

**TRIBOLOGY OF SELF-LUBRICATING
SU-8 COMPOSITES FOR MICRO-ELECTRO
MECHANICAL SYSTEMS (MEMS) APPLICATIONS**

PRABAKARAN SARAVANAN

NATIONAL UNIVERSITY OF SINGAPORE

2015

**TRIBOLOGY OF SELF-LUBRICATING
SU-8 COMPOSITES FOR MICRO-ELECTRO
MECHANICAL SYSTEMS (MEMS) APPLICATIONS**

BY

PRABAKARAN SARAVANAN
(B.E-Mech.Engg., Anna University, India)

A THESIS SUBMITTED

FOR THE DEGREE OF DOCTOR OF PHILOSOPHY

DEPARTMENT OF MECHANICAL ENGINEERING

NATIONAL UNIVERSITY OF SINGAPORE

2015

Preamble

This thesis is submitted for the degree of Doctor of Philosophy in the Department of Mechanical Engineering, National University of Singapore under the supervision of Dr. Duong Hai Minh, Dr. Sujeet Kumar Sinha and Dr. Christina Lim. I assure the examiner that no part/content of this thesis has been submitted for any degree or diploma at any other Universities or Institution and the contents of this thesis are purely original. Parts of this thesis have been published/accepted and under review for publication as listed below:

(A) Patents:

- 1) **Prabakaran Saravanan**, S K Sinha, Satyanarayana N, SU-8 Nano-Composites with Improved Tribological and Mechanical Properties, **US PCT Application No. 2013/0130951 A1**, Filing date: 23 May 2013.

(B) Peer-Reviewed Journal Publications:

- 1) **Prabakaran Saravanan**, N. Satyanarayana and S. K. Sinha, Self-lubricating SU-8 Nanocomposites for micromechanical systems applications, *Tribology Letters* **49** (1) (2013) 169-178.
- 2) **Prabakaran Saravanan**, Nalam Satyanarayana and S. K. Sinha, Wear Durability Study on Self-lubricating SU-8 composites with perfluoropolyether, multiply-alkylated cyclopentane and base oil as the fillers, *Tribology International* **64** (2013) 103-115.

- 3) **Prabakaran Saravanan**, Nalam Satyanarayana, Duong Hai Minh and Sujeet K. Sinha, An *in-situ* heating effect study on tribological behavior of SU-8+PFPE composite, *Wear* **307** (2013) 182-189.
- 4) **Prabakaran Saravanan**, Nalam Satyanarayana and Sujeet K. Sinha, SU-8 Composite Based “Lube-tape” for a Wide Range of Tribological Applications, *Micromachines* **5** (2014) 263-274.
- 5) **Prabakaran Saravanan**, Sundaramurthy Jayaraman, Duong Hai Minh and Sujeet K. Sinha, A Role of Functional End Groups of Perfluoropolyether - Z-dol and Z-03 Lubricants in Augmenting the Tribology of SU-8 composites, *Tribology Letters* **56** (2014) 423-434.

(C) Conference Publications/Presentations (Peer Reviewed):


- 1) **Prabakaran Saravanan**, Satyanarayana N, Sinha SK, “ Tribology of Self-lubricating SU-8 composites for MEMS Applications”, **WTC2013-657**, *Proceedings of 5th World Tribology Congress 2013*, Turin, Italy.
- 2) **Prabakaran Saravanan**, N. Satyanarayana, P. C. Siong, H. M. Duong and S. K. Sinha., "Tribology of self-lubricating SU-8+PFPE composite based Lub-tape"., *Procedia Engineering* **68** (2013) 497-504. (Organised by MITC,2013, Sabah, Malaysia)
- 3) **Prabakaran Saravanan**, Sinha SK, “SU-8 Composites for Micro-systems Applications”, **TSI914677**, *Proceedings of ASIATRIB -2014*, Agra, India.

(D) Conference Poster Presentations:

- 1) **Prabakaran Saravanan**, N. Satyanarayana and S. K. Sinha., “SU-8 Nanocomposites with self-lubricating properties for Microelectromechanical Systems Applications”, *International Conference of Young Researchers on Advanced Materials (MRS-ICYRAM 2012)*, July 1-6, 2012, Singapore.
- 2) **Prabakaran Saravanan**, Nalam Satyanarayana, Duong Hai Minh and Sujeet K Sinha, “Tribological Behaviour of *In-Situ* heated SU-8+PFPE composites”, *International Nanotribology Forum 2014*, Kerala, India.

Declaration

I hereby declare that the work presented in this thesis is purely my original work and it has been conceived and written entirely by me. It was neither copied nor reproduced from anywhere else. I have duly acknowledged all the information sources used in this thesis with appropriate and adquete citations. According to my knowledge, I also declare this thesis has not been submitted for any degree in any university previously for any courses of study .

| | |
|----------------------|---|
| Prabakaran Saravanan |  |
| Date | 14/05/2015 |

Acknowledgements

Undoubtedly, doing a PhD is one of the best journeys one can ever have in life. I would not have reached my final destination in that journey without the help, support and guidance of a few amazing people whom I have come across during the four years of my PhD program. Hence, I would like to take this opportunity to thank and acknowledge all those people who supported me during all these years.

Above all, I offer my deepest appreciation to my PhD mentors, A/P. Sujeet Kumar Sinha, A/P. Duong Hai Minh and A/P. Christina Lim, for their incredible support and guidance provided for grooming me in my PhD research. I am very grateful to Prof. Sinha for his extended support for the conversion of my M.Eng to PhD. His style of mentoring, and analyzing and solving problems and his unending encouragement have always inspired me and made me strive to do better and in fact, it is precisely that which drives my passion towards research. I cannot express enough appreciation for Prof. Duong for his patience and dedication towards me in last two years of my PhD program. He was very helpful in various occasions starting from mentoring, advice regarding conference funding and other technical discussions. Last but not least, I offer my sincere thanks to Prof. Christina Lim of the Materials Division for being my co-supervisor, for her direct and indirect help in many aspects and occasions for the completion of my PhD.

I would like to express my genuine thanks to Dr. Nalam Satyanarayana, who co-authored with me more than five journal papers and conference proceedings. His assistance and support were truly indispensable for the successful completion of my PhD. The time and effort spent by him for my PhD is immense and his patience and humility is always striking. He has given me valuable advice during every stage of my PhD program

and continues to guide me even to this day. My accomplishments would not be possible without him. I also thank Dr. Sundaramurthy Jayaraman for his assistance in unlocking the mystery of chemical interactions by performing a series of XPS tests. His help saved a significant amount of my effort and time. His exceptional guidance and advice were absolutely essential to my progress.

I also appreciate the assistance provided by the Materials Lab technical staff members, Mr. Thomas Tan Bah Chee, Mr. Abdul Khalim Bin Abdul, Mr. Ng Hong Wei, and Mr. Juraimi Bin Madon in helping me perform many of my experiments. I am also grateful for the help provided by the staff in other labs, in particular Nano-Biomechanics (Ms. Brenda and Dr. Zhang) and Lab-in-Charge Prof. CT Lim.

I would like to thank all my colleagues in the lab for helping me on many occasions and for their friendship (Minn, Sandar, Bau, Sharon, Siew Fah and many others). I would like to thank all my friends Hemanth, Adthiya, Sanjay, Amutharaj, Truc, Gopi, Sasi, Mohan, Venkat, Akshay, Kwodwo, Moon, Kalai, Deepan, Balaji, Simbu, Venky, Sleepy and many others for their help, constant support and late night chats.

Finally, I want to thank my family for their support and encouragement, and most of all, my mother, followed by brothers Gopinathan and Rajesh, my sister Ramya, my uncles Sendhilvel and Kandasamy for their incredible support throughout my life and having confidence in me. No words are sufficient to express my gratitude and thanks for support offered by my entire family, those who not mentioned here.

Table of Contents

| | Page Number |
|---|-------------|
| Preamble | i |
| Acknowledgements | v |
| Table of Contents | vii |
| Summary | xiv |
| List of Tables | xvi |
| List of Figures | xvii |
| List of Notations | xxii |
| Chapter 1: Introduction | 1 |
| 1.1 Background | 1 |
| 1.2 Introduction to MEMS and Its Tribology | 3 |
| 1.3 Research Objectives and Scope | 5 |
| 1.4 Outline of the Thesis | 6 |
| Chapter 2: Literature Review | 11 |
| 2.1 Tribological Challenges of MEMS | 11 |
| 2.2 Case Studies: MEMS Failure..... | 14 |
| 2.2.1 Polysilicon Electrostatic Micromotor | 14 |
| 2.2.2 Microturbine | 15 |
| 2.2.3 Micro Gearbox | 15 |
| 2.2.4 Digital Micromirror Device (DMD) | 17 |
| 2.3 Solutions to MEMS Tribological Challenges | 19 |
| 2.3.1 Liquid Lubricant Films | 20 |

| | |
|--|-----------|
| 2.3.2 Self-Assembled Monolayers (SAMs) | 22 |
| 2.3.3 Nano Patterning/ Texturing of Surfaces | 24 |
| 2.3.3.1 Analysis of Contact Interface..... | 26 |
| 2.3.3.2 Composite Interface | 27 |
| 2.4 Polymer and Composites for MEMS Applications | 28 |
| 2.4.1 PDMS (polydimethylsiloxane) Elastomer | 30 |
| 2.4.2 Polymer Nanocomposites..... | 31 |
| 2.4.3 Self-lubricating Nanocomposites..... | 33 |
| 2.5 SU-8 Polymer for MEMS Applications..... | 37 |
| 2.5.1 Research Strategy Followed in this Thesis | 42 |
| Chapter 3: Materials and Experimental Procedure | 44 |
| 3.1 Materials | 44 |
| 3.1.1 Silicon | 44 |
| 3.1.2 SU-8 Resin | 45 |
| 3.1.2.1 SU-8 Processing | 46 |
| 3.1.2.2 Mechanical and Physical Properties of SU-8..... | 48 |
| 3.1.3 Perfluoropolyether | 50 |
| 3.1.4 Multiply-alkylated cyclopentanes (MACs) and SN 150 base oil ... | 51 |
| 3.2 SU-8 / SU-8 composite Film Preparation and Characterizations | 51 |
| 3.2.1 SU-8 Sample Preparation..... | 51 |
| 3.2.2 Contact Angle and Surface Free Energy Characterization | 54 |
| 3.2.3 Tribological Characterization | 55 |
| 3.2.4 Nano-mechanical Characterization..... | 57 |

| | |
|--|-----------|
| 3.2.5 X-ray Photoelectron Spectroscopy (XPS) Characterization | 58 |
| 3.2.6 AFM Characterization | 59 |
| 3.2.7 FESEM and EDS Characterization..... | 59 |
| 3.2.8 Time-of-Flight Secondary-ion Mass Spectroscopy (TOF-SIMS) Characterization | 59 |
| 3.2.9 Nano - tribological Characterization..... | 60 |
| 3.2.10 Optical profiler Characterization | 60 |
| 3.2.11 Thermogravimetric Analysis (TGA)..... | 61 |
| 3.2.12 Perfluoropolyether (PFPE) Dip-coating on SU-8 | 61 |
| Chapter 4: Development of Self-Lubricating SU-8 Composites for MEMS | |
| Applications | 62 |
| 4.1 Introduction..... | 62 |
| 4.2 Materials and Experimental Procedures | 63 |
| 4.3 Results and Discussion | 64 |
| 4.3.1 Water Contact Angle Characterization | 64 |
| 4.3.2 X-ray Photoelectron Spectroscopy (XPS) Characterization of Freshly Cured and Cross-linked Surface | 65 |
| 4.3.3 Tribological Characterization | 67 |
| 4.3.4 Discussion..... | 70 |
| 4.3.5 XPS and WCA of Worn Surfaces..... | 72 |
| 4.3.6 Nano-Mechanical Characterization | 74 |
| 4.3.7 Optical Characterization of Worn Surfaces | 75 |
| 4.4 Conclusions..... | 77 |

| | |
|--|-----|
| Chapter 5: Chemical Bonding in SU-8 Composites | 78 |
| 5.1 Introduction..... | 78 |
| 5.2 Materials and Experimental Procedures | 80 |
| 5.3 Results and Discussion | 81 |
| 5.3.1 AFM Surface Images | 81 |
| 5.3.2 Surface Free Energy Calculations (for fresh Surface) | 83 |
| 5.3.3 XPS Characterization (on fresh Surface)..... | 84 |
| 5.3.4 Tribological Characterization | 87 |
| 5.3.5 Surface Free Energy Calculations (Worn Surface)..... | 90 |
| 5.3.6 Physical Boundary Self- Lubrication Mechanism | 91 |
| 5.3.7 EDS Characterization..... | 95 |
| 5.3.8 XPS Characterization (Worn Surface)..... | 97 |
| 5.3.9 Nano-Mechanical Characterization | 100 |
| 5.3.10 Three-Dimensional (3D) Optical Profiler Images | 101 |
| 5.3.11 Surface Characterization of Worn Surfaces..... | 103 |
| 5.4 Conclusions..... | 108 |
| Chapter 6: Effects of Functional End Groups of Perfluoropolyether (PFPE) Z-dol and Z-03 in Tribology of SU-8 Composites | 109 |
| 6.1 Introduction..... | 109 |
| 6.2 Materials and Experimental Procedures | 112 |
| 6.3 Results and Discussion | 112 |
| 6.3.1 Wettability Analysis..... | 113 |
| 6.3.2 Surface Free Energy Calculations..... | 114 |

| | |
|--|-----|
| 6.3.3 Tribological Characterization | 117 |
| 6.3.4 Nano-tribological Characterization..... | 118 |
| 6.3.5 Surface Chemical Analysis | 120 |
| 6.3.6 Thermogravimetric Analysis (TGA)..... | 124 |
| 6.3.7 Surface Characterization of Worn Surfaces..... | 126 |
| 6.4 Conclusions..... | 129 |

Chapter 7: A Comprehensive Investigation of Physical Self-Lubrication

| | |
|--|------------|
| Mechanisms of SU-8 Composites..... | 131 |
| 7.1 Introduction..... | 131 |
| 7.2 Materials and Experimental Procedures | 139 |
| 7.2.1 Micro-tribological Characterization..... | 139 |
| 7.3 Results and Discussion | 140 |
| 7.3.1 Coefficient of Friction (COF) versus Sliding Velocity Plot | 140 |
| 7.3.2 Discussion..... | 142 |
| 7.3.2.1 Lubrication Mechanism at Zone 1..... | 142 |
| 7.3.2.2 Lubrication Mechanism at Zones 2 and 3 | 144 |
| 7.3.3 Effects of Normal Load and Sliding Rotational Speed..... | 150 |
| 7.3.4 Tribological High-Low Speed Tests..... | 153 |
| 7.3.5 EDS Elemental Mapping | 157 |
| 7.4 Conclusions..... | 159 |

Chapter 8: Effects of Curing Temperature and In-situ Heating on Thermal Stability

| | |
|---------------------------------|------------|
| of SU-8 Composites | 161 |
| 8.1 Introduction..... | 161 |

| | |
|---|------------|
| 8.2 Materials and Experimental Procedures | 163 |
| 8.2.1 Materials | 163 |
| 8.2.2 Tribological Characterization | 163 |
| 8.3 Results and Discussion | 165 |
| 8.3.1 Surface Free Energy Calculations | 165 |
| 8.3.2 Tribological Characterization | 168 |
| 8.3.3 Migration of lubricant | 171 |
| 8.3.4 Surface Area Coverage Calculation..... | 177 |
| 8.3.5 Nano-Mechanical Characterization | 178 |
| 8.3.6 Surface Characterization of Worn Surfaces..... | 180 |
| 8.4 Conclusions..... | 182 |
| Chapter 9: Conclusions and Future Work | 183 |
| 9.1 Conclusions..... | 183 |
| 9.1.1 Development of Self-lubricating SU-8 composites | 183 |
| 9.1.2 Wear Durability Study for Chemical Bonding Investigation | 184 |
| 9.1.3 Physical Self-Lubrication Investigation..... | 186 |
| 9.2 Limitations and Future Work | 187 |
| 9.2.1 Adapting this Approach for Other Photo-resist Polymers | 187 |
| 9.2.2 Utilizing SU-8 composites in Real-time Applications..... | 187 |
| 9.2.3 Addition of Additives and Surfactants..... | 188 |
| 9.2.4 Mechanical Properties of SU-8..... | 188 |
| 9.2.5 Cross-linking Density Analysis of SU-8 and SU-8 Composites | 189 |
| 9.2.6 Graphite-PFPE Lubrication | 189 |

Table of Contents

| | |
|---|------------|
| 9.2.7 Dip-coating of SU-8 Composite for Commercial Applications | 190 |
| References..... | 191 |

Summary

The photo-resistive property of epoxy-based SU-8 polymer makes it a potential structural material for micro-fabrication of MEMS devices using the photo-lithography process. However, its poor tribological and mechanical properties are major concerns, if SU-8 has to replace Si, which is the mainstay structural material for making MEMS. Low moduli and hardness present problems in the fabrication and functioning of the micro-machines. Poor tribology will lead to adhesion, friction, wear and early failure of the components. This thesis deals with the preparation of novel SU-8 based composites to enhance the tribological and mechanical properties of the base polymer. It is observed that adding liquid PFPE (Perfluoropolyether; Z-dol 4000) lubricant to SU-8 as filler promotes chemical reactions between the molecules of SU-8 and PFPE, which helps in forming a physical boundary lubrication layer (~10 nm) when this composite is subjected to tribological contacts. This enhances the wear durability of SU-8 by more than four orders of magnitude over its pure form. The chemical reaction is further investigated by adding other two lubricants, a base oil (SN 150) and a multiply-alkylated cyclopentane (MAC) oil, to the SU-8 matrix. Both lubricants are alkanes, chemically less reactive, and have no polar reactive terminal groups unlike PFPE (Z-dol 400) which has –OH polar terminal groups. SU-8+PFPE, SU-8+SN 150 and SU-8+MAC composites have enhanced wear life exceeding that of SU-8 by 1000, 500 and 200 times, respectively at very mild lubricant concentration (2 wt%) for a given set of experimental conditions of a normal load of 100 g and a sliding speed of 1000 rpm. It is postulated that proper lubricant dispersion and possible chemical bonding of PFPE (Z-dol) molecules with SU-8 are responsible for the

superior tribological properties of SU-8+PFPE composites, in comparison to other SU-8 composites.

The nature of the chemical bonding is further investigated by comparing PFPE Z-dol performance with another PFPE lubricant Z-03. Both Z-dol and Z-03 have the same chemical back bone chain, however, they have polar ($-OH$) and non-polar (CH_3) end groups, respectively. SU-8+Z-dol yielded ~8 times greater wear life than that for SU-8+Z-03. This has proven that the polar component of Z-dol provides sites for the etherification reaction and bonding of PFPE with SU-8 molecules. The physical self-lubrication mechanism along with chemical bonding was found to be responsible for the dramatic rise in the wear durability of SU-8+ PFPE (Z-dol).

The physical self-lubrication was investigated further by plotting the coefficient of friction versus sliding velocity plot for 5 wt% SU-8+Z-dol composite. Three different zones were identified based on their exhibited frictional behaviour with speed. Zone 1, Zone 2 and Zone 3 exhibit a steep increase, marginal increase and linear increase in coefficient of friction (COF) with increasing speed, respectively. At low speeds, the entire wear track is covered by lubricant, because there is enough time for the displaced mobile lubricant to diffuse to the wear track again. As the speed increases, there is not enough time for the displaced lubricant to diffuse to the wear track between consecutive cycles. Hence, the increase in sliding speed leads to more and more asperity contact and initiates the surface wear. Once the wear process reaches the next layer of fresh lubricant droplets, further lubricant is released. Thus, the COF is stabilized. Further increase in speed increases the COF linearly. The increase in COF is attributed to lubricant displacement and starvation. As soon as it reaches the dry contact, a new batch of

lubricant is released and the COF drops to a lower value and stabilizes again. However, a gentle rise in the coefficient of friction is encountered, along with a further increase in speed.

The effects of curing temperature on tribological properties and thermal stability of pristine SU-8 and SU-8+PFPE composite were also studied by *in-situ* heating from room temperature (25 °C) to 100 °C. The heating did not lead to any observable change in the tribological behaviour of pristine SU-8, whereas the heating of SU-8+PFPE reduced the initial and steady-state coefficients by ~2 and ~7 times, respectively, and increased the wear life (n) by more than three times than that of SU-8+PFPE at room temperature. The *in-situ* heating provided greater surface area coverage by the PFPE lubricant and the migration of additional PFPE from the bulk to the surface. Overall, these two aspects made the surface enriched with more PFPE, which reduced friction and wear. Various characterizations such as surface energy, TOF-SIMS have also confirmed the phenomenon. This study shows that apart from MEMS applications, the SU-8+PFPE composite can also find application in moderately high temperature engineering applications where tribology is a major concern.

In summary, the newly developed self-lubricating lubricant droplet-filled SU-8 composite has exhibited superior tribological properties, compared to pristine SU-8. The physical and chemical mechanisms responsible for this tribological enhancement were analyzed comprehensively in this thesis. This tribologically enhanced SU-8 composite can also have numerous applications in bearings, raceways, gears, bio-devices, precision-positioning stages, and components in consumer electronics, such as cameras and printers, in addition to micro-systems applications.

List of Tables

| | | Page Number |
|-----------|---|------------------------|
| Table 2.1 | Description of list of polymer composites (1-6) and nanocomposites (6-14), their matrix, filler, dispersion technique and lowest wear rate concentration (vol%) | 32 |
| Table 2.2 | Common polymers and fillers used for developing the self-lubricating composites | 34 |
| Table 2.3 | Self-lubricating composites and their applications in space industry | 35 |
| Table 3.1 | Physical, Mechanical and dimensional properties of Si wafers used | 44 |
| Table 3.2 | Mechanical and physical properties of SU-8 photoresist | 48 |
| Table 3.3 | Physical and chemical properties of Z-dol and Z-03 lubricants | 50 |
| Table 3.4 | Physical properties of MAC and SN 150 lubricants | 51 |
| Table 3.5 | Polar, dispersive and total surface tensions of reference liquids used for surface energy calculation | 55 |
| Table 4.1 | Initial coefficient of friction (μ_i), Steady-state coefficient of friction (μ_s) and wear life (number of sliding cycles) of SU-8 and SU-8 composites obtained from sliding tests against 4 mm diameter Si_3N_4 ball at different normal loads and sliding rotational speeds | 67 |
| Table 5.1 | Composite nomenclature, compositional description, category and grade for all SU-8 composites | 80 |
| Table 5.2 | AFM images of freshly spin-coated Pristine SU-8 and 2wt%SU-8 composites surfaces before and after washing. In addition to the table, alphabetical identification is also given. Before washing: (a) Pristine SU-8 (b) SU-8+PFPE (c) SU-8+SN 150 (d) SU-8+MAC. After washing: (e) SU-8+PFPE (f) SU-8+SN 150 (g) SU-8+MAC | 82 |
| Table 5.3 | Initial coefficient of friction (μ_i), Steady-state coefficient of friction (μ_s) and wear life (number of sliding cycles) of pristine SU-8 and SU-8 composites obtained from sliding tests against 4 mm diameter Si_3N_4 ball at different normal loads and sliding | 88 |

| | | |
|-----------|---|-----|
| | rotational speeds. | |
| Table 6.1 | Initial coefficient of friction (μ_i), steady-state coefficient of friction (μ_s) and wear life (number of sliding cycles, n) of different composites obtained from sliding tests against 4 mm diameter Si_3N_4 ball pristine at different normal loads and sliding rotational speeds. (a) SU-8 and 2wt% SU-8 composite tested at a normal load of 150g and a sliding rotational speed of 1000 rpm. (b) 0.5wt% PFPE dip-coated on SU-8 tested at a normal load of 20mN and a sliding rotational speed of 100 rpm | 117 |
| Table 7.1 | Summary of coefficient of friction (μ_s) values for 5wt% SU-8+Z-dol composite obtained from sliding tests against 4 mm diameter Si_3N_4 ball at a fixed normal load of 300g and various sliding rotational speeds and their corresponding counterface ball and worn surface image after sliding test, respectively. | 147 |
| Table 7.2 | Summary of co-efficient of friction values of 5wt% SU-8 composites were obtained from sliding tests against 4 mm diameter Si_3N_4 ball at fixed normal load of 300 g and various sliding rotational speeds. The corresponding optical micrographs of counterface ball after sliding tests and micrographs of counterface ball after cleaning with solvent were also shown. The sliding tests were conducted from high speed of 3000 rpm to low speeds of 10, 100, 500 and 1000 rpm, respectively. | 156 |
| Table 8.1 | Initial coefficient of friction (μ_i), Steady-state coefficient of friction (μ_s) and wear life (number of sliding cycles) of pristine SU-8 and SU-8+PFPE composite obtained from sliding tests against 4 mm diameter Si_3N_4 ball for a normal load of 300g and a sliding linear velocity of 7mm/s at various temperatures. | 169 |
| Table 8.2 | Initial coefficient of friction (μ_i), Steady-state coefficient of friction (μ_s) and wear life (number of sliding cycles) of pristine SU-8 and SU-8+PFPE composite obtained from sliding tests against 2 mm diameter Si_3N_4 ball for a normal load of 20 mN and a sliding rotational speed of 100 rpm at various surface conditions | 172 |

List of Figures

| | | Page Number |
|-------------|---|------------------------|
| Figure 2.1 | The failure mode and mechanism of this resonator are broken beams and overload stress induced by rough handling, respectively | 12 |
| Figure 2.2 | Typical failure mechanisms identified in MEMS devices | 12 |
| Figure 2.3 | (a) Schematic top view of the measurement of adhesion as a function of relative humidity using interferometry. The dark spots correspond to the bending of the beam by adhesive forces. (b) Capillary condensation between two contacting surfaces | 14 |
| Figure 2.4 | SEM image of MEMS devices (a) electrostatic micromotor. (b) Microturbine rotor and nozzle guided vanes on the stator | 15 |
| Figure 2.5 | SEM image of microgear speed reduction unit after wear test | 16 |
| Figure 2.6 | Images of digital micromirror device for digital projection displays | 18 |
| Figure 2.7 | Schematic illustrates the possible mechanism for wear and stiction in SAMs coatings on DMD | 18 |
| Figure 2.8 | Tribological solutions developed to the wear and stiction issues in MEMS devices | 19 |
| Figure 2.9 | Wear test results i.e. Number of cycles Vs frictional force and COF, for PFPE Z-dol , Z-15 and Si(100). Schematic diagram demonstrates molecular interaction between Z-15 molecules and AFM tip over a number of passes (bottom) | 21 |
| Figure 2.10 | Formation of SAMs coating on a substrate using simple immersing technique | 23 |
| Figure 2.11 | (a) Droplet on a smooth and rough surface with the contact angle of θ_0 and θ , respectively. (b) Contact angle for rough surface (θ) as a function of the roughness factor (Rf) for various contact angles of the smooth surface (θ_0) | 27 |
| Figure 2.12 | (a) Formation of solid-liquid-air composite interface by a liquid droplet on a rough surface | 28 |
| Figure 2.13 | PDMS microchip for generating localized plasma | 30 |

| | | |
|-------------|---|----|
| Figure 2.14 | Schematic illustration shows the anatomy of nanocomposite, where two phases co-exist, polymer matrix and nanoparticles | 31 |
| Figure 3.1 | Schematic illustrating distinction between the negative and positive photoresists | 45 |
| Figure 3.2 | Chemical structure of (a) SU-8, (b) a solvent such as gamma-butyrolactone (GBL), and (c) a photoacid generator such as triaryl sulfoniumsalts | 46 |
| Figure 3.3 | The processing sequence for SU-8 processing | 47 |
| Figure 3.4 | Step-by-step procedure adopted for fabrication of pristine SU-8 and SU-8 composite films | 53 |
| Figure 3.5 | Digital image of water contact angle measurement apparatus | 54 |
| Figure 3.6 | CETR ball/pin-on-disk sliding test setup. (a) Rotational sliding test set up; (b) Reciprocating (To and Fro) sliding test setup | 56 |
| Figure 4.1 | WCA values for pristine SU-8 and SU-8 based composites over fresh (pristine surface of composites before experiment) and worn surfaces (wear track). (a) : Non-PFPE combinations at 10^4 cycles (composites did not contain PFPE). (b): PFPE combinations at 10^6 cycles | 65 |
| Figure 4.2 | XPS Wide-scan survey spectrum results for freshly cured and cross-linked surfaces (a) pristine SU-8, (b) SU-8+PFPE composite | 66 |
| Figure 4.3 | Coefficient of friction versus number of cycles plot for SU-8, SU-8+PFPE, SU-8+SiO ₂ , SU-8+CNTs and SU-8+graphite composites obtained from the ball-on-disk sliding tests against 4 mm diameter Si ₃ N ₄ ball at different normal loads and sliding speeds. (a) A normal load of 30g and a rotating sliding speed of 200 rpm. (b) A normal load of 300 g and a rotating sliding speed of 2000 rpm. The tests were stopped at 1 million cycles because of the long test duration as the samples had not failed | 69 |
| Figure 4.4 | (a) A depiction of the cross-linking in SU-8+PFPE composite through the formation of ether bonds. (b) Digital Image of a 200 micron thick gear made of SU-8+PFPE composite using UV lithographic process. | 71 |
| Figure 4.5 | XPS Wide-scan survey spectrum results for inside the wear track of SU-8+PFPE composite after sliding for 1 million cycles at a normal load of 300g and a rotational speed of 2000 rpm. | 73 |

| | | |
|------------|--|----|
| Figure 4.6 | Elastic Modulus (E) and Hardness (H) values of pristine SU-8 and SU-8 composites from nano-indentation characterization | 74 |
| Figure 4.7 | Optical micrographs of worn surfaces: (a) Bare SU-8 (at 10,000 cycles), (b) SU-8+Nanoparticles(SiO ₂ ,CNT) (at 10,000 cycles), (c) SU-8+PFPE (at 1 million cycles), (d) SU-8+PFPE+CNTs (at 1 million cycles), (e) SU-8+PFPE+SiO ₂ (at 1 million cycles), (f) SU-8+PFPE+graphite (at 1 million cycles). Images (g), (h), (i), (j), (k),(l) and (m), (n), (o), (p), (q), (r) are Optical micrographs of the counter face balls surface after sliding tests and micrographs of the tested counterface balls after cleaning with acetone corresponding to the worn surfaces shown in (a), (b), (c), (d), (e) and (f) respectively. The length of the scale bar is 100 μm in all images | 76 |
| Figure 5.1 | Polar, dispersive and total Surface energies at the freshly spin-coated surface of pristine SU-8 and 2wt% SU-8 composites | 84 |
| Figure 5.2 | XPS analysis Cls scan (left) and At% table (right) for pristine SU-8 and 2wt% SU-8 composites at freshly spin-coated surfaces. (a) Pristine SU-8. (b) SU-8+PFPE. (c) SU-8+SN 150. (d) SU-8+MAC | 86 |
| Figure 5.3 | Typical coefficient of friction versus number of cycles plot for pristine SU-8 and SU-8 composites obtained from the ball-on-disk sliding tests against 4 mm diameter Si ₃ N ₄ ball at different normal load and sliding speed. (a) Pristine SU-8 and 10wt% SU-8 composites tested at a normal load of 300g and a sliding speed of 2000 rpm. The tests stopped after 1 million cycles without any failure for the composites. (b) Pristine SU-8 and 2 wt% SU-8 composites tested at a normal load of 100g and a sliding speed of 1000rpm. | 89 |
| Figure 5.4 | Polar, dispersive and total Surface energies at the wear track (worn surface) of pristine SU-8 and 2 wt% SU-8 composites after 500,000 sliding cycles | 90 |
| Figure 5.5 | SEM cross-sectional images of ~100 μm thick pristine SU-8 and 2 wt% SU-8 composite films. (a) Pristine SU-8 (b) SU-8+PFPE (c) SU-8+SN 150 (d) SU-8+MAC | 92 |
| Figure 5.6 | Coefficient of friction versus number of cycles plot for washed 10 wt% SU-8 composites obtained from the ball-on-disk sliding tests against 4 mm diameter Si ₃ N ₄ ball at a normal load of 300 g and a sliding speed of 1000 rpm | 93 |
| Figure 5.7 | Cross-sectional SEM images of SU-8+PFPE and corresponding | 96 |

| | | |
|-------------|---|-----|
| | EDX atomic percent (At. %) table. (a) SU-8+PFPE before washing. (d) SU-8+PFPE after washing. (c) PFPE layer at surface before washing. (d) PFPE layer at surface after washing | |
| Figure 5.8 | XPS analysis Cls scan (left) and At% table (right) for 2wt%SU-8 composites at inside the wear tracks (worn surfaces) after 500,000 sliding cycles. (a) SU-8+PFPE. (b) SU-8+SN 150. (c) SU-8+MAC | 99 |
| Figure 5.9 | Hardness (H) values of pristine SU-8 and 2 wt% SU-8 composites from nano-indentation characterization | 101 |
| Figure 5.10 | 3D Optical profiler images of the wear track (worn surface) for 2 wt% SU-8 composites after 500,000 sliding cycles at normal load of 100 g and sliding speed of 1000 rpm. (a) SU-8+PFPE. (b) SU-8+SN 150. (c) SU-8+MAC | 103 |
| Figure 5.11 | Optical micrographs of worn surfaces: (a) Pristine SU-8(at 10,000 cycles) (b) SU-8+PFPE (at 500,000 cycles) (c) SU-8+SN 150 (at 270,000 cycles) (d) SU-8+MAC (at 100,000 cycles). Images (e), (f), (g), (h) and (i), (j), (k), (l) are Optical micrographs of the counterface balls surface after sliding tests and micrographs of the tested counterface balls after cleaning with solvents corresponding to the worn surfaces shown in (a), (b), (c) and (d) respectively. The length of the scale bar is 100 μ m in all images | 105 |
| Figure 5.12 | SEM images of wear track (worn surface) of 2wt%SU-8 composites after sliding tests of 100g normal load and 1000 rpm. (a) SU-8+PFPE (at 500,000 cycles). (b) SU-8+SN 150 (at 270,000cycles). (c) SU-8+MAC (at 100,000 cycles) | 107 |
| Figure 6.1 | Visual images of contact angle measurements of 0.5 μ l droplets of PFPE lubricants with SU-8 surface. (a) Z-03, (b) Z-dol and (c) Surface area coverage comparison between 2 μ l of PFPE lubricants | 113 |
| Figure 6.2 | Polar, dispersive and total surface energies of freshly spin-coated (completely UV-cured and cross-linked) pristine SU-8 and 2wt% SU-8 composites. The data scatter was within ± 0.2 for all cases | 114 |
| Figure 6.3 | Water contact angle (WCA) measurements of freshly spin-coated (completely UV-cured and cross-linked) pristine SU-8 and 2wt% SU-8 composites for different conditions after UV exposure; (a) immediately – after UV exposure, (b) one day – after UV exposure, and (c) after washing | 115 |
| Figure 6.4 | Typical coefficient of friction versus number of cycles plot for different samples fetched from the ball-on-disk sliding tests against | 119 |

| | | |
|------------|--|-----|
| | 4 mm diameter Si ₃ N ₄ ball at a different normal load and a sliding rotational speed. (a) SU-8 and 2wt% SU-8 composite tested at a normal load of 150g and a sliding rotational speed of 1000 rpm. (b) 0.5wt% PFPE dip-coated on SU-8 tested at a normal load of 20mN and a sliding rotational speed of 100 rpm | |
| Figure 6.5 | Figure 6.5: XPS Cls scan for freshly spin-coated (completely cured and cross-linked) Pristine SU-8 and 2wt%SU-8 composites, corresponding to the XPS of washed surfaces shown in Figure 6.6. (a) Pristine SU-8. (b) SU-8+Z-03. (c) SU-8+Z-dol. | 121 |
| Figure 6.6 | XPS analysis of Cls scan for freshly spin-coated (completely cured and cross-linked) 2wt%SU-8 composites after rinsing, followed by 20 min sonication. (a) Pristine SU-8. (b) SU-8+Z-dol. (c) SU-8+Z-03. | 122 |
| Figure 6.7 | Thermogravimetric analysis results of pristine SU-8 and 2wt%PFPE dip-coated onto SU-8 for various surface conditions | 125 |
| Figure 6.8 | Optical micrographs of counterface balls surface after sliding tests: (a) Pristine SU-8(at 70,000 cycles);(b) SU-8+Z-dol (at 500,000 cycles);(c) SU-8+Z-03 (at 70,000 cycles). Images (d), (e), (f) and (g),(h),(i)are optical micrographs of the counterface balls surface after cleaning with solvents and the worn surfaces corresponding to the images of counterface balls shown in (a),(b),(c),respectively. The length of the scale bar is 100 μm in all images | 127 |
| Figure 6.9 | Schematic diagram explains the interaction between SU-8 and PFPE Z-dol and Z-03 molecules in SU-8 composites | 128 |
| Figure 7.1 | Stribeck curve explains the how lubrication behaviour in reality from thetextbooks, especially at low stribeck numbers | 132 |
| Figure 7.2 | Schematic diagram demonstrates execution of micro tribological tests, carried out on the same spot where macro tribo test was conducted | 140 |
| Figure 7.3 | Coefficient of friction (COF) versus sliding velocity plot for 5wt% SU-8+Z-dol composite tested at a normal load of 300g and different sliding velocitiesfor a fixed number of 10,000 sliding cycles. | 141 |
| Figure 7.4 | Possible lubrication mechanisms at the ball-surface interface during Zone 1 of low speed sliding in a sequence. (a) Before sliding. (b) Beginning of the sliding. (c) Ending of the sliding. | 143 |
| Figure 7.5 | Possible lubrication mechanisms at the ball-surface interface during | 145 |

-
- Zone 2 and 3 of high speed sliding in a sequence. (a) After few sliding cycles. (b) Lubricant starved contact. (c) Wear releases new batch of lubricant due to self-lubrication.
- Figure 7.6 Effect of sliding rotational speed (V) and Normal load (N) on frictional behaviour of 5wt% SU-8+Z-dol composite tested against 4 mm diameter Si₃N₄ ball with the ball-on-disk sliding configuration at a different normal load and a sliding rotational speed. (a)COF Vs sliding rotational speed plot:5wt% SU-8 +Z-dolcomposite tested at a range of sliding rotational speeds from 10 to 3000 RPM for normal loads from 10 to 300 g. (b)COF VsNormal load plot: 5wt% SU-8+Z-dol composite tested at a range of normal loads from 10-300g for sliding rotational speeds from 10 to 3000 RPM.[Standard Error: ± 0.02] 152
- Figure 7.7 Typical coefficient of friction versus number of sliding cycles plot of 5wt% SU-8+Z-dol composite tested against 4 mm diameter Si₃N₄ ball with the ball-on-disk sliding configuration at different normal loads and sliding rotational speeds for a fixed test duration of 10,000 cycles 153
- Figure 7.8 EDS elemental mapping carried out on the random spot of wear track (worn surface) of 5wt% SU-8+Z-dol composite tested at macro tribological test conditions of normal load of 300g and sliding rotational speed of 3000 rpm for a fixed test duration of 10,000 cycles. 158
- Figure 8.1 Schematic of the experimental heating set-up used for the tribological characterization 164
- Figure 8.2 Polar, dispersive and total surface energies of pristine SU-8 and SU-8+PFPE composite at various temperatures from RT (25°C) to 110°C. (a) Pristine SU-8, (b) SU-8+PFPE composite fresh surface, and (c) SU-8+PFPE composite after washing. Standard error (S.E) is ± 0.2 for all cases 166
- Figure 8.3 Typical coefficient of friction versus number of cycles plot for pristine SU-8 and SU-8+PFPE composite obtained from the ball-on-disk sliding tests against 4 mm diameter Si₃N₄ ball at a normal load of 300g and a sliding velocity of 7 mm/s for different temperatures from room temperature (25°C) to 100°C. (a) Pristine SU-8; (b) SU-8+PFPE composite. The tests stopped after 0.2 million cycles without any failure for the SU-8+PFPE composite at all temperatures (50-100°C) 170
- Figure 8.4 Coefficient of friction versus number of cycles plot for pristine SU- 173

-
- 8 and SU-8+PFPE composite at various surface conditions, obtained from the ball-on-disk sliding tests against 2 mm diameter Si₃N₄ ball at a normal load of 20 mN and a sliding speed of 100 rpm. The inset at middle of the plot shows the initial co-efficient of friction (μ_i) of all series shown in the plot.
- Figure 8.5 Schematic explaining possible migration of PFPE from bulk to surface after heating at 100°C for 12 hrs 174
- Figure 8.6 Typical 2D TOF-SIMS elemental mapping for SU-8+PFPE composite. (a) Elemental mapping for SU-8+PFPE after washing. (b) Elemental mapping for the same washed SU-8+PFPE after heating at 100°C for 12 hrs. The samples were preserved in clean container before TOF-SIMS analysis to avoid any surface contamination. The total count number presented here are for one selected sample and the same trend was observed for other samples as well 175
- Figure 8.7 Graphical illustration of ratio between element counts for SU-8+PFPE composite. (a) Elemental count ratio for SU-8+PFPE after washing. (b) Elemental count ratio for the same washed SU-8+PFPE after heating at 100°C for 12 hrs 176
- Figure 8.8 Surface area coverage calculations for fresh surface of SU-8+PFPE composite at different temperatures 178
- Figure 8.9 Hardness (H) and elastic modulus (E) values of pristine SU-8 and SU-8+PFPE composite before and after heating at 100°C for about 12 hrs, measured using nano-indentation characterization 179
- Figure 8.10 Optical micrographs of worn surfaces: (a) Pristine SU-8(at 100,000 cycles). Images (b),(c),(d),(e) and (f): SU-8+PFPE composite at RT(25°C),60°C, 80°C, 90°C and 100°C, respectively (at 200,000 cycles). Images (g), (h), (i), (j), (k), (l) are optical micrographs of the counterface balls surface after sliding tests and (m), (n), (o), (p), (q), (r) are micrographs of the tested counterface balls after cleaning with solvents corresponding to the worn surfaces shown in (b),(c),(d),(e),(f),respectively. The length of the scale bar is 200 μ m in all images 180

List of Notations

5wt% SU-8+Z-03: SU-8 with 5wt% PFPE Z-03

5wt% SU-8+Z-dol: SU-8 with 5wt% PFPE Z-dol

AFM: Atomic force microscopy

CNT: Carbon nanotube

COF (μ): Coefficient of friction; μ_i and μ_s : Initial and steady-state coefficient of friction

CSM: Continuous Stiffness Measurement

E: Elastic Modulus (GPa)

FE-SEM: Field Emission- Scanning Electron Spectroscopy

GBL: gamma-butyrolactone

H: Hardness (GPa)

HDPE: High density polyethylene

L-B: Langmuir-Blodgett method

LFM: Lateral Force Microscopy

LIGA: A German acronym for lithography, electroplating and molding

MAC: multiply-alkylated cyclopentane

MEMS: Micro-electro-mechanical systems

MPa: Mega Pascal

MWCNT: Multi walled CNT

NEMS: Nano-electro-mechanical systems

NP: Nanoparticles such as SiO₂, CNTs and Graphite

PAA: Polyamic acid

PDMS: Polydimethylsiloxane

PE: Polyethylene

PEB: Post exposure bake

PEEK: Poly ether ether ketone

PFPE: Perfluoropolyether

PI: Polyimide

PMMA: Polymethylmethacrylate

PS: Polystyrene

PTFE: Polytetrafluoroethylene

RMS- Root mean square roughness

RT: Room Temperature

SAM: Self-assembled monolayer

EDS: Energy-dispersive X-ray spectroscopy

SFA: Scanning Force Apparatus

Si₃N₄: Silicon nitride

SiO₂: Silicon dioxide

SN 150: Alkane based base oil

SU-8+PFPE+NP: Hybrid composite of SU-8 with 5wt% PFPE and 5wt% NP

TGA: Thermogravimetric analysis

ToF-SIMS: Time of Flight-Secondary Ion Mass Spectroscopy

UHMWPE: Ultra-high-molecular-weight polyethylene

UV: Ultra Violet

WCA: Water Contact Angle

XPS: X-ray photoelectron spectroscopy

Chapter 1

INTRODUCTION

1.1 Background

Tribology is the study of the friction, wear and lubrication of contacting surfaces in relative motion. Friction is a work of Mother Nature that involves the phenomenon whereby two surfaces come into contact and the elastic energy of the material in contact is released through atomic lattice vibrations in the form of heat. Friction is also the energy dissipation at the interface due to the work done in deforming the surface asperities plastically and fracturing at the surface. The effect of friction is wear (debris generation), which is a gradual process of material removal from the surface, and lubrication is the counteracting process against friction and wear, to protect the surfaces. Hence, friction, wear and lubrication can be considered as cause, effect and counter measure, respectively.

The word “Tribology” was acquired from the Greek word “tribos”, which means rubbing. A famous quote from Nobel Prize physicist Wolfgang Pauli, “God made solids, but the surfaces were the work of the devil”, illustrates the significance and challenges of tribology in all scales from macro to nano scale. Friction and wear are not completely undesirable, as many of our everyday activities such as walking, holding, and braking are facilitated by friction. But in most engineering applications, friction and wear affect the lifespan of mechanical devices and hence it is necessary to minimize them to the lowest level possible.

Arguably, the history of tribology begins as early as 0.2 million years ago when fire was invented by rubbing stones against each other, followed by the invention of the

wheel at about 3500 BC. The Egyptians were the first recorded tribologists in history (2400 B.C.). They used water, sticky and greasy substances with a melting point of 49.5 °C as lubricants to transport giant structures, statues and tombs. The next known tribologist was the man of many talents: Leonardo da Vinci (1452-1519), who was the first person to approach tribology more scientifically by conducting friction experiments. He postulated that contact area has no effect on friction and it is only the normal load that controls the frictional force. This discovery of Da Vinci was followed by Amonton in 1699, who conceived the first and second laws of friction, which state that the coefficient of friction (μ) is the ratio of the frictional force (F) to the normal force (N) and the frictional force does not depend on the apparent contact area, respectively.

In 1778, Leonhard Euler proved that the static and kinetic friction coefficients are distinguishable and also proposed a theory that the tangent of interlocking angle of asperities is equal to the coefficient of friction ($\mu = \tan\theta$). Following this, Charles Augustine de Coulomb postulated in 1785 that the frictional force is independent of the relative velocity as he surmised that friction is the interlocking of surface asperities and has no effect on the rate of sliding. This is also called the third law of friction [Dowson 1998].

The contributions to tribological research from various researchers around the globe have increased substantially over the last century. Some notable contributions are from Hardy (1925), Prandtl (1928), Bradley (1932), Bowden and Tabor (1950), Courtney-Pratt (1955), Tabor and Winterton (1969), Johnson, Kendall and Roberts (1971) and Israelachvili and Tabor (1972). In the present day, utmost attention is given to tribology as the focus of research shifts from macro scale to micro or nano scale. Recent

developments in the computer industry, hard disk storage industry, nanotechnology, telecommunication, electronic industries, modern automobile and automation have opened up new areas of micromachinery such as micro and nano electro mechanical systems (MEMS and NEMS). As tribological issues are of key concern in MEMS industries, new coatings, lubricants, lubrication techniques and characterization techniques have been developed. The technique of using crossed atomically smooth mica cylinders to measure the real contact area and shear strength of monolayer lubricants between the mica surfaces was developed by Bailey and Courtney Pratt [1955], and was followed by the invention of the first actual Surface Force Apparatus (SFA) [Tabor and Winterton 1969 and Israelachvili and Tabor 1972].

The next milestone was the invention of AFM/FFM [Mate et al 1987] to record the near atomic friction between a tungsten tip and a graphite surface. The second and third laws of friction were found to be invalid at small scales and the frictional forces such as surface forces were proportional to the apparent contact area which was in agreement with the frictional behaviour of macro contacts studied by Bowden and Tabor [1950]. Frictional forces such as surface and interfacial forces become detrimental to the operation of micro and nano-scale devices when the surface area to volume ratio is high [Bhushan 2007, Mate 2007 and Kim 2007].

1.2 Introduction to MEMS and its Tribology

Microelectromechanical systems (MEMS) are small scale devices with dimensions in the range of a few to over a hundred micrometers, designed to perform certain operations by integrating mechanical and electronic systems through microfabrication technology.

Some examples for commonly used MEMS are pressure sensors, gyroscopes, optical MEMS, accelerometers, flow sensors, micrometers, microgears, comb-drive, Lab-on-a-chip systems and micro channels [Chau and Sulouff 1998, Yeow et al 2001 and Cao et al 2001]. Micro-fabrication allows us to fabricate the devices for various functions such as sensing and actuating [Muller et al 1990, Sze 1994, Beyzek 1994, Madou 2002].

In majority of the cases, the polycrystalline Silicon (Si) is used as a conventional structural material for MEMS fabrication because of process knowledge acquired from semi-conductor industries in which integrated chips have been fabricated from Si. The three main MEMS fabrication techniques are electroforming, surface-micromachining and Silicon-on-Insulator technology (SOI) [Madou 2002]. The life span of these devices may vary between a few hundred thousand to a few billion cycles, which increases the necessity for new materials and methodology [Bhushan 2007]. The scale-dependent mechanical properties of materials make tribology an important factor influencing the reliability and performance of these devices [Bhushan 2007, 1996].

When the size of the device scales down, the volume decreases by several folds more than the surface area. As a result, the surfaces forces such as van der Waals , capillary, chemical, and electrostatic attractions may become important factors as the surface area to volume ratio becomes extremely large [Kim 2007, Bhushan 1996 , Komvopoulos 1996, Tas 1996, Mastrangelo 1997, Maboudian and Howe 1997, Maboudian 1998, Bhushan 1998, De Boer 2001]. A large static friction between the two surfaces is normally referred as “Stiction”, which is when the magnitude of surface forces exceeds the magnitude of driving force. The above mentioned tribological challenges limit the commercial viability, reliability, life span and performance of MEMS devices.

Hence, new methodologies must be adapted to face the tribological challenges and to cope up with a shrinking scale for the prevention of friction and wear [Kim et al 2007]. Hence, there has been a great demand for the development of new materials, coatings and approaches for tribological solutions in MEMS devices.

1.3 Research Objectives and Scope

The overall objectives of this thesis are to improve the tribological properties of SU-8 photo-resist without compromising any of its inherent mechanical or physical properties using the approach of liquid-filled composite fabrication. SU-8 is an emerging negative UV photo-resist polymer, invented by IBM in 1989. SU-8 has three basic chemical elements: (a) an EPONTM SU-8 epoxy resin; (b) a solvent such as gamma-butyrolactone (GBL); and (c) a photoacid generator such as triaryl sulfonium salts. The name SU-8 is given due to the count of eight epoxy rings in each molecule of SU-8 [Gelrome et 1989]. Chapter 3: Materials and Experiments contains the elaborated description about SU-8 chemical structure, property and processing.

Scope of the thesis:

1. To characterize the liquid-filled SU-8 composites tribologically and mechanically.
2. To investigate the science, i.e. physics and chemistry, behind the workings of a newly developed lubrication approach.
3. To study the commercial viability of the developed approach.
4. To fabricate a small scale device to prove the viability of the newly developed approach in lubricating the MEMS devices.

The scope and the objectives of the research were carefully set after having carried out a literature survey on the current state-of-the-art technology in improving the tribology of SU-8 polymer.

1.4 Outline of the Thesis

The entire thesis consists of nine chapters. Chapter 2 and 3 are literature review and materials and experimental procedures, respectively. Chapter 4 elaborates on development and fabrication and testing of self-lubricating SU-8 composites, which are filled with perfluoropolyether (PFPE) droplets. A simple methodology has been used to fabricate SU-8 composites, which improved its tribological properties dramatically. Then, the chemical and physical mechanisms behind this dramatic improvement in tribological properties were analyzed thoroughly in chapters 5 and 6, and chapter 7, respectively. Chapter 8 discusses the effect of curing temperature and in-situ heating on the tribological performance of these composites. Chapter 9 provides overall conclusions for the entire thesis and also provides the directions for further work.

➤ Chapter 2 : Literature Survey

Chapter 2 covers the following:

- A review of tribological challenges, such as adhesion, friction and wear, to the effective operation of MEMS devices.
- The status of SU-8 as an MEMS structural material and the tribological challenges faced by the use of SU-8 as an MEMS material.

- The major works carried out so far to improve the tribological and mechanical properties of SU-8, the disadvantages of current techniques followed, and the need for a new approach.

➤ **Chapter 3: Materials and Experimental Procedure**

This chapter includes a detailed description of the materials and experimental procedures used in this research to fabricate the self-lubricating SU-8 composite. It also provides the explanations for the characterization methods used to estimate the physical, chemical, mechanical and tribological properties of the fabricated films.

➤ **Chapter 4: Development of Self-lubricating SU-8 Composites for MEMS Applications**

The motivation for this development of self-lubricating SU-8 composites comes from literature survey along with our expertise in this field. SU-8 composites were developed by adding the liquid lubricant i.e. perfluoropolyether (PFPE), which reduced the initial friction coefficient by ~9 times and increased the wear life by more than four orders of magnitude. In addition to that, a few nanoparticles such as SiO₂, CNTs, and graphite were also added to SU-8 and they have resulted in a marginal increment of mechanical properties (elastic modulus and hardness) by ~ 0.4 times. It was also observed that adding liquid PFPE (Perfluoropolyether; Z-dol 4000) lubricant to SU-8 promotes a chemical reaction between the molecules of SU-8 and PFPE, which helps in forming a more durable boundary lubrication layer.

➤ **Chapter 5: Chemical Bonding Study of SU-8 Composites**

The objective of this study was to investigate and confirm the possibility of chemical bonding observed between the SU-8 (epoxy ring) and PFPE (-OH groups) molecules upon UV exposure as demonstrated in the last chapter. Hence, another two different lubricants, a base oil and a multiply-alkylated cyclopentane (MAC) oil, were separately added to SU-8, in addition to PFPE. Both lubricants are alkanes, chemically inert and have no polar reactive terminal groups unlike PFPE which has -OH polar terminal groups. The SU-8+PFPE composite exhibited higher wear life than all SU-8 composites at all wt% of the lubricant content. The possible formation of ether bonds (C-O) between SU-8 and PFPE molecules was also postulated. From the XPS characterization, the SU-8+PFPE composite has shown more C-O group intensity than pure SU-8, but the chemical bonding cannot be verified for sure, because C-O might have come from PFPE as well. This ambiguity in chemical bonding has led to further study. Nevertheless, proper dispersion and possible chemical bonding of PFPE molecules with SU-8 were found to be responsible for the superior tribological properties of the SU-8+PFPE composite when compared with other SU-8 composites.

➤ **Chapter 6: Effects of End Groups of Perfluoropolyether Z-Dol and Z-03 in Tribology of SU-8 Composites**

The nature of chemical bonding was investigated using another fluorocarbon lubricant PFPE Fomblin[®] Z-03, which has very similar physical and chemical properties as Z-dol 4000 used in previous chapters. Both lubricants have the same chemical main chain but with different end groups. Z-dol has polar (-OH) end groups whereas Z-03 has

non-polar (CF₃) end groups. Tribological evaluation has shown that the SU-8+Z-dol offered ~8 times greater wear life than SU-8+Z-03. The various characterizations, i.e. XPS, TGA and WCA, have validated the role of the polar end functional group of Z-dol in covalent binding with SU-8 upon UV plasma treatment that resulted in the improved tribological properties.

➤ **Chapter 7: A Comprehensive Investigation on Physical Self-lubrication Mechanisms of SU-8 Composites**

It was also observed in prior chapters that physical self-lubrication helped to form a boundary film over the SU-8 surface using the lubricant droplets in the matrix. The chemical bonding helped the formed boundary film to stay undamaged for a longer time. However, the physical self-lubrication mechanism, along with chemical bonding, was found to be responsible for the dramatic rise in the wear durability of SU-8+ PFPE (Z-dol). Hence, the self-lubrication phenomenon was investigated further by plotting the coefficient of friction versus sliding velocity graph for the speed range of 0.0001 m/s to 0.73 m/s. Three different Zones were indentified based on their exhibited friction behavior with speed. Zone 1, Zone 2 and Zone 3 exhibit the steep increase, marginal increase and linear increase in COF with increase in speed, respectively. The lubrication mechanism responsible for frictional behavior observed Zone 1, 2, 3 and after Zone 3 is elaborated with ample evidences.

➤ **Chapter 8: Effects of Curing Temperature and In-situ heating on Thermal Stability of SU-8 Composites**

The motivation for this work arose from two key questions: “Can this SU-8 composite work at temperatures higher than room temperature (RT)?” and “Will the curing temperature affect the performance of the SU-8 composite?” The tribological evaluation of pristine SU-8 and SU-8+PFPE composite was performed under the condition of *in-situ* heating from room temperature (25°C) to 100°C. The heating did not cause any change in the tribological behaviour of pristine SU-8, whereas the heating of SU-8+PFPE has reduced the initial and steady-state coefficients by ~2 and ~7 times respectively, and increased the wear life (n) by more than three times than that of SU-8+PFPE at room temperature. The *in-situ* heating has provided greater surface area coverage by the PFPE lubricant and the migration of additional PFPE from the bulk to the surface. Overall, these two aspects enriched the surface with PFPE, which reduces friction and wear. Various characterization results have also ascertained the mentioned phenomenon. This study shows that besides in MEMS fabrication, the SU-8+PFPE composite can also be used in moderately high temperature applications where tribology is a major concern.

Chapter 2

Literature Review

2.1 Tribological Challenges of MEMS

MEMS is an emerging industry with much scope and growth to be realized. The research and development potential of the industry is also growing at a fast pace. However, the commercialization of MEMS devices is far more lacking than would be expected. The commercial viability of these devices is very much limited by the reliability issues associated with them such as friction, wear and failure. The remarkable feat by Texas instruments of bringing the digital micromirror device (DMD) chip to market nearly took more than 10 years after its demonstration [Douglass 2003]. Most of the issues encountered by the design engineers are with respect to the reliability of the device. The last 10 years of research were mainly invested in investigating the failure mechanisms and modes of the devices. Solving the reliability issues, which are related to the tribological challenges, would be key to bringing MEMS devices to common usage level. Hence, intense research in this direction is expected to continue [Van Spengen 2003].

Failure modes and failure mechanisms are different concepts. A failure mode is an apparent failure pattern, whereas a failure mechanism provides the reason behind the failure. See the example below in Figure 2.1, whereby the brittle fracture of the resonator beams represents a failure mode, whereas the cause of the failure such as overload due to stiction or physical over load represents the failure mechanism [Miller et al. 1998]. Some common MEMS failure mechanisms are listed in the chart below in Figure 2.2.

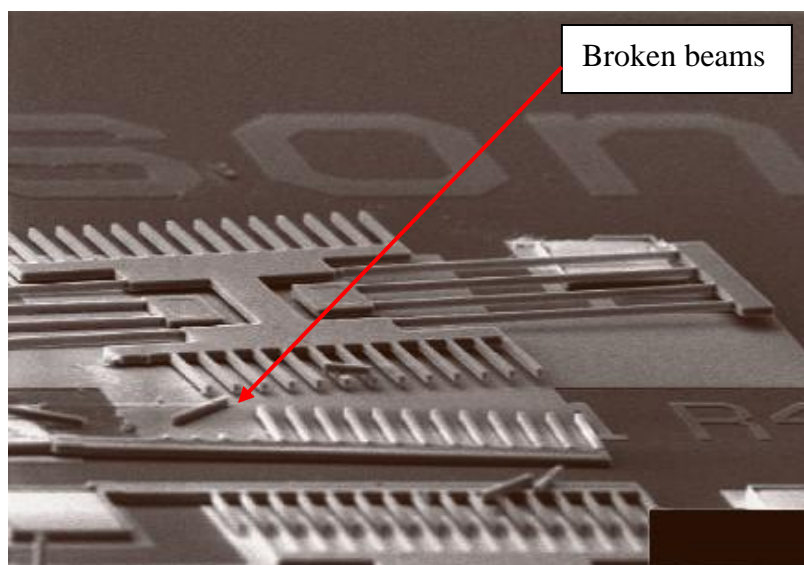


Figure 2.1: The failure mode and mechanism of this resonator are broken beams and overload stress induced by rough handling, respectively. [Reproduced from Miller et al. 1998]

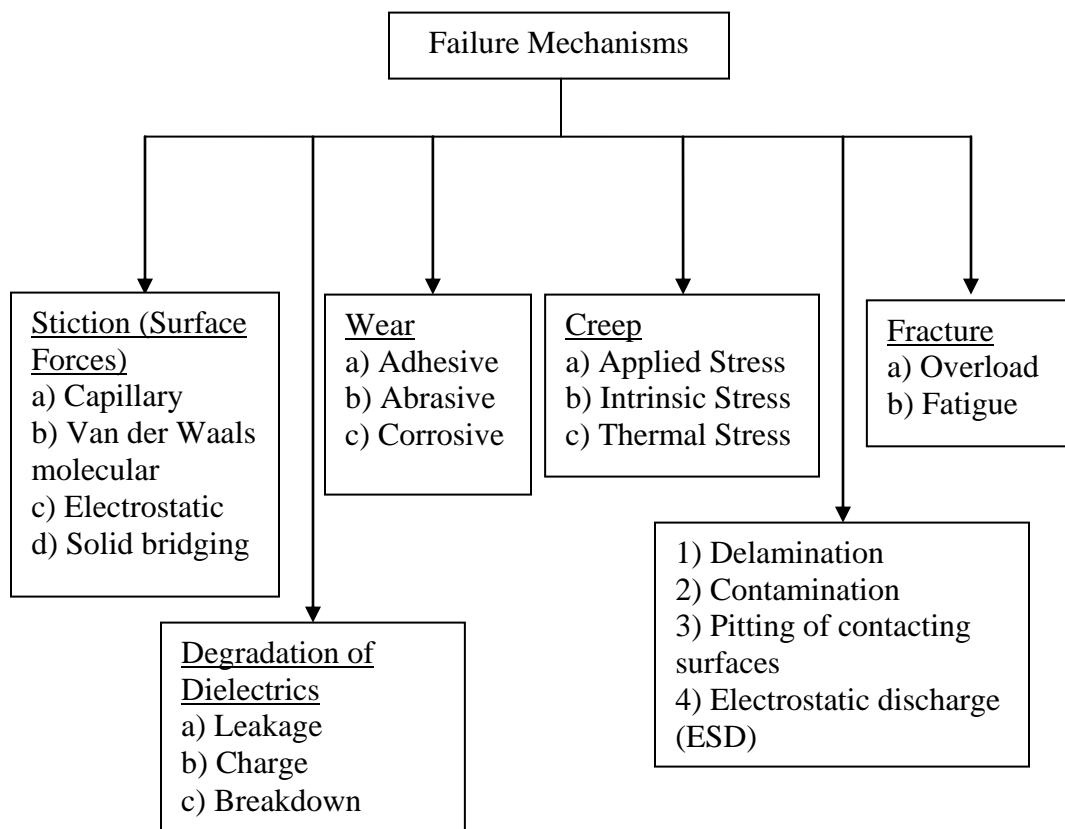


Figure 2.2: Typical failure mechanisms identified in MEMS devices [Stark 1999].

Figure 2.2 shows common failure mechanisms found in MEMS devices such as stiction, creep, fracture, wear, delamination and contamination. The tribology at micro scale, as encountered in MEMS, differs from that at macro scale. Amonton's law, which states that friction is independent of the apparent contact area, remains valid at the macro scale whereas at micro-scale, asperity level contact with nano-meter size contact area causes friction to be highly dependent on area of contact [Kim 2007]. Surface forces have a more dominant and significant effects on friction, as the inertial forces of a small component are much smaller in comparison.

When the size of the machine decreases by a scale of three orders of magnitude, the surface area to volume ratio increases by a factor of thousand [Bhushan 1996]. As a result, the surface forces i.e. capillary, van der Waals, adhesion, drag forces, increase four orders of magnitude more than the actual area-volume ratio. Stiction is the largest static frictional force experienced by two surfaces to initiate a relative motion between them [Bhushan 1996, 1998, 2007, Timbe 2005]. There are two types of stiction named as "release stiction" and "in-use stiction" and in-use stiction is considered to be more important for better reliability. Stiction occurs primarily because of the etching process, where the solvents and liquids used for etching form capillary condensation between the surfaces. Even after it gets evaporated, the surfaces come together and show strong adhesion. Hence, many methods have been proposed to dry them to avoid capillary bridge formation [de Boer et al.1999, Mastrangelo et al 1993 (a) & (b)]. The effect of humidity on surface interaction energy was demonstrated by de Boer [de Boer et al.1999], as shown in Figure 2.3. He recorded the adhesion between the array of free-standing cantilever beams using the interference. The bending of cantilever beams is

more pronounced in high humidity cases than low humidity cases (Figure 2.3). He concluded that the capillary condensation induced surface interaction energy changes notably with the relative humidity. The capillary liquid bridges will form while the hydrophilic surfaces are in contact.

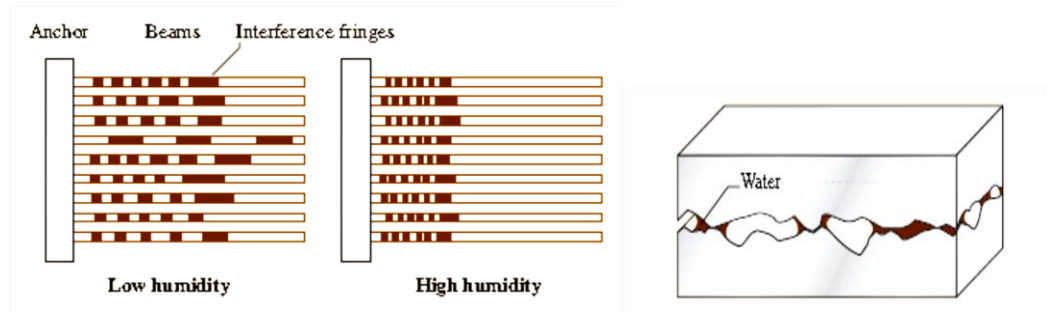


Figure 2.3: (a) Schematic top view of the measurement of adhesion as a function of relative humidity using interferometry. The dark spots correspond to the bending of the beam by adhesive forces. (b) Capillary condensation between two contacting surfaces. [Reproduced from de Boer et al.1999]

2.2 Case Studies of MEMS Failure

Some examples of well-known microsystems and the description of the systems, their tribological issues and the solutions proposed to those issues are presented below.

2.2.1 Polysilicon Electrostatic Micromotor

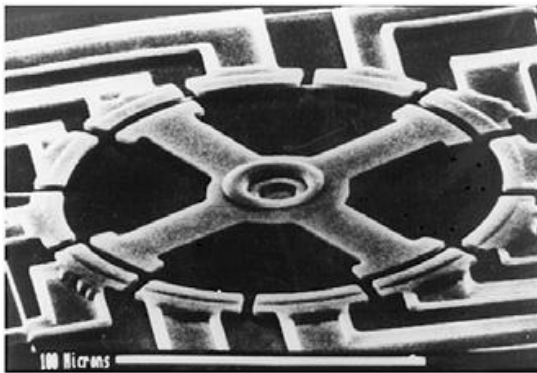
(a) Description: The surface micro-machined polysilicon electrostatic micromotor (Figure 2.4(a)) has a rotor with a diameter of 120 μm and the gap between the rotor and stator is just 2 μm . The motor can run up to a speed of 100,000 rpm [Tai et al 1989].

(b) Tribological Issue: The wear and high stiction issues arise from the interfacial physical contact between the rotor-hub flange pair. Also, the interfacial intermittent contact between rotor-stator pair affects the operation of the device considerably.

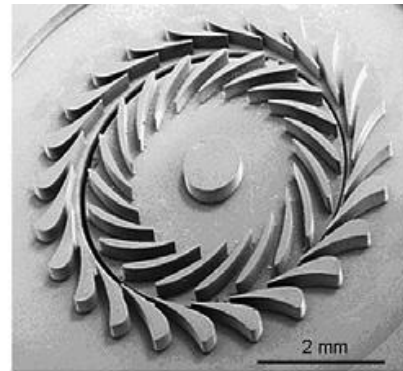
2.2.2 Microturbine

(a) Description: Figure 2.4 (b) shows the SEM image of a silicon based microturbine rotor produced by the micromachining process. The complete assembly of bladed rotor and nozzle guide vanes located on the stator is together less than 1 mm. The maximum attainable speed, rotor diameter and specific power of this high temperature turbine are 1 million RPM, 4-6mm and 10 W, respectively [Spearing et al 2001, Frechette et al 2005].

(b) Tribological Issue: Wear durability of the blades, vanes, nozzles and microbearings to withstand such a severe operating speed are the main concerns.



Electrostatic micromotor
(Tai et al., 1989)



Microturbine bladed rotor and
nozzle guide vanes on the stator
(Spearing and Chen, 2001)

Figure 2.4: SEM images of MEMS devices (a) Electrostatic micromotor. (b) Microturbine rotor and nozzle guided vanes on the stator.

2.2.3 Micro Gearbox

(a) Description: The micromachined polysilicon multiple microgear speed reduction unit shown in Figure 2.5 is a kHz frequency range operating device, developed by Sandia National Laboratories, USA for electrostatically driven microengines. The fabricated unit

was subjected to a wear test in air and worn surfaces were investigated. [Tanner et al 2000, Garcia et al 1995].

(b) Tribological Issue: Figure 2.5 clearly shows the wear in various parts such as the hub, clip and pin hole. It is found that humidity played a vital role in initiating the wear process.

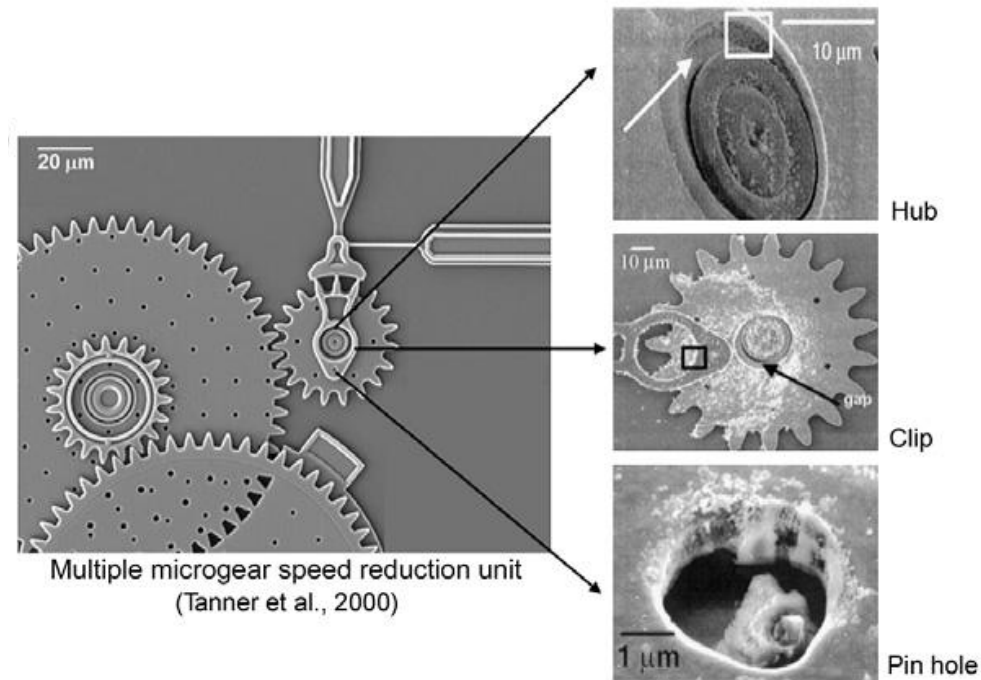


Figure 2.5: SEM images of microgear speed reduction unit after wear test. [Reproduced from Tanner et al 2000]

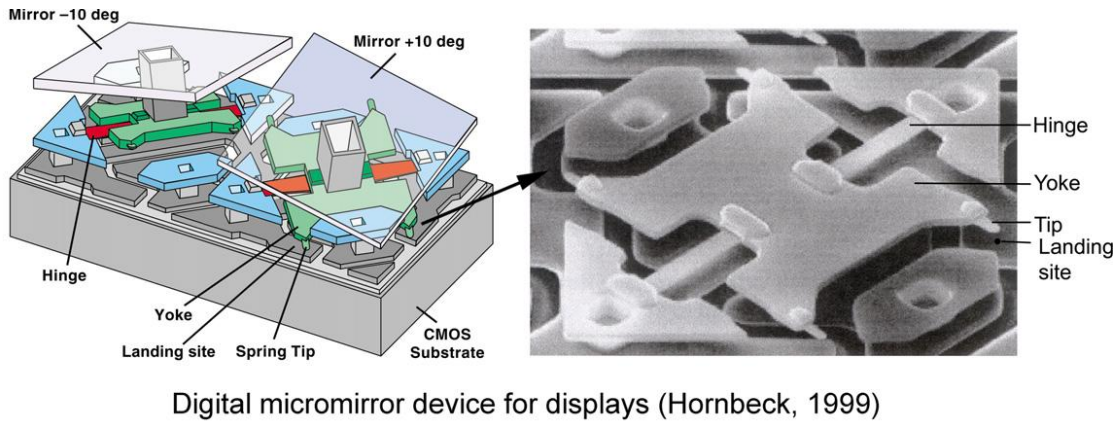
(c) Tribological Solutions: (a) 20 nm CVD (chemical vapor tungsten) based tungsten coating was coated on the rubbing surfaces at 450°C to improve wear resistance [Mani et al 2000]. Though there was an improvement in the wear behaviour, tungsten-coated microengines have never matched expectations. Alternatively, self-assembled monolayers (SAMs) were tried, which increased the yield, but durability was marginal [Hankins et al 2003].

2.2.4 Digital Micromirror Device (DMD)

(a) Description: The first digital micromirror device was developed by Texas Instruments in 1987 and it took more than 10 years for the product to hit the market due to reliability issues. The DMD chip set has several hundred thousand rotatable aluminium alloy coated micromirrors, fabricated over a CMOS static integrated RAM (Random Access Memory) unit. More than two million independently maneuvered reflective micromirrors work at a frequency range of 5000-7000 times a second due to the electrostatic charge between structure and electrode. The common applications of DMD are digital light processing (DLP) technology for digital projection displays in computer projectors, high definition television (HDTV) sets, and movie projectors [Hornbeck 1999, 2001, Hornbeck et al 1988].

(b) Tribological Issue: The major threats affecting the reliability of the device are stiction and wear between the contacts of the Al alloy spring-landing site pair, slide mirror pair and also ambient conditions such as humidity, dirt, shock and vibration failure [Douglass 2003, Henck 1997].

(c) Tribological Solutions: Self-assembled monolayers consisting of a fatty acid – perfluorodecanoic acid (PFDA) were deposited on surfaces of the tip and landing sites to reduce stiction and wear using vapor deposition process.



Digital micromirror device for displays (Hornbeck, 1999)

Figure 2.6: Images of digital micromirror device for digital projection displays.

The SAMs coating on the DMD devices still failed to stop the wear of the landing sites. The failure mechanism for SAMs on DMD was proposed by Liu and Bhushan, shown in Figure 2.7 [Liu et al 2004]. It was reported in the literature that the vapor deposited SAMs were expected to cover about 97% of a lubricated surface.

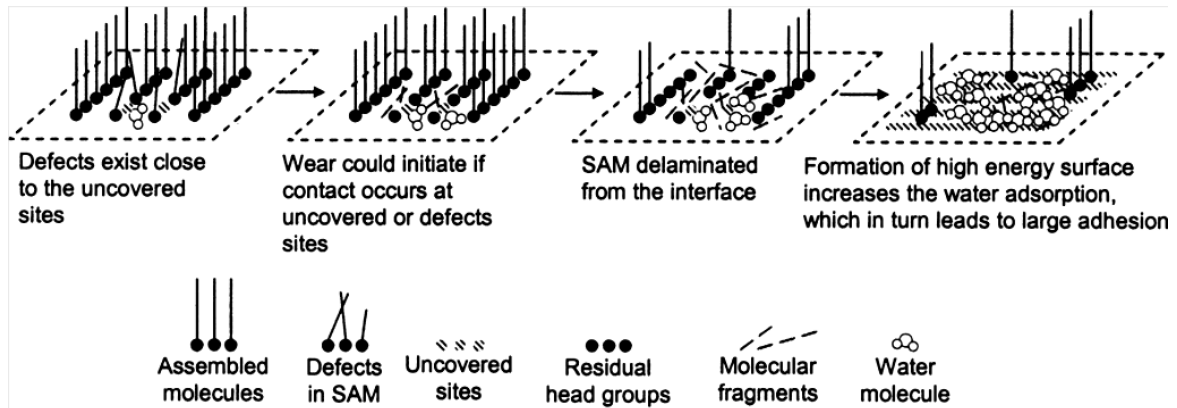


Figure 2.7: Schematic illustrating the possible mechanism for wear and stiction in SAM coatings on DMD [Reproduced from Liu et al. 2004].

The SAM molecules very near to the uncovered sites were expected to be vulnerable to de-bonding from the surface because of low interfacial bonding. Hence, the neighboring

molecules next to the uncovered site and the uncovered site in the SAM coating were referred to as “defects”. Possible contact at the defective sites could initiate the delamination of SAM coating. The delamination propagated further due to the newly exposed high energy surface and increased solid-solid contact area as the density of the SAM molecules collapsed. The fresh surface also attracted moisture and other contaminants which accelerated the stiction, delamination and wear. The durability of SAMs on DMD can be improved by enhancing the surface coverage and wear resistance of the coatings.

2.3 Solutions to MEMS Tribological Challenges

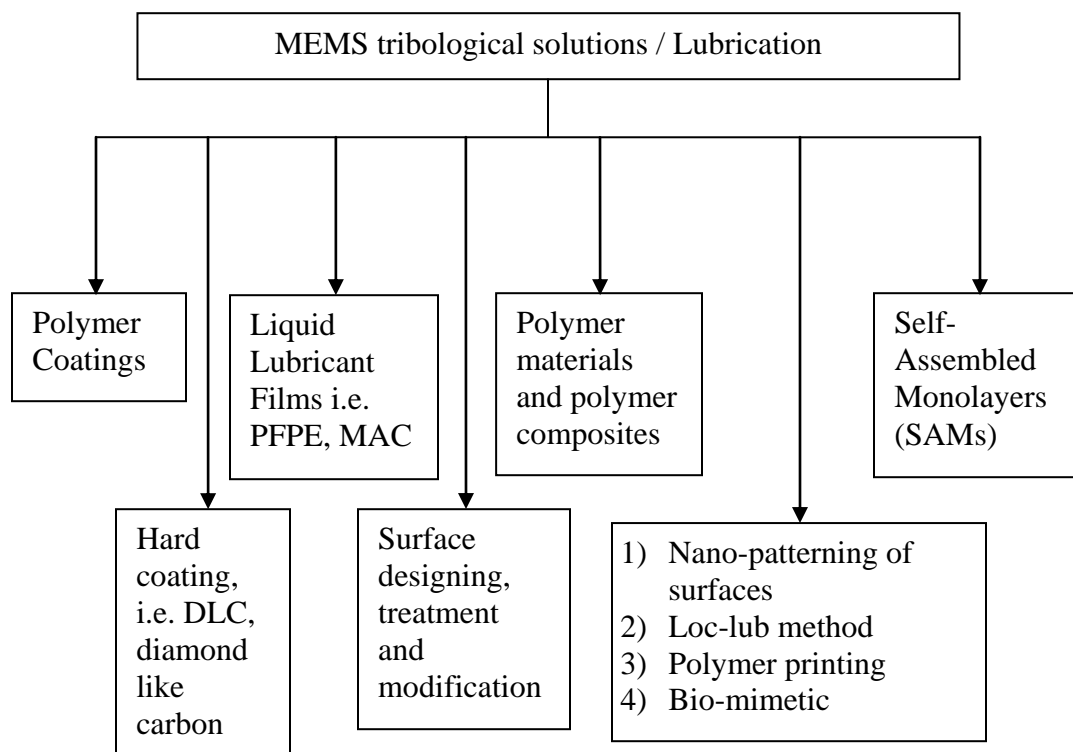


Figure 2.8: Tribological solutions developed to address the wear and stiction issues in MEMS devices.

The case studies and examples mentioned earlier also suggested that the adhesion, friction, and wear are the key issues which limit the commercialization of MEMS devices with moving components where dynamic contact occurs. Conventional lubrication methods such as the use of a pool of lubricants and grease in macro machines cannot be adopted for micro scale devices. The drag forces from viscous lubricants would eventually affect the rotation of micro devices, through power dissipation, more resistance to inertia and increased stiction, which affects the rapid mechanical response against inertia. It is essential to develop new techniques to lubricate the micromachines. Figure 2.8 shows the tribological solutions developed so far to alleviate the friction and wear issues in MEMS. Every single technique listed above has its own merits and demerits. Among them, liquid lubricants are widely used for lubrication because of the relatively very simple coating process [Eapen et al 2002].

2.3.1 Liquid Lubricant Films

The lubrication of MEMS devices using multi-molecular layers of liquid lubricants is an effective approach [Eapen et al 2002, Liu et al 2003, Singh et al 2011]. There could be either a chemical absorption or physical absorption of lubricant molecules to the substrate or a combination of both. One such popular lubricant used in the hard-disk industry is perfluoropolyether (PFPE), which is a molecularly thin lubricant with extremely low vapor pressure and high thermal stability [Bhushan 1996].

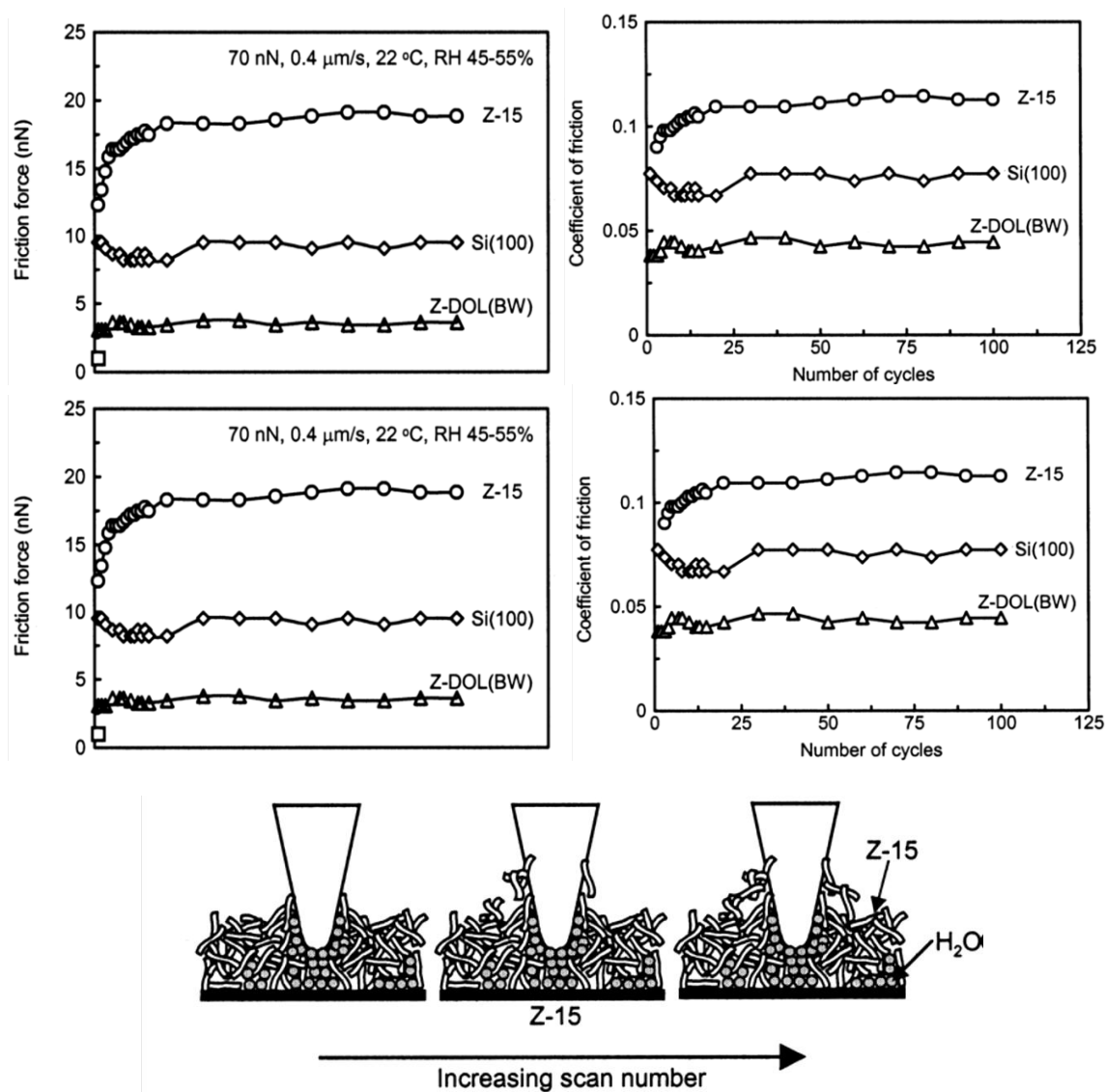


Figure 2.9: Wear test results i.e. Number of cycles Vs frictional force and COF, for PFPE Z-dol , Z-15 and Si(100). Schematic diagram demonstrates molecular interaction between Z-15 molecules and AFM tip over a number of passes (bottom). [Bhushan 2007]

Figure 2.9 shows the wear test results performed by AFM (Atomic Force Microscopy) on pure Silicon (Si 100), functionalized PFPE Z-dol dip-coated on Si and non-functionalized PFPE Z-15 dip-coated on Si. The results show that the Z-15 exhibited more friction than for an unlubricated Si surface, whereas Z-dol exhibited the least friction. The non-functionalized Z-15 molecules were not able to bond with Si properly,

which led to the molecules getting absorbed to the tip of the AFM. The cohesive force between the Z-15 molecules on the surface and the molecules on the AFM tip increased the adhesion and friction. After the removal of the adsorbed layer from the AFM tip by scanning it several times, the COF remained constant and high at certain values. The low COF for Z-dol films shows that the Z-dol molecules remained attached to the surface properly after 100 cycles of scanning, whereas the Z-15 molecules get displaced easily because of their end groups [Bhushan 2007].

Nowadays, many other liquid lubricants are also used for the lubrication of MEMS devices. Some of them are: multiply-alkylated cyclopentanes (MAC), hexadecane, octadecylamine, baseoils, ionic liquids, fatty acids and other bio-lubricants [Venier et al 1991, Leong et al 2013, and Satyanarayana et al 2005].

2.3.2 Self-Assembled Monolayers (SAMs)

SAMs are ordered two-dimensional molecular assemblies formed at the interface by the spontaneous attachment of an active surfactant over a solid surface as the system attains equilibrium state [Ulman 1991, Liu et al 2001, Bhushan et al 1995, Satyanarayana et al 2005]. Most of the lubricant molecules have two groups, starting with a head group and ending with a functional or tail group. The head groups are attached to the surface, the terminal groups keeps the outer surface of the film exposed to all interactions and the main chain (back bone) determines the film thickness. SAMs of functionalized long-chain alkanes are most frequently used as building blocks of supermolecular structures. Figure 2.10 shows the SAMs formation process over a substrate, which uses the Langmuir-Blodgett (LB) deposition technique.

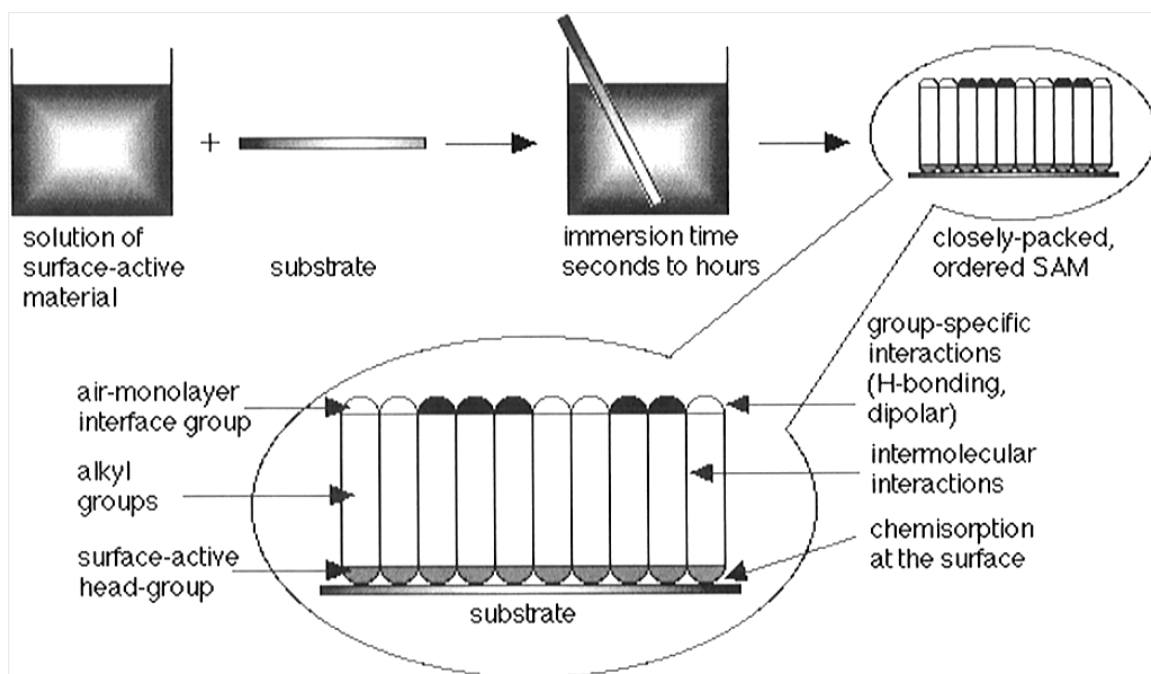


Figure 2.10: Formation of SAM coating on a substrate using a simple immersion technique. [Reproduced from Ulman 1991]

Langmuir-Blodgett films are formed by attaching the array of closed packed molecules using weaker surface forces like electrostatic and van der Waals forces. The weak physical bonding between the LB films and substrate makes these films less wear resistant. Another approach to deposit the SAMs is by grafting the molecules using strong chemical interactive bonds such as covalent, ether and amine bonds [Ulman 1991]. SAMs represent one of the best approaches for the boundary lubrication of MEMS devices because of the customization in chain length and terminal group offered by SAMs.

Many SAM coatings have been tested for improving the tribology of Si. For example, perfluorodecyltrichlorosilane (PFTS), n-octyldimethyl (dimethylamino) silane (ODMS) ($n = 7$), and n-octadecylmethyl (dimethylamino) silane (ODDMS) ($n = 17$) vapor phase SAMs have been coated onto Si and tribologically evaluated. The results of wear tests performed by AFM have shown that the PFTS/Si pairing with higher contact

angles offered lower adhesive forces in comparison to that of ODMS/Si and ODDMS/Si pairings [Bhushan et al 2005, Kasai et al 2005, Tambe et al 2005]. Other SAMs such as octylphosphonate (OP) and octadecylphosphonate (ODP) coated on Al substrate exhibited frictional behaviour similar to the ODMS/Si and ODDMS/Si pairings and indeed, showing that the substrate has almost no effect on frictional behaviour. The effects of a decrease in film thickness and normal load on the wear of SAMs with respect to various substrates such as Si, Al have been studied [Kasai et al 2005, Tambe et al 2005]. The studies revealed a critical normal load beyond which the height of the film decreases as it gets conformed. The decrease in height initiated wear and this effect of chain length on the tribological performances has been observed in ODDMS/Si and ODP/Al SAMs.

The role of interfacial bonding strength between molecules and substrate in the wear behaviour of fluoropolymer multilayers and fluorosilane monolayers on Si and a selected fluorosilane on PDMS as substrate were investigated [Bhushan et al 2006, Lee et al 2005]. All fluorosilane SAMs were found to be more durable and hydrophobic. Fluorosilane monolayers increased the contact angle up to 100° with water and showed less adhesive forces [Bhushan et al 2006].

2.3.3 Nano Patterning/Texturing of Surfaces

Surface morphology can be designed or modified to exhibit the hydrophobicity or non-wetting behaviour, which helps in reducing meniscus formation, and thus, stiction and wear. It is also useful in fluid flow applications and microfluidics [Jung et al 2007]. Surface modification (hydrophobic or hydrophilic) can be done either by the earlier

mentioned way of coating with low surface energy materials such as PFPE or wax, or by creating the surface roughness. The air trapped between the ridges of roughness helps in reducing the contact between the surfaces and reduces the apparent surface energy by supporting the water droplets when they fall on the surface. This famous phenomenon has been reported in literature as the creation of a solid-air-liquid interface (Wenzel 1936, Cassie and Baxter 1944, Nosonovsky and Bhushan 2005, Jung et al 2006, Bhushan et al 2007, Bhushan 2007). This effect is also known as the “lotus effect”, as the lotus leaf does self-cleaning to prevent the contamination on its leaf from micro-organisms by making the leaf rough and hydrophobic (Barthlott and Neinhuis 1997). The lotus also exhibits super hydrophobic behaviour towards water because it has a layer of wax in addition to the surface texture. Thus, water droplets on a lotus leaf collect impurities, while they roll over the leaf.

The lotus leaf has controlled surface patterns such as micro or nano bumps (pillars) and a wax compound on its surface. The wax is an aliphatic compound. The inspirations from the lotus leaf have led to the introduction of surface roughness on various surfaces to enhance tribological performances (Burton et al 2006, Jung et al 2007). This lotus effect is also considered as “biomimetics”, which means mimicking and implementing ideas from nature for real engineering applications. The idea of creating roughness induced hydrophobic surfaces has been investigated and implemented in numerous applications (Shibuichi *et al* 1996, Hozumi et al 1998, Coulson *et al* 2000, Miwa *et al* 2000, Oner and McCarthy 2000).

2.3.3.1 Analysis of Contact Interface

Figure 2.11(a) shows a droplet on an ideal smooth and rough surface with contact angles of θ_0 and θ , respectively. The droplet on the ideal smooth surface without air pockets or the solid-liquid interface is referred to as a homogenous interface (Wenzel 1936).

$$\cos \theta = R_f \cos \theta_0 \quad (\text{Eq 2.1})$$

where θ is the contact angle for a rough surface, θ_0 is the contact angle for a smooth surface, and R_f is the roughness factor defined as the ratio of the solid-liquid area, A_{SL} , to its projection on a flat plane, A_F .

$$R_f = \frac{A_{SL}}{A_F} \quad (\text{Eq 2.2})$$

Figure 2.11(b) shows the effect of roughness factor (R_f) on the contact angle with respect to the value of θ_0 , according to equation 2.1. The wetting of a liquid on a surface is characterized by the contact angle values between the solid and liquid surfaces. If the contact angle value is between 0° and 90° , the surface is referred to as a hydrophilic surface, while if the contact angle value is between 90° and 150° , the surface is considered as a hydrophobic surface [Bhushan 2006]. When the contact angle is more than 150° , the surface is called a super-hydrophobic surface. According to the model, the hydrophobic and hydrophilic surfaces become more hydrophobic and hydrophilic, respectively, with an increase in roughness factor (R_f) (Nosonovsky and Bhushan 2005, Jung and Bhushan 2006). This shows that roughness can modify surface properties such as hydrophobicity and hydrophilicity independently.

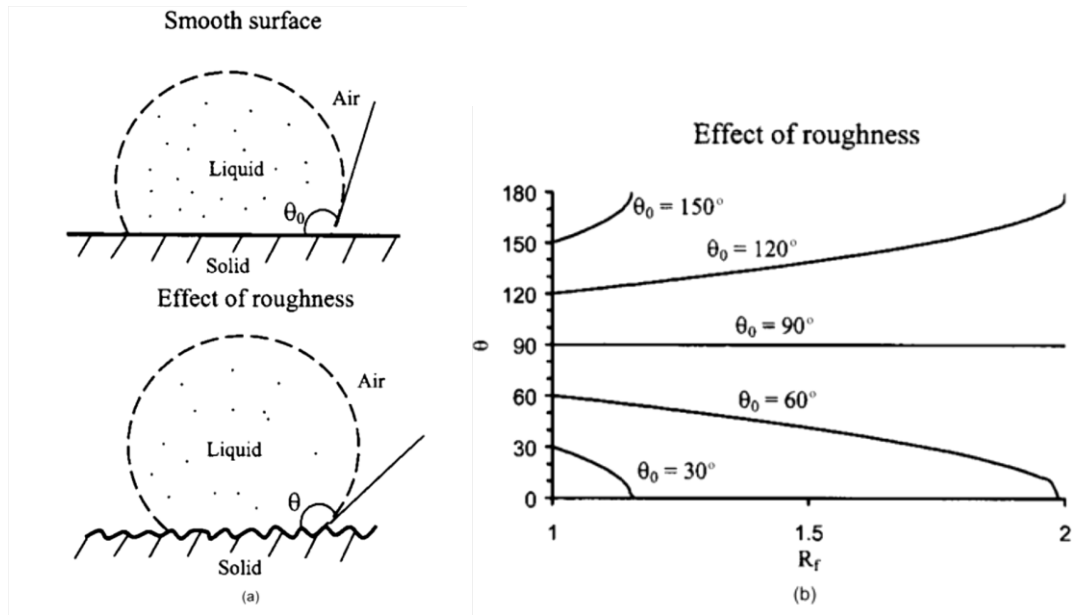


Figure 2.11: (a) Droplet on a smooth and rough surface with the contact angle of θ_0 and θ , respectively. (b) Contact angle for a rough surface (θ) as a function of the roughness factor (R_f) for various contact angles of the smooth surface (θ_0), [Reproduced from Nosonovsky and Bhushan 2005].

2.3.3.2 Composite Interface

Figure 2.12 shows that the composite interface consists of solid, liquid and air rather than the typical homogenous solid-liquid interface [Cassie and Baxter (1944)]. The air pockets might be formed because of the inability of the liquid to wet the cavity or just the entrapment of air at the cavity. Thus, the composite interface is generated. The common Wenzel equation involves a solid-liquid interface with area wetted by liquid. Here, an additional fractional area with air pockets is to be considered. Thus, the Wenzel equation was modified for a composite surface.

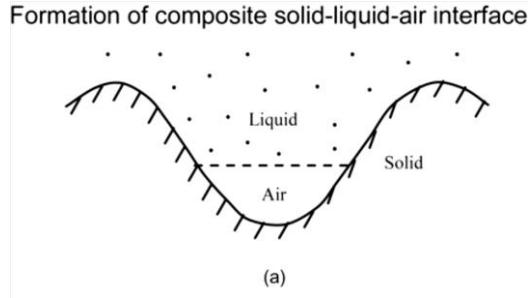


Figure 2.12: (a) Formation of solid-liquid-air composite interface by a liquid droplet on a rough surface [Reproduced from Jung and Bhushan 2006].

Hence, the modified Wenzel equation is given below:

$$\cos \theta = R_f \cos \theta_0 - f_{LA}(R_f \cos \theta_0 + 1) \quad (\text{Eq 2.3})$$

where f_{LA} is the fractional flat geometrical area of the liquid–air pockets interface below the droplet. This equation suggests that the contact angle (θ) of a smooth surface increases with an increase in f_{LA} . The hydrophobic surfaces show greater water contact angle (hence lower apparent surface free energy) with an increase in roughness factor.

2.4 Polymers and Composites for MEMS Applications

Polymer materials are emerging materials and have been used in several MEMS applications as structural materials, substrates, coatings and thin films [Kim et al 2001, Srinivasan et al 1998, Frechette et al 2006]. The commonly used polymers are Parylene, polyimide, acrylics (PMMA), photopatternable epoxy, and polydimethylsiloxane (PDMS) elastomer, etc. Polymers are classified into three major categories: fibers, plastics and elastomers.

The following are the main advantages of introducing polymer materials into MEMS applications:

- a) Though Si has excellent mechanical properties such as a Young's modulus (E) of 130 GPa and hardness (H) of 12 GPa, its brittle nature with high surface free energy makes it vulnerable to various failure modes [Sharpe et al 2001& 2004]. Polymers are relatively tougher than Si and yield more during failure. Direct contact MEMS applications such as tactile and flow sensors desperately require polymers for their success [Engel et al 2005 & 2006].
- b) Processing of polymers such as photoresists are far easier than those of Si. Thus, it lowers the cost of the devices significantly.
- c) The size of the polymer substrate can be customized with respect to specific applications, unlike Si wafers which are obtained in standard sizes.
- d) The flexibility available in polymer processing is abundant and new processing methods can be developed, whereas processing techniques in the semi-conductor industry are very much limited and fixed. Vapor depositions, lithography, thin film processing and printing are the some innovative polymer processing techniques developed recently [Shen et al 2002, Cui et al 2005, Yoon et al 2006, Fang et al 2004, Lau et al 2013].
- e) Polymers can be easily customized to render any desired physical, chemical, mechanical and biological properties not found in any materials. For example, poly carbonate films can have holes with controlled nanoscopic dimensions, which are produced by energetic ion track etching [Kuo et al 2003].

2.4.1 Polydimethylsiloxane (PDMS) Elastomer

PDMS is a promising elastomeric material for micro fabrication because of its benefits such as biocompatibility, elastomeric properties, gas permeability, optical properties, ease of microfabrication, easy bonding to wide variety of substrates, low processing and manufacturing cost, and high chemical resistivity [Belanger et al 2001, Duffy et al 1998, Jo et al 2000, Yang et al 1998]. The easy and simple processing of PDMS makes it popular among biologists and chemists especially in microfluidic applications. PDMS is widely used in contact printing, which is a technique for direct attachment or deposition of functionalized molecules on surfaces for microfluidic applications [Xia et al 1998, Menard et al 2005].

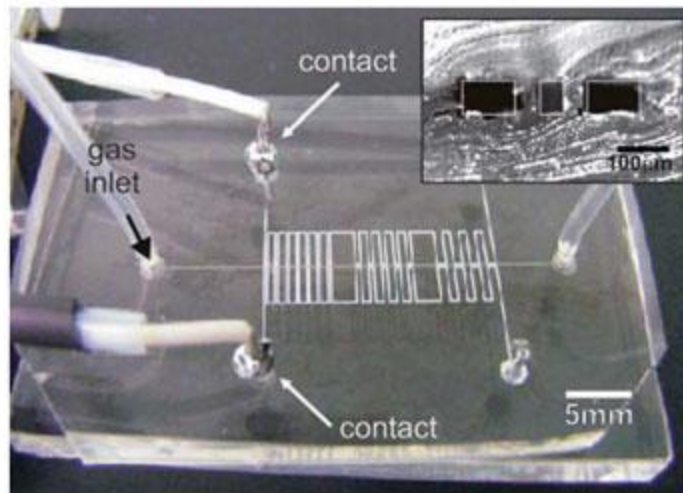


Figure 2.13: *PDMS microchip for generating localized plasma [Priest et al 2011].*

PDMS can be molded at temperatures slightly above room temperature ($\sim 60^{\circ}\text{C}$) to replicate any structures to be molded. The formed mold pieces are then attached together to fabricate the microfluidic channels. Figure 2.13 shows a PDMS chip designed to produce localized plasma. A few other components such as valves [Thorsen et al

2002], pumps [Khoo et al 2001] and mixers [Thorsen et al 2002, Unger et al 2000] have been successfully fabricated and integrated using PDMS.

2.4.2 Polymer Nanocomposites

Nanocomposites are new materials formed by integrating two or more materials to combine their properties. Various nanoparticles such as carbon nanotubes (CNTs), graphene, silica particles and other nanoparticles, have been added into various polymers such as PMMA, SU-8, PDMS, PEEK, PTFE and UHMWPE [David et al. 2007].

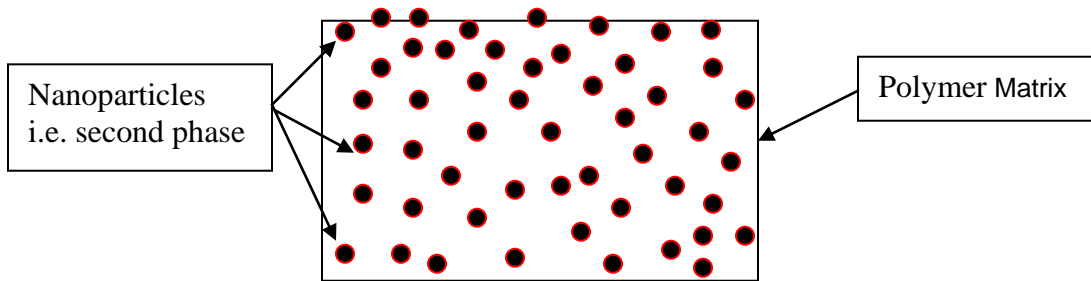


Figure 2.14: Schematic illustration shows the anatomy of nanocomposite, where two phases co-exist — polymer matrix and nanoparticles.

Doping with nanoparticles changes the electrical properties of many polymers for energy and display applications. The percolation limit regulates the concentration of nanoparticles beyond which the material properties changes drastically. The resistivities of four types of nanocomposite materials — multi-wall carbon nanotubes (MWNT) in PDMS matrix, MWNT in polyurethane (PU) matrix, carbon black (CB) particles in PDMS, and CB in PU matrix — have been studied and it was found that these nanocomposites act as a strain gauge [Samel et al 2007]. Nanocomposite elastomers have

been used for precision screen printing technology and MEMS devices are made by integrating them with other non-conductive elastomers [Ryu et al 2004].

Table 2.1 provides a detailed list of polymer composites and nanocomposites, their matrix, filler materials, dispersion technique and concentration at lowest wear rate observed. These are some of the commonly used polymers and their corresponding nano fillers for various applications such as aerospace, automobile, data recording and MEMS.

Table 2.1: List of polymer composites (1-6) and nanocomposites (6-14), their matrix, filler, dispersion technique and lowest wear rate concentration (vol%). (Reproduced from David et al 2007)

| S. No | Matrix | Filler | Dispersion techniques | Concentration of fillers (Vol%) at lowest wear rate observed |
|-------|--------|--------------------------------|----------------------------|--|
| 1 | PTFE | FEP | Mechanical | >50 |
| 2 | PEEK | PTFE | Ultrasonication | 20 |
| 3 | PEEK | PTFE | N/A | 5 |
| 4 | PA | PE | Twin screw extrusion | >40 |
| 5 | PA | GF | Melt mixed | >20 |
| 6 | PMIA | PTFE | Mechanical | 20 |
| 7 | PTFE | Al ₂ O ₃ | Jet mill | 0.5 |
| 8 | PTFE | Al ₂ O ₃ | Jet mill | >10 |
| 9 | PTFE | Al ₂ O ₃ | Jet mill | >5 |
| 10 | PTFE | CNT | Ultrasonication/Mechanical | 20 |
| 11 | PTFE | ZnO | Ultrasonication/Mechanical | 15 |
| 12 | PEEK | Si ₃ N ₄ | Ultrasonication | 4 |

| | | | | |
|----|------|--------------------------------|-----------------|-----|
| 13 | PEEK | SiC | Ultrasonication | 1 |
| 14 | PEEK | SiO ₂ | Ultrasonication | 4 |
| 15 | PEEK | ZrO ₂ | Ultrasonication | 3 |
| 16 | PET | Al ₂ O ₃ | Melt mixing | 0.7 |
| 17 | PPS | Al ₂ O ₃ | Mechanical | 2 |

[Note: PEEK - Poly ether ether ketone, PTFE - Polytetrafluoroethylene, PE- Polyethylene, PA - Polyamide, PE - Polyethylene, PPS - Poly(p-phenylene sulfide), ZnO - Zinc Oxide, SiC - Silicon Carbide, ZrO₂ - Zirconium dioxide, PMIA - poly(m-phenylene isophalamide) , PET - Polyethylene terephthalate, FEP - Fluorinated ethylene propylene, GF - Glass Fiber, Al₂O₃ - Alumina, SiO₂ - Silica and CNT- carbon naotube.]

2.4.3 Self-lubricating Nanocomposites

It is almost impossible to use liquid lubricants in space applications to protect surfaces. The difference in pressure and temperature from the Earth causes these lubricants to be less viscous, evaporate or freeze. Thus, the best alternative is to use solid lubricants by coating them over surfaces using binders. In any case, failure of the binder or coating would lead to massive wear of costly equipments. Hence, self-lubricating composites have been developed to solve this problem by dispersing solid lubricants into the matrix. The solid lubricant particles embedded in the matrix lubricates the surface as the wear reaches fresh lubricant particles beneath the worn surface. Commonly used solid lubricants are graphite, molybdenum disulphide (MoS₂) and polytetrafluoroethylene (PTFE). Graphite works well only in the presence of moisture, whereas MoS₂ works better in dry environments and thus, is referred to as a dry lubricant [Fusaro 1990]. In

addition, it has a shortened life in air and is vulnerable to decomposition due to long period storage.

The motivations for making polymer composites by embedding other materials to its matrix are given below [Booser 1984]:

- 1) The load carrying capacity of a pure polymer is enhanced by adding some materials like fibers and nanoparticles.
- 2) The addition of lubricants or additives reduces friction and wear rate. Perfect combinations of some lubricating and non-lubricating fibers are also used in certain applications.
- 3) Some desirable and unique properties like thermal, electrical and optical properties can be obtained by adding some variety of materials.

Dynamic stress in self-lubricating composites is an important design concern and interfacial shear strength should be very low for easy sliding and smooth sliding. Development of an interfacial shear layer between the sliding surfaces is necessary to avoid adhesive and ploughing interactions between them.

Table 2.2: *Common polymers and fillers used for developing the self-lubricating composites (Reproduced from Booser 1984)*

| Polymer Description | Max. Temperature (°C) |
|-----------------------------------|-----------------------|
| (a) Thermoplastics Polymer | |
| Polyethylene (High MW and UHMW) | 80 |
| Polyacetal | 125 |
| Nylons | 130 |
| Poly (phenylene sulphide) | ~200 |

| | |
|--|------|
| Poly (tetrafluoroethylene) | 275 |
| Poly (P-oxybenzionate) | 300 |
| (b) Thermosetting Polymer | |
| Phenolics | ~150 |
| Cresylics | ~150 |
| Epoxies | ~200 |
| Silicones | ~250 |
| Polyimides | ~300 |
| (c) Reinforcements | |
| Glass fibers, asbestos fibers and textiles (polyester, cotton and micas) | |
| (d) Friction and wear reducing additives / Thermal conductivity materials | |
| Graphite, molybdenum disulphide, polytetrafluoroethylene (PTFE), metal oxides, silicone fluids, bronze, graphite and silver | |

Table 2.3: *Self-lubricating composites and their applications in the space industry (Reproduced from Fusaro 1990)*

| Composite | Applications |
|------------------------------------|--------------------------------------|
| PTFE/glass fiber | Bearing cages |
| PTFE/glass fiber/MoS ₂ | Bearing cages, gears |
| Polyacetal homopolymer/ co-polymer | Bearing cages, gears, bushes, brakes |
| Reinforced phenolics | Bearing cages, gears |
| Polyimide / MoS ₂ | Bearing cages, gears |
| PTFE/ woven glass fiber/ resin | Bushes |

| | |
|---------------------|-----------------------|
| PTFE/ bronze sinter | Bushes, rotating nuts |
|---------------------|-----------------------|

As we mentioned earlier, the low shear strength and the easy sliding nature of solid lubricants make them suitable materials for making self-lubricating composites. The friction and wear rate are reduced drastically by the addition of fillers such as PTFE, molybdenum (MO) and graphite. The addition of MO and PTFE fillers to UP (unsaturated polyester) has been studied [Yamaguchi 1990]. 3% vol. MO was shown to have no effect on the wear of UP, whereas 5% vol. PTFE reduced the wear rate of UP by 48 fold. Similar results were reported when 3% MoS₂ and 5% PTFE were added to DAP (Diallyl Phthalate) resin [Lancaster 1972]. Overall, results suggest that PTFE is more effective than MO in reducing the wear of UP and DAP.

It was also reported in literature that PTFE has yielded better wear rates with PEEK in all proportions from 5% to 100% vol. [Briscoe et al 1985]. This indicates that the wear-reducing action of PTFE is specific to the polymer. The effect of MO and graphite fillers on the wear rates of PTFE, polyamide (PA) 66, and polyimide (PI) have been investigated [Friedrich 1989, Giltrow 1973, West 1973]. Fillers such as 3% PTFE and 12% graphite have exhibited a reduction in wear rates by 54 fold when added to polyamide-imide (PAI) [Jain et al 1987].

Another study reported that the graphite-PI composite exhibited a wear life that was 3 times better than that of MO-PI composite. The effectiveness of filler materials in reducing the wear of PPS (Polyphenylene sulfide) is in the following ascending order: PTFE, graphite and MO. The effect of PTFE concentration on the wear rates of POM and PA was studied and it was observed that 10wt% PTFE is the optimum concentration such

that both polymers exhibit low wear rates [Yamaguchi et al 1984]. Another similar study also concluded that the wear rate of PI+40% graphite was greater than that of PI+15% graphite [Yamaguchi 1990]. A small amount of reduction in wear was observed when an additional 10% PTFE was added to PI+15% graphite composite [Gong et al 1989]. From the above literature, it is clear that using an optimum concentration is the key to producing a polymer composite with a minimum wear rate. The literature also reports that the optimum concentrations of PTFE and MoS₂ in a polymer composite for better wear rates are ~10-15wt% and ~15-20wt% respectively.

2.5 SU-8 Polymer for MEMS Applications

As mentioned previously in section 2.4, polymers are useful materials for fabricating MEMS devices because of the numerous advantages offered by them as compared to Si. The MEMS industry also puts stringent requirements on materials to be developed into new polymers, composites, coatings. The complicated fabrication process and highly brittle nature of Si make it an unfavorable MEMS material though it has good mechanical properties [Sharpe 2001, 2004]. Some commonly used polymers are polyimide, PMMA, photo-patternable epoxy resins, bio-degradable polymers, polydimethylsiloxane (PDMS), hydrogels, paraffins, piezoelectric polymers and liquid crystal elastomers [Wang 2003, Harris 2007, Ryu 2006, Carlen 2002, Zhang 2007, Delille 2006, Armani 2000]. Among them, SU-8 is an emerging negative UV photo-resist, invented by IBM in 1989. SU-8 has three basic chemical elements: (a) an EPONTM SU-8 epoxy resin; (b) a solvent such as gamma-butyrolactone (GBL); and (c) a photoacid generator such as triaryl sulfonium

salts. The name SU-8 is given due to the count of eight epoxy rings in each molecule of SU-8 [Gelrome et 1989].

UV-LIGA (German Abbreviation: Lithographie Galvanoformung Abformung) is a processing technique, developed in Germany, used to produce high thickness and high aspect ratio MEMS structures using near UV lithography [Wenmin 1998, Holmes 1998]. UV-LIGA can achieve a few tens of micron thick micromolds because UV light may not be able to pass further. EPON SU-8 photo-resist has become an alternative structural material for applications with thick molds (>1 mm) and high aspect ratio (>50) [Lbianca 1993, Lee 1995, Dellmann 1997, Guerin 1997, Lorenz 1998 (a)&(b), Mann 1998, Renaud 1998, Bertsch 1998, Arocott 1999, Jo at 2000].

Besides its compatibility with the lithography process, SU-8 has several attractive advantages over other MEMS materials such as chemical stability and resistance to most solvents and bio-compatibility [Weisenberg et al 2002, Abgrall et al 2007], optimum mechanical and optical properties compared to other MEMS polymers such as PDMS, PMMA [Ruano 2006, Foulds 2006, Jiguet 2006 (a) & (b)], favourable electrical [Jiguet 2004] and magnetic properties [Damean 2005], and very good adhesion to a wide range of substrates such as Si and Gold [Ewan et al 2002]. However, SU-8 has two major drawbacks which are poor mechanical and tribological properties (COF: SU-8 ~ 0.5, Si ~0.7) [Jiguet et al 2006 (a) & (b)]. Hence, SU-8 has been identified as a potential MEMS material if the drawbacks can be properly addressed. A few works have been carried out to improve the mechanical and tribological properties of SU-8.

13 nm sized silica nanoparticles (NP) were added to SU-8 at a concentration of 5wt% and the effect of the addition of NP on the frictional behaviour of SU-8 was investigated [Jiguet et al 2006 (a) & (b)]. The steel and polyoxymethylene (POM) balls were used as a counterface for sliding tests. The resulting SU-8 nanocomposites have marginally improved tribological properties compared to SU-8. The response to a heat treatment of 150 °C for 2 hours on the frictional properties of SU-8 was also investigated and it was found that the heat treatment has considerably reduced the wear rate of pristine SU-8 and SU-8 nanocomposites.

The two-step surface modification method was developed to improve the tribological properties of SU-8 [Singh et al. 2011 (a)] and indeed, it has enhanced the tribological properties of SU-8 surfaces by several fold. Firstly, the SU-8 surface is treated with oxygen plasma, which introduces functional hydroxyl groups by removing the contaminants from the surface. This also enhances the adhesion between the substrate and the coating [Jiguet et al 2006 (a)]. After an oxygen plasma treatment, the surface is coated with lubricants such as PFPE using the dip-coating technique. The two-step surface modification method produces a 500 nm thick perfluoropolyether (PFPE) coating on a 50 µm thick SU-8 film on Si substrate. Tribological characterization has shown that the initial coefficient of friction has been reduced by ~4-7 times, the steady-state coefficient of friction has been reduced by ~2.5-3.5 times and the wear durability has been increased by >1000 times. However, the two-step surface modification method has slightly reduced the elastic modulus and hardness of pristine SU-8 thick films as observed in the nanoindentation tests.

Another method developed to improve the tribological properties of SU-8 is the two-step chemical modification technique [Singh et al.2011 (b)]. The SU-8 surface is treated with ethanolamine-sodium phosphate buffer first, followed by a coating of PFPE lubricant. It comprises of two-steps. Thus, it is called the “Two-step chemical modification technique”. The results showed that the steady-state coefficient of friction has been reduced by ~4-5 times and the wear durability has been increased by >1000 times at the loading conditions of a normal load of 150 g and a rotational speed of 200 rpm. The bonding between the –OH functional groups of ethanolamine treated SU-8 films and the –OH functional groups of PFPE was found to be responsible for the superior tribological properties such as a reduction in friction coefficients and an increase in wear life, exhibited by the chemically modified SU-8. However, it is noted that both surface modification methods can be costly for manufacturing, as they require additional processing steps.

The impregnation of liquid lubricants and natural absorbents to PTFE based composites were investigated [Okhlopkova et al 2008], in order to improve the tribology of those composites. They also reduced the molding pressure of the polymer materials to increase the porosity of the polymer and these porosities absorb the lubricants inside for tribological improvement. The new materials have a long-lasting self-lubrication effect and increase the load bearing capacity.

The self-lubricating ultra-high molecular weight polyethylene (UHMWPE) composites were developed by blending two solid lubricants (MoS₂ and carbon black)

and one liquid lubricant (PFPE) with UHMWPE [Esa Puukilainen et al 2007]. The tribological properties of those composites were characterized. They have noticed a marginal reduction in the coefficient of friction with increasing amount of PFPE, yet, with a considerable reduction in tensile strength and abrasion properties.

The inclusion of lubricant-filled microcapsules as a filler material into epoxy resins have formed self-lubricating composites which provide better tribological performance [Guo et al 2009]. The lubricant stored inside the capsules is released by the wear process which involves the breaking of the capsules by asperity contacts. The released oil gets into the contact area or wear track to form boundary lubrication, thereby reducing friction and wear.

The epoxy resin surface-modified SiO_2 nanoparticles with 20nm diameter were added into the epoxy photo resist to improve the lithographic, optical and mechanical properties of the pristine material. [Voigt et al 2007]. The addition of the epoxy resin surface-modified SiO_2 nanoparticles to epoxy resin yielded the greatest increase in Young's modulus of up to 8.7 GPa, with the lowest concentration of surface modified SiO_2 nanoparticles of 2 wt%.

The responses of reinforcements of diamondoids and SWCNTs (single-walled carbon nanotubes with average diameter: 0.8 nm and concentrations: 1 wt% and 5 wt%) on the mechanical properties of SU-8 were also investigated [Chiamori et al 2008]. Results of uniaxial tensile tests have shown that the reinforcements of diamondoid and SWCNTs with SU-8 resulted in elastic moduli of 1.9 GPa and 1.3 GPa, respectively,

compared to the elastic modulus of 1.6 GPa for pristine SU-8. This decrease in mechanical properties could be attributed to the agglomeration of SWCNTs, which affects the cross-linking and curing ability of SU-8.

Mionic et al. [Mionic et al 2010] have demonstrated the inclusion of MWCNTs (multi-walled carbon nanotubes) (concentration: 5 wt%) in SU-8 in developing SU-8+MWCNTs composites. They determined their mechanical properties using nanoindentation. The study was also extended to investigate the impact of SU-8 solvent on the structural homogeneity and mechanical properties of the composites. The solvent type and the surface functionalization of MWCNTs were the factors deciding the Young's modulus of the composite. They have also reported a 104% increase in the Young's modulus of SU-8 from that of pristine SU-8 when acetone was used as the solvent.

2.5.1 Research Strategy Followed in this Thesis

The above presented literature reviews covered the scope of the polymers and their composites in MEMS industries, and the tribological challenges to their effective operation. Among the emerging polymers, SU-8 is an attractive negative photo-resist with excellent potential to be a structural material to replace traditional Si. However, its poor mechanical and tribological properties restrict its commercial viability. The reported literatures showed that very few works have been carried out so far to improve the tribological properties of SU-8 by developing novel composites and coatings. These composites and coatings have improved the tribological properties of SU-8 very

marginally and also included additional processing steps, and hence incurring additional costs.

Therefore, a new method of lubrication is desired in terms of viability, processing and cost. Thus, in the present thesis, we have developed self-lubricating SU-8 composites by adding perfluoropolyether (PFPE) lubricant into them. These self-lubricating SU-8+PFPE composites have shown a reduction in the initial coefficient of friction by ~6-9 times and increased wear life by more than four orders of magnitude [Prabakaran et al 2013 (a)]. It was also observed that adding PFPE lubricant to SU-8 possibly promoted a chemical reaction between the molecules and helped in the boundary lubrication enhancing the wear durability of SU-8 by more than four orders of magnitude. It is believed that the combination of physical self-lubrication mechanism and chemical bonding between SU-8 and PFPE molecules have yielded dramatic improvement in the wear life of SU-8 [Prabakaran et al 2013 (b), Prabakaran et al 2014]. Therefore, the science and mechanisms behind these superior tribological properties of SU-8 composites will be investigated throughout this thesis.

Overall, the thesis aims to fulfill the three major objectives listed in Chapter 1 and below as well:

1. To develop self-lubricating SU-8 composites for MEMS applications.
2. To investigate the chemical bonding between SU-8 and PFPE molecules.
3. To investigate the physical self-lubrication mechanism assisting in forming the boundary layer lubrication.
4. To investigate the effect of curing conditions on the self-lubricating mechanism of SU-8 composites and analyze the lube migration mechanism.

Chapter 3

Materials and Experiments

This chapter describes the materials and experimental procedures used in this research to fabricate the self-lubricating SU-8 composite films. It also provides detailed explanations on the characterization methods used to determine the physical, chemical, mechanical and tribological properties of the fabricated films.

3.1 Materials

3.1.1 Silicon

10.5 cm diameter p-type Si wafer with crystal orientation of <100> (Supplied by Sigma-Aldrich) was used as a substrate material to form the films. The mechanical and physical properties of the wafers are given below.

Table 3.1: *Physical, mechanical and dimensional properties of Si wafers used.*

Top of Form

| Properties | Units | Values |
|--|--------------------|--|
| Wafer diameter | mm | 100 |
| Wafer thickness | μm | 455-475 |
| Bulk modulus of elasticity | GPa | 102 |
| Density | g/cm^3 | 2.329 |
| Hardness | GPa | 12.4 |
| Surface microhardness (using Knoop's pyramid test) | kg/mm^2 | 1150 |
| Elastic constants | dyne/cm^2 | $C_{11} = 16.60 \cdot 10^{11}$ $C_{12} = 6.40 \cdot 10^{11}$ $C_{44} = 7.96 \cdot 10^{11}$ |
| Young's Modulus (E) | GPa | 129.5 |

| | | |
|---------------------------|-------------------------|----------------------|
| Shear Modulus | GPa | 64.1 |
| Poisson's Ratio | - | 0.22 to 0.28 |
| Thermal expansion, linear | $^{\circ}\text{C}^{-1}$ | 2.6×10^{-6} |
| Thermal conductivity | W / (m. K) | 148 |

(Note: The properties mentioned here are taken from Sigma-Aldrich product data sheets.)
<http://www.sigmaaldrich.com/>Bottom of Form

3.1.2 SU-8 Resin

SU-8 is a negative UV photo-resist, contrary to Poly (methyl methacrylate) (PMMA) , which is a positive photo-resist. Figure 3.1 shows the difference between the positive and negative resists. In negative resists, the area of the resist exposed to UV light remains over the substrate after the development and etching. While in the positive resist case, the exposed area is washed away and the unwashed area remains over the surface after the development process. The UV light exposure promotes cross-linking in negative resists, whereas the UV exposure demotes cross-linking in positive resists. [Reichmanis et al 1989]. The grade used in this research is SU-8 2050.

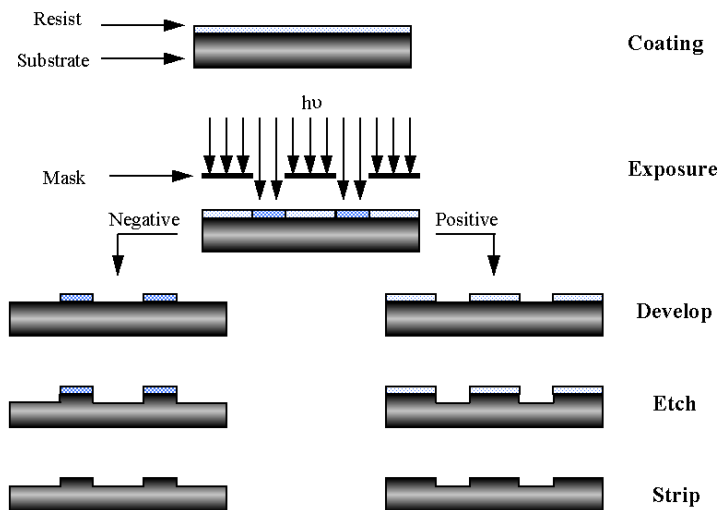


Figure 3.1: Schematic illustrating the distinction between the negative and positive photoresists. [Reichmanis et al 1989]

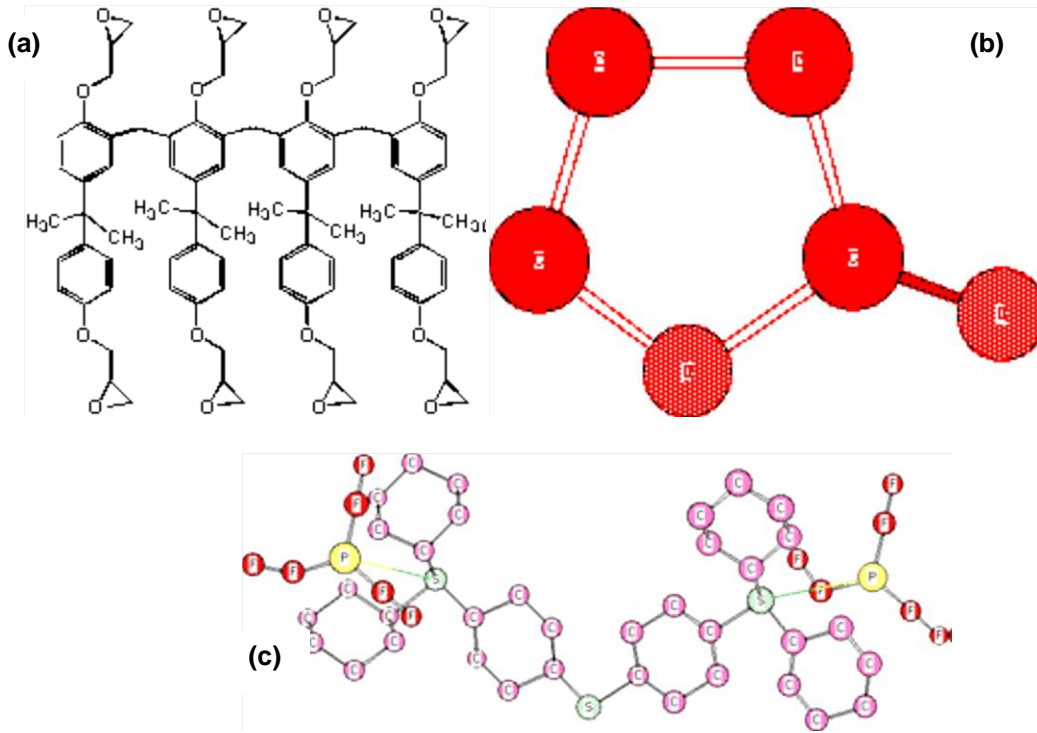


Figure 3.2: Chemical structure of (a) SU-8, (b) a solvent such as gamma-butyrolactone (GBL), and (c) a photoacid generator such as triaryl sulfonium salts [www.somisys.ch/microfluidics.htm].

3.1.2.1 SU-8 Processing

Processing steps for different grades of SU-8 such as SU-8 2000, 2050, 3100, are almost similar, but the processing parameters may change from one to another. The processing sequence for SU-8 is given below in Figure 3.3. The processing starts with pre-treatment of substrate using piranha or any other solvents such as acetone, ethanol [Singh et al 2011 (a)& (b)], followed by the drying of the substrates using nitrogen gas. The cleaned substrates can be cleaned again using plasma cleaning techniques to improve the bonding

between the substrate and the coating. The following steps are used to spincoat the respective grade of SU-8 over the substrates (Si). The spin speed, spinning time, acceleration (ramping) can be selected according to the desired thickness. Edge bead removal (EBR) is the process of removing resist build-up at the edges of the substrate to avoid contamination of the hot plate and mask aligner by resist.

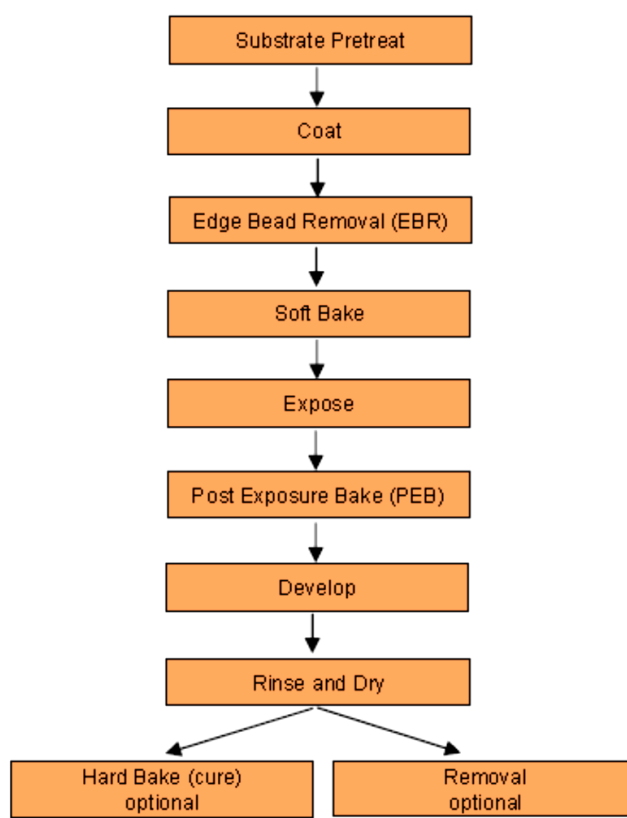


Figure 3.3: *The sequence for SU-8 processing.* [Reproduced from MCC: (www.microchem.com)].

The GBL solvent in SU-8 helps the resist to remain in the resin state. Soft-baking is the process of heating the sample at the recommended temperature for the recommended duration, mentioned in the data sheet [www.microchem.com]. Soft baking evaporates the solvent and thereby, the resin viscosity changes significantly. The cross-linking is carried out in two steps; the first step is UV exposure, followed by post

exposure bake. UV exposure introduces strong acids such as Lewis acid ($H + A^-$) which acts as a catalyst for cross-linking of SU-8 during the post exposure bake (PEB) step. The development of SU-8 photoresist can be done in several ways such as immersion, spray or spray-puddle processes with MicroChem's SU-8 developer. Ethyl lactate and diacetonealcohol are a few developers commonly used [www.microchem.com]. The patterns and structures can be obtained with good accuracy by using an ultrasonic or megasonic bath. The developed structure or pattern may be washed in a fresh solution of developer to remove the residues, followed by rinsing with isopropyl alcohol (IPA), and finally it is dried with nitrogen gas. A hard bake or final cure step is recommended to increase the cross-linking further, which keeps the SU-8 structures intact. It is also advisable to expose the SU-8 to a higher temperature than the service temperature of the device to keep the mechanical properties and shape unchanged.

3.1.2.2 Mechanical and Physical Properties of SU-8

Table 3.2 shows the mechanical and physical properties of SU-8 before and after curing. The conditions given here have been taken from the references listed in the last column.

Table 3.2: *Mechanical and physical properties of SU-8 photoresist.* [<http://memscyclopedia.org/su8.html>]

| Properties | Units | Value | Conditions | Reference |
|---------------------------|-------|-------|---|---------------------------|
| Modulus of elasticity (E) | GPa | 4.02 | In tension, post-baked at 95°C, screw tensile testing machine | Lorenz et al 1997 |
| Hardness (H) | GPa | 0.27 | - | Prabakaran et al 2013 (a) |

| | | | | |
|--|------|---------------|---|----------------------|
| Bi-axial modulus of elasticity | GPa | 5.18 +/- 0.89 | Post-baked at 95°C, thermal cycling test on Si wafer | Lorenz et al 98(a) |
| Poisson ratio | - | 0.22 | Post-baked at 95°C, SM blend | Sotec Micro |
| Film stress | MPa | 19 - 16 | For 0 - 400 µm thick SU-8 film coated on a 3" 375 mic. thick Si wafer, prebaked, illuminated, postbaked at 95°C and brought back to room temperature (20°C) | Lorenz et al 98(b) |
| Max stress | MPa | 34 | Hardbaked at 200°C, lateral deflexion FEM analysis | Dellmann et al 97 |
| Max shear stress | - | 0.009 | Hardbaked at 200°C, lateral deflexion FEM analysis | Dellmann et al 97 |
| Friction coefficient : (µ) | - | 0.19 | Postbaked at 95°C, pin-on-disc installation (10 g load), Polymer ball | Lorenz et al 97 |
| Bond strength | MPa | 4.8 +/- 1.2 | SU-8 on Au, Instron pull test | Nordstrom et al 2005 |
| | | 5.6 +/- 2.5 | SU-8 on Ti, Instron pull test | |
| | | 12.1 +/- 2.8 | SU-8 on Al, Instron pull test | |
| | | 20.7 +/- 4.6 | SU-8 on Si, pull test | |
| Glass transition temperature (T _g) | °C | ~50 | Unexposed film (not polymerized) | LaBianca et al 95 |
| | | >200 | Fully crosslinked film (hard baked) | |
| | | ~55 | Micro chem. Corp. (MCC) blend before PEB (post-exposure bake) | MCC |
| Thermal conductivity | W/mK | 0.2 | General value for thermoplastic not for SU-8 | Guerin et al 97 |

| | | | | |
|----------------------------|-------------------|-------|---|-----|
| Density: ρ | kg/m ³ | 1233 | Density of the raw SU8 resin (not for the PR) | MCC |
| Kinematic viscosity: ν | cSt | 12900 | SU-8 2050 (71.6% solid), 20°C | MCC |

3.1.3 Perfluoropolyether (PFPE)

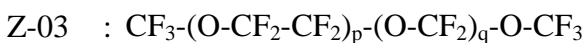
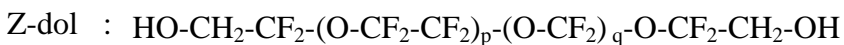
The physical and chemical properties of perfluoropolyether (PFPE) lubricant used in this research (obtained from Solvay Solexis, Singapore) are summarized in Table 3.3. H-Galden, SV60 (obtained from Ausimont INC) is a solvent used to dissolve both PFPE Z-dol and Z-03 and also used for washing the SU-8+PFPE composites.

Table 3.3: *Physical and chemical properties of Z-dol and Z-03 lubricants.*

[www.solvayplastics.com/]

| Properties | Z-dol | Z-03 |
|----------------------------------|-------|------|
| Kinematic Viscosity(Cst) at 40°C | 18.2 | 18 |
| Surface Tension (mN/m) | 22 | 23 |
| Molecular Weight (g/mol) | 4000 | 4000 |
| Density (kg/cm ³) | 1800 | 1850 |

The chemical structures of the lubricants are as follows:



where p/q ratio is 2/3, for both lubricants.

3.1.4 Multiply-Alkylated Cyclopentanes (MACs) and SN 150 base oil

SN 150 and multiply-alkylated cyclopentanes (MACs) are alkane-based base oil lubricants. Table 3.4 summarizes the physical properties of SN 150 and MAC lubricants.

Table 3.4: *Physical properties of MAC and SN 150 lubricants.*

| Lubricant name | Chemical category | Grade and manufacturer | Lubricant solvent | Kinematic viscosity (Cst) at 40°C | Surface tension (mN/m) |
|----------------|-------------------|--|-------------------|-----------------------------------|------------------------|
| SN 150 | Alkane based | Paraffinic based SN 150, Chevron | n-Hexane | 23 | 26 |
| MAC | Alkane based | MAC based synthetic oil 2001A, Pennzoil lubricants | n-Hexane | 108 | 32 |

[Ref. - MAC: <http://www.nyelubricants.com/>; SN 150: <http://www.chevron.com/>]

3.2 SU-8 and SU-8 Composite Film Preparation and Characterization

3.2.1 SU-8 Sample Preparation

Figure 3.4 shows the step-by-step process flow diagram for fabrication of SU-8 and SU-8 composite films. Si wafers were cut into ~2 cm x 2 cm pieces and were thoroughly cleaned with detergent water (house-hold soap), distilled water and isopropyl alcohol (IPA, 99.9% purity obtained from Sigma -Aldrich) sequentially, and finally dried with N₂ gas. The cleaned Si wafers were then subjected to heating at 150°C for about 3-4 min inside a dry-cabinet to remove any adsorbed moisture and then subsequently treated with

oxygen plasma for about 15-20 min, using plasma cleaner PDC-32G (Harrick plasma, NY, USA). The purpose of oxygen plasma treatment was to remove the contaminants and to generate hydroxyl groups on the surface which enhance adhesion between the substrate and the coating [Jiguet et al 2006 (a)].

The cleaned Si wafers were then subjected to SU-8 (grade 2050 supplied by Microchem Ltd USA) spin-coating immediately on SCS P6700 spin coater (Speciality Coating Systems, Indiana, USA). SU-8 was spin-coated onto Si at an initial speed of 500 rpm for a duration of 5 seconds, followed by 3000 rpm for a duration of 30 seconds which results in SU-8 films with a thickness of ~100 microns. The spin-coated SU-8 films were then subjected to pre-baking at a temperature of 65°C for 4 minutes, and then at 95°C for 9 minutes. The pre-baked SU-8 films were then exposed to UV rays (wavelength: 365 nm and power: 210 mJ/cm²) for a duration of 30-60 seconds using Black-Ray B-100SP UV lamp (UVP, LLC, upland, CA, USA).

A post exposure bake was carried out at a temperature of 65°C for 1 minute, followed by a temperature of 95°C for 7 minutes. The samples were then stored in the desiccators before any further characterization. The conditions of the spin-coating, pre-baking, UV curing, post- exposure baking were approximately the same for both pristine SU-8 films and SU-8+PFPE composite films. The digital image of ~100 μm thick completely cured and cross-linked pristine SU-8 is shown in Figure 3.4 (b).

The samples after UV curing and post-exposure bake (cross-linked) are called “freshly spin-coated samples” throughout this thesis for convenience. For the preparation of the SU-8+PFPE composite, 5 wt% of lubricants such as PFPE and MAC were added to SU-8 (grade 2050) and then the composite materials were thoroughly mixed using a

sonicator for about 12 hrs before spin-coating. Sonication breaks the lubricant droplets into the smallest sizes ($<1 \mu\text{m}$) possible by overcoming their intermolecular forces using sound waves.

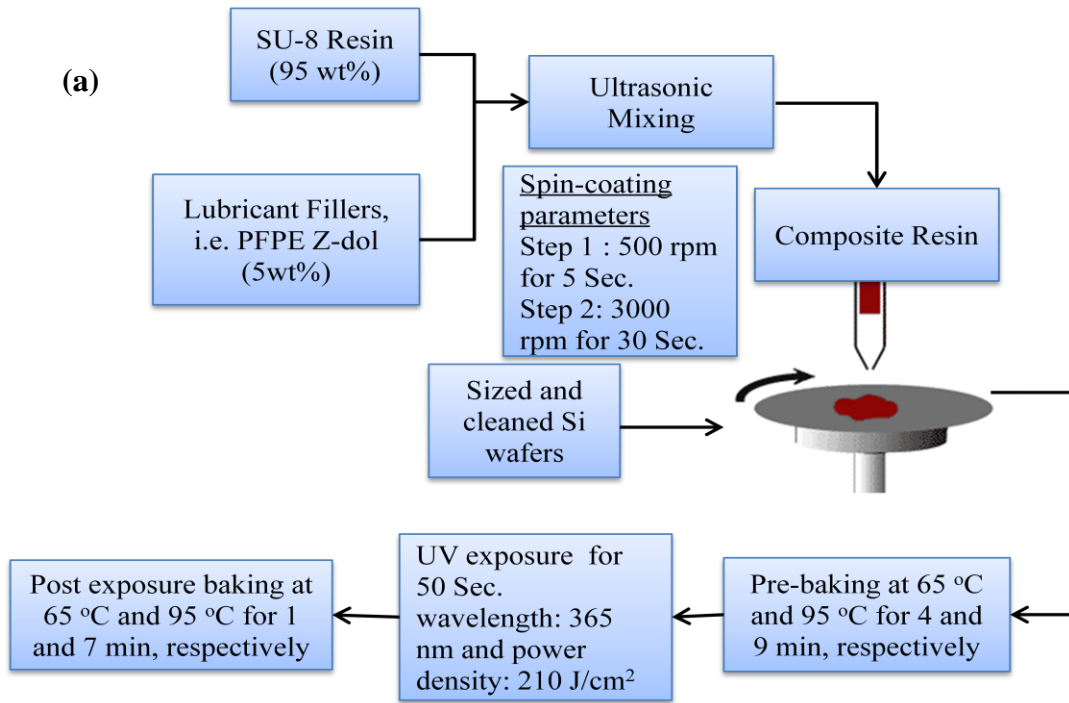


Figure 3.4: (a) *Step-by-step procedure adopted for fabrication of pristine SU-8 and SU-8 composite films.* (b) *Visual image of freshly cured and cross-linked pristine SU-8 film on Si.*

Before coating, the uniform size of the droplets has to be ensured using dynamic light scattering (DLS) characterization, which reveals the particulate dispersive index (PDI). PDI is a measure of the homogeneity of the second phase in the solution. The sonication time can be extended until homogeneous droplet distribution is achieved.

3.2.2 Contact Angle and Surface Free Energy Characterization

VCA Optima contact angle system (AST Products Inc, USA) was used to characterize the surface free energies of both pristine SU-8 and SU-8 composites by experimentally measuring the static water contact angles (WCAs). The ambient temperature and relative humidity were 25°C and 60%, respectively.

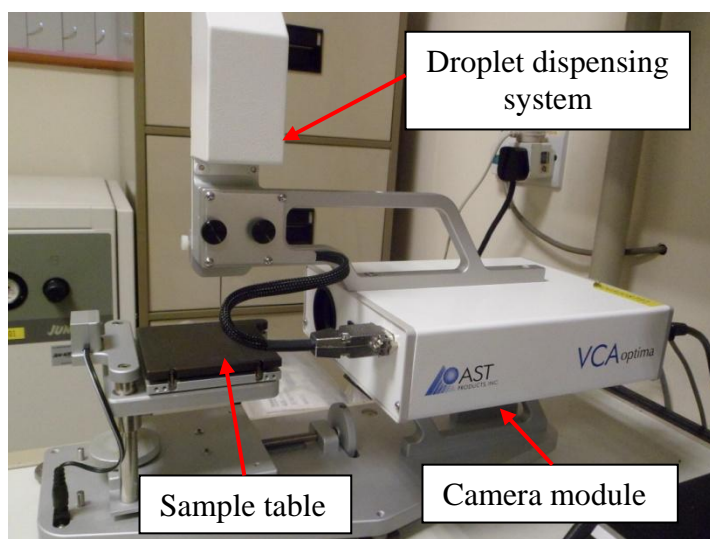


Figure 3.5: *Digital image of water contact angle measurement apparatus.* [AST Products Inc, USA]

Owens-Wendt equation was used for the surface energy calculations [Loeb et al 1992],

$$(1 + \cos\theta_i)\gamma_i = 2\left(\sqrt{\gamma_i^d\gamma_s^d} + \sqrt{\gamma_i^p\gamma_s^p}\right) \quad (\text{Eq 3.1})$$

where,

θ_i is the apparent contact angle, γ_i^d and γ_i^p are the dispersive and polar surface tensions of liquids, respectively. γ_s^d and γ_s^p are the dispersive and polar surface energies of the surface, respectively, to be determined.

Two polar liquids, water and ethanol, and one non-polar liquid, hexadecane, were used as droplets of 0.5 μl volume for the contact angle measurements and their corresponding polar and dispersive surface tension values were summarized in Table 3.5. The variation in water contact angles at various random locations of a sample and the measurement error were within $\pm 3^\circ$ and $\pm 1^\circ$, respectively. The water contact angle measurement and surface free energy calculation were also performed inside the wear tracks after tribological tests.

Table 3.5: Polar, dispersive and total surface tensions of reference liquids used for surface energy calculation. [<http://www.accudynetest.com/>]

| Reference Liquids | Polar Surface Tension (mN/m) | Dispersive Surface Tension (mN/m) | Total Surface Tension (mN/m) |
|-------------------|------------------------------|-----------------------------------|------------------------------|
| Water | 50.7 | 22.1 | 72.8 |
| Ethanol | 2.6 | 18.8 | 46.07 |
| Hexadecane | 0 | 27.5 | 27.5 |

3.2.3 Tribological Characterization

Friction and wear tests were carried out using UMT-2 (Universal Micro Tribometer, CETR, USA) in a ball-on-disk setup where the coefficient of friction was measured with respect to the number of sliding cycles. Figure 3.6 illustrates the ball-on-disk wear test setup for rotating and reciprocating sliding test configurations. Si_3N_4 balls of 4 mm diameter with a surface roughness of 5 nm were used as the counterface. The roughness of the Si_3N_4 counterface ball was measured using the Wyko NT1100 optical profiling system with a vertical measurement range of 1 nm to 1 mm with a resolution of < 0.1 nm Ra and the arithmetic mean method was used to determine the surface roughness.

The tests were conducted at different normal loads (up to 300 g, Hertzian contact pressure: 0.14 GPa) and at different rotational speeds (up to 2000 rpm). All experiments were performed openly at room temperature (23 °C) and at a relative humidity of approximately 60%. From the sliding tests, an initial coefficient of friction (μ_i) was noted as an average of the first twenty sliding cycles.

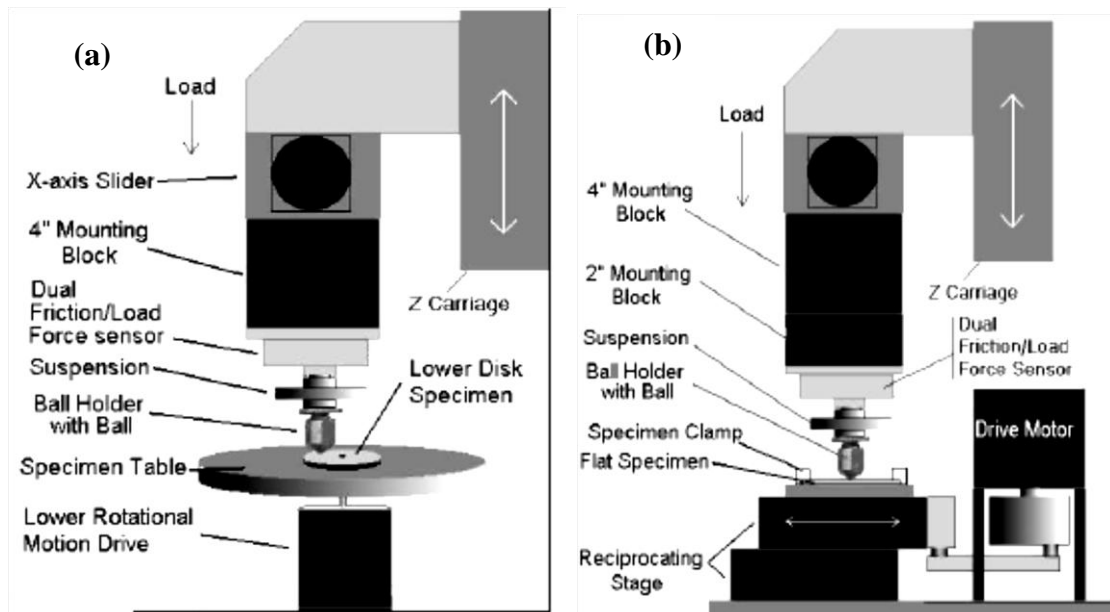


Figure 3.6: *CETR ball/pin-on-disk sliding test setup. (a) Rotational sliding test set up; (b) Reciprocating (To and Fro) sliding test setup. [Ref: <http://www.cetr.com/eng/products/umt-2.html>]*

The steady-state coefficient of friction (μ_s) was measured as the average of all coefficients of friction from the point where the steady-state behaviour (after the observation period of initial coefficient of friction) was observed until the end of the test or until the failure point, whichever was earlier. The wear life for the tested conditions was taken as the number of sliding cycles after which the coefficient of friction exceeded 0.3 or a visible wear track was observed on the substrate with abnormally fluctuating friction values, whichever occurred earlier. Similar definitions for wear life determination have been used in the literature [Hu et al 2012, Neidhardt et al 2004, Sugimoto et al 1998] and present authors' works [Satyanarayana et al 2005, Singh et al 2011]. Very similar wear definitions can be found in ASTM G99 standard for Pin-on-disk. For each composite, at least 3 tests were repeated and average data are reported. An optical microscope was used to image the worn surfaces after the sliding tests to assess the damage to the film surfaces and the ball, respectively.

The specifications of ball-on-disk and reciprocating test module are given below,

Ball/pin-on-disk wear test: Maximum rotational speed – 5,000 RPM; Maximum normal load – 0.5 kg. (Contact pressure: 0.16 GPa)

Reciprocating wear test: Maximum linear speed – 0.01 – 100 mm/s; Maximum travel – 75 mm; Maximum normal load – 0.5 kg;

3.2.4 Nano-mechanical Characterization

The elastic modulus and the hardness of the pristine SU-8 and SU-8 composite films were measured using MTS Nano Indenter XP with a continuous stiffness measurement (CSM) technique. A triangular pyramid Berkovich diamond indenter was employed for nanoindentation tests. The depth of indentation was set to 3,000 nm. The CSM technique has the load and the displacement resolutions at 50 nN and <0.01 nm, respectively. A total of 10 indents were conducted on each sample and the tests were repeated on 3 different samples and an average value was reported.

3.2.5 X-ray Photoelectron Spectroscopy (XPS) Characterization

XPS characterization of pristine SU-8 and SU-8 composites was done using VG ESCA Lab-220i XL XPS. Mg Ka X-ray was employed for analysis of one spot on each sample with photoelectron take-off angle of 90°. The analysis area was 4 mm x 4 mm, whereas the maximum analysis depth lies in the range of ~4-8 nm. Charge compensation was performed by means of low-energy electron flooding and further correction was made based on adventitious C1s at 285.0 eV using the manufacturer's standard software. The voltage of the X-ray beam was 15 KV. The pass energies for the survey scan and high resolution scans were 150 eV and 20 eV, respectively.

XPS characterization was also done inside the wear track after tribological tests on SU-8 composite samples using the Thermo Fisher Scientific Theta-probe XPS. Monochromatic Al Ka X-ray was employed for the analysis of one spot on each sample with photoelectron take-off angle of 50° (with respect to surface plane normal). The analysis area was 100 µm x 100 µm. The maximum analysis depth lay in the range of ~4-

8 nm. A specially designed electron flood gun with a few eV Ar⁺ ions was used for the charge compensation. Electron beam and ion beam were focused and steered towards the analysis position. The voltage of the X-ray beam was 15 KV. The pass energies for survey scan and high resolution scans were 200 eV and 40 eV, respectively.

3.2.6 AFM Characterization

3D surface images of pristine SU-8 and SU-8 composites were taken using DI dimension Nanoscope 3100 AFM, (Digital Instruments, USA). The silicon cantilever tip with stiffness of 1.5 N/m with gold coating at the back side was used and AFM tapping mode was used.

3.2.7 FESEM and EDS Characterization

The surface morphologies of the wear track and the cross-section of pristine SU-8 and SU-8 composite films were studied using Field Emission Scanning Microscopy (FESEM) (FESEM S-4300, Hitachi High-Technologies Inc, Canada). Prior to FESEM imaging, the samples were gold coated at 10 mA for 30 s using a JEOL, JFC-1200 Fine Coater. The same FESEM attached with EDS was used to analyze the chemical elements of pristine SU-8 and SU-8 composites.

3.2.8 Time-of-Flight Secondary-ion Mass Spectroscopy (TOF-SIMS) Characterization

The TOF-SIMS measurements were performed on SU-8 composites using a TOFSIMS IV instrument from IONTOF GmbH, equipped with Bi⁺ ion gun for analysis and Ar⁺ or

Cs⁺ ion guns for sputtering. The SU-8+PFPE composites after complete washing and after heating at 100°C for 12 hrs were subjected to ToF-SIMS analysis. The surface scans were obtained using a pulsed 25keV Bi⁺ beam with the detection of negative secondary ions. The beam current was ~ 1pA and raster size was 300 μm by 300 μm. Sample charging was compensated using a low-energy electron flood gun which was pulsed between each ion gun pulse.

3.2.9 Nano-tribological Characterization

Nano-tribological tests for pristine SU-8 and SU-8 composites were carried out on a ball-on-disk arrangement of CSM-Nanotribometer (CSM, Switzerland). A silicon nitride ball of diameter Ø2 mm with a surface roughness of 5 nm (Salem specialty balls, USA) was used as the counterface material. The wear track radius was fixed at 1 mm for all the tests. The ball was cleaned thoroughly with acetone before the beginning of each test. The normal load (N), rotational sliding speed and the calculated maximum hertzian contact pressure for corresponding load used were 20 mN, 100 rpm (linear speed = 0.01 m/s) and 0.04 GPa, respectively. After each test, the counterface and sample surfaces were examined under an optical microscope to investigate the wear mechanisms. All experiments were performed in open air at room temperature (25°C) and at a relative humidity of approximately 60%. For all friction and wear life criteria, section 3.2.3 on Tribological characterization can be referred.

3.2.10 Optical profiler Characterization

The thickness of the pristine SU-8 and SU-8 composite was measured using an optical profiler (wyko NT1100, Veeco, USA). For the thickness measurement, a step was formed over Si by exposing half of the sample to UV and subsequently, the unexposed other half was etched by the solvent. The bare silicon substrate surface was set as a reference and step height was measured as the thickness of the coating.

3.2.11 Thermogravimetric Analysis (TGA)

The thermogravimetric analysis of pristine SU-8 and 2wt% PFPE dip-coated SU-8 was performed using Shimadzu DTG-60H thermal analyzer (Shimadzu scientific instruments, USA). The following parameters have been adapted for this study: a heating rate of 10°C/min, a hold temperature at 600°C, an atmosphere of argon gas, an airflow rate of 25 ml/min, a sample cell of alumina (Al₂O₃) and a sample weight of 2-10 mg. The weight loss (%) against corresponding temperature were plotted to analyze the thermogravimetric behaviour. The variation in the weight loss data was within ±3-5%.

3.2.12 Perfluoropolyether (PFPE) Dip-coating on SU-8

Pristine SU-8 films were subjected to both PFPE Z-dol and Z-03 dip-coating for nanotribological characterization. After thorough cleaning, the SU-8 thin films were immediately dip-coated with a 0.5wt% PFPE in H-Galden SV60 solvent. The samples were dipped into a beaker containing the solution of PFPE for a duration of 1 min with a withdrawal speed of 2.1 mm/s. The thickness of the dip-coated PFPE films on SU-8 were measured using a variable angle spectroscopic ellipsometer (M-2000U, Woollam, Lincoln, NE, USA) at wavelengths from 400 to 1000 nm at 10-nm intervals and at

incidence angles of 65° , 70° and 75° . The measured film thickness is 10 nm. Average film thickness taken from three measurements was reported.

Chapter 4

Development of Self-Lubricating SU-8 Composites for MEMS

Applications

This chapter describes the development of self lubricating SU-8 composites and the motivation for their development. Their tribological and mechanical properties were obtained from various characterizations. The reasons behind their superior tribological behaviour and applications of these composites will also be discussed.

4.1 Introduction

In MEMS devices, surface forces such as van der Waals, capillary, electrostatic, and chemical forces become more dominant than gravity and inertial forces, as well as the forces that are used to run the devices. Thus, tribological issues such as high friction, high adhesive forces and low wear durability become major impediments against their smooth operation [Kim 2007, de Boer et al 2001]. A newly emerging polymer MEMS material, SU-8 photoresist, has been replacing the mainstay structural material - silicon (Si), for fabricating MEMS devices [Labianca 1993, Lorenz 1998 (a) & (b)]. Although Si is mechanically strong (elastic modulus: 130 GPa and hardness: 12 GPa), it has many inherent drawbacks. The SU-8 has some advantages over Si but it also has some major limitations such as a low elastic modulus ($E \sim 4$ GPa), low hardness ($H \sim 0.28$ GPa) and poor tribological properties [Weisenberg et al 2002, Abgrall et al 2007, Jiguet et al 2006 (a) & (b)]. Hence, researchers have developed some nanometer to sub-micrometer thin films (mostly solid lubricants) which reduce friction, adhesion force and wear. These thin

films include self-assembled monolayers (SAMs), polymer coatings, vapor deposited organic layers, fluorine-based organic layers, solid coatings etc, which have been developed and tested on Si surfaces [Eapen et al 2002, Henck 1997, Ma et al 2007, Satyanarayana et al 2005].

From the literature survey in Chapter 2, it is clear that very minimal work on improving the tribological properties of bulk SU-8 has been found. The improvements in tribological behaviour from the above mentioned literature were not only very marginal but also involved additional processing steps and cost. In this PhD thesis, self-lubricating SU-8 composites were developed by adding a liquid PFPE lubricant and nanoparticles such as SiO₂, CNTs and graphite for tribological and mechanical property enhancement, respectively. These self-lubricating SU-8+PFPE and SU-8+PFPE+ nanoparticle (SU-8+PFPE+NP) composites have shown a reduction in the initial coefficient of friction by ~6-9 times and an increased wear life by more than four orders of magnitude. Mechanical properties such as the elastic modulus and the hardness have increased by ~0.4 times. These SU-8 composites can be used as a self-lubricating structural material for MEMS applications with no external lubrication needed.

4.2 Materials and Experimental Procedures

Details of the materials, experimental procedures and the various characterization techniques and procedures used in this study have been elaborated in Chapter 3. For the preparation of SU-8+PFPE and SU-8+PFPE+NP (NP stands for nanoparticle, SiO₂ of 100% purity (size: 15 nm), MWNTs of 95% purity (diameter: 9.5 nm and length: 1.5 μm), graphite of 99.9% purity (size: 20 μm)), 5 wt% of PFPE and 5 wt% of NP were

added to SU-8 (grade 2050). All nanoparticles (NP) used in this study were supplied by the Sigma-Aldrich Corporation [<http://www.sigmaaldrich.com/>].

4.3 Results and Discussion

4.3.1 Water Contact Angle Characterization

Figure 4.1 shows the water contact angles on pristine SU-8 and SU-8 composite surfaces under two different conditions: freshly spin-coated (completely UV-cured and cross-linked or before tribo-test) and after tribological tests (inside worn regions). Pristine SU-8 showed a water contact angle of 84° whereas the SU-8+NP showed water contact angle values ranging from 79° to 89° (SU-8+graphite: 79° , SU-8+SiO₂: 85° and SU-8+CNTs: 89°). SU-8+PFPE showed a water contact angle of 98° whereas the SU-8+PFPE+NP composites showed water contact angles ranging from 91° to 106° (SU-8+PFPE+CNTs: 91° , SU-8+PFPE+graphite: 91° and SU-8+PFPE+SiO₂: 106°).

Generally, the composites containing PFPE have increased the water contact angle of SU-8. The highest water contact angle (106°) was observed when both PFPE and SiO₂ particles were added, which was about 22° higher than that of pristine SU-8. Due to the fluorocarbons in the PFPE, it was observed that the PFPE-contained composites are hydrophobic. The enhanced hydrophobicity of the fluorinated surfaces are a result of their poorer van der Waals interactions with water. Since fluorocarbons are unable to form hydrogen bonds [Dalvi et al 2010], the polarization of water which is able to form hydrogen bonds internally, repels the fluorinated non-polarized surfaces.

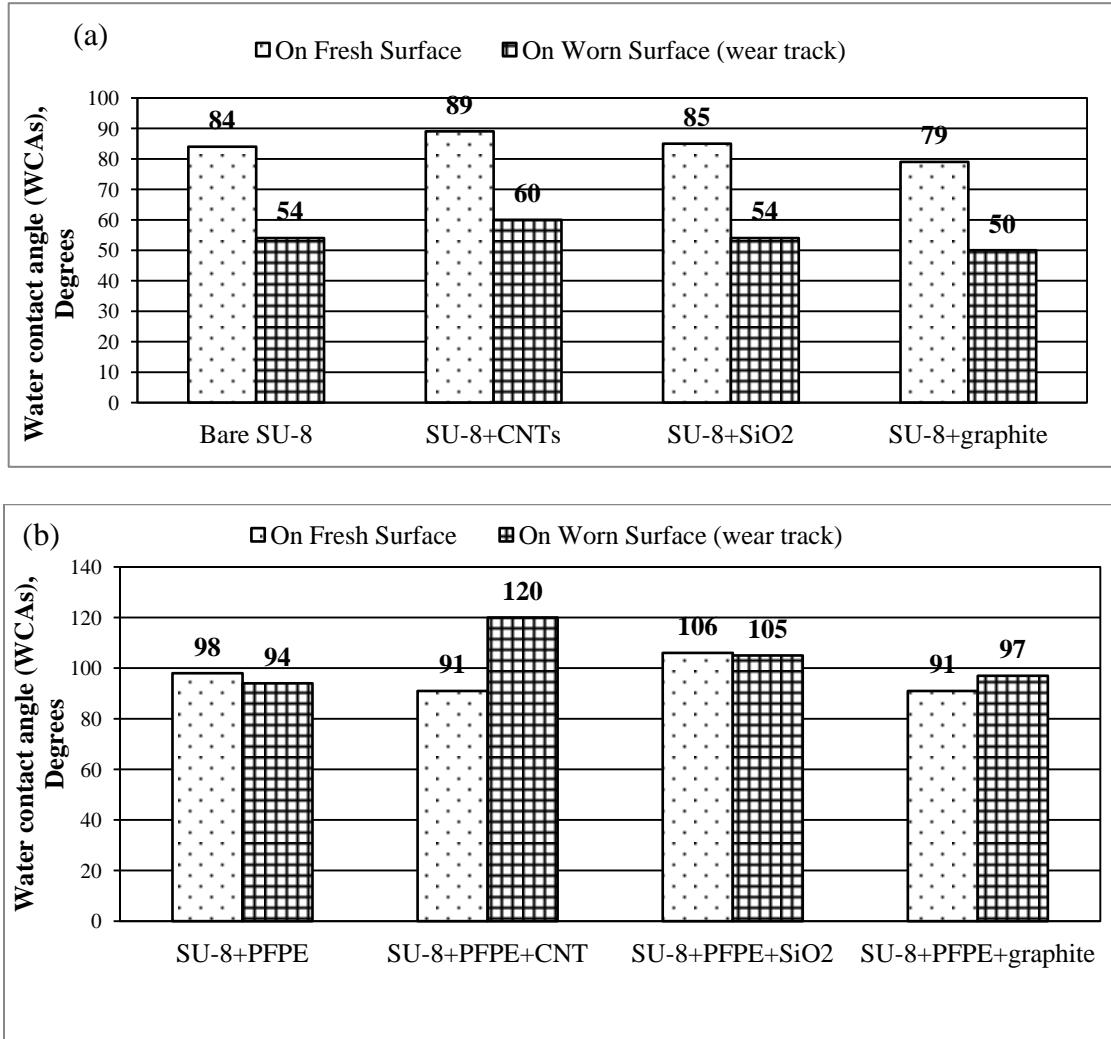


Figure 4.1: WCA values for pristine SU-8 and SU-8 based composites over fresh (pristine surface of composites before experiment) and worn surfaces (wear track). (a) Non-PFPE combinations at 10^4 cycles (composites did not contain PFPE). (b) PFPE combinations at 10^6 cycles.

4.3.2 X-ray Photoelectron Spectroscopy (XPS) Characterization of Freshly Cured and Cross-linked Surfaces

XPS characterization was carried out on freshly spin-coated surfaces (cured and cross-linked) of pristine SU-8 and SU-8+PFPE composites, with Figures 4.2 (a) and 4.2 (b) showing the respective wide-scan spectra. The insets in Figures 4.2 (a) and 4.2 (b) shows

the major peaks observed, together with the corresponding bond assignments and atomic percentages.

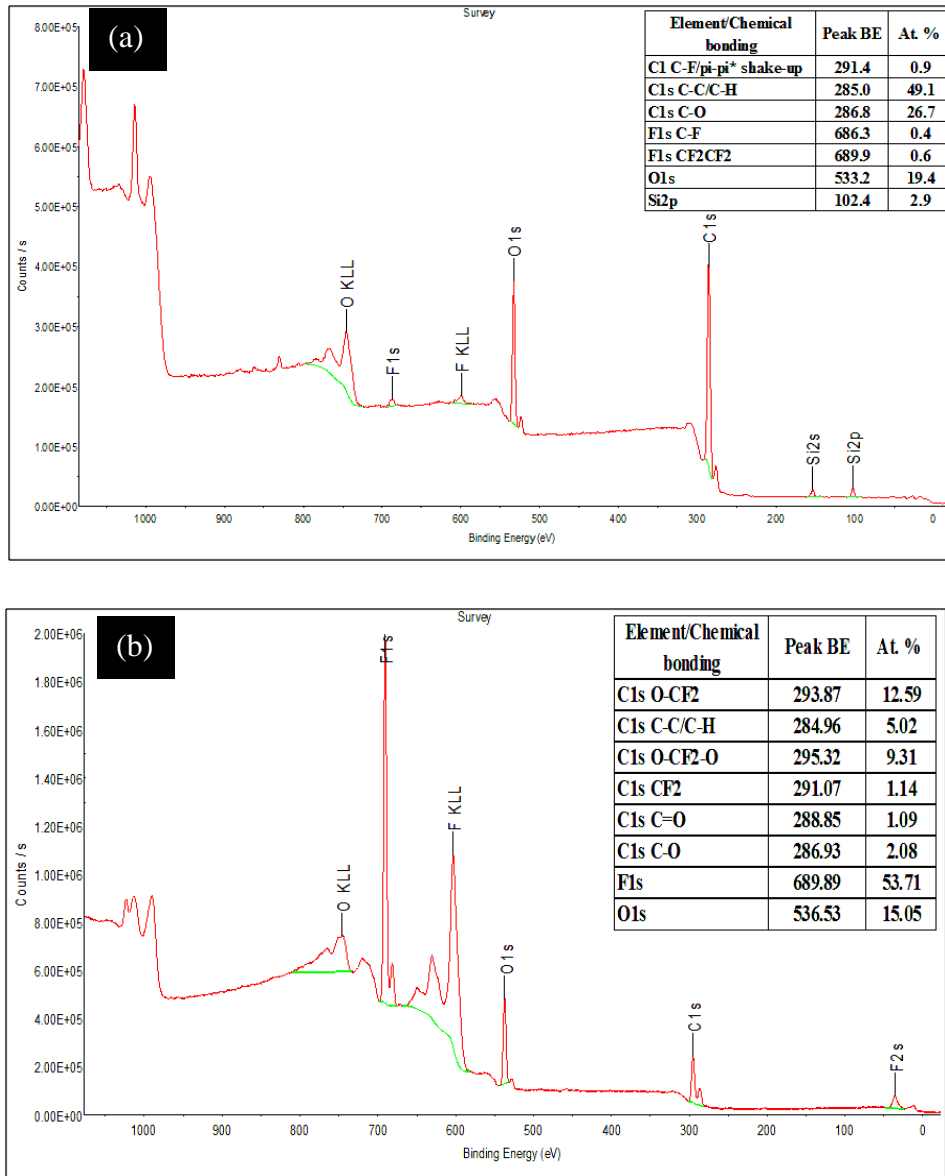


Figure 4.2: XPS wide-scan survey spectrum results for freshly cured and cross-linked surfaces for (a) pristine SU-8 and (b) SU-8+PFPE composite.

The SU-8+PFPE wide-scan spectrum shows a high intensity F1s peak which not only confirms the presence of PFPE in the composite but also confirms the presence of PFPE on the top surface of the composite coating. SU-8+PFPE also showed O-CF₂, O-CF₂-O

and CF_2 groups which were not present on the pristine SU-8 and have mainly arisen from the presence of PFPE.

4.3.3 Tribological Characterization

Table 4.1 shows the initial coefficient of friction (μ_i), steady-state coefficient of friction (μ_s) and wear-lives of pristine SU-8 and SU-8 composites which have been tested at two different normal loads and sliding rotational speeds.

Table 4.1: Initial coefficient of friction (μ_i), steady-state coefficient of friction (μ_s) and wear life (number of sliding cycles) of SU-8 and SU-8 composites obtained from sliding tests against a 4 mm diameter Si_3N_4 ball at different normal loads and sliding rotational speeds.

| Composite Description | Initial coefficient of friction, COF (μ_i) | Steady- state coefficient of friction, COF (μ_s) | Wear Life (Number of Cycles) |
|--|--|--|------------------------------|
| 5wt% SU-8 composites / Normal load :30 g, Sliding Speed: 200 rpm, Spin Coated on Si | | | |
| Pristine SU-8 | 0.82 | - | 0 |
| SU-8+ SiO_2 | 0.77 | - | 0 |
| SU-8+CNTs | 0.39 | - | 0 |
| SU-8+graphite | 0.35 | - | 0 |
| SU-8+PFPE | 0.03 | 0.09 | >100,000 |
| 5wt% SU-8 composites / Normal load :300 g, Sliding Speed: 2000 rpm, Spin Coated on Si | | | |
| Pristine SU-8 | 0.52 | - | 0 |
| SU-8+PFPE | 0.07 | 0.09 | >1,000,000 |
| SU-8+PFPE+ SiO_2 | 0.04 | 0.11 | >1,000,000 |
| SU-8+PFPE+CNTs | 0.11 | 0.17 | >1,000,000 |
| SU-8+PFPE+graphite | 0.09 | 0.14 | >1,000,000 |

[Note: The experiment was stopped due to the long test duration for all PFPE contained films. No μ_s were reported for all non-PFPE samples as they failed very early on in the experiment.]

In this section, the tribological properties obtained at a normal load of 300 g and a rotational speed of 2000 rpm will mainly be discussed and the data for other testing conditions can be referred to Table 4.1. The tribological properties summarized in Table 4.1 have been obtained from the coefficient of friction versus the number of sliding cycles plot shown in Figures 4.3 (a) and (b). It should be noted that although the test was stopped at 100,000 sliding cycles because of the long test duration at a lower rpm, the SU-8+PFPE sample at 30 g load and 200 rpm rotational speed performed equally as well as all the other PFPE contained composites. The pristine SU-8 film showed high frictional properties (μ_i : 0.52) and low wear-life ($n \sim 0$) when tested at a normal load of 300 g and a rotational speed of 2000 rpm.

Under the loading conditions of a normal load of 300 g and a rotational speed of 2000 rpm, SU-8+PFPE showed very low coefficients of friction (μ_i : 0.07 and μ_s : 0.09) and high wear-life ($n > 1,000,000$). This is a significant improvement when compared with the pristine SU-8. The composites of SU-8+PFPE showed significant improvement in tribological properties (μ_i has been reduced by ~ 8 times and wear life has improved by $> 10^4$ times). The incorporation of nano-particles has not improved the tribological performance much; they only slightly reduced the coefficient of friction of SU-8 and marginally improved wear durability. When tested at a normal load of 30 g and a rotational speed of 200 rpm, the SU-8+NP samples were found to have μ_i in the range of 0.35 to 0.77 and wear-lives ranging from zero to a few cycles.

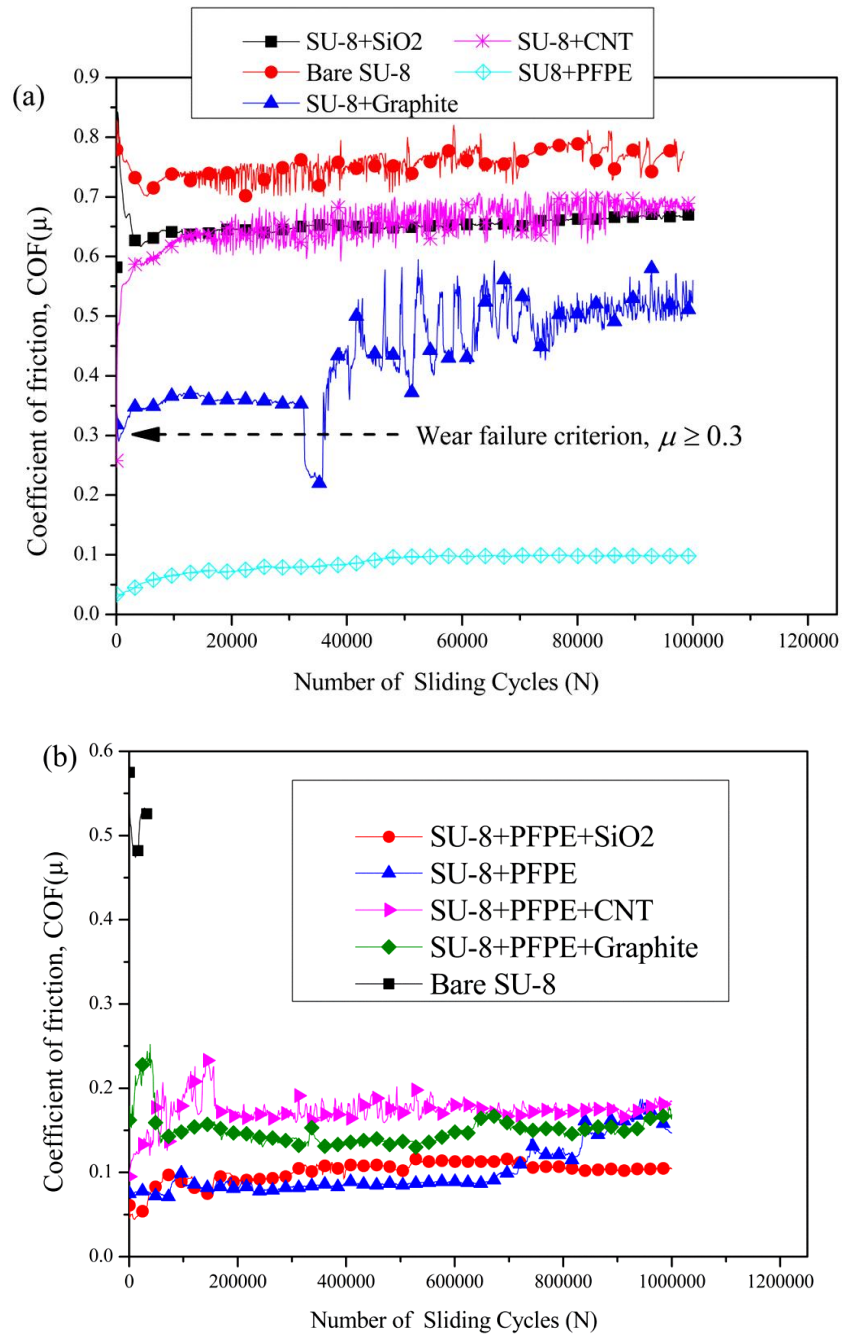


Figure 4.3: Coefficient of friction versus number of cycles plot for SU-8, SU-8+PFPE, SU-8+SiO₂, SU-8+CNTs and SU-8+graphite composites obtained from the ball-on-disk sliding tests against a 4 mm diameter Si₃N₄ ball at two different normal loads and sliding speeds: (a) A normal load of 30g and a rotating sliding speed of 200 rpm and (b) A normal load of 300 g and a rotating sliding speed of 2000 rpm. The tests were stopped at 1 million cycles because of the long test duration and the samples had not failed yet.

The presence of graphite seems to produce better effects on the coefficient of friction and wear life when compared to other nano-fillers (i.e CNTs and SiO₂). SU-8+PFPE+SiO₂ was shown to have a μ_i of 0.04, μ_s of 0.11 and a wear life (n) greater than 1,000,000 cycles. When compared with SU-8+PFPE, SU-8+PFPE+SiO₂ showed similar tribological performance and improved mechanical properties. SU-8+PFPE+CNTs was shown to have a μ_i of 0.11, μ_s of 0.17 and a wear life (n) of >1,000,000 cycles whereas SU-8+PFPE+graphite was shown to have a μ_i of 0.09, μ_s of 0.14 and a wear-life of >1,000,000 cycles. All three hybrid SU-8 composites have shown similar improvements in their tribological performance. The reason for the superior tribological performance of PFPE and the poor tribological performance of the nanoparticles will be elaborated in the following discussion section.

4.3.4 Discussion

Cross-linking is expected to improve in the SU-8+PFPE composite because of the etherification reaction between hydroxyl groups of PFPE and epoxy groups of SU-8 [François et al 2001, Tanaka et al. 1964, Surface coatings et al 1993]. The possible etherification reaction is depicted in Figure 4.4 (a). Currently, this reaction cannot be verified using XPS because the PFPE molecules themselves have ether linkages; hence, any ether linkage formed due to chemical bonding between PFPE and SU-8 cannot be shown exclusively. Another possibility is that the presence of OH functional groups in the PFPE polymer will interact with the carbocations (C⁺) in the SU-8 polymer (epoxide ring), hence, breaking the existing bond and forming a new linkage known as an ether bond.

It is postulated that the improved tribological properties of SU-8 hybrid composites are a result of the good cross-linking in the composites through ether bonds between SU-8 and PFPE. Also, the presence of lubricant throughout the composite matrix resulting in the supply of the lubricant on demand (in-situ supply), contributing to the maintenance of a thin PFPE film and improved bulk mechanical properties. It is also postulated that the PFPE molecules, SU-8 molecules and/or the nanoparticles might form some kind of cohesive 3D network which shows anti-wear properties and delay the initiation of the wear process unlike the case of pristine SU-8, whereby the wear particles are generated quite early in the sliding process.

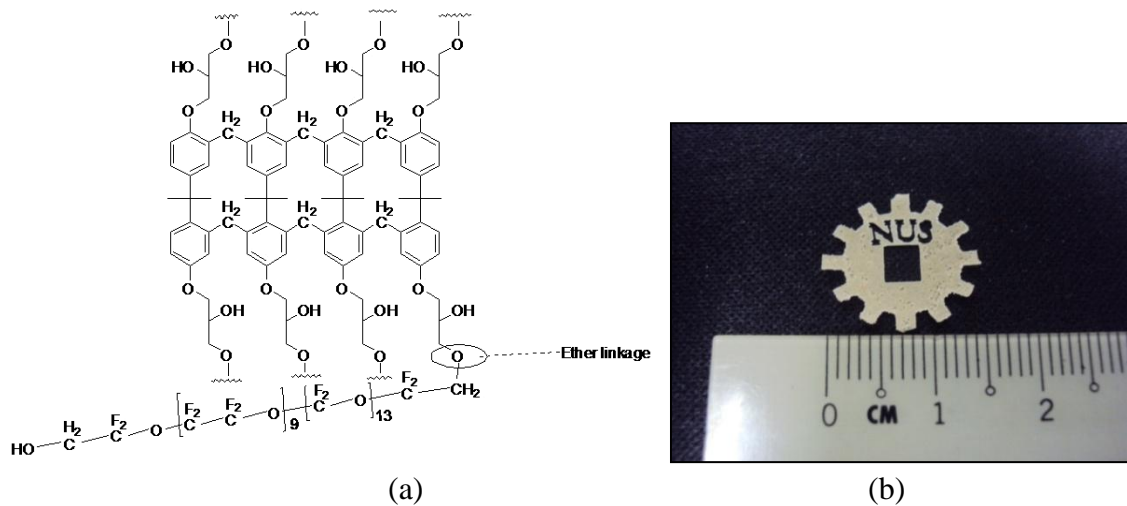


Figure 4.4: (a) A depiction of the cross-linking in the SU-8+PFPE composite through the formation of ether bonds. (b) A digital image of a 200 micron thick gear made of SU-8+PFPE composite, via the UV lithographic process.

Furthermore, the abundant amount of PFPE nanolubricant available in the sliding region reduces friction and eventually minimizes wear particle generation. When the wear process starts, the lubricant in the inside region will be exposed to the sliding contact and reduce further wear. Hence, the SU-8 hybrid composites have improved the

tribological properties to a large extent. From this study, it is not very clear whether or not the addition of nanoparticles played any role in enhancing the wear durability of SU-8+PFPE because the SU-8+PFPE and SU-8+PFPE+NP samples have shown the same wear-lives under the tested tribological conditions. Further work is necessary to elucidate the effect of nanoparticles on enhancing SU-8+PFPE wear durability. A millimeter-scale gear was fabricated (with letters: “NUS” on top of it) using the SU-8+PFPE composite via the UV-lithography process to demonstrate that the addition of PFPE does not deteriorate the photo-patternable property of SU-8. A digital picture of the fabricated gear is shown in Figure 4.4(b). This proves that the addition of PFPE does not affect or deteriorate the photo-patternable property of SU-8. In the current study, the improved tribological behaviour of SU-8 composites was also ascertained at the very low loads of 10g and 5g and at a high speed of 3000 rpm (data not included).

4.3.5 XPS and WCA (Water Contact Angle) of Worn Surfaces

Figure 4.1 shows the WCAs of all tested samples measured inside the wear tracks after an appropriate number of sliding cycles (after 100,000 cycles for SU-8 and SU-8+NP samples and after 1 million cycles for the remaining samples). As there was a distinct visible wear track after 1 million cycles of sliding in the case of all SU-8 composites, WCAs inside the wear tracks were measured for all tested samples and XPS characterization inside the wear track of SU-8+PFPE was carried out to qualitatively ascertain the extent of wear. In the case of the pristine SU-8, the WCA inside the worn region was about 30° less than that observed on the untested region. This can be

attributed to the removal of a large amount of SU-8 inside the wear track and an introduction of high energy new surfaces.

In the case of SU-8+NP samples, there was a reduction of about 29° - 31° of WCA inside the wear tracks, as compared to those on the untested regions, hence, also indicating a loss of material inside the wear track. However, for all the SU-8+PFPE+NP composites, there was either no change or an increase in the WCAs inside the worn regions, when compared to the corresponding WCAs on untested regions, thus clearly indicating very minimal loss of material inside the worn regions. The increase in the WCAs in the worn regions in the case of SU-8+PFPE+graphite and SU-8+PFPE+CNTs can be attributed to the sliding induced morphological changes inside the worn region. Section 2.3.3.1 Analysis of Contact Interface can be referred for the exact mechanism causing the increase in WCAs for both of these composites.

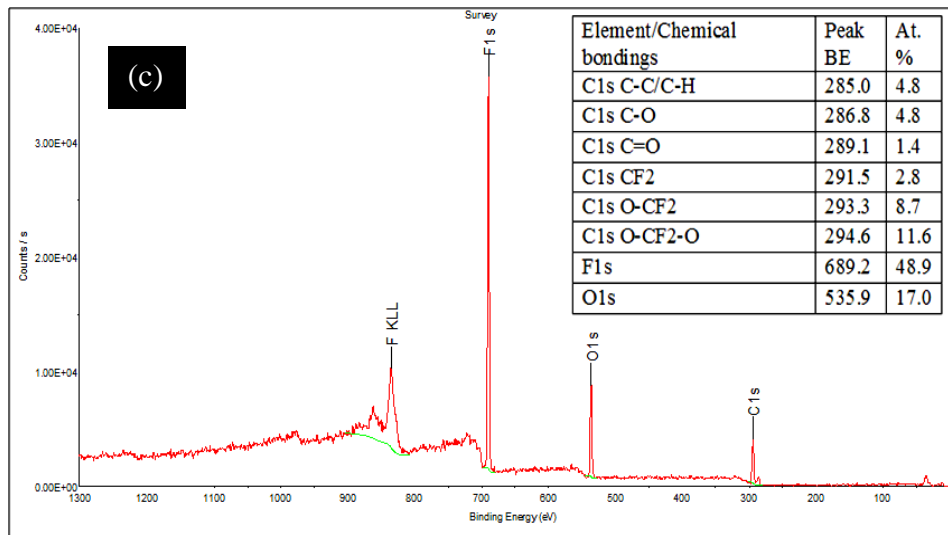


Figure 4.5: XPS Wide-scan survey spectrum results for the inside of the wear track of SU-8+PFPE composite after sliding for 1 million cycles at a normal load of 300g and a rotational speed of 2000 rpm.

The wide scan spectrum inside the worn region of the SU-8+PFPE sample after sliding for 1 million cycles at a normal load of 300 g and a rotational speed of 2000 rpm is shown in Figure 4.5 (the inset shows the major peaks observed with their bond assignments). The distinct F1s peak in the spectrum clearly shows the presence of PFPE inside the worn region, despite sliding for 1 million cycles under severe loading conditions. From this result, it can be inferred that the SU-8 hybrid composite samples still have an improved lubricous property withstanding beyond 1 million cycles.

4.3.6 Nano-Mechanical Characterization

The pristine SU-8 (Figure 4.6) has shown elastic modulus (E) and hardness (H) values of ~3.8 and ~0.27 GPa respectively whereas SU-8+PFPE has shown E and H of ~4 and ~0.32 GPa respectively. The improvement in mechanical properties of SU-8 caused by PFPE addition can be attributed to the chemical bonding between SU-8 and PFPE, which results in increased cross-linking.

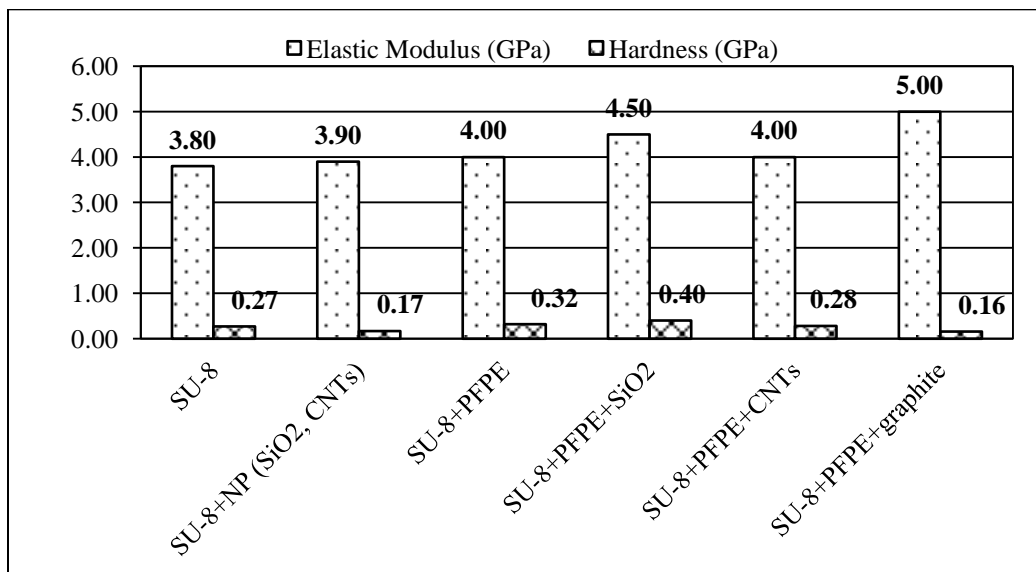


Figure 4.6: Elastic Modulus (E) and Hardness (H) values of pristine SU-8 and SU-8 composites from nano-indentation characterization.

SU-8+PFPE+SiO₂ has shown a H of ~0.4 GPa, which is a 40% increase in H. SU-8+PFPE+Graphite has shown an E of ~ 5 GPa, which is a 22% increase in E. Overall, mechanical properties such as the elastic modulus and hardness have increased by ~0.4 times. However, selection of the right composite depends entirely on the application (i.e. high hardness/modulus) requirements.

4.3.7 Optical Characterization of Worn Surfaces

Figure 4.7 shows the optical micrographs of the ball surface after sliding tests, the tested balls after cleaning with acetone and the optical images of worn surfaces after an appropriate number of sliding cycles. The optical images of SU-8 after 10,000 cycles shows severe damage to the surface, whereby the accumulation of wear debris along the wear track has also transferred to the ball (Figures 4.7 (a) and 4.7 (g) respectively). After sliding for 10,000 cycles (Figure 4.7 (m)), a slight wear of the ball was also observed after cleaning the ball with acetone.

After sliding for 1 million cycles at a normal load of 300 g and at a rotational speed of 2000 rpm, the SU-8+PFPE composite showed a distinct wear mark with some material transfer on the counterface ball, but with no wear to the ball surface (Figures 4.7 (c), 4.7 (i) and 4.7 (o)). After sliding for 10,000 cycles, the SU-8+NP samples showed severe wear to the sample surface as well as the ball surface (Figures 4.7 (b), 4.7 (h) and 4.7 (n)). Additionally, the SU-8+NP samples showed an E of 3.9 GPa and an H of 0.17 GPa respectively.

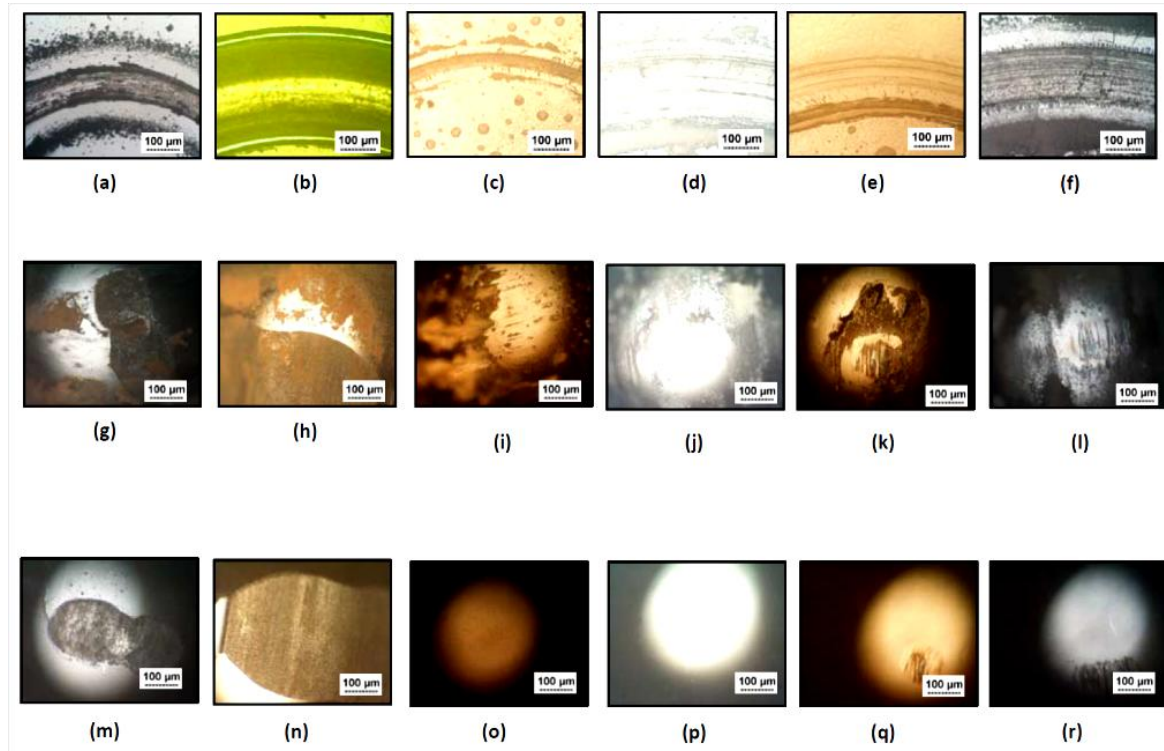


Figure 4.7: Optical micrographs of worn surfaces: (a) bare SU-8 (at 10,000 cycles), (b) SU-8+Nanoparticles (SiO_2 , CNT) (at 10,000 cycles), (c) SU-8+PFPE (at 1 million cycles), (d) SU-8+PFPE+CNTs (at 1 million cycles), (e) SU-8+PFPE+ SiO_2 (at 1 million cycles) and (f) SU-8+PFPE+graphite (at 1 million cycles). Corresponding to the worn surfaces shown in images (a), (b), (c), (d), (e) and (f), images (g), (h), (i), (j), (k) and (l) are optical micrographs of the counterface balls' surface after sliding tests whilst images (m), (n), (o), (p), (q), and (r) are micrographs of the tested counterface balls after cleaning with acetone. The length of the scale bar is 100 μm in all images.

For these three SU-8 hybrid composites, there was a distinct wear track with the generation of transfer material on the counterface ball but no wear to the ball surface (Figures 4.7 (d-f), 4.7 (j-l) and 4.7 (p-r)). It is clear that the high coefficient of friction and brittle nature of SU-8 (SU-8 being a thermoset, exhibits brittleness in its fully cross-linked state) leads to the generation of wear particles within the first cycle of sliding and the probability that the sliding process will change from two-body to three-body sliding which will eventually accelerate the wear process.

4.4 Conclusions

Self-lubricating SU-8 hybrid composites have been developed using in situ nanolubricant (PFPE) and nanoparticles (SiO₂, CNTs and graphite as filler materials). The developed SU-8 composites are hydrophobic (with a maximum water contact angle of 106° for SU-8+PFPE+SiO₂), highly lubricous and have exceptional wear durability without any detrimental effect on their photo-sensitive curing property. When compared with pristine SU-8, the SU-8+PFPE and SU-8+PFPE+nanoparticle composites have reduced the initial coefficient of friction by ~6-9 times, increased the wear life by >104 times and increased the elastic modulus and the hardness by ~0.4 times.

The presence of PFPE film at the interface due to in situ lubricant supply is the main reason for superior tribological performance, whereas the nanoparticles help in the mechanical property enhancement. The chemical bonding between SU-8 and PFPE molecules were partially verified by XPS and water contact angle characterizations indirectly. These SU-8 composites can be used as self-lubricating structural materials for MEMS, requiring no external lubrication. Apart from this, the SU-8 composite can also find application as a lubricous and wear resistant coating for several tribological components made from different materials. Examples are journal bearings, raceways of a ball bearing, gears, medical equipments and tools, bio-devices, precision positioning stages, electronics components such as those inside cameras and printers, plastic bearings, etc.

Chapter 5

Chemical Bonding in SU-8 Composites

This chapter presents an extensive investigation of the chemical bonding between SU-8 and PFPE molecules in self-lubricating SU-8 composites. The same chemical interaction as surmised and postulated in the previous chapter will be ascertained using various characterizations.

5.1 Introduction

In the previous chapter, it was postulated that the tribological properties of SU-8 composites were improved due to good cross-linking through ether bonds between SU-8 and PFPE, in addition to a uniform presence of lubricant droplets throughout the composite matrix which results in the supply of lubricant in-situ and improved mechanical properties. The exact nature of the chemical interaction between the lubricant and SU-8 still needs further investigation with different types of lubricants.

Therefore, two other lubricants namely, base oil (SN 150) and multiply-alkylated cyclopentane (MAC), were selected for the purpose of investigating their effects on the tribological properties of SU-8 when they are added as filler materials. The properties of these two composites (i.e. SU-8+SN 150 and SU-8+MAC) have been compared with the SU-8+PFPE composites obtained under the same testing conditions. The lubricants in both the SU-8+SN 150 and SU-8+MAC composites are alkanes, chemically inert and have no polar reactive terminal groups unlike PFPE which has –OH polar terminal groups [www.solvayplastics.com/]. SN 150 is a chemically inert alkanes-based base oil

lubricant [www.chevron.com/]. This base oil is a part of the paraffinic alkane oils, synonymous to mineral oil. The general chemical formula for alkanes is C_nH_{2n+2} whereby for the base oil, the carbon ranges from C_{15} to C_{40} . Hence, the chemical structure of the base oil ranges between $C_{15}H_{32}$ to $C_{40}H_{82}$ and has a relatively lengthy molecular chain with non-polar CH_3 end groups. The SN 150 is expected to increase the hydrophobic behaviour of SU-8 due to the absence of polar chemical groups. Also, the base oil is very cheap and industrially attractive for economical production of the composites.

Multiply-alkylated cyclopentanes (MACs) [www.nyelubricants.com/] are novel alkane lubricants, composed of one cyclopentane ring with about 2 to 5 alkyl groups substituted on the ring. MACs are synthesized by reacting dicyclopentadiene with alcohols of various lengths, which produces a lubricant with selectable range of physical properties [Venier et al 1991]. MACs have been identified as suitable lubricants for space applications [Cutler et al 2000, Dube et al 2003, Gill et al 2010, Ohno et al 2010] and MEMS (micro-electro mechanical systems) lubrication purposes [Ma et al 2007 & 2009, Wang et al 2010].

Therefore, we have selected the MAC lubricant for comparison with PFPE and the SN 150 base oil in terms of their effectiveness in improving the tribological properties of SU-8 when used as a filler material. Lubricants were initially added at 10 wt% but since tribological tests have shown equally good wear durability behaviour for all the three composites (i.e. SU-8+PFPE, SU-8+SN 150 and SU-8+MAC), the lubricants were subsequently added at a lower weight percent (2%) to experimentally distinguish their wear durability performances. The tribological results were interpreted in terms of the chemical and/or physical interactions between the lubricant and SU-8 molecules. The

worn surfaces were subjected to optical and electron microscopy observations, XPS characterization and surface energy measurements and analysis. Based on the tribological properties observed, a physical explanation of the self-lubricating behaviour is proposed and explained.

5.2 Materials and Experimental Procedures

The physical and chemical properties of SU-8 2050, perfluoropolyether, base oil SN 150 and MAC lubricants have already been presented in Chapter 3. A comprehensive comparison between the physical properties of the lubricants is illustrated below in Table 5.1.

Table 5.1: Composite nomenclature, compositional description, category and grade of all SU-8 composites

| Composite Nomenclature | Compositional Description | Chemical Category | Grade and Manufacturer | Lubricant solvent | Kinematic Viscosity (Cst) at 40°C |
|------------------------|---|---------------------|--|------------------------|-----------------------------------|
| SU-8+PFPE | SU-8 blended with perfluoropolyether (PFPE) | Fluoro carbon based | Z-DOL 4000, Fomblin | H- Galden (grade SV55) | 18 |
| SU-8+SN 150 | SU-8 blended with SN150 grade base oil | Hydro carbon based | Paraffinic based SN 150, Chevron | n-Hexane | 23 |
| SU-8+MAC | SU-8 blended with multiply-alkylated Cyclopentane (MAC) Oil | Hydro carbon based | MAC based synthetic oil 2001A, Pennzoil lubricants | n-Hexane | 108 |

[Ref. – PFPE: www.solvayplastics.com/; MAC: <http://www.nyelubricants.com/>; SN 150: <http://www.chevron.com/>];]Bottom of Form

The sample preparation procedures from sizing the Si wafer substrates to obtaining completely cured SU-8 and SU-8 composites film and other characterizations have been detailed in Chapter 3. The two lubricant concentrations used in this chapter are 2 wt% and 10 wt%.

5.3 Results and Discussion

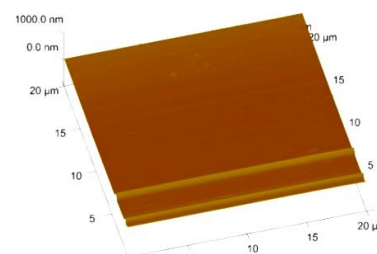
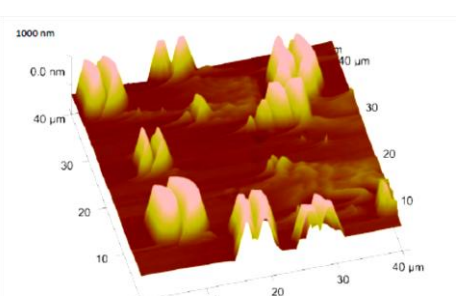
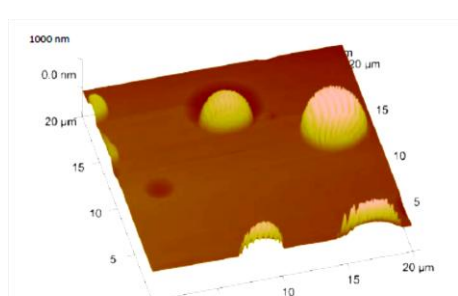
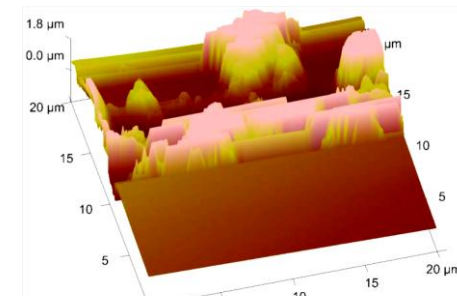
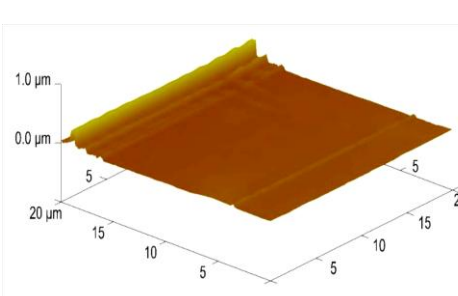
5.3.1 AFM Surface Images

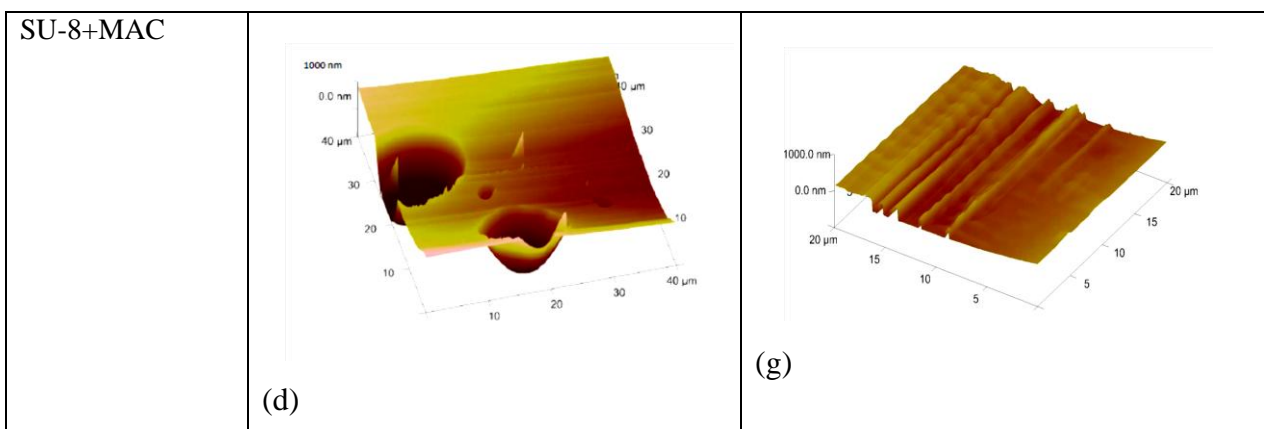
Table 5.2 shows the AFM images of the pristine SU-8 and freshly spin-coated 2 wt% SU-8 composites, before and after washing respectively. In Table 5.2, the ‘before washing’ column shows the surfaces of freshly spin-coated pristine SU-8 and SU-8 composites (in their prepared condition). Pristine SU-8 shows a plain and featureless surface (Image (a)), whereas SU-8+PFPE (Image (b)) shows a proper dispersion of lubricant droplets over the surface without any agglomeration. SU-8+SN 150 (Image (c)) shows a poor dispersion of lubricant droplets with agglomeration, whilst the SU-8+MAC composite (Image (d)) shows cavities without any lubricant droplets. The lubricant in those cavities gets agglomerated and appears as a bigger droplet over the surface. If the lubricant is not present to lower the shear stresses, cavities over the surface can act as a stress raiser to promote wear towards catastrophic failure.

Subsequently, the SU-8 composite surfaces were washed with their respective solvents: H-Galden for PFPE and n-Hexane for SN 150 and MAC. The objective for washing is to check whether the droplets present on the surface were chemisorbed on the surface or physically bonded with the surface. AFM imaging for all the SU-8 composites

after washing can be observed under the ‘after washing’ column in Table 5.2 (Images (e), (f) and (g)) for SU-8+PFPE, SU-8+SN 150 and SU-8+MAC respectively.

Table 5.2: AFM images of freshly spin-coated Pristine SU-8 and 2wt% SU-8 composites surfaces before and after washing. **Before washing:** (a) Pristine SU-8, (b) SU-8+PFPE, (c) SU-8+SN 150 and (d) SU-8+MAC. **After washing:** (e) SU-8+PFPE, (f) SU-8+SN 150 and (g) SU-8+MAC.

| Composite Description | Conditions | |
|-----------------------|---|--|
| | Before Washing | After Washing |
| Pristine SU-8 | (a)  | |
| SU-8+PFPE | (b)  | (e)  |
| SU-8+SN 150 | (c)  | (f)  |



For SU-8+PFPE, the uniformly distributed PFPE droplets remained present on its surface, even after washing. However, both SU-8+SN 150 and SU-8+MAC showed plain surfaces with insignificant residual lubricant film after washing. These AFM images indicate that the PFPE molecules may have undergone chemical bonding with SU-8, since the micro-features of PFPE are reflected in SU-8. These observed features above have a strong effect on the tribological properties of the composites which will be discussed later.

5.3.2 Surface Free Energy Calculations (Freshly cured (as prepared))

Surface free energy values for freshly spin-coated surfaces of pristine SU-8 and 2 wt% SU-8 composites were calculated as shown in Figure 5.1. Since pristine SU-8 shows the highest surface free energy of 32.64 mN/m, it offers the greatest adhesion and friction followed by SU-8+MAC, SU-8+SN 150 and SU-8+PFPE which show surface free energies of 29.42, 27.96 and 24.14 mN/m respectively. Also, whilst the three SU-8 composites show a polar surface energy ranging from 2.54 to 3.92 mN/m, the pristine SU-8 shows a polar surface energy of 12 mN/m. This high polar nature of pristine SU-8 makes the surface much more hydrophilic than the other composites. The high polar

component of the surface free energy in pristine SU-8 also leads to high adhesion and friction.

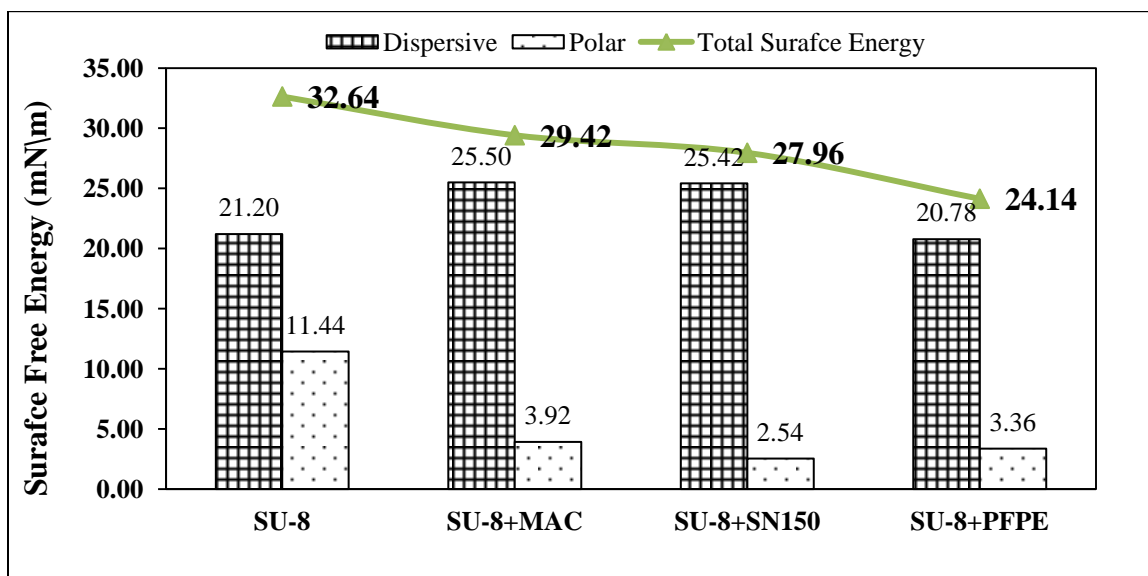
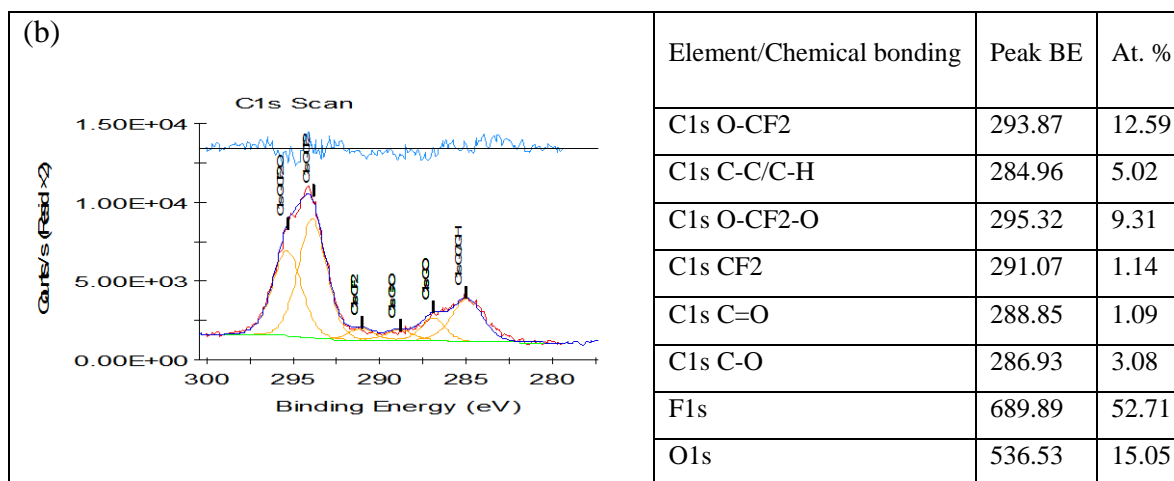
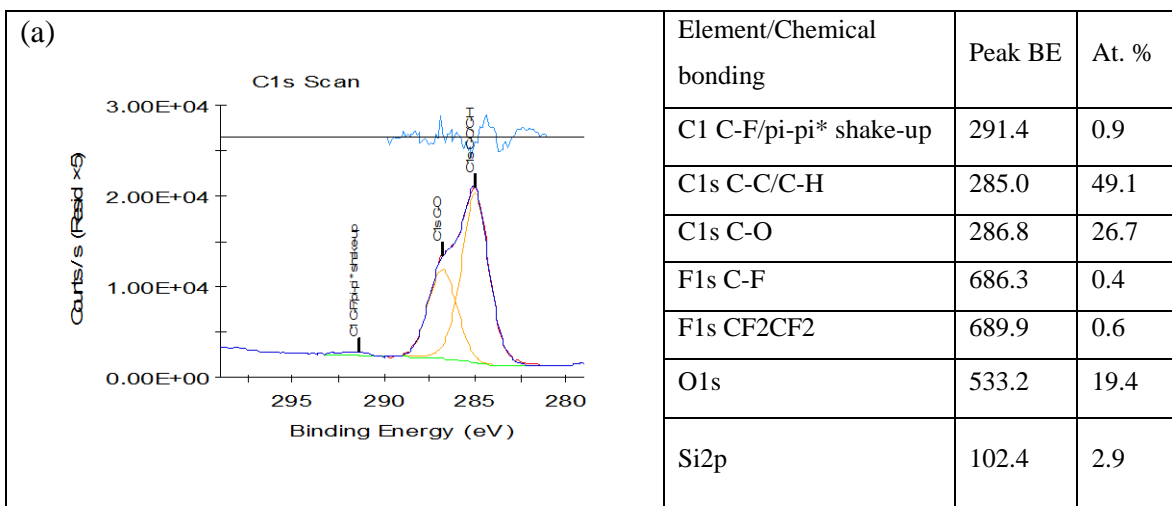


Figure 5.1: Polar, dispersive and total surface energies at the freshly spin-coated surface of pristine SU-8 and 2 wt% SU-8 composites

5.3.3 XPS Characterization (on fresh surface)

Figures 5.2(a), (b), (c) and (d) show the atomic percentage (At%) table (tables are on the right side of the scan) and C1s scan of pristine SU-8, SU-8+PFPE, SU-8+SN 150 and SU-8+MAC samples respectively. Since the pristine SU-8 is an organic polymer, C-C/C-H forms its major chemical groups, followed by C-O. The At% table of SU-8+PFPE in Figure 3(b) shows the new groups of O-CF₂, O-CF₂-O and CF₂, which confirms the presence of PFPE, since none of these chemical groups are present in pristine SU-8 (At% table of Figure 5.2(a)). The (C-C/C-H)/C-O ratio was reduced from 1.8 for pristine SU-8 to 1.6 for SU-8+PFPE, thus indicating the possibility of chemical interaction between the SU-8 and PFPE molecules. However, the chemical reaction cannot be confirmed since the C-O bond appears in PFPE as well.

Figure 5.2(c) shows the At.% table and C1s scan for SU-8+SN 150. Since SN 150 is a alkane lubricant, the only difference that can be seen in the At% table is that there is an increase in atomic percentages of C-C/C-H chemical groups to 67 from 49 for pristine SU-8. The ratio of (C-C/C-H) / C-O have also increased to ~3.9 from ~1.83 for pristine SU-8, thus confirming the presence of base oil SN 150. Figure 5.2(d) shows the At% table and C1s scan for SU-8+MAC, which is also a alkane lubricant but the only difference that can be seen in the At% table is that there is an increase in the atomic percentages of C-C/C-H chemical groups to 77 from 49 for pristine SU-8.



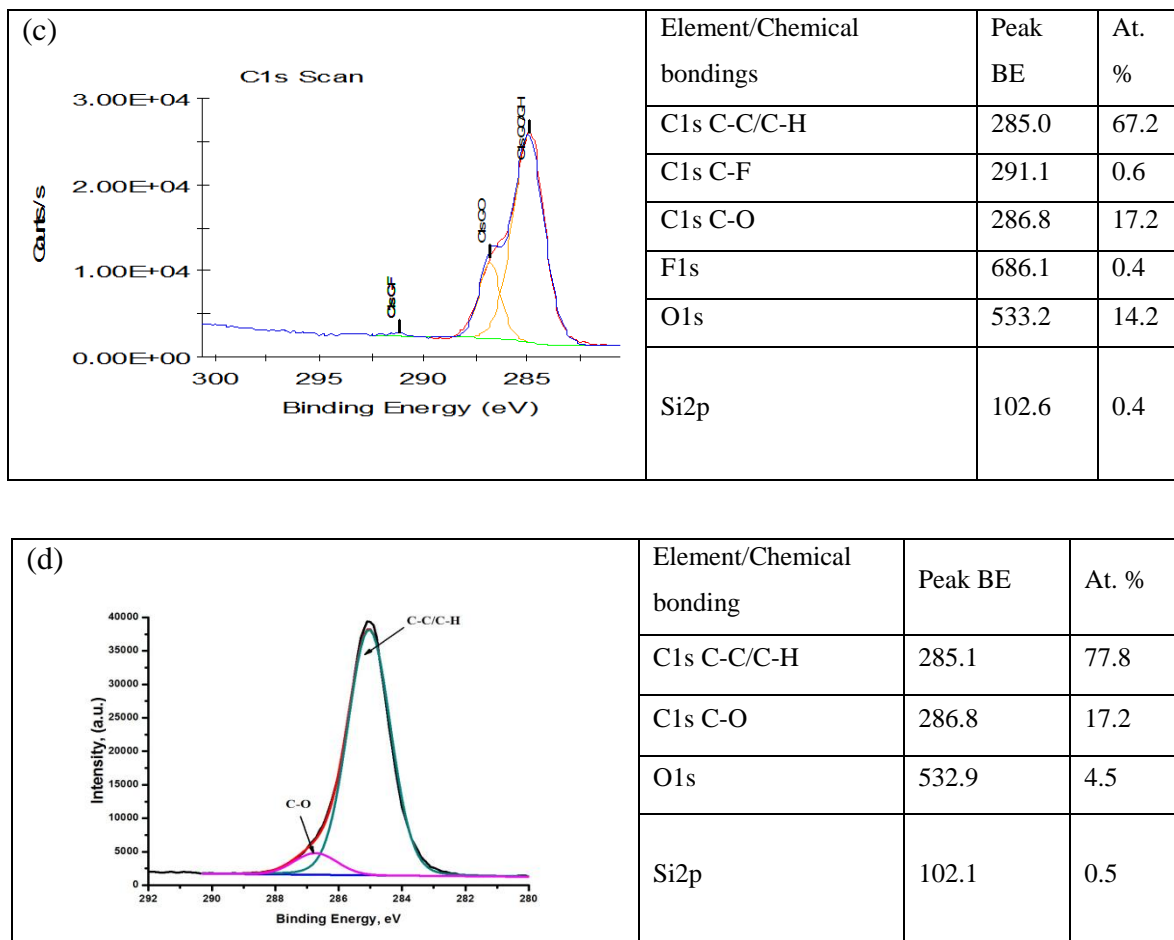


Figure 5.2: XPS analysis *C1s* scan (left) and *At%* table (right) for pristine SU-8 and 2 wt% SU-8 composites at freshly spin-coated surfaces. (a) Pristine SU-8. (b) SU-8+PFPE. (c) SU-8+SN 150. (d) SU-8+MAC.

The ratio of (C-C/C-H) / C-O increases to ~4.5 from ~1.83 for pristine SU-8. This clearly shows the dominance of the MAC lubricant over the presence of both SU-8 and MAC's presence.

5.3.4 Tribological Characterization

The tribological test results for pristine SU-8 and 10 wt% SU-8 composites, tested at a normal load of 300 g and a sliding rotational speed of 2000 rpm until 1,000,000 (1 million) sliding cycles are summarized in Table 5.3 (top half) and were obtained from the coefficient of friction (CoF) versus number of sliding cycles (N) plots shown in Figure 5.3(a). Pristine SU-8 showed a low wear life ($n \sim 10$) with a high initial and steady-state coefficient of friction of $\mu_i \sim 0.55$ and $\mu_s \sim 0.52$ respectively. In comparison, SU-8+PFPE showed $\mu_i = 0.08$ and $\mu_s = 0.07$, SU-8+SN 150 showed $\mu_i = 0.14$ and $\mu_s = 0.13$ and SU-8+MAC showed $\mu_i = 0.08$ and $\mu_s = 0.07$. These three composites have shown a high wear durability of $>1,000,000$ (experiments were stopped after 1 million cycles due to long test duration), which is several orders of magnitude higher than that for pristine SU-8. In order to make a clear difference between the wear lives of the three composites, the lubricant concentration was reduced to 2 wt% and the new composites with 2 wt% lubricant were subsequently subjected to tribological tests.

The bottom half of Table 5.3 shows the initial coefficient of friction (μ_i), steady-state coefficient of friction (μ_s) and the wear lives of pristine SU-8 and 2 wt% SU-8 composites tested at a normal load of 100 g and a rotational speed of 1000 rpm, respectively. The tribological data summarized in Table 5.3 were obtained from these plots in Figure 5.3(b). The pristine SU-8 film showed high frictional coefficients ($\mu_i = 0.19$ and $\mu_s = 0.35$) and low wear life ($n = 500$) whereas SU-8+PFPE showed low frictional coefficients with $\mu_i = 0.12$ and $\mu_s = 0.11$ and a wear life of $n > 500,000$. SU-8+SN 150 also showed low frictional coefficients ($\mu_i = 0.15$ and $\mu_s = 0.2$) and a moderate

wear life ($n \sim 270,000$), whereas SU-8+MAC showed low frictional coefficients ($\mu_i = 0.13$ and $\mu_s = 0.09$) and a low wear life ($n \sim 100,000$).

Table 5.3 : Initial coefficient of friction (μ_i), Steady-state coefficient of friction (μ_s) and wear life (number of sliding cycles) of pristine SU-8 and SU-8 composites obtained from sliding tests against a 4 mm diameter Si_3N_4 ball at different normal loads and sliding rotational speeds.

| Composite Description | Initial coefficient of friction, COF (μ_i) | Steady- state coefficient of friction, COF (μ_s) | Wear Life (Number of Cycles, N) |
|---|--|--|---------------------------------|
| 10wt% SU-8 composites /Test Parameter: 300g, 2000rpm | | | |
| Pristine SU-8 | 0.55 | 0.52 | ~ 10 |
| SU-8+PFPE | 0.08 | 0.07 | $>1,000,000$ |
| SU-8+SN150 | 0.14 | 0.13 | $>1,000,000$ |
| SU-8+MAC | 0.08 | 0.07 | $>1,000,000$ |
| 2wt% SU-8 composites /Test Parameter: 100g, 1000rpm | | | |
| Pristine SU-8 | 0.19 | 0.35 | 500 |
| SU-8+PFPE | 0.12 | 0.11 | $>500,000$ |
| SU-8+SN 150 | 0.15 | 0.2 | $\sim 270,000 \pm 3,000$ |
| SU-8+MAC | 0.13 | 0.09 | $\sim 100,000 \pm 7,000$ |

Since pristine SU-8 has very poor tribological properties in nature, these composites (even with only 2 wt% of lubricants) have not only enhanced its wear life by several folds but have also reduced the coefficients of friction. SU-8+PFPE, SU-8+SN 150 and SU-8+MAC have enhanced the wear life of pristine SU-8 by >1000 , ~ 500 and ~ 200 times, respectively and have also, approximately reduced the initial (μ_i) and steady-state coefficient friction (μ_s) by ~ 2 and $\sim 2-4$ times respectively.

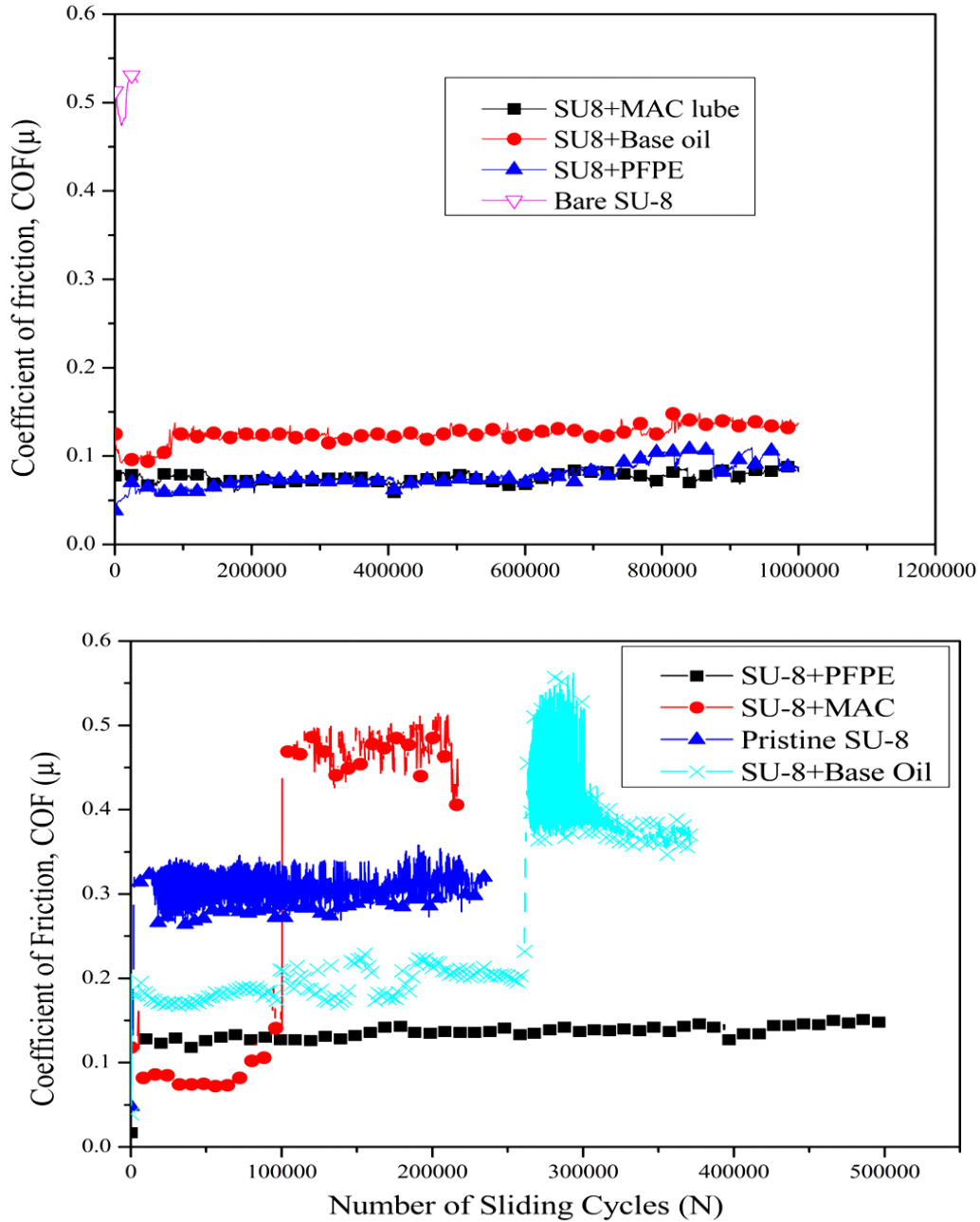


Figure 5.3: Typical coefficient of friction versus number of sliding cycles plot for pristine SU-8 and SU-8 composites obtained from the ball-on-disk sliding tests against a 4 mm diameter Si_3N_4 ball at different normal loads and sliding speeds. (a) Pristine SU-8 and 10 wt% SU-8 composites tested at a normal load of 300g and a sliding speed of 2000 rpm. The tests were stopped after 1 million cycles without any failure by the composites. (b) Pristine SU-8 and 2 wt% SU-8 composites tested at a normal load of 100g and a sliding speed of 1000rpm.

The reason for this high wear life enhancement will be discussed in the following sections. However, it should be noted that the SU-8+PFPE composite outperforms the other two composites even when the wt% of the lubricant is reduced to 2 wt%.

5.3.5 Surface Free Energy Calculations (Worn Surface)

Figure 5.4 shows the surface free energies at the wear tracks (worn surface) of pristine SU-8 and 2 wt% SU-8 composites after 500,000 sliding cycles at a normal load of 100 g and sliding speed of 1000 rpm respectively. The pristine SU-8 shows the highest total surface free energy of 49.48 mN/m, which is 17 mN/m more than the total surface free energy at fresh surface. This high surface free energy can be highly attributed to the polar component of the surface energy of 26.1 mN/m, which is 15 mN/m more than the polar surface energy of 11.4 mN/m at fresh surface.

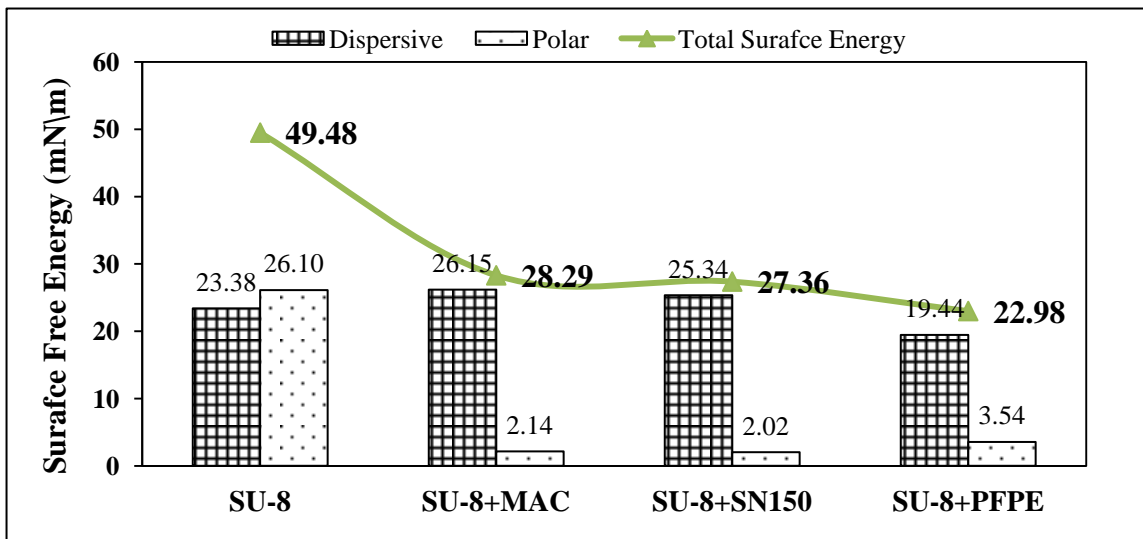


Figure 5.4: Polar, dispersive and total surface energies at the wear track (worn surface) of pristine SU-8 and 2 wt% SU-8 composites after 500,000 sliding cycles.

The surface of pristine SU-8 is polar in nature but after tribological testing, the new worn-out surface showed a much higher surface energy than that for the fresh one, due to unsatisfied, broken bonds over the surface [Dalvi et al 2010]. Hence, the polar component becomes highly dominant over the dispersive component and makes the surface highly hydrophilic. For the SU-8 composites, the surface remains hydrophobic with a distinct wear track after tribological testing. For both SU-8+SN 150 and SU-8+MAC, their surface free energy remains similar for the fresh surface; with minimal change because of the formation of a boundary layer which covers the surface with enough lubricant. The SU-8+PFPE wear track showed a surface free energy of 22 mN/m which is 2 mN/m lesser than that for its fresh surface. This reduction is probably due to the complete coverage of the wear track by fluorinated PFPE molecules in contrast to the fresh surface, whereby the boundary lubrication further confirms the presence of lubricants inside the matrix. The SU-8+PFPE wear track also showed a marginal increase in polar surface energy due to the unbounded PFPE available at the surface.

5.3.6 Physical Boundary Self- Lubrication Mechanism

Figures 5.5 (a) to (d) show the SEM cross-sectional images of pristine SU-8, SU-8+PFPE, SU-8+SN 150 and SU-8+MAC. Since all the composites exhibit the characteristic of self-lubrication, it can be argued that the physical boundary layer lubrication may become the source for their prolonged wear life. Before curing and UV exposure, the composite resin is in the gluey state and the SU-8 matrix has lubricant (PFPE, SN 150 and MAC) droplets of sizes ranging from a few nm to μm dispersed throughout its matrix [Prabakaran et al 2013 (b)]. After UV exposure and curing, the SU-

8 undergoes cross-linking and becomes solid. As the lubricant remains unaffected by UV radiation, the droplets remain trapped inside the solid SU-8 bulk. This trapped lubricant in the tiny cavities gives the advantage of storing lubricants for self-regeneration and lubrication. The SEM cross-sectional images show that the pristine SU-8 cross-section surface has no lubricant cavity. Amongst the three composites, SU-8+PFPE has a better distribution of PFPE droplets; it has a much smaller and more uniform droplet size than the other two composites.

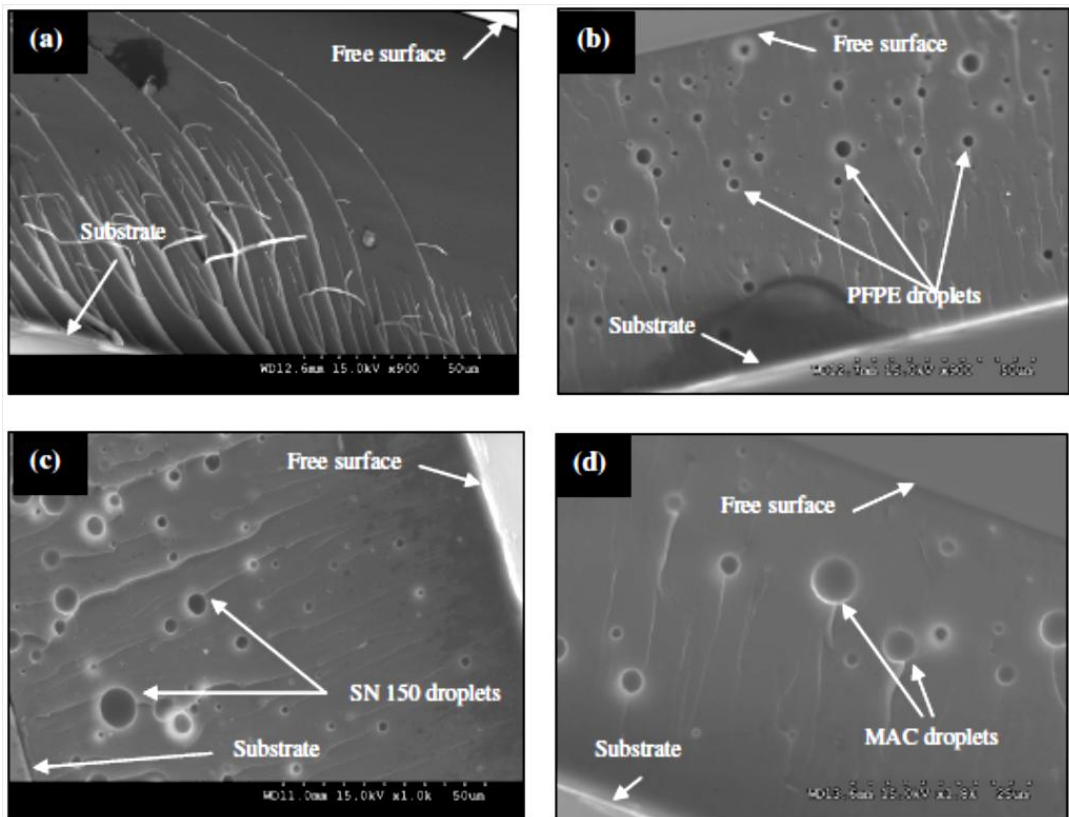


Figure 5.5: SEM cross-sectional images of $\sim 100 \mu\text{m}$ thick pristine SU-8 and 2 wt% SU-8 composite films. (a) Pristine SU-8 (b) SU-8+PFPE (c) SU-8+SN 150 (d) SU-8+MAC.

At the beginning of the test, the SU-8 composites have some lubricant droplets over the surface to provide resistance against friction and wear. Once the lubricant layer

over the surface has worn away with counterface sliding, the lubricant droplets beneath the worn surface are released to form the boundary layer that reduces friction and wear. This same cycle is repeated until the composite completely wears out. This model also emphasizes that the tribological performance of the composites is dependent on the uniform dispersion of the lubricants. Although the function of the physical mechanism has been well depicted by SEM images earlier, it is further supported by some additional tribological tests to confirm the presence of lubricants inside the matrix. The surfaces of all SU-8 composites were washed with their respective solvents and tribological tests were performed over the washed surfaces.

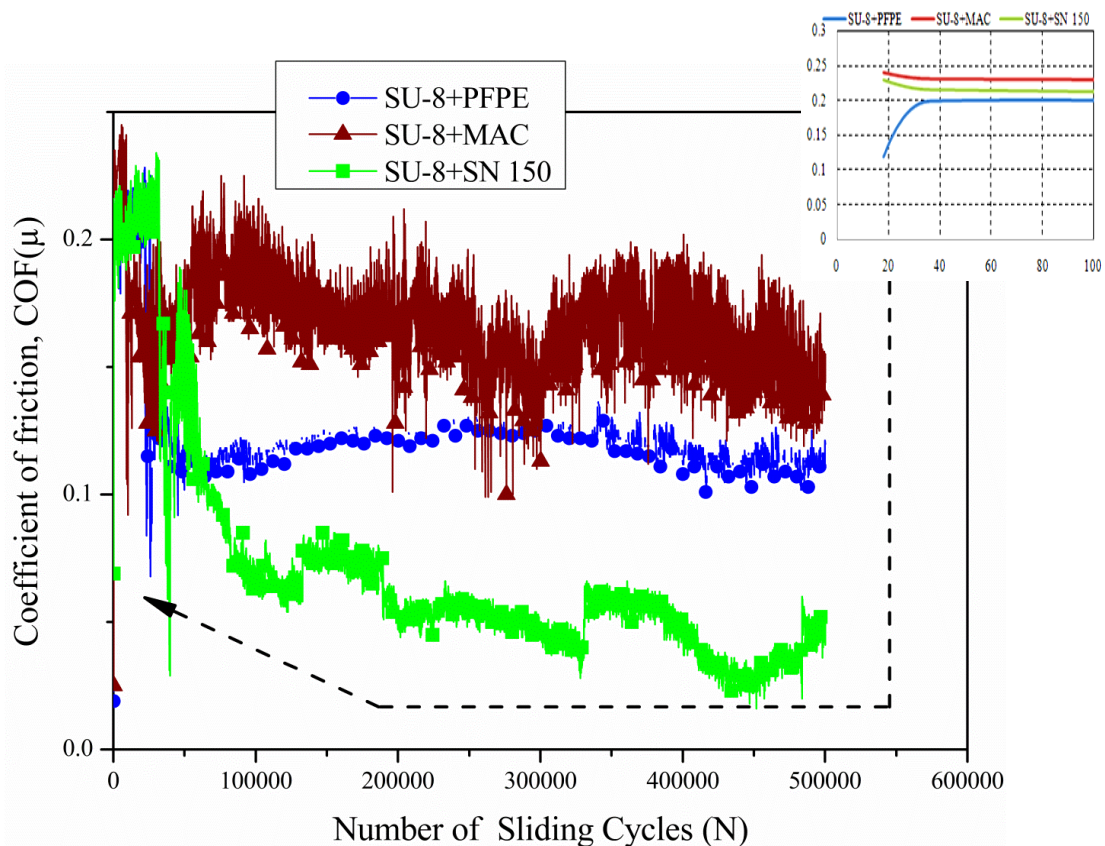


Figure 5.6: Coefficient of friction versus number of cycles plot for washed 10 wt% SU-8 composites obtained from the ball-on-disk sliding tests against a 4 mm diameter Si_3N_4 ball at a normal load of 300 g and a sliding speed of 1000 rpm

From the AFM images of the washed surfaces shown in Table 5.2 earlier, all the washed surfaces were deprived of lubrication except for SU-8+PFPE. The washed 10 wt% SU-8 composites were tested at a normal load of 300 g and a sliding speed of 1000 rpm and their corresponding coefficient of friction vs number of sliding cycles (N) plots can be seen in Figure 5.6. The initial coefficient of friction (μ_i) values for all composites can also be seen in the inset in Figure 5.6. SU-8+PFPE has shown a high initial friction coefficient (μ_i) of ~ 0.19 and a steady-state friction coefficient (μ_s) of 0.12 with a visible wear track (signs of a worn surface).

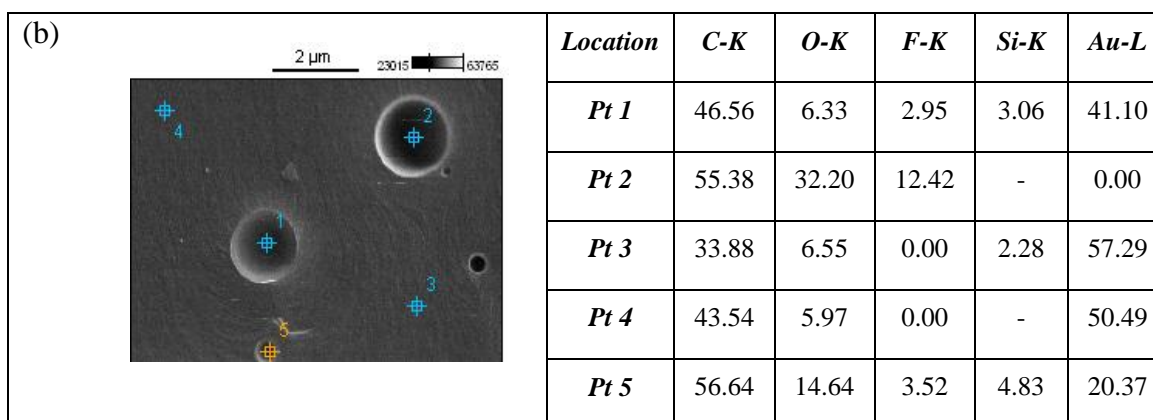
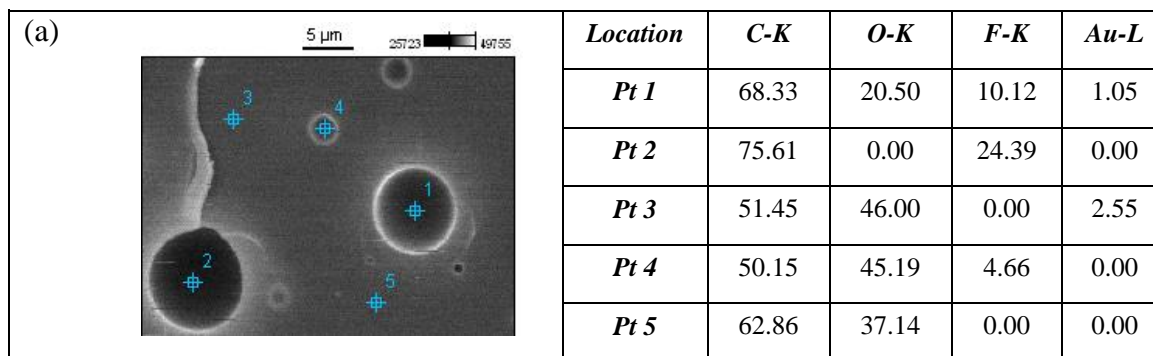
The low initial coefficient of friction not only supports the presence of PFPE lubricant over the surface even after washing. It also shows that a portion of the lubricant has been chemically bonded over the surface because a slight increase in μ_i from the fresh surface and a sudden decrease in μ_s supports the physical boundary layer lubrication mechanism. For SU-8+SN 150, it showed a high initial friction coefficient (μ_i) of ~ 0.23 and a steady-state friction coefficient (μ_s) of ~ 0.07 with a distinct severely worn wear track which has almost reached up to the substrate. Interestingly, although the composite film had failed rapidly like the pristine SU-8 film, the coefficient of friction remained low till the end of the test. This unusual tribological behaviour of SU-8+SN 150 with high friction at the beginning and a sudden drop to low friction after initial wear clearly indicates that the lubricant was indeed present inside the matrix.

SU-8+MAC showed a high initial friction coefficient (μ_i) of ~ 0.24 and a steady-state friction coefficient (μ_s) of ~ 0.15 with a severely worn wear track which almost reached up to the substrate. It also exhibited a tribological trend similar to SU-8+SN150, as explained earlier. The lower initial coefficient of friction for SU-8+PFPE surface after

washing proves that some PFPE molecules do indeed chemically bond with SU-8 during cross-linking. The nature of the interfacial tribology after washing is that once the wear process is initiated, the wear debris will immediately be caught in between the sliding bodies and will hasten the process of surface failure. Although the lubrication occurs after initial wear and the wear rate is reduced considerably, this may not stop the surface failure.

5.3.7 EDS Characterization

Energy dispersive X-ray spectroscopy (EDS) characterization was carried out at random locations on the cross-sections of the pristine SU-8 and 2 wt% SU-8 composites. Although the cross-sectional SEM images of the SU-8 composites in a preceding section showed cavities in their matrices, it is necessary to confirm the lubricant's presence in those cavities.



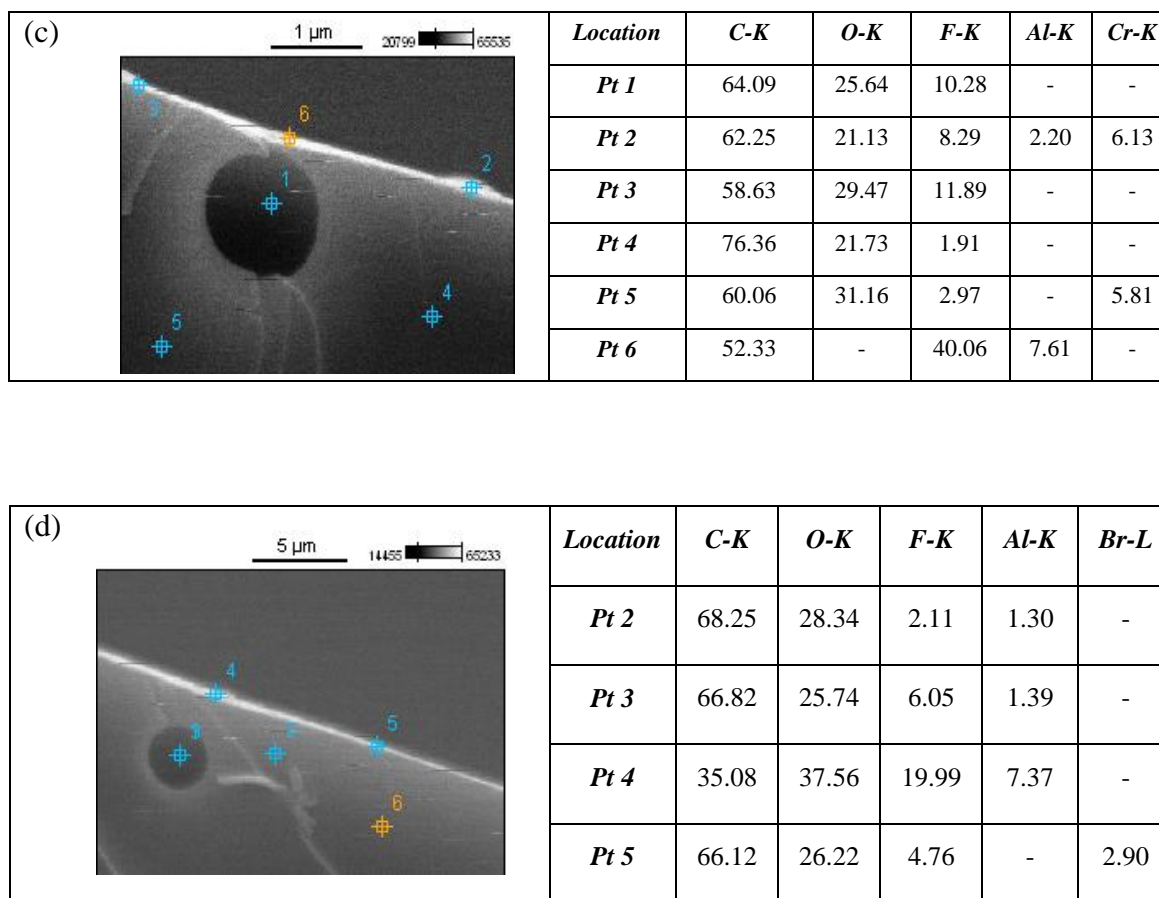


Figure 5.7: Cross-sectional SEM images of SU-8+PFPE and the corresponding EDX atomic percent (At. %) table. (a) SU-8+PFPE before washing. (d) SU-8+PFPE after washing. (c) PFPE layer at surface before washing. (d) PFPE layer at surface after washing.

Pristine SU-8, SU-8+SN 150 and SU-8+MAC did not show any distinct chemical compounds corresponding to SN 150 and MAC. This is obviously because SU-8, SU-8+SN 150 and SU-8+MAC are alkanes comprising of only C and H. Figures 5.7 (a) to (d) show cross-sectional SEM images (on the left) depicting the random locations of EDS analysis and the corresponding atomic percentages (At.%) are shown in the tables on the right. Figure 5.7(a) shows an EDS analysis at five random locations of SU-8+PFPE before washing. Locations 1, 2 and 4 on the cavities show higher fluorine (F) At% than in

comparison to locations 3 and 5 on the SU-8 surface. The reason for the difference in F At% between the cavities can be attributed to the removal of chemically unbounded PFPE. SU-8+PFPE was washed in H-Galden SV55 using ultrasonication for about 1 hour and the same step was repeated thrice for thorough washing before subjecting it to EDS analysis. It is observed from the results in Figure 5.7 (b) that although more than 60% of PFPE was washed away, a portion of the PFPE has chemically bonded with SU-8.

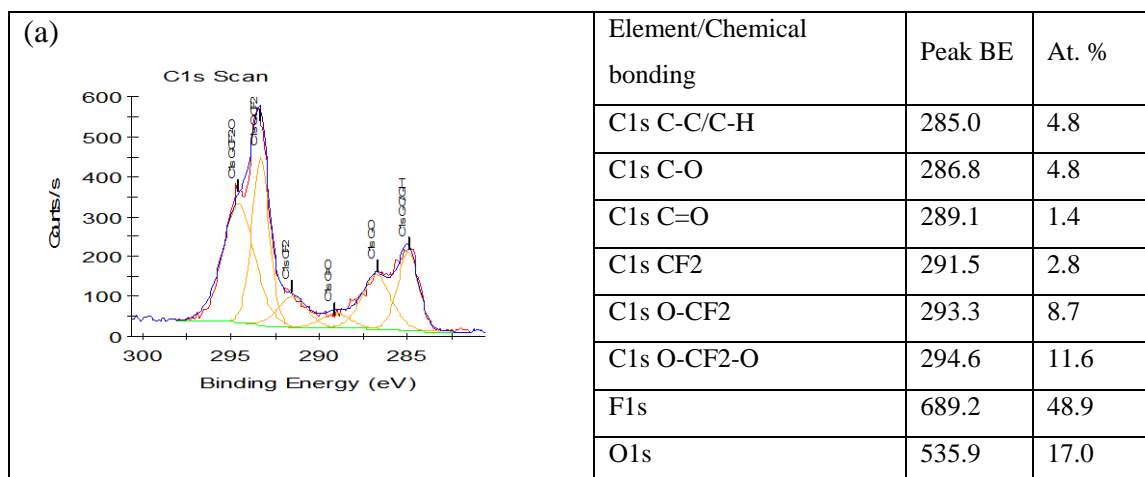
A PFPE layer was detected over the surface which acts as a lubrication layer at the beginning of the sliding test. The top layer has enriched fluorine percentage in contrast to the inside of the composite, as can be seen from Figure 5.7(c). After thorough washing, the PFPE layer over the top surface could still be detected with little difference in fluorine content from the unwashed sample (Figure 5.7(d)). This clearly shows the possibility of a chemically-bonded PFPE layer formed over the top surface. Overall, the EDS results have confirmed that there is a chemically-bonded PFPE layer over the surface that controls the friction and wear life performances to a large extent. It is also possible that the PFPE molecules are chemically-bonded with SU-8 in bulk.

5.3.8 XPS Characterization (Worn Surface)

XPS analysis was also carried out inside the wear tracks (worn surface) after 500,000 sliding cycles at a normal load of 100g and a sliding speed of 1000 rpm. The XPS C1s scan (left image) and atomic percentage (At%) table (right image) for the SU-8+PFPE, SU-8+SN 150 and SU-8+MAC samples are presented in Figures 5.8 (a), (b) and (c) respectively. The SU-8+PFPE At% table shows the presence of PFPE inside the wear

track by exposing new chemical groups such as O-CF₂, O-CF₂-O and CF₂ which have mainly arisen from PFPE and not from SU-8. The SU-8+PFPE At% table also shows that the atomic percentages of the elements are almost similar to that of the fresh surface results with only minor variations. The (C-C/C-H)/C-O ratio was reduced to 1 from 1.8 for pristine SU-8, which indicates the possibility of a chemical interaction between the SU-8 and PFPE molecules.

Figure 5.8 (b) shows the At% table and C1s scan for SU-8+SN 150 at the wear track. As SN 150 is also a alkane, the only difference that can be seen in the At% table is that there is an increase in the atomic percentages of C-C/C-H chemical groups to 80 from 67 for fresh surface of SU-8+SN 150.



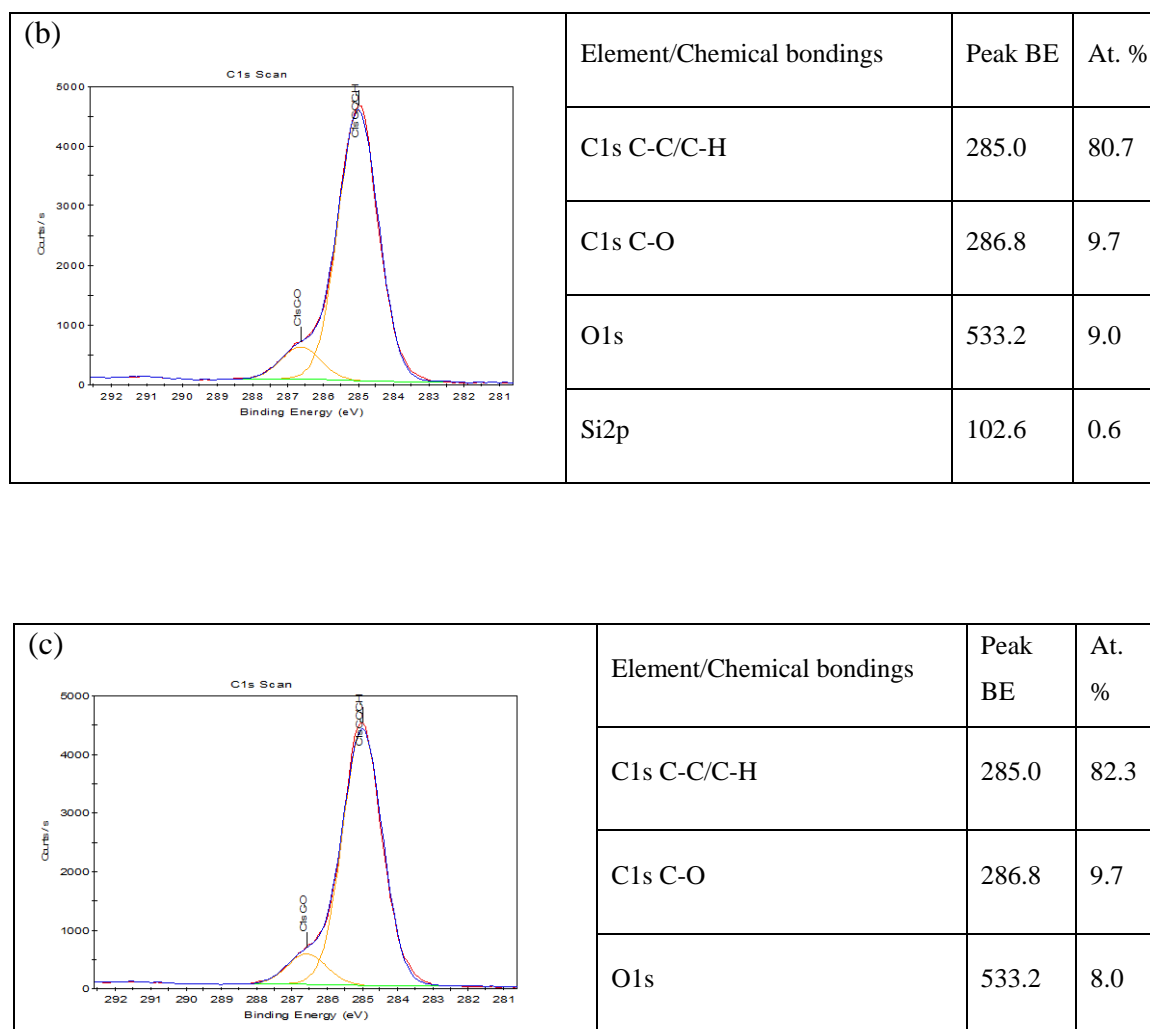


Figure 5.8: XPS analysis C1s scan (left) and At% table (right) for the 2 wt% SU-8 composites' inner wear tracks (worn surfaces) after 500,000 sliding cycles. (a) SU-8+PFPE. (b) SU-8+SN 150. (c) SU-8+MAC.

The ratio of (C-C/C-H)/C-O has increased to ~ 8.3 from ~ 3.9 for the fresh surface of SU-8+SN 150, thus confirming the presence of the base oil, SN 150. A thicker layer of lubricant film may be covering the entire wear track with no SU-8 exposed to XPS. Therefore, the XPS results have been dominated by the lubricant's chemistry alone. Figure 5.8(c) shows the At% table and C1s scan for SU-8+MAC. Since the MAC lubricant is a alkane, the only difference that can be seen in the At% table is the increase in the atomic percentages of C-C/C-H chemical groups to 82 from 77 for the fresh

showed a hardness (H) value of 0.27 GPa whilst SU-8+PFPE showed a H value of 0.32 GPa which is a ~19% increase in hardness. This increase in hardness can be attributed to some chemical bonding between SU-8 and PFPE molecules which might have increased the cross-linking. Since PFPE is a lubricant, it is expected to act as a plasticizer; however, it acted somewhat like a hardener. This increase in hardness might have contributed to an increase in the wear resistance. For both SU-8+SN 150 and SU-8+MAC, the lubricants acted as a plasticizer and reduced the hardness from 0.27 GPa to 0.22 GPa and 0.21 GPa, respectively for the pristine SU-8. These mechanical characterization results also support the chemical reaction in SU-8+PFPE.

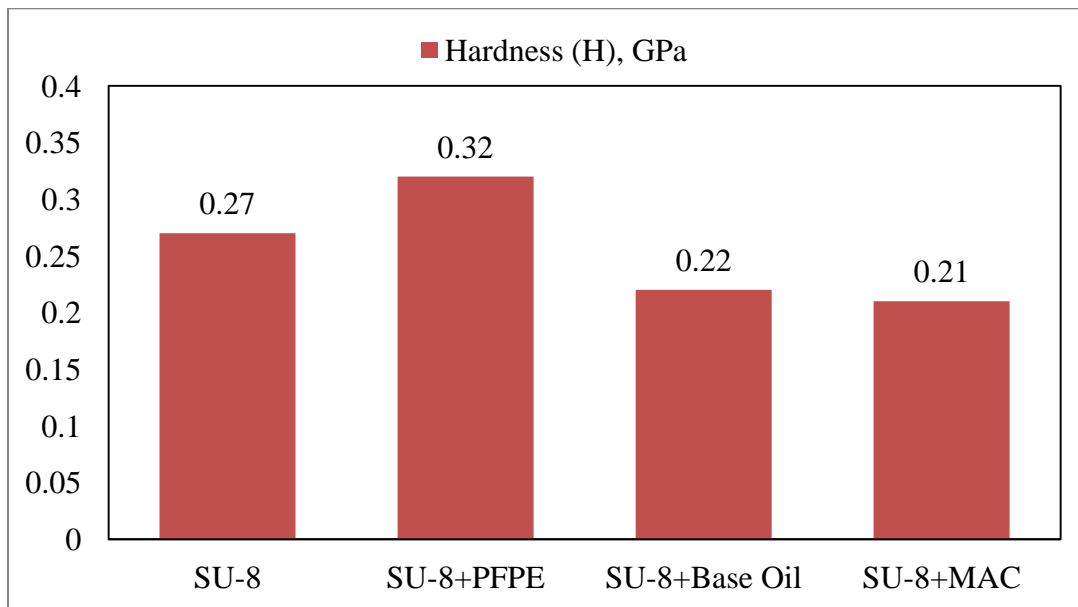
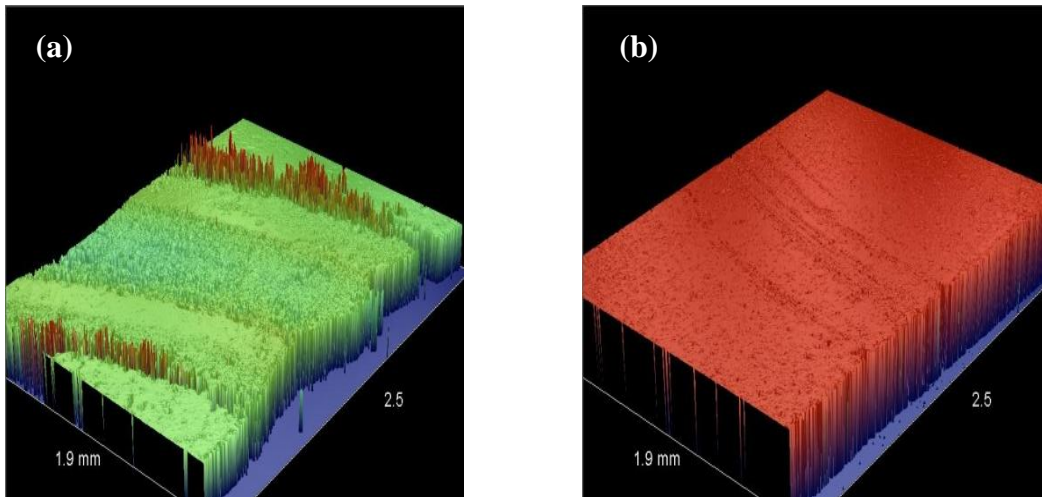


Figure 5.9: Hardness (H) values of pristine SU-8 and 2 wt% SU-8 composites from nano-indentation characterization.

5.3.10 Three-Dimensional (3D) Optical Profiler Images

Figures 5.10 (a), (b) and (c) show the 3D optical profiler images of the wear track for SU-8+PFPE, SU-8+SN 150 and SU-8+MAC respectively. The profiles were taken after 500,000 cycles of sliding at a normal load of 100 g and a rotational speed of 1000 rpm.

Although SU-8+PFPE has high H which may be one of the reasons for its high wear resistance, its high H has limited the wear track depth (h) to 0.8 μm as shown in Figure 5.10(a). For SU-8+SN 150, it showed an h of 8 μm which is 10 times greater than that for SU-8+PFPE, as shown in Figure 5.10(b). For SU-8+MAC, it showed an h of $>30 \mu\text{m}$ which almost reached the Si substrate, as shown in Figure 5.10(c). Despite almost similar hardness values, SU-8+SN 150 and SU-8+MAC have shown remarkably different wear lives. This shows that hardness is only one of the factors contributing to wear life. Having an excellent supply of lubricant on the interface and having low surface free energy (the lower polar component gives its hydrophobic nature) are other important factors for a longer wear life. However, it has been noted that a higher hardness of the materials may provide the additional benefit of a smaller contact area when other factors are favorable.



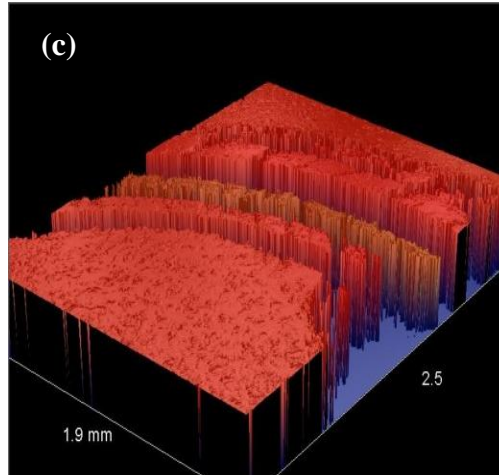


Figure 5.10: 3D Optical profiler images of the wear track (worn surface) for 2 wt% SU-8 composites after 500,000 sliding cycles at a normal load of 100 g and a sliding speed of 1000 rpm. (a) SU-8+PFPE. (b) SU-8+SN 150. (c) SU-8+MAC.

5.3.11 Surface Characterization of Worn Surfaces

Figure 5.11 shows the optical micrographs of pristine SU-8 and 2 wt% SU-8 composites after sliding tests at a normal load of 100 g and a sliding speed of 1000 rpm. Figures 5.11 (a), (e) and (i) correspond to the optical micrographs of the wear track (worn surface) on SU-8, the counterface ball immediately after the test and the counterface ball after cleaning with a solvent for pristine SU-8 respectively. A physical observation of the counterface ball before and after cleaning will reveal information about the amount of material transfer onto the counterface ball, the mode of wear and the damages caused to the counterface ball. Pristine SU-8 shows severe wear with a wide and deep wear track accompanied by a loss of material too. The counterface ball also shows a thick layer of material with some damages to the counterface ball and a distinct wear track after cleaning with acetone. These images qualitatively support the tribological behaviour mentioned in the preceding sections.

Figures 5.11(b), (f) and (j) correspond to the optical micrographs of the wear track on SU-8+PFPE, the counterface ball and the counterface ball after cleaning with the solvent of SU-8+PFPE. SU-8+PFPE shows a very mild wear track with little material removed and the presence of lubricant droplets on the counterface can also be observed. Additionally, some micro-sized cracks are also observed at a spot on the wear track as shown in Figure 5.11 (a). There was very little material transfer onto the counterface ball which confirms a lesser chance of adhesive wear with no wear debris accumulated in and around the wear track. It is necessary to analyse the contents of the transferred material in terms of whether it is a SU-8 or PFPE film. Therefore, the counterface ball was washed with the PFPE solvent - H-Galden - which washed away ~80% of the transfer material and left behind only ~20% which may be SU-8 and could be cleaned with acetone. The counterface ball was very clean after washing with no sign of any scratch or damage observed. These images again confirm that qualitatively, the presence of an intermediate layer of lubricant restricts direct interaction between the SU-8 surface and the counterface ball.

Figures 5.11 (c), (g) and (k) correspond to the optical micrographs of the wear track, the counterface ball after sliding tests and the counterface ball after washing and cleaning with solvents, respectively for SU-8+SN 150. SU-8+SN 150 showed a very distinct wear track with wear and material loss but not much scratching or plowing and the very little wear debris observed in and around the wear track were in the shape of large flakes. This confirms the signs of surface fatigue wear and more interestingly, there are some micron-sized surface wavy patterns across the wear track as can be seen in the SEM image in Figure 5.12 (b).

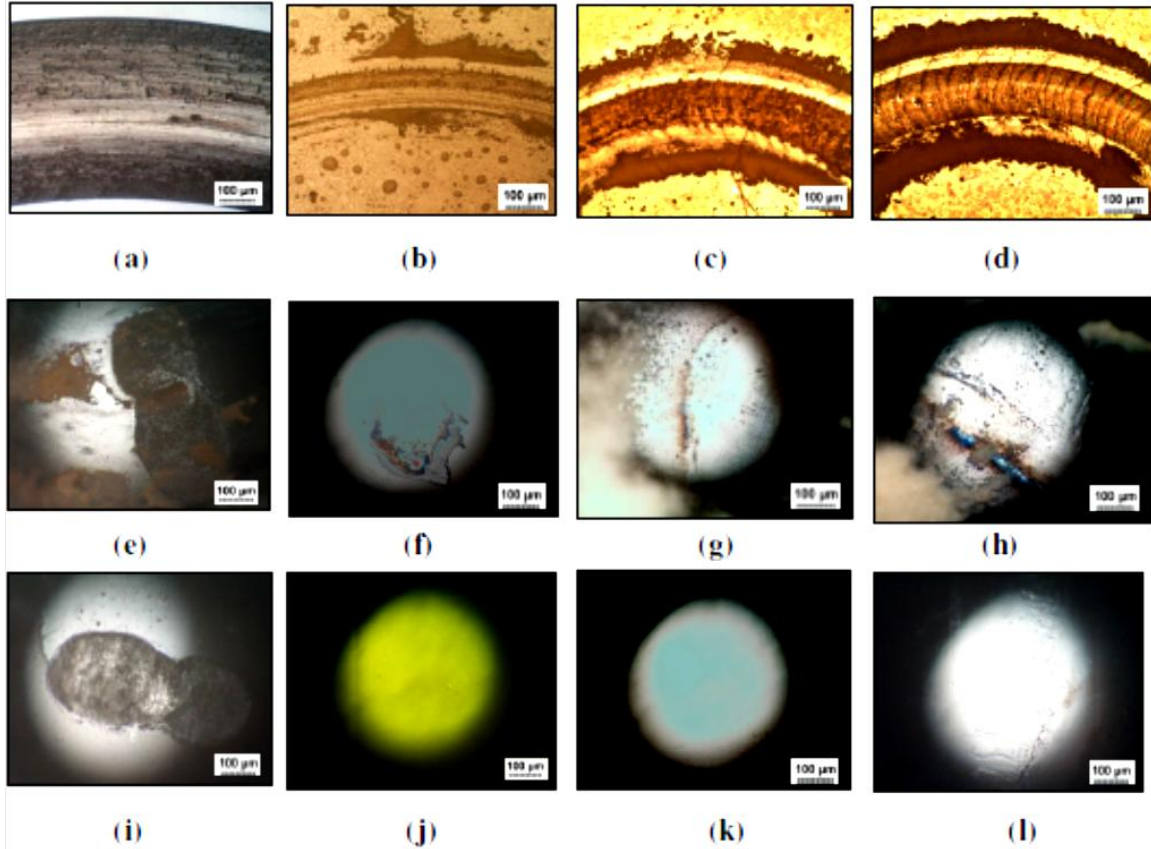


Figure 5.11: *Optical micrographs of worn surfaces: (a) Pristine SU-8 (at 10,000 cycles), (b) SU-8+PFPE (at 500,000 cycles), (c) SU-8+SN 150 (at 270,000 cycles) and (d) SU-8+MAC (at 100,000 cycles). Corresponding to the worn surfaces shown in (a), (b), (c) and (d), images (e), (f), (g) and (h) are the optical micrographs of the counterface balls' surface after sliding tests, whilst images (i), (j), (k) and (l) are the optical micrographs of the tested counterface balls after cleaning with solvents. The length of the scale bar is 100 μm in all images.*

Those patterns are micro-cracks which have mainly arisen from micro surface fatigue wear. When the surface is repetitively loaded under the movements of the counterface ball, the contact area plastically deforms in a cyclic manner and gets strain hardened. As the strain level reaches the critical value, breakage of the tie molecular chains and amorphous disentanglement may occur [Shi et al. 2000].

Since SU-8 is brittle in nature, micro-cracks - which are highly detrimental to brittle material - perpendicular to the surface area, leads to a rapid propagation of cracks

and eventually, the catastrophic failure of the surface. These cracks get interlinked as they propagate further, followed by a spall-off of material in large chunks [Shi et al. 2000]. Since SU-8 is brittle in nature, once the contact stress exceeds the elastic limit, it may cause surface cracks to appear. It has also been observed that the micro-cracks are quite visible and distinct at a higher normal load of 300 g although it is not presented in this report. The counterface ball showed much of the material transferred onto it but ~40% of the transfer material was removed when it was washed with the SN 150 solvent n-hexane; the remaining transfer material could be cleaned away by using acetone. This again confirms that the adhesive wear and the surface is not completely covered by lubricant, hence, resulting in an enhanced interaction between SU-8 and the counterface.

Figures 5.11(d), (h) and (l) correspond to the optical micrographs of the wear track on SU-8+MAC, the counterface ball after the test and the counterface ball after washing and cleaning with the solvents of SU-8+MAC. SU-8+MAC shows a very wide and deep wear track with a large amount of material loss. The surface shows distinct micro-cracks similar to that of SU-8+SN 150, thus confirming surface fatigue wear as explained earlier. Moreover, the micro-cracks have become very severe across the wear track and have propagated deeper, leading to considerable wear, since flakes of a larger size rather than just particles are shown in Figure 5.12(c), which is the magnified SEM image of the wear track. Wear debris in the form of flakes were observed in and around the wear track. Once these cracks are formed over the surface, they act as surface defects and stress raisers for any subsequent wearing process. The counterface rotating at a higher velocity will exert impact load as it passes through the cracks.

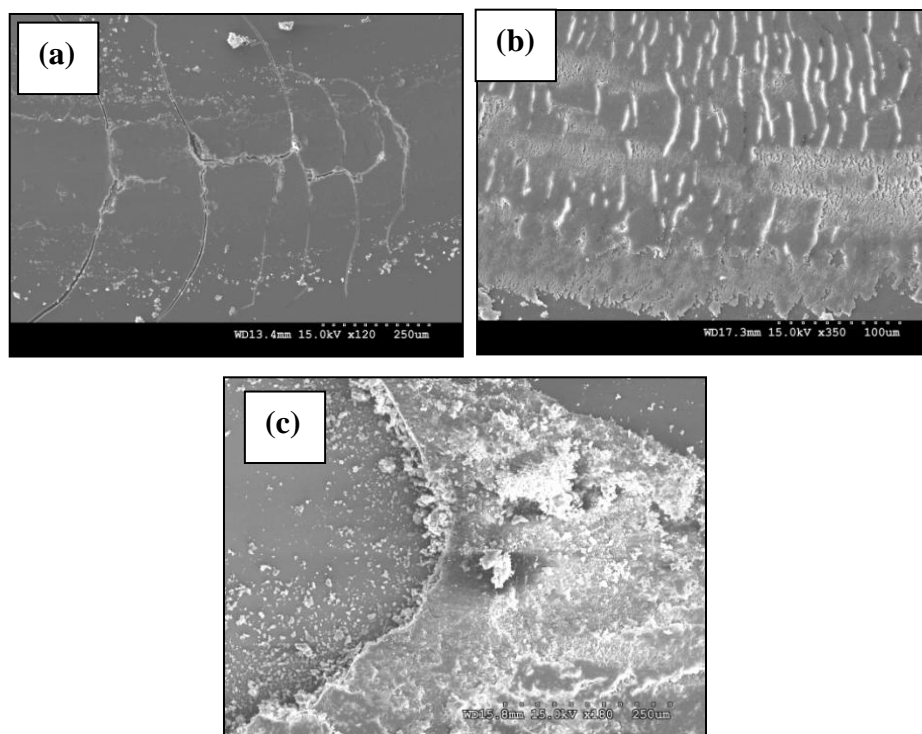


Figure 5.12: SEM images of the wear track (worn surface) of 2 wt% SU-8 composites after sliding tests of a normal load of 100g and at a rotational speed of 1000 rpm. (a) SU-8+PFPE (at 500,000 cycles). (b) SU-8+SN 150 (at 270,000cycles). (c) SU-8+MAC (at 100,000 cycles).

Commonly, brittle materials are very vulnerable to impact load and surface defects. A larger amount of material was transferred onto the counterface ball as compared to the other two cases. After washing with the MAC solvents - hexane and acetone, a thick transfer film was observed over the counterface. This shows good adhesion between SU-8+MAC and the counterface ball. Hence, this analysis confirms strong adhesive wear.

5.4 Conclusions

In summary, self-lubricating SU-8 composites were developed using lubricants such as PFPE, base oil SN 150 and MAC (multiply-alkylated Cyclopentane) oil. The 10 wt% (lubricant) SU-8 composites have enhanced the wear life of pristine SU-8 by more than five orders of magnitude without any failure. However, the 2 wt% SU-8 composites exhibited some clear distinction in their wear lives in the comparison study. At a 2 wt% lubricant concentration, SU-8+PFPE, SU-8+SN 150 and SU-8+MAC have an enhanced wear life of 1000, 500 and 200 times respectively.

For both SU-8+SN 150 and SU-8+MAC, the physical boundary layer self-lubrication mechanism is responsible for their superior tribological properties. For SU-8+PFPE, the physical boundary layer self-lubrication mechanism and the chemical reaction between the SU-8 and PFPE molecules are responsible for its more superior tribological properties over the other SU-8 composites. The presence of the physical boundary layer self-lubrication mechanism was confirmed through surface energy measurements and XPS analysis on the wear track after sliding tests.

The chemical reaction between SU-8 and PFPE have been ascertained by the EDS analysis, the AFM images after washing, the high wear resistance of the rinsed specimen and the nano-mechanical and optical characterizations. These SU-8 composites can be used as self-lubricating structural materials for MEMS, requiring no external lubrication and can also be used in the form of coatings in other applications such as journal bearings, raceways of a ball bearing, gears, medical equipments and tools, bio-devices, precision positioning stages, electronics components such as those inside cameras and printers, plastic bearings, etc.

Chapter 6

Effects of Functional End Groups of Perfluoropolyether (PFPE) Z-dol and Z-03 in the Tribology of SU-8 Composites

This chapter presents a further investigation on the postulated chemical bonding between the SU-8 and PFPE molecules as explained in Chapter 5. The same chemical interaction is analyzed intensively using various characterizations.

6.1 Introduction

The SU-8+PFPE composite has exhibited more superior tribological properties over other SU-8 composites such as SU-8+SN 150 and SU-8+MAC in the previous chapter. This good tribological performance was attributed to the improved cross-linking of SU-8 through the formation of ether bonds between SU-8 and PFPE, in addition to a uniform presence of the lubricant droplets throughout the composite matrix, which resulted in an in-situ supply of the lubricant and improved both the tribological and mechanical properties. The exact nature of the chemical interaction between the PFPE and SU-8 molecules requires further investigation with different types of PFPE lubricants. First, a thorough literature survey on the comparative tribological performance of various PFPE will be presented before moving on to the materials, results and discussions.

Chen et al. [Chen et al 2011] studied the surface energy and adhesion of one functionalized PFPE (Z-dol) and two non-functionalized PFPEs (Z and D) on carbon overcoated hard disk surfaces. They observed that Z-dol had better adhesion via strong

hydrogen bonding, whereas Z and D had weak interactions between their backbone oxygen and the polar dangling bonds of the hard disk surface.

Tani et al. [Tani et al. 2012] have reported the tribology of molecularly thin dip-coated PFPE (Z-tetraol and Z-03) films on magnetic disks. Particularly, they studied the effect of film thicknesses of PFPE lubricants on their frictional behaviour. It was found that the Z-03 films showed no dramatic decrease in friction with an increase in film thickness, whereas PFPE Z-Tetraol films showed a dramatic decrease in friction when the film thickness was increased beyond 1.2 nm. This was attributed to the increased surface coverage in the contact area by Z-tetraol molecules (-OH polar groups) as they maintain good bonding with the surface. Hence, the friction and adhesion forces decreased drastically. The Z-03 film with the non-functional end group (-CF₃) forms no proper bonding with the surface and can be easily displaced from the surface, allowing for local solid-solid contact. Hence, the Z-03 films exhibited very marginal decrease in adhesion and friction forces. The difference in tribological behaviour between PFPE Z-Tetraol films and Z-03 films is due to their end group functionality. The surface coverage increases only after a certain thickness for functionalized PFPEs.

Chen et al. studied the relationship between the surface coverage of ~1 nm thick PFPE lubricant films with different terminal groups coated on carbon overcoat (COC) by measuring their dispersive surface energy [Chen et al. 2006]. They reported that the PFPE with stronger end groups (i.e. Z-Tetraol) comprising of two -OH groups at each end, had a smaller surface coverage, whereas PFPE with weaker end groups (i.e. no -OH functional groups) had greater surface coverage. The mobility of the Z-tetraol molecules was restricted by the chemical bonding of the end group to the surface. They also

postulated that functionalized PFPE films with thickness more than 1 nm or a few monolayers will decrease the dispersive surface energy. Thus, a decrease in dispersive energy increases the surface coverage in functionalized PFPE films due to its multi-layering property. In another study, Tyndall *et al.* demonstrated that the PFPE Z-dol covered the CH_x surface completely at the thickness of ~ 1.4 nm whereas PFPE Z did not cover the entire surface within the study range of up to ~ 5 nm. The complete surface coverage by Z-dol was attributed to the decrease in dispersive surface energy of functionalized PFPEs with higher thickness [Tyndall et al. 1999].

Waltman *et al.* have studied the intermolecular interactions between the hydroxyl-terminated different PFPEs (Z-dol, Z-dol-TX and Z-Tetraol) on the sputtered amorphous SiN_x surface [Waltman et al. 2005]. They reported that the hydroxyl end groups of PFPE formed hydrogen bonds with the SiN_x surface. It had a direct function with the number of end groups. However, moisture is known to weaken the bonding between PFPE end groups and the SiN_x surface as water molecules can also form hydrogen bond at preferential sites. Zhang *et al.* have addressed the effect of UV irradiation on lubricant bonding with the disk surface of tailor made PFPE AM3001 lubricant films coated on a magnetic hard disk [Zhang et al. 2005]. UV irradiation decreased the dispersive and polar surface energies by 20% and 80% respectively and increased the bonding thickness. The polar and dispersive interaction between the lubricant molecules and the disk surface were strengthened by UV irradiation.

In this chapter, the chemical interaction between the PFPE and SU-8 molecules via end group functionality will be investigated. Two PFPE lubricants with the same backbone chains but with different functional end groups have been chosen for this study.

These functional end groups are -OH and -CF₃ which are present in Z-dol and Z-03, respectively. The liquid lubricant concentrations in the respective composites are maintained at a 2 wt% of PFPE, with the remaining 98 wt% comprising of SU-8. Comparative tribological performances along with the results from other characterizations such as the surface energy analysis, surface chemical analysis and thermogravimetric analysis for these two composites will be presented in the following sections.

6.2 Materials and Experimental Procedures

The physical and chemical properties of SU-8 2050, perfluoropolyether Z-dol and perfluoropolyether Z-03 lubricants have already been summarized in Chapter 3. Bottom of Form The sample preparation procedure from the sizing of the Si wafer substrates to the completely cured SU-8 and SU-8 composites film and other characterizations have been detailed in Chapter 3. In this chapter, the lubricant concentration used is 2 wt%.

6.3 Results and Discussion

The surface roughness (R_a) values for pristine SU-8, SU-8+Z-dol and SU-8+Z-03 are 30 nm, 70 nm and 120 nm respectively, as measured using an optical profiler (Brucker Inc, USA). The higher roughness values in the composites are a result of the lubricant droplets sticking out at the surface. SU-8+Z-03 had a higher roughness value than SU-8+Z-dol since SU-8+Z-03 showed bigger agglomerated droplets over the surface.

6.3.1 Wettability Analysis

Figures 6.1 (a) and (b) show the images of the contact angle measurements of $0.5 \mu\text{l}$ droplets of raw (without mixing with the solvent) PFPE lubricants on the SU-8 surface. PFPE Z-03 has shown a contact angle value of $27 \pm 3^\circ$ on the SU-8 surface, whereas Z-dol has shown a contact angle of $8 \pm 3^\circ$ on the SU-8 surface. It is well understood that the wettability of Z-dol on the SU-8 surface is much greater than that of the wettability of Z-03 on the SU-8 surface. This behaviour could be attributed to the chemical affinity between the Z-dol molecules and the SU-8 molecules.

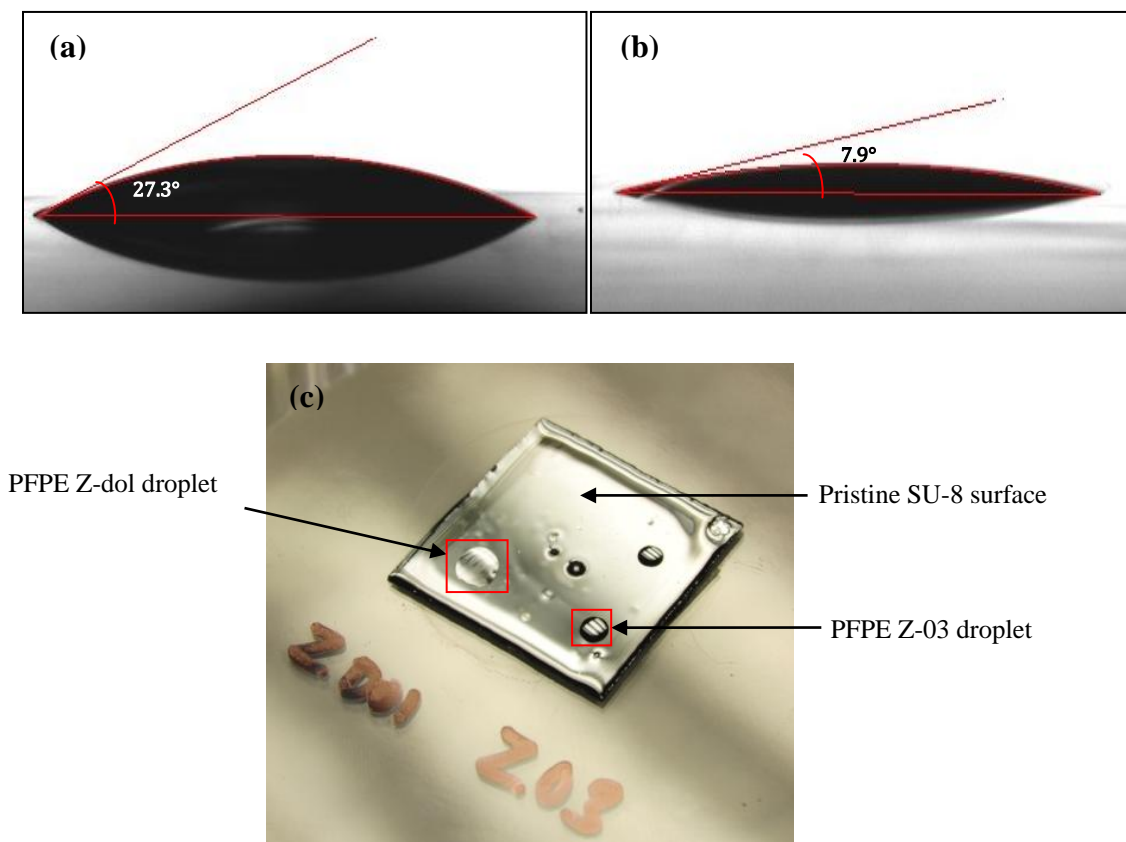


Figure 6.1: Visual images of the contact angle measurements of $0.5 \mu\text{l}$ droplets of PFPE lubricants with the SU-8 surface: (a) Z-03 and (b) Z-dol. (c) A surface area coverage comparison between $2 \mu\text{l}$ of the two PFPE lubricants.

This wetting behaviour has indeed helped Z-dol to disperse uniformly inside the SU-8 matrix more easily than the other lubricants, apart from also providing a larger surface area coverage. Surface area coverage of PFPE lubricants over the SU-8 surface can be seen from Figure 6.1(c). The uniform dispersion and surface area coverage of the lubricants were found to have influenced the tribology of SU-8 composites in our prior studies [Prabakaran et al. 2013 (b) and (c)].

6.3.2 Surface Free Energy Calculations

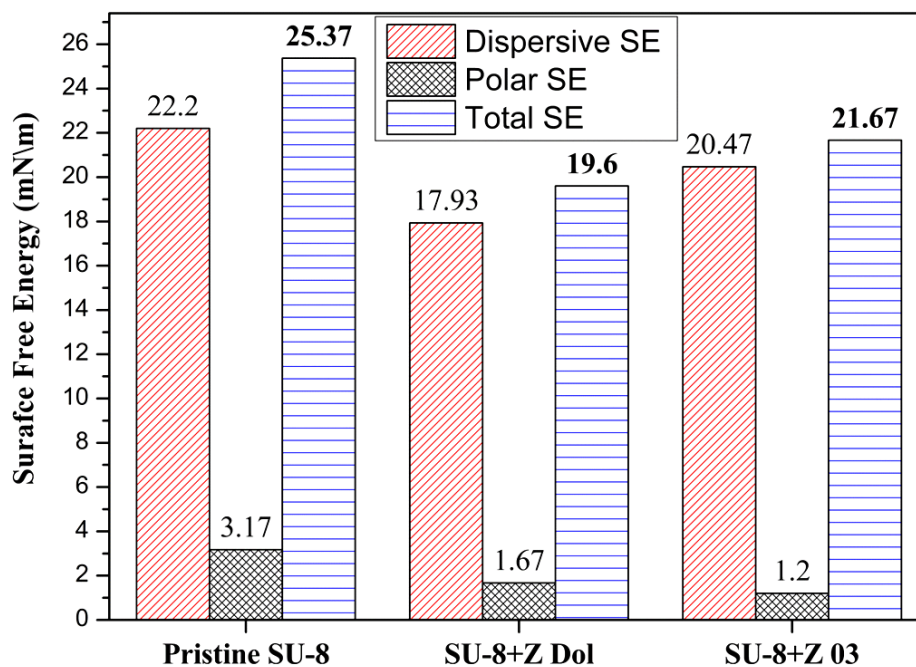


Figure 6.2: Polar, dispersive and total surface energies of freshly spin-coated (completely UV-cured and cross-linked) pristine SU-8 and 2 wt% SU-8 composites. The data scatter value was within ± 0.20 for all cases.

[Note: Contact angle values for the surface energy calculations were measured immediately after completely curing and cross-linking (after UV and PEB) the sample to avoid contamination.]

The surface free energy values for pristine SU-8 and the 2 wt% SU-8 composites are shown in Figure 6.2. Pristine SU-8 shows the highest surface free energy of 25.37 mN/m

and a polar surface energy of 3.17 mN/m. The total surface energy of SU-8+Z-03 and SU-8+Z-dol surfaces are ~21 and ~19 mN/m respectively. Although SU-8+Z-dol exhibited the lowest total surface energy, SU-8+Z-03 exhibited the lowest polar surface energy. It is clear that the polar end groups from the unbonded Z-dol lubricant molecules on the surface give rise to polar surface energy. The SU-8+Z-dol composite showed the lowest dispersive surface energy of ~17 mN/m, indicating that Z-dol has better surface coverage on the SU-8 surface than Z-03 [Chen et al. 2006 and Tyndall et al. 1999]. The effect of this observed behaviour on their tribological properties will be discussed in the following sections.

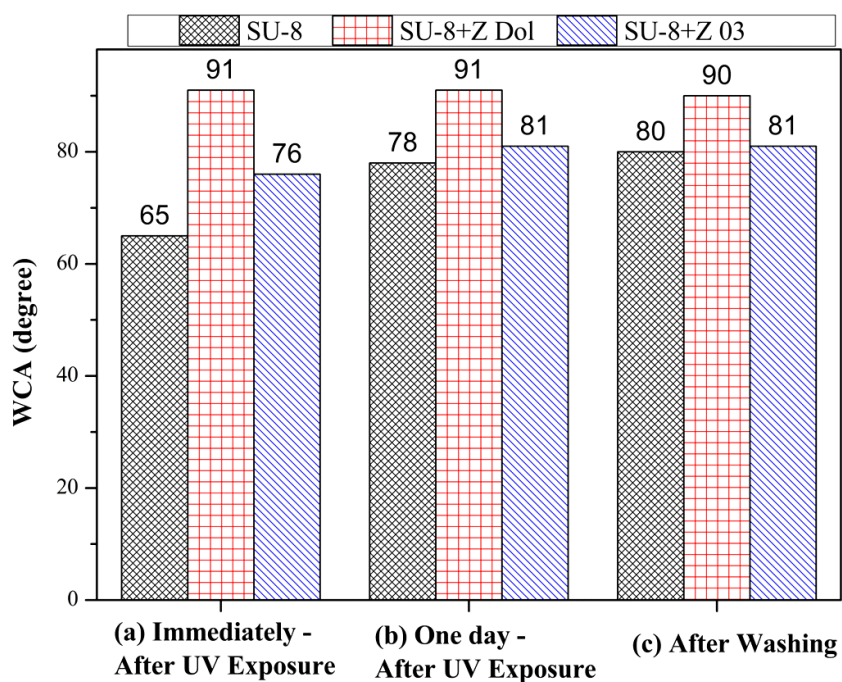


Figure 6.3: Water contact angle (WCA) measurements of freshly spin-coated (completely UV-cured and cross-linked) pristine SU-8 and 2 wt% SU-8 composites for different conditions after UV exposure: (a) immediately – after UV exposure, (b) one day – after UV exposure and (c) after washing.

[Note: The same completely cured and cross-linked samples were used for characterizations shown in Figure 6.2 and Figure 6.3. The WCA in Figure 6.3 were measured at different intervals.]

Figure 6.3 shows the water contact angle values for pristine SU-8 and 2 wt% SU-8 composites obtained immediately (Figure 6.3(a)) and one day (Figure 6.3(b)) after UV exposure. The wetting behaviours of the samples obtained immediately after UV exposure for SU-8+Z-dol, SU-8+Z-03 and SU-8 can be inferred from their WCA values of 91° , 76° and 65° respectively. These results indicate that the UV exposure has generated more polar (hydrophilic) end groups on the SU-8 surface; after one-day (kept inside the desiccator) of UV exposure, the same surface becomes less hydrophilic accompanied by a rise in WCA values.

UV irradiation have also been used to introduce functional end groups on the various polymer surfaces [Situma et al. 2004, Nahar et al. 2004, Welle et al. 2005, Xing et al. 2005, Owens 1975 and Borger et al. 2000]. The introduction of these functional groups has helped Z-dol to spread across the surface and remain dispersed via chemical interaction, thereby maintaining hydrophobic contact angle values. However, the absence of functional hydroxyl groups in Z-03 does not permit the molecules to disperse and they remain bonded with the SU-8 molecules. Hence, the wetting behaviour varies for the two composites from immediately after UV exposure to one day after UV exposure. The same samples were then washed with PFPE solvent H-Galden SV60 and subjected to water contact angle measurement. Both pristine SU-8 and SU-8+Z-03 showed a similar contact angle of approximately $\sim 80^\circ$, whereas the SU-8+Z-dol surface maintained a high contact angle of $\sim 90^\circ$. These WCA values after solvent washing indicates that a very little amount of Z-03 remained on the composite surface, whereas Z-dol remained bonded to the composite surface.

6.3.3 Tribological Characterization

Table 6.1 (a) provides a summary of the tribological tests of pristine SU-8 and 2 wt% SU-8 composites at a normal load of 150 g and a rotational sliding speed of 1000 rpm until 500,000 sliding cycles.

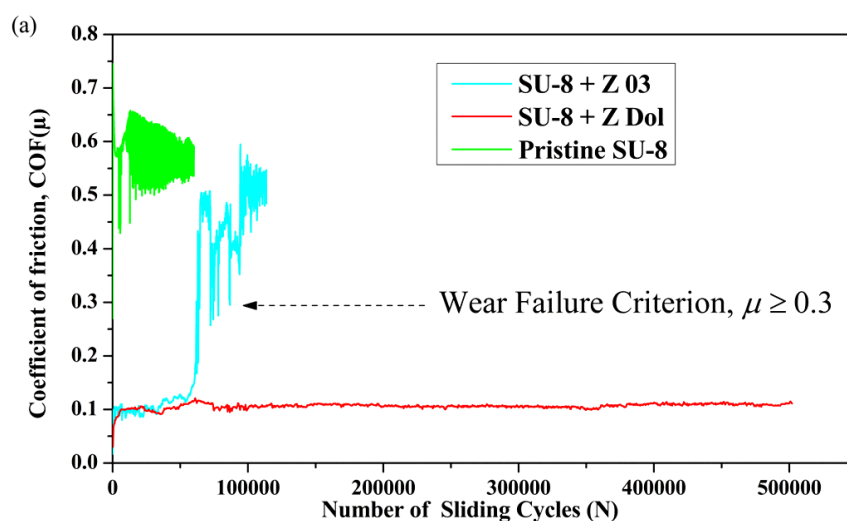
Table 6.1: *Initial coefficient of friction (μ_i), steady-state coefficient of friction (μ_s) and wear life (number of sliding cycles, n) of different composites obtained from sliding tests against a 4 mm diameter Si_3N_4 ball at different normal loads and sliding rotational speeds. (a) Pristine SU-8 and 2 wt% SU-8 composites tested at a normal load of 150 g and a sliding rotational speed of 1000 rpm. (b) Pristine SU-8 and 0.5wt% PFPE dip-coated onto SU-8, tested at a normal load of 20mN and a sliding rotational speed of 100 rpm.*

| Composite Description | Initial coefficient of friction, COF (μ_i) | Steady- state coefficient of friction, COF (μ_s) | Wear Life (Number of Cycles, n) |
|--|--|--|---|
| a) Pristine SU-8 and 2wt% SU-8 composites /Test Parameters: 150g, 1000 rpm | | | |
| Pristine SU-8 | 0.6 | - | 0 |
| SU-8 + Z-dol | 0.03 | 0.10 | >500,000 |
| SU-8 + Z-03 | 0.08 | 0.11 | 60,000±5,000 |
| b) Pristine SU-8 and 0.5wt% PFPE dip-coated onto SU-8/Test Parameters: 20 mN, 100 rpm | | | |
| Pristine SU-8 | 0.7 | - | 0 |
| SU-8 + Z-dol (FS) | 0.03 | 0.03 | >10,000 |
| SU-8 + Z-dol (AW) | 0.03 | 0.19 | >10,000 |
| SU-8 + Z-03 (FS) | 0.04 | 0.02 | >10,000 |
| SU-8 + Z-03 (AW) | 0.33 | - | 0 |

[Note: Legend: FS – fresh surface; AW – after washing.]

Figure 6.4(a) shows the typical coefficient of friction (CoF) versus number of sliding cycles (n) plot and this data has been summarized in Table 6.1 (a). The pristine SU-8 has shown high initial coefficient of friction ($\mu_i \sim 0.6$) and zero wear life ($n \sim 0$) as per the definition of wear life. The SU-8+Z-dol composite has shown $\mu_i \sim 0.03$, $\mu_s \sim 0.1$ and wear life (n) of >500,000 cycles (experiment was stopped due to a long test duration) whereas SU-8+Z-03 has shown $\mu_i \sim 0.03$, $\mu_s \sim 0.1$ and wear life (n) of $\sim 60,000$. No difference can be seen between SU-8+Z-dol and SU-8+Z-03 except for a wear life increase of more than eight times for SU-8+Z-dol. It is important to note the difference in wear life between these composites, even though they have a similar chemical backbone chain. Z-dol shows a better surface area coverage than Z-03, due to its end group interaction with the surface and a lower dispersive surface energy component [Chen et al. 2006 and Tyndall et al. 1999].

6.3.4 Nano-Tribological Characterization



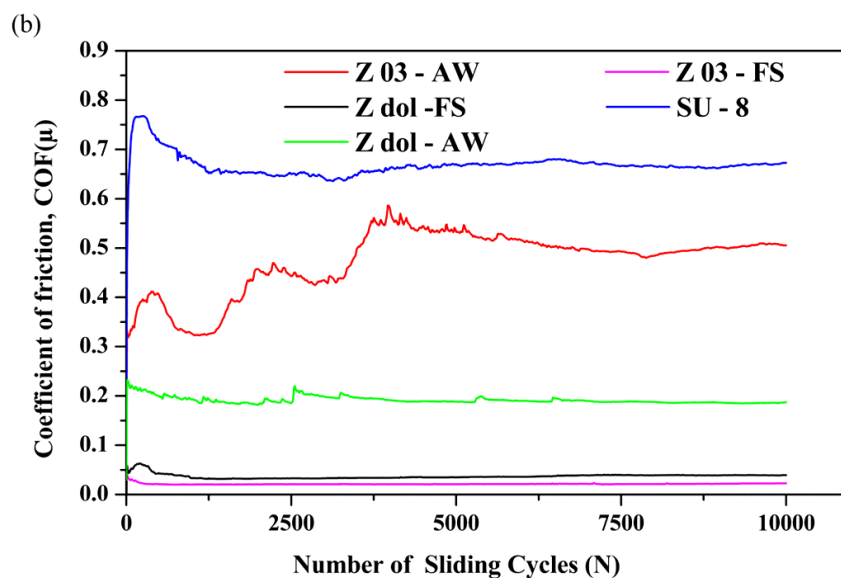


Figure 6.4: Typical coefficient of friction versus number of cycles plot for different samples obtained from the ball-on-disk sliding tests against a 4 mm diameter Si_3N_4 ball at different normal loads and sliding rotational speeds. (a) SU-8 and 2 wt% SU-8 composite tested at a normal load of 150g and a sliding rotational speed of 1000 rpm. (b) 0.5wt% PFPE dip-coated on SU-8 tested at a normal load of 20mN and a sliding rotational speed of 100 rpm.

Table 6.1(b) contains a summary of the nano-tribological test results for 0.5 wt% PFPE (Z-dol and Z-03) dip-coated SU-8 formed under the conditions provided in Section 2.7; tested at a normal load of 20 mN and a sliding rotational speed of 100 rpm under different surface conditions (i.e. fresh surface, after washing with the solvent). The data obtained from the typical coefficient of friction versus number of cycles plot is shown in Figure 6.4(b). The objective of these nano-tribological tests was to confirm whether the dip-coated PFPE was physically or chemically adsorbed onto the SU-8 surface. If there were no chemisorptions of the lubricant, the dip-coated SU-8 was expected to exhibit similar tribological behaviour as the pristine SU-8 after intensive washing.

From Table 6.1(b), the pristine SU-8 shows a high initial coefficient of friction of $\mu_i \sim 0.7$ and a low wear life ($n \sim 0$). The fresh surface of SU-8+Z-dol showed low initial

and steady-state coefficients of friction of $\mu_i \sim 0.03$ and $\mu_s \sim 0.03$ respectively and a wear life of (n) >10,000. After thorough washing with PFPE solvent H-Galden SV60, the washed surface of SU-8+Z-dol showed $\mu_i \sim 0.03$, $\mu_s \sim 0.19$ and a wear life of (n) >10,000. The fresh surface of SU-8+Z-03 showed $\mu_i \sim 0.04$, $\mu_s \sim 0.02$ and a wear life of (n) >10,000 whilst its washed surface (AW) showed $\mu_i \sim 0.33$ and a wear life of (n) >0 with a noticeable wear track. These results strongly suggest that a chemical interaction has occurred between the SU-8 and Z-dol molecules even after intensive washing. It is understood that the -OH end groups are responsible for bond formation with SU-8. The chemical interpretation of this tribological behaviour will be discussed in the following sections through an extensive surface chemical analysis.

6.3.5 Surface Chemical Analysis

The surface chemical nature and composition of UV cured pristine SU-8, SU-8+Z-dol and SU-8+Z-03 were investigated by XPS analysis before (Figure 6.5) and after solvent washing, and following vigorous ultra-sonication washing (Figure 6.6). Upon UV curing, the Z-dol and Z-03 molecules tended to graft themselves with SU-8 both physically and chemically via corresponding chemical interactions of functional groups. Rinsing followed by sonication removes the physically adsorbed Z-dol and Z-03 molecules leaving behind only the chemically modified SU-8 molecules [Zhang et al. 2005 & 2011]. An XPS study after the rinsing and sonication of SU-8 composite films was carried out to understand and to reveal new insights on surface nature and improved tribological performances due to chemical interactions. The deconvoluted C1s spectra of UV cured SU-8 constitutes of peaks centered at 284.6 eV, 286.2 eV, 286.9 eV 288.8 eV

and 290.9 eV corresponding to C-C/C-H, C-O, C=O, -O-C=O and shake-up peaks (i.e. due to $\pi-\pi^*$ interactions) (Figure 6.5 (a)) [Walther et al. 2010]. Shake-up are appearing due to non-covalent interactions such as an electrostatic interaction where a region of negative charge interacts with a positive charge, the electron-rich π system can interact with a metal (cationic or neutral), an anion, another molecule and even another π system. Mostly, weak physical interactions based peaks are called as shake-up peaks and they have no significance in XPS results of polymers.

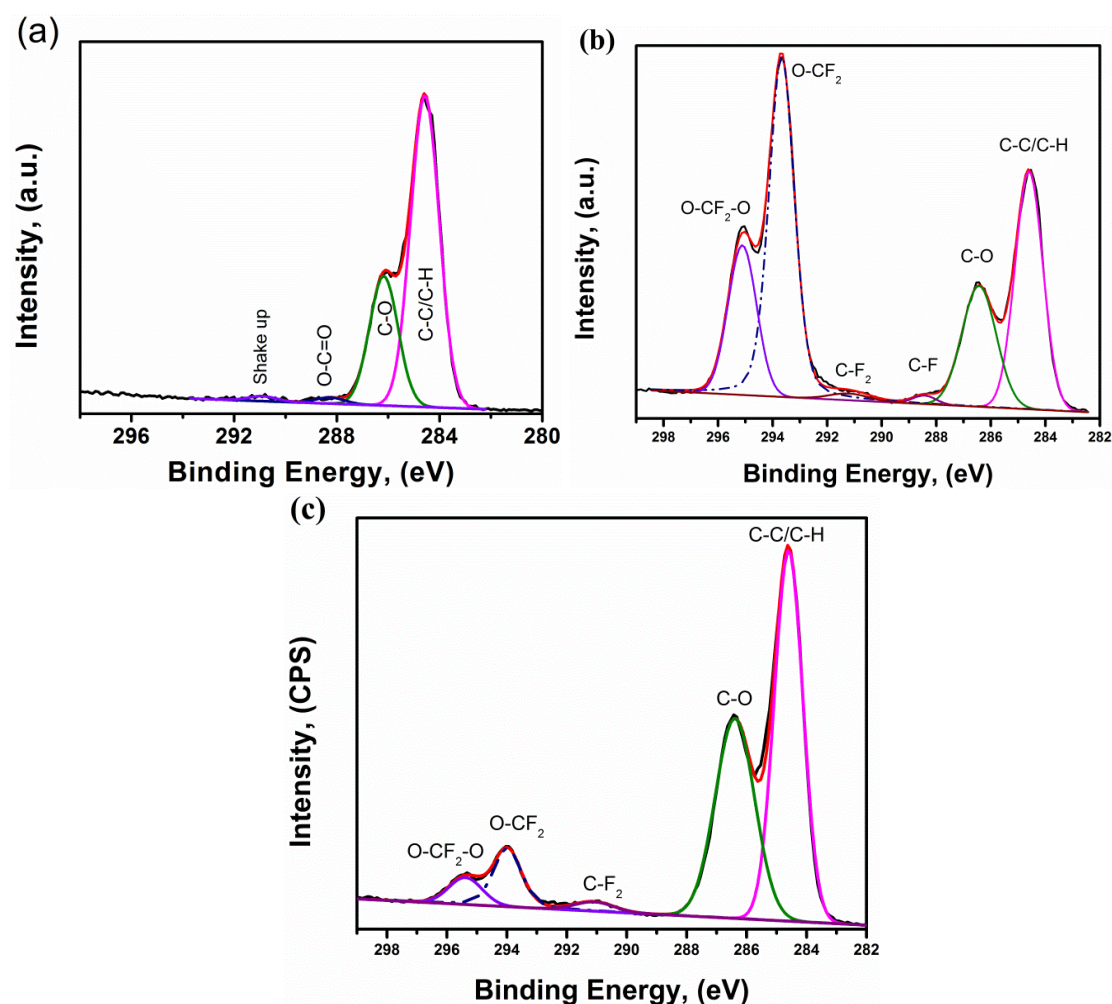


Figure 6.5: XPS Cls scan for freshly spin-coated (completely cured and cross-linked) pristine SU-8 and 2 wt% SU-8 composites corresponding to the XPS of the washed surfaces shown in Figure 6.6. (a) Pristine SU-8. (b) SU-8+Z-03. (c) SU-8+Z-dol.

After UV curing the SU-8, the oxygen content had increased significantly due to the formation of C-O, C=O and -O-C=O functional groups, similar to that reported in the literature [Wang et al. 2006, Gabriela et al. 2008 and Lin et al. 1991]. Z-dol is an amphiphilic polymer possessing hydroxyl end groups, while Z-03 has non-polar CF₃ end-groups [Li et al. 2012].

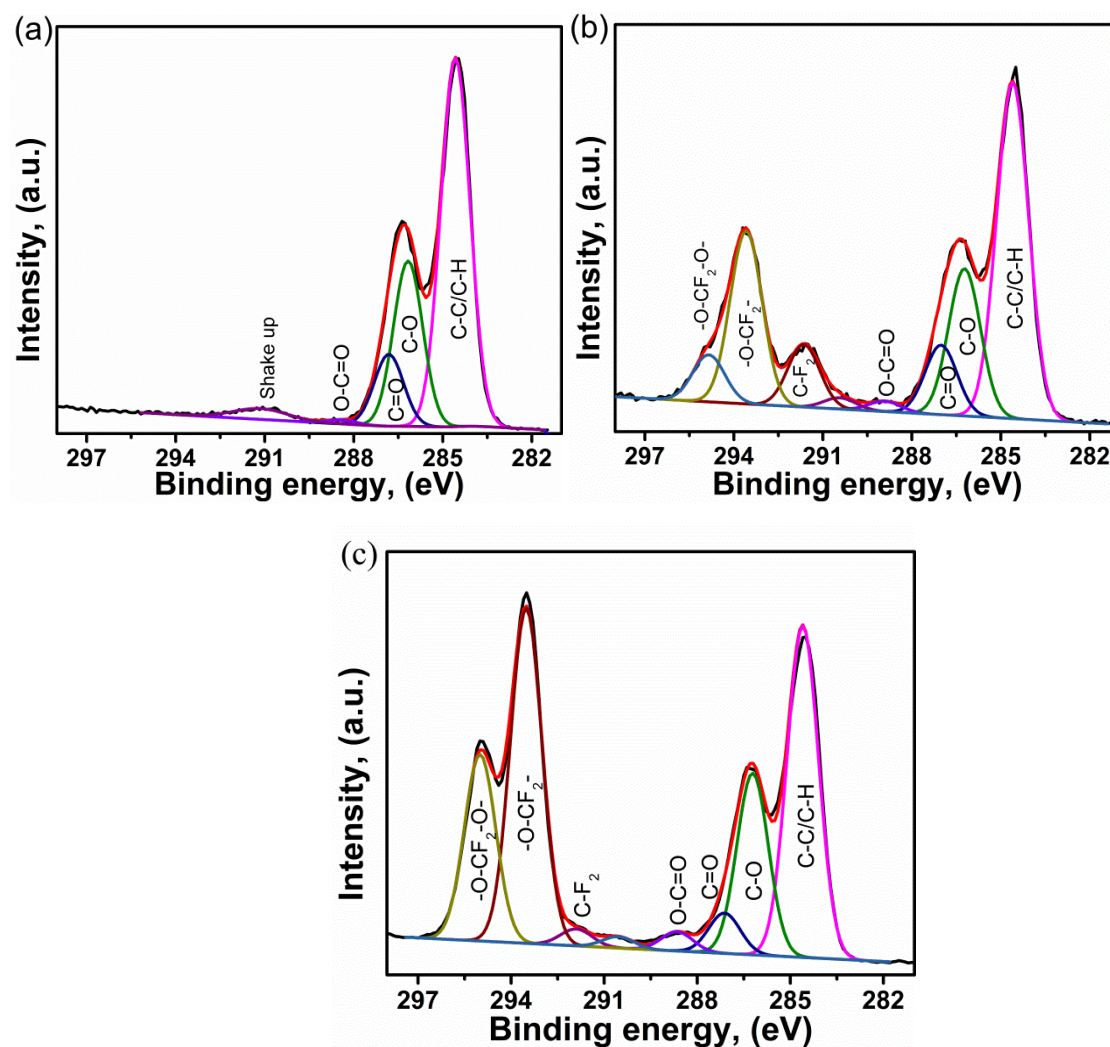


Figure 6.6: XPS analysis of C1s scan for freshly spin-coated (completely cured and cross-linked) 2 wt% SU-8 composites after rinsing, followed by a 20 minute sonication. (a) Pristine SU-8. (b) SU-8+Z-dol. (c) SU-8+Z-03.

The XPS C1s spectra of the UV cured SU-8+Z-dol and SU-8 + Z-03 in Figure 6.5 have exhibited similar peaks with varied intensities depending on the amount of functional groups present in Z-dol and Z-03. No noticeable difference in peaks and peak positions corresponding to the presence of additional functional groups were observed. The UV curing initiates both the chemically cross-linking/grafting of end functional groups in the two polymers as well as the cross-linking of the individual polymers [Zhang et al. 2005, Lin et al. 1991, Thomas et al. 2003 and Heeb et al. 2009].

Both physically and chemically adsorbed films were formed on the surfaces but it is difficult to differentiate via XPS analysis due to the limitation of polymeric film thicknesses. Therefore, after rinsing the films in the solvent H-Galden SV 60 and sonicating for 20 minutes, the unbonded and physically adsorbed polymeric films were removed. Figures 6.6(b) and 6.6(c) show the XPS C1s spectra of SU-8+Z-dol and SU-8+Z-03 respectively; after UV curing and rinsing, followed by sonication. The peaks centered around 284.6 eV, 286.2 eV, 286.9 eV, 288.8 eV, 290.5 eV, 291.6 eV, 293.5 eV and 295 eV correspond to C-C/C-H, C-O, C=O, -O-C=O, shake-up/C-F peaks, CF₂, O-CF₂ and O-CF₂-O bonds respectively [Li et al. 2012 and Mathew et al. 1991]. Both the Z-dol and Z-03 spectra exhibited similar peak positions due to the same backbone chains and both clearly differed from the pristine SU 8. The peaks of CF₂, O-CF₂ and O-CF₂-O bonds were very prominent (Figure 6.6 (b) &(c)), but they differed from each other in terms of corresponding intensities due to differences in their end group chemical interactions and bonding with SU-8.

Similar to pristine SU-8, the mixed polymer films also exhibited an increase in oxygen content due to the formation of C-O, C=O and -O-C=O functional groups, since

the SU-8 made up the majority amount. In SU-8+Z-dol films, the ratio between the -O-CF₂- and C-O was ~1.2, which is very close to the stoichiometric chemical reaction between oxygen-nourished SU-8 during UV curing and the polar -OH end groups of Z-dol. Also, the -CF₂ peak at 291.6 eV was very prominent and confirmed that no polymeric chain breakage occurred during UV curing. In the case of Z-03, the -CF₃ end groups were non-polar and less reactive upon UV exposure.

Hence, there will be no possible interaction between the two polymers SU-8 and Z-03 as proven by the ratio between the -O-CF₂- and C-O peaks [Chen et al. 2011, Tani et al. 2012, Zhang et al. 2005, Lin et al. 1991 and Ruhe et al. 1994]. The higher ratio (~1.85) was due to a low residual amount of physically trapped, unwashed Z-03 on the SU-8 films as a result of physical bonds such as van der Waal's and other weak force interactions. Also, there was a significant decrease in the intensity of the CF₃ end functional group which confirmed the removal of Z-03 molecules upon solvent rinsing and sonication. The above observations of chemical binding between SU-8 and Z-dol were further supported by the superior tribological behaviour of SU-8+Z-dol films and the contact angle analysis, which showed that even after washing was done to remove the physically deposited Z-dol, the chemically bonded lubricant molecules remained on the SU-8 surface.

6.3.6 Thermogravimetric Analysis (TGA)

Figure 6.7 shows the thermogravimetric analysis of pristine SU-8 and 2 wt% PFPE dip-coated onto SU-8 samples for various surface conditions (e.g. fresh surface and after washing). The objective of the analysis was to confirm whether or not the PFPE

molecules chemically absorbed to SU-8. The pristine SU-8 began to degrade at about 300 °C and decomposed completely at 620 °C. The minor weight loss of SU-8 (~ 2 wt%) before 300 °C was attributed to the moisture content. The fresh surface (FS) of Z-dol began to degrade at about 250 °C and decomposition occurred completely at 550 °C which is ~70 °C lesser than that for the pristine SU-8. Z-dol's (FS) degradation at temperatures lower than that of the SU-8 was attributed to the volatilization of the Z-dol lubricant from the SU-8 surface.

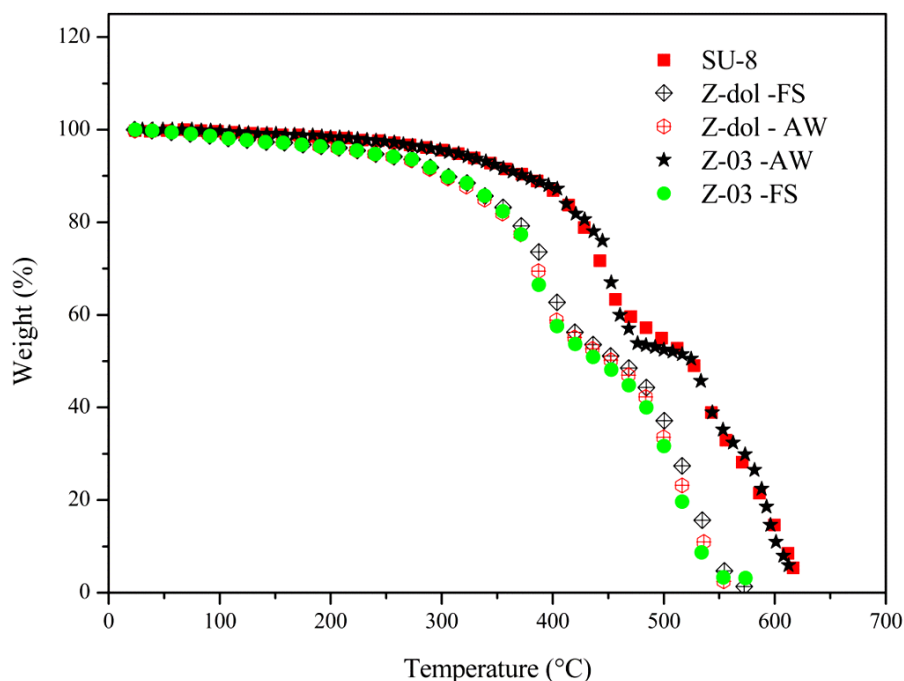


Figure 6.7: Thermogravimetric analysis results of pristine SU-8 and 2 wt% PFPE dip-coated onto SU-8 for various surface conditions. [Note: Legend: FS – Fresh Surface; AW – After Washing; Z-dol – PFPE Z-dol lubricant dip-coated on SU-8; Z-03– PFPE Z-03 lubricant dip-coated on SU-8.]

The FS of Z-03 also exhibited similar weight loss behaviour as the FS of Z-dol. After that, the dip-coated samples were washed in the PFPE solvent H-Galden using sonication for about an hour and the same process was repeated twice. The surface of Z-

dol after washing (AW) showed similar weight loss characteristics as the FS of Z-dol with marginal variation, thus confirming the retention of an appreciable amount of the lubricant by SU-8 through chemical bonding. On the other hand, the Z-03 AW showed the same weight loss as pristine SU-8, hence indicating no noticeable presence of lubricant over SU-8 to influence the weight loss behaviour. Thus, the TGA results strongly support the chemical interaction between the SU-8 and PFPE Z-dol molecules as both the TGA spectra before and after sonication followed a similar trend. However, the CF_3 groups in Z-03 did not initiate any chemical interaction with SU-8 [Chen et al 2011].

6.3.7 Surface Characterization of Worn Surfaces

Figure 6.8 shows the optical micrographs of pristine SU-8 and 2 wt% SU-8 composites after sliding tests at a normal load of 150 g and a rotational sliding speed of 1000 rpm. Figures 6.8 (a), (d) and (g) correspond to the optical micrographs of the counterface ball immediately after the test, the counterface ball after cleaning with a solvent and the wear track (worn surface) of pristine SU-8 at 70,000 sliding cycles of wear life, respectively. A physical observation of the counterface ball before and after cleaning is necessary to assess the amount of material transfer onto the counterface ball, the mode of wear and damages caused to the counterface ball.

The pristine SU-8 counterface ball (Figure 6.8(a)) exhibits an appreciable amount of material transfer onto it from surface wear, but after cleaning with acetone, it exhibits a few scratches on the Si_3N_4 ball without much damage. The SU-8 surface (Figure 6.8(g)) shows very severe wear with a wide and deep distinct wear track. Figure 6.8(b), (e) and (h) correspond to the optical micrographs of the counterface ball immediately after the

test, the counterface ball after cleaning with a solvent and the wear track of SU-8+Z-dol, respectively. The counterface ball (Figure 6.8(b)) exhibits no wear with a transfer layer of PFPE lubricant on it but after cleaning with acetone, it exhibits a clean surface identical to a new ball surface. No distinct wear track can be seen other than a thin sliding trail (an impression) that of plastically deformed asperities, on the surface of SU-8+Z-dol. The counterface ball of SU-8+Z-03 (Figure 6.8(c)) shows no wear with a small transfer layer of PFPE lubricant on it even after cleaning with acetone. Figure 6.8(f) shows a clean surface which appears as good as a new ball surface until 70,000 cycles.

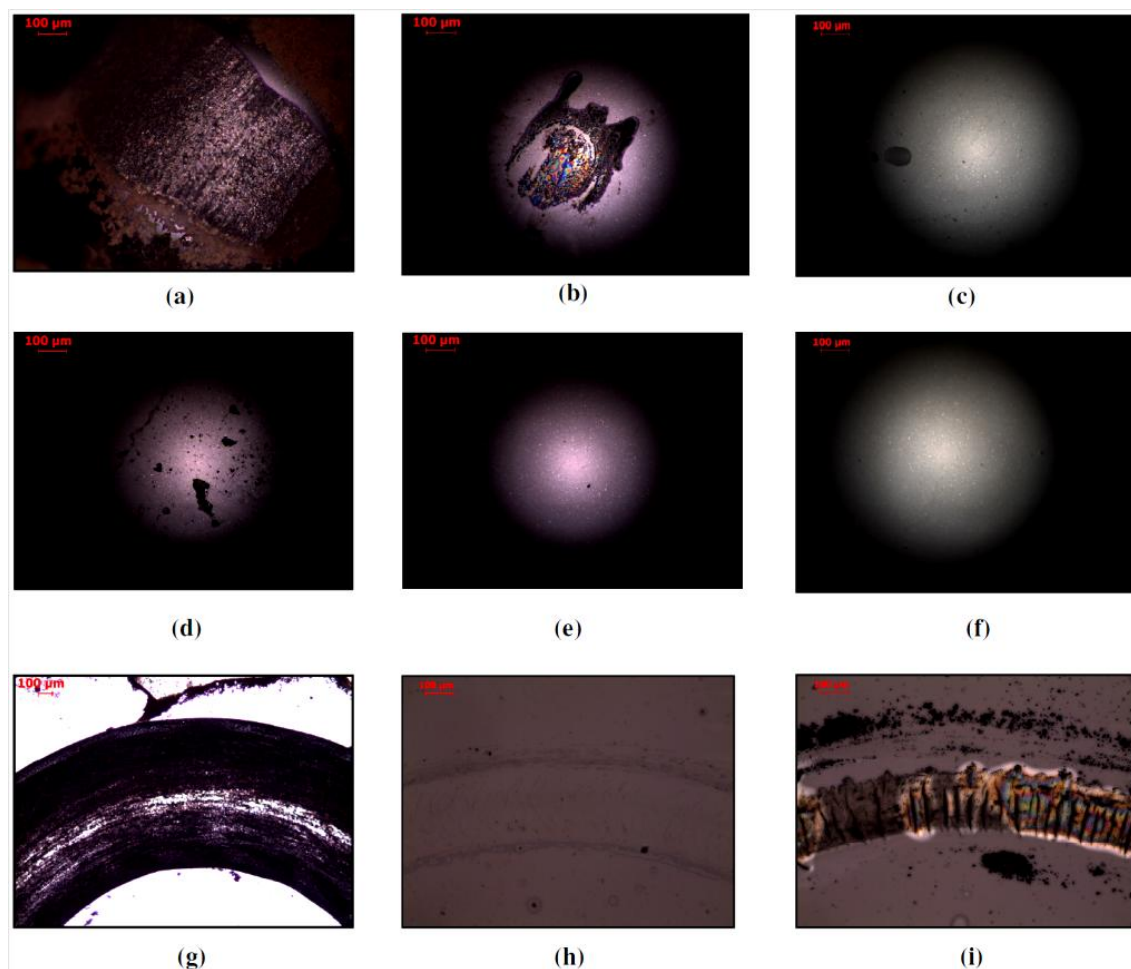


Figure 6.8: Optical micrographs of the counterface ball's surface after sliding tests: (a) Pristine SU-8 (at 70,000 cycles), (b) SU-8+Z-dol (at 500,000 cycles) and (c) SU-8+Z-03

(at 70,000 cycles). Corresponding to the images of the counterface balls shown in (a),(b) and (c), images (d), (e) and (f) are optical micrographs of the counterface ball's surface after cleaning with solvents and images (g),(h) and (i) are optical micrographs of the worn surfaces respectively. The length of the scale bar is 100 μm in all images.

The surface of SU-8+Z-03 (Figure 6.8(i)) shows a very distinct wear track with a series of surface cracks, which indicates the signs of surface fatigue [Shi et al. 2000]. Moreover, the lower dispersive energy of SU-8+Z-dol has helped the Z-dol lubricant (shown in Figure 6.8(h)) to form a thin film-like coating spread across the SU-8 surface. In contrast, SU-8+Z-03 (Figure 6.8(i)) shows droplets over the surface instead of film-like spreading, thus, showing more hydrophobic behaviour towards SU-8. The micrographs also strongly support the tribological behaviour explained in the preceding sections.

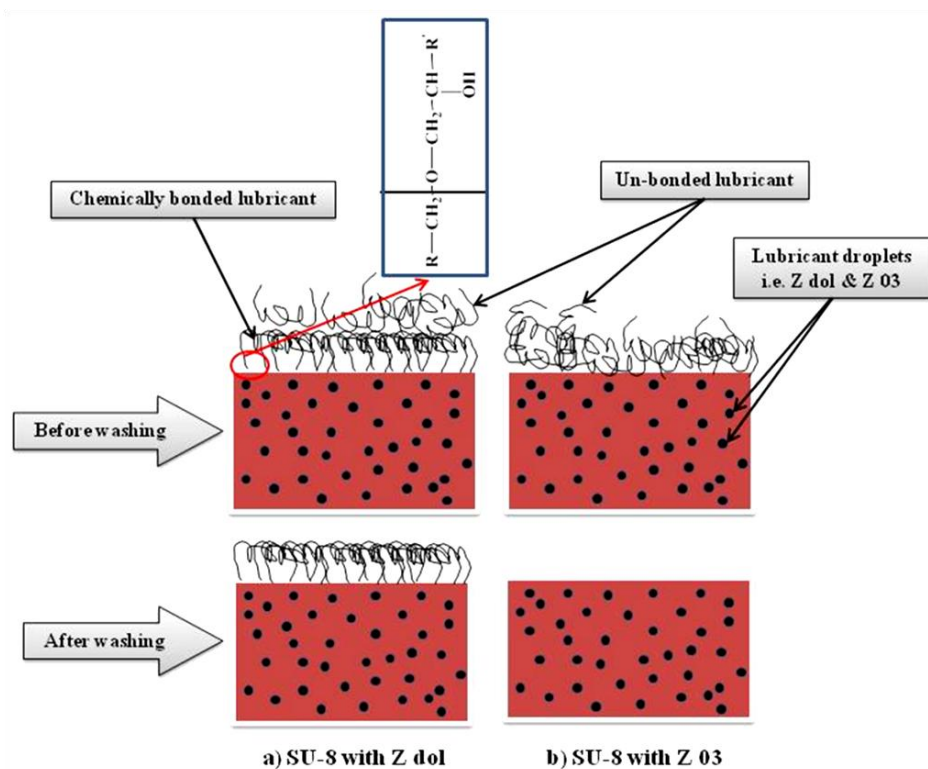


Figure 6.9: Schematic diagram explaining the interaction between SU-8, PFPE Z-dol and PFPE Z-03 molecules in the SU-8 composites.

From the mechanical, chemical and physical characterizations, the following mechanism during the curing process between SU-8 and PFPE composites (Figure 6.9) has been proposed. Before washing, SU-8+Z-dol had few physical and chemisorbed monolayers of lubricant, over which there were few layers of mobile and unbonded lubricant. After washing, the physically bonded molecules were removed but the chemically bonded Z-dol molecules remained on the SU-8 surface. UV exposure helped to create a C-O bond between Z-dol and SU-8 and a full account of the evidences has been provided in Chapter 4, 5 and in the references therein [Tanaka et al. 1964, François et al. 2004 and Surface coatings 1993]. On the other hand, SU-8+Z-03 had a few layers of physisorbed mobile lubricant, which could be easily removed by washing the surface. The increase in C-O group intensity in SU-8+Z-dol was much more evident than SU-8+Z-03 or SU-8, as has been demonstrated by XPS surface chemical analysis.

6.4 Conclusions

In this chapter, the development of SU-8 composites and a wide-spectrum of results proving the chemical interaction between SU-8 and PFPE Z-dol molecules via –OH end groups have been presented. Due to the chemical bonding between the SU-8 and Z-dol molecules, the SU-8+Z-dol composite showed a more superior wear life of ~8 times and a better magnitude of more than four orders ($>10^4$) in comparison with SU-8+Z-03 and pristine SU-8. The following conclusions are drawn from the current study:

- The dispersive surface free energy of SU-8+Z-dol was lower than that for SU-8+Z-03, thus indicating that Z-dol had better dispersion and more affinity towards SU-8.

This was also verified by worn surface micrographs where Z-03 droplets showed hydrophobic behaviour towards SU-8, whereas Z-dol remained uniformly spread across the SU-8 surface.

➤ Nano-tribological results demonstrated that the Z-dol dip-coated SU-8 samples performed better than the Z-03 dip-coated SU-8 samples even after washing and did not fail until 10,000 cycles. This superior tribological behaviour was attributed to the formation of chemical bonds between the Z-dol and SU-8 molecules.

➤ From the XPS results, the SU-8+Z-dol showed an increase in C-O groups in comparison to SU-8+Z-03 although both have the same polymer backbone chain.

➤ TGA characteristics of the Z-dol dip-coated SU-8 samples proved that the Z-dol lubricants' molecules were retained through chemical bonding with the SU-8 molecules even after intensive solvent washing.

Chapter 7

A Comprehensive Investigation of Physical Self-Lubrication

Mechanisms of SU-8 Composites

This chapter presents a detailed investigation on the self-lubrication mechanisms of SU-8 composites (SU-8 with PFPE Z-dol). Chapters 5 and 6 have improved our understanding about the nature of chemical bonding between PFPE and SU-8 molecules and its role in tribological mechanisms. Another essential aspect of the SU-8 composite is the physical self-lubrication mechanism, which needs thorough investigation.

7.1 Introduction

In Chapter 5, it was ascertained that the etherification reaction between SU-8 and PFPE molecules, along with the physical self-lubrication mechanism, have been found responsible for the superior tribological properties of the SU-8 composite [Prabakaran et al 2013 (b)]. Ether bonding between SU-8 and PFPE molecules has enhanced the wear resistance of PFPE molecules over SU-8, which was fully investigated and validated in Chapter 6 [Prabakaran et al 2014]. Another essential aspect of the SU-8 composite is the physical self-lubrication mechanism, which needs thorough investigation. A clearer understanding needs to be obtained about the release of lubricant from the pockets within the matrix, lubricant behaviour at the ball-surface interface, effects of normal load, as well as sliding speed on lubrication and underlying lubrication mechanisms.

Few others have also studied the lubrication mechanism on a micro scale. Among them, Spencer et al. [Spencer et al 2012] have objected to the concept of the conventional

Stribeck curve shown in textbooks, which shows the boundary lubrication regime as the constant friction regime with high COF values. But in reality, the chemistry at the sliding interface plays an important role in reducing friction to the lowest value ($\text{COF} < 0.1$). Boundary friction may increase or decrease with the sliding speed. In addition, molecular structure, chain length, chain orientation and chemistry of the additives or friction modifiers can have a greater influence on the friction at the interface in a boundary lubrication regime than in a hydrodynamic lubrication regime. Direct contact between the sliding surfaces is prevented by absorbed monolayers and they also provide low interfacial shear strength to reduce friction and wear [Spencer et al 2012]. Figure 7.1 illustrates the difference between boundary lubrication as portrayed in textbooks and typical friction modifier-assisted boundary lubrication.

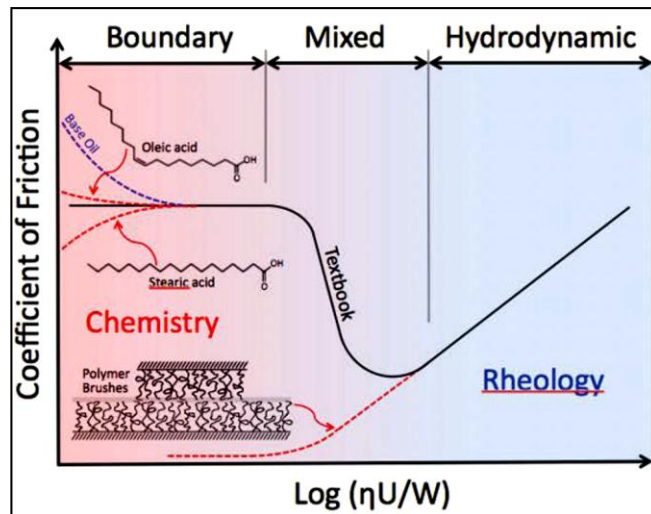


Figure 7.1: Stribeck curve explaining how lubrication behaviour differs in reality from textbooks, especially at low Stribeck numbers. [Reproduced from Spencer et al 2012]

Campen et al. [Campen et al 2012] have investigated the effect of sliding speed on boundary friction. Firstly, they reported from the existing literature that friction increases

along with sliding speed in the boundary lubrication regime, where friction modifiers and additives are present in both the cases of deposited monolayer and self-assembled monolayers. It was also observed that the saturated friction modifiers generally exhibited low friction which increased with the logarithm of sliding speed, whereas the unsaturated friction modifiers exhibited high friction that was less speed-dependent. The reason is that low frictional behaviour at very low speeds depends on the ability of the monolayers adsorbed onto the surface in an orderly closely-packed manner, whereas the unsaturated modifiers may not be able to form such a closely-packed monolayer.

Spikes [Spikes 1997] has done a complete review addressing mixed lubrication regimes, including techniques used to study these regimes, present progress and future prospects. At low Stribeck numbers, the thickness of the roughness is more likely to be higher than lubricant film thickness. Thus, contact operates completely within the boundary regime. It was also reported that the coefficient of friction has a typical value between 0.08-0.12 at this regime and was found to be mostly independent of normal load as long as an effective boundary film exists. The non-conformal contacts, such as point contacts in bearings and gears, were found to operate in elastohydrodynamic regimes only at moderate and high speeds. The film thickness in these regimes follows a trend $(U\eta)^{0.7}$, where the friction is independent of viscosity and reaches a limiting value between 0.02-0.1 based on the chemical structure of the lubricant. It was also reported that surface roughness affects the lubricant film formation considerably in all lubrication regimes.

Bielecki et al. [Bielecki et al 2013] have reported that employing polymer-brush based surface modification is an effective lubrication strategy. Poly (alkyl methacrylates)

with hexyl, dodecyl and octadecyl side chains were prepared on both silicon and iron substrates by means of surface-initiated atom-transfer radical polymerization. Three different lubricants, i.e. hexadecane, ethanol and toluene were used as mobile lubricants between the polymer brushes. From the Stribeck plots, the brush-brush samples showed speed-independent friction behaviour with constant low COF ($\mu \sim 0.01$) at low *speed x viscosity* numbers. They attributed this behaviour to the brush-lubrication regime. After the transition regime, COF increases with the increase of the *speed x viscosity* number in the hydrodynamic lubrication regime. The reason for this behaviour was attributed to the squeezing of film, which in turn increases the effective viscosity, the interfacial shear stress values and friction.

Prathima et al. [Prathima et al 2013] have investigated the nanotribological properties of PEG/ dextran brushes over silica surfaces by using colloidal-probe lateral force microscopy as a function of shear viscosity in various aqueous solvent mixtures. Nano-scale Stribeck curves were constructed for bare silica surfaces in certain aqueous co-solvent mixtures. It was found that the existence of a surface-solvating thin film, due to the adsorption of hydrated ions, prevented direct physical contact at the boundary lubrication regime. The polymer brush surfaces were found to reduce the friction in particular solvent mixtures. They also reported that the presence of an interfacial solvent film for solvated polymer brushes shifts the hydrodynamic lubrication regime to smaller values of Stribeck number ($U\eta$). Hence, the frictional behaviour of polymer brushes is very much determined by the effective viscosity of interfacial solvent film, at lower and higher Stribeck numbers respectively.

Ingram et al. [Ingram et al 2011] investigated the frictional properties of automatic transmission fluids. For efficient operation of clutches without stick-slip, friction should increase with sliding speed and this trend would be maintained over a large range of sliding speeds. Additives and friction modifiers are able to provide low friction at low speeds, and increase friction with increasing speed. They also discussed the literature and main models about hydrodynamic film forming at high sliding speeds and fluid drag supplementing friction as sliding speed increases.

A new model was proposed based on the following two principles: (1) Wet clutch morphology ensures that the contact remains in the boundary lubrication regime over the whole range of sliding speeds, (2) Adsorbed boundary films from organic friction modifiers were found to increase friction with an increase in the logarithm of sliding speed. Conformal contacts were not achieved because of the porosity of friction material in clutches and steel protrusions from the disc, which meant that hydrodynamic lubrication would never be achieved at all speeds. It was postulated that the partial disruption of the organic friction modifier film at higher sliding speeds increases the interpenetration of molecules and asperities from the sliding surfaces. Hence, this increases the shear stress at the interface, which in turn increases friction.

It was also stated that the presence of polar functional groups such as $-OH$ and $-COOH$ exhibited a trend of a rapid increase in friction with increasing speed, followed by a fall in friction. This was attributed to insufficient time to restore the broken bonds between the friction modifiers and the pad surface at high speeds.

Albertson [Albertson 1963] studied the frictional effect of paraffin oil containing anti-squawk additives on common surfaces such as steel and oxidized surfaces. It was

postulated that the damaged boundary film due to sliding processes could be reformed over a short period of time at lower sliding velocities. At higher sliding velocities, there would not be enough time for the damaged boundary film to heal because of enhanced asperity contact. He surmised that the damaged boundary film can only be restored by diffusion of molecules from the lubricant solution to the surface. He developed equations for the rate of reformation of a boundary film, by absorption of additives and molecules from the solution, as a function of the dynamic coefficient of friction:

$$\mu_v = \mu_d - (\mu_d - \mu_\infty) \left[1 - e^{\left[\frac{-c}{v} \right]} \right] \quad (\text{Eq 7.1})$$

where μ_v is the friction coefficient at sliding velocity (v), μ_d and μ_∞ are the friction coefficients of the fully damaged boundary film and fully effective boundary film (especially at low speeds) respectively, c is the parameter that defines the rate of diffusion of additives and molecules to the surface, which accounts for additive concentration and lubricant viscosity.

Another explanation for increased friction with sliding speed is the concept of activated slip models proposed by Eyring [Eyring 1936]. This model postulates that friction is increased because a group of atoms in one layer is trying to pass across the group of atoms with energy barrier “E”. Thus, the activation energy is the energy required to slip across the arising potential barrier between neighboring molecules or atoms. The potential barrier has been overcome by applied shear stress and random thermal fluctuations, and it differs in forward and backward directions with respect to the direction of applied force. When the amount of energy lowers in the forward direction,

the same amount will add in the backward direction. So the combination of these two factors can be derived as:

$$K_f - K_b = A(e^{-(E-\sigma\phi/2)/kT} - e^{-(E+\sigma\phi/2)/kT}) \quad (\text{Eq 7.2})$$

where K_f and K_b are the rates of passage across the potential barriers, λ is the distance moved by the molecules from one side to another across a potential barrier, σ is shear stress, ϕ is the shear activated volume ($\lambda \times A$), A is the area on which the forces act, k and T are the Boltzmann constant and absolute temperature respectively.

The relative velocity, v , between faster molecular layers moving against slower molecular layers, is derived as:

$$v = A\lambda e^{-E/kT} (e^{\sigma\phi/2kT} - e^{-\sigma\phi/2kT}) \quad [\text{Since } \sin(x) = (e^x - e^{-x})/2] \quad (\text{Eq 7.3})$$

$$\text{Thus, it can be rewritten as: } v = 2A\lambda e^{-E/kT} \sinh(\sigma\phi/2kT) \quad (\text{Eq 7.4})$$

For low applied shear stress, $kT \gg (\sigma\phi/2)$, hence the equation can be rewritten as:

$$v = A\lambda e^{-E/kT} (\sigma\phi/2kT) \quad (\text{Eq 7.5})$$

Eq 7.5 shows velocity increasing linearly with applied shear stress at low levels.

For high applied shear stress, $e^{(\sigma\phi/2kT)} \gg e^{-(\sigma\phi/2kT)}$. Thus, Eq 7.4 can be modified as:

$$v = A\lambda e^{-E/kT} e^{(\sigma\phi/2kT)} \quad (\text{Eq 7.6})$$

The above equation shows that velocity increases exponentially with applied shear stress at high levels. Briscoe et al. [Briscoe et al 1982] have demonstrated that interfacial shear stress increases logarithmically with sliding speed when pressure and temperature are kept constant. The results discussed here are from a study of sliding friction between two highly oriented monolayers using molecularly smooth mica substrates in the form of contacting orthogonal cylinders. They assumed that the height of

the potential barriers increases linearly with the applied hydrostatic pressure (p), which was included into Eq 7.6. When shear stress exponentially increases with velocity, $(\sigma\phi / kT) \gg 1$ and Eq 7.6 can be modified for high stress limits as:

$$v = v_0 e^{-(E+p\Omega)} e^{(\sigma\phi/2kT)} \quad (\text{Eq 7.7})$$

Equation (Eq 7.7) is thus equivalent to: $\sigma = (kT / \phi) \ln\left(\frac{v}{v_0}\right) + \frac{1}{\phi}(E + p\Omega)$ (Eq 7.8)

where Ω is the pressure activation volume and v_0 is the unknown and reference velocity.

Thus, the relation between v and σ can be given using the prediction from Eq 7.8 as follows:

$$\sigma = \sigma_1 + \theta \ln(v); \mu_v = x + y \ln(v) \quad (\text{Eq 7.9})$$

$$\sigma_1 = \frac{1}{\phi}(E + P\Omega - kT \ln v_0); \theta = \frac{kT}{\phi};$$

σ_1 and θ are constants for the monolayer of the given acid. Since the friction coefficient is largely influenced by interfacial shear strength, it can be written as an equation in terms of the friction coefficient [Campen et al 2012] and experiments are also in agreement with the postulated Equation (Eq 7.9) [Briscoe et al 1982]. In addition, the thermally activated model developed by Briscoe and Evans is in agreement with the Eyring model, which suggests a rate-limiting step or characteristic relaxation process during shear that involves several molecules. Hence, the relaxation process is achieved by the relative movement of blocks of molecules.

From the aforementioned literature, it is suggested that the boundary lubrication is mostly independent of normal load, and friction was found to be low at the boundary

regime because of friction modifiers. Also, friction was found to increase with sliding speed at all regimes in a variety of cases. Various unconventional lubrication regimes appear to exist at different Stribeck numbers. The lubrication at the micro/nano scale requires deeper understanding. Hence, we have further investigated the lubrication mechanism of SU-8 composites over a sliding rotational speed range of 0.0001-0.73 m/s (0.5-3500 RPM), and four different lubrication zones were observed. Those lubrication regimes will be explained with adequate results.

7.2 Materials and Experimental Procedures

The physical and chemical properties of SU-8 2050 and PFPE Z-dol lubricant have already been presented in Chapter 3. The sample preparation procedure from sizing the Si wafer substrates to completely cured SU-8 and SU-8 composite films was also detailed in Chapter 3, as well as various characterization techniques and procedures used in this study. The completely cured and cross-linked (after UV and PEB) SU-8 composite (SU-8+5wt% Z-dol) films have shown thickness and surface roughness (R_a) of $\sim 100 \mu\text{m}$ and $\sim 70 \text{ nm}$ respectively.

7.2.1 Micro-tribological Characterization

Micro-tribological behaviour of the SU-8+Z-dol composite was estimated using a ball-on-disk arrangement of the CSM-Nanotribometer (CSM, Switzerland). The tests were performed on a wear track (worn surface) created by a macro-tribological test carried out by a UMT-2 tribometer at a normal load of 300 g and a sliding speed of 3000 rpm as shown in Figure 7.2. The diameter and surface roughness of the silicon nitride (Si_3N_4)

counterface balls (supplied by Salem Specialty Balls, USA) were 2 mm and 5 mm respectively.

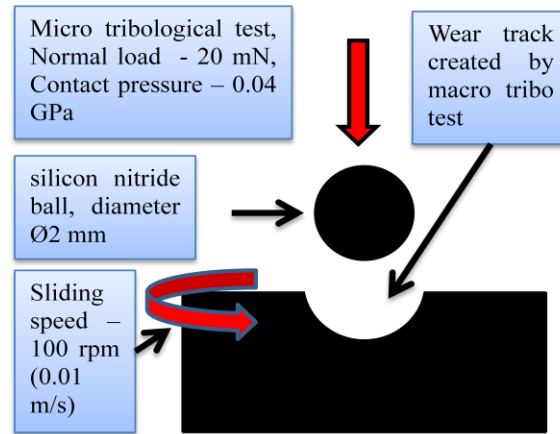


Figure 7.2: Schematic diagram demonstrates execution of micro tribological tests, carried out on the same spot where the macro tribo-test was conducted.

The wear track radius was fixed at 2 mm for all the tests. Each ball was cleaned thoroughly with acetone before the beginning of each test. The normal load (N), rotational sliding speed and the calculated maximum Hertzian contact pressure are shown in Figure 7.2. After each test, the counterface and sample surfaces were examined under an optical microscope to investigate the wear mechanisms. All experiments were performed in air at room temperature (25°C) at a relative humidity of approximately 60% and the average values are reported here.

Important Note: All sliding speeds / sliding velocities reported here are sliding rotational speeds (RPM) only. Sliding velocities reported in this chapter are conversion of actual sliding rotational speeds (RPM) used for testing.

7.3 Results and Discussion:

7.3.1 Coefficient of Friction (COF) versus Sliding Velocity Plot

Figure 7.3 shows typical coefficient of friction (COF) values versus sliding velocity plot for the 5wt% SU-8+Z-dol composite which was tested at a normal load of 300 g and different sliding velocities. The COF is observed for a fixed number of 10,000 cycles irrespective of sliding velocity.

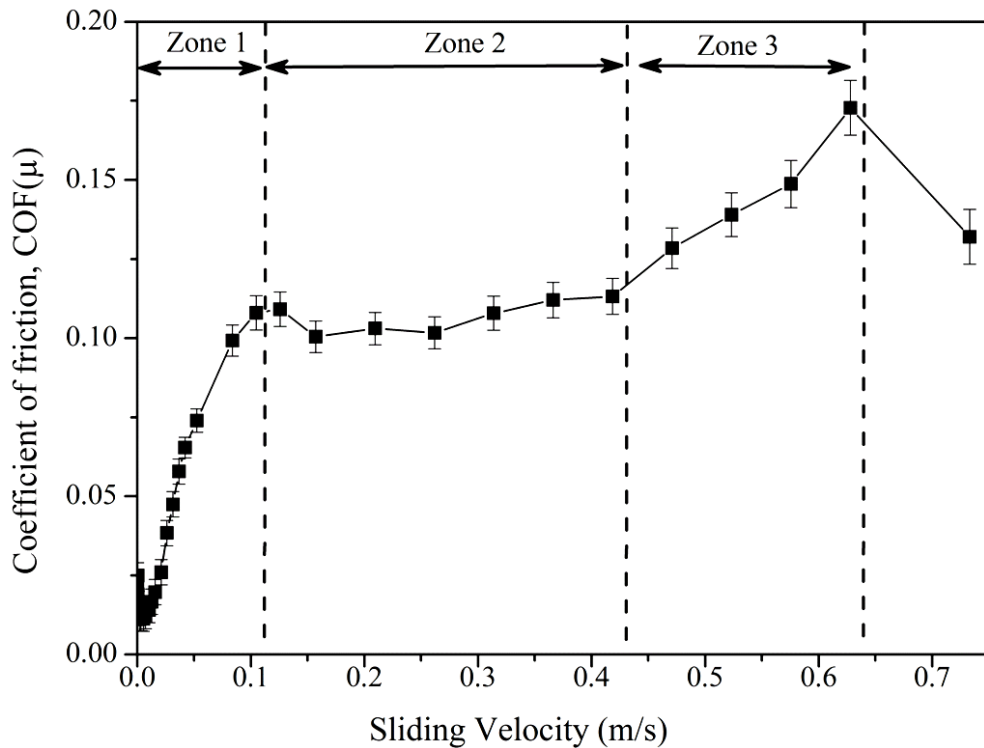


Figure 7.3: Coefficient of friction (COF) versus sliding velocity plot for 5wt% SU-8+Z-dol composite tested at a normal load of 300g and different sliding velocities for a fixed number of 10,000 sliding cycles. Zone 1, Zone 2 and Zone 3 are three regimes with different frictional behaviour. Zone 1: COF increases steeply (0-0.12 m/s (600 RPM)). Zone 2: COF increases marginally (0.15-0.36 m/s) (750-1500 RPM). Zone 3: COF increases linearly (0.41-0.73 m/s) (2000-3000 RPM).

Three different zones or regimes were identified based on their exhibited frictional behaviour with speed. Zone 1, Zone 2 and Zone 3 exhibit a steep increase, marginal increase and linear increase in COF respectively, as speed increases. At Zone 1, a steep increase in COF from 0.02 to 0.11 was observed, while Zone 2 exhibited a marginal increase in COF from 0.11 to 0.12. Zone 3 exhibited a linear increase in COF from 0.12 to 0.17. After Zone 3, there was a sharp drop in COF from 0.17 to 0.13 at 0.73 m/s. The lubrication mechanism responsible for frictional behaviour observed in Zone 1, 2, 3, and after Zone 3 is elaborated in succeeding paragraphs with ample evidence.

7.3.2 Discussion

7.3.2.1 Lubrication Mechanism at Zone 1 (Low Speeds):

Figure 7.4 shows a sequence of possible lubrication mechanisms at the ball-surface interface during Zones 1, 2 and 3 (shown earlier in Figure 7.3). Zone 1 sliding speed ranges from 0.0001 – 0.125 m/s (0.5-600 RPM), where the COF rises steeply. Figure 7.4 (a), (b) and (c) corresponds to the schematic of ball-surface interface before the start of the sliding test, at the beginning of sliding cycle, and at the ending of the sliding cycle, respectively. Before sliding (Figure 7.4(a)), the surface has few layers of bonded lubricant and many layers of un-bonded mobile lubricant.

Next, Figure 7.4(b) shows the beginning of the sliding cycle where the counterface ball slides against the surface with defined normal load. The bonded monolayers of PFPE at the interface behave in a similar fashion to polymer brushes, and over where there is mobile PFPE lubricant [Bielecki et al 2013, Prathima et al 2013]. Though the molecules in the bonded layer have conformed to a packed configuration, the

presence of mobile lubricant between them lowers the interfacial shear strength, which maintains the boundary lubrication. As the counterface ball moves away, the bonded molecules spring back to their original configuration and mobile lubricant flow backs to the contact point (Figure 7.4(c)).

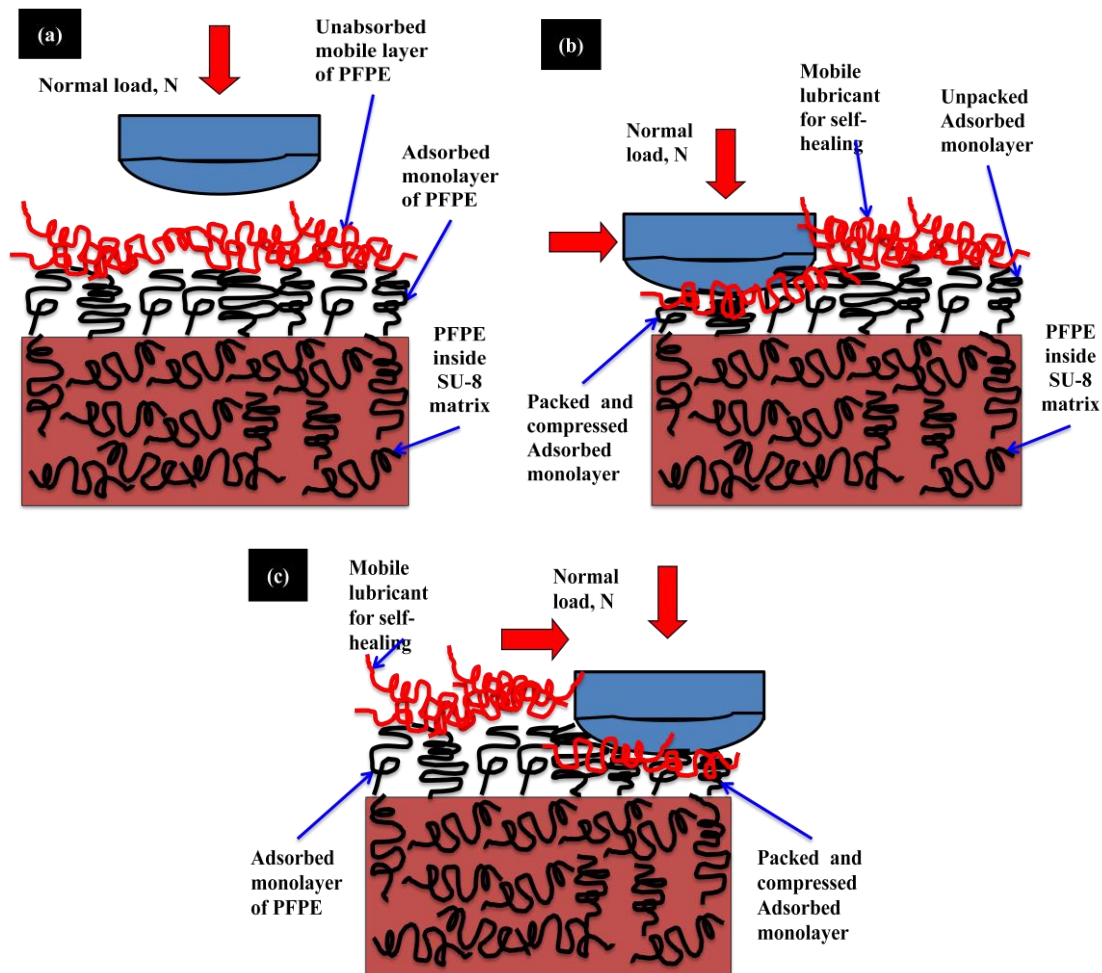


Figure 7.4: Possible sequence of lubrication mechanisms at the ball-surface interface during Zone 1, where low speed sliding takes place. (a) Before sliding. (b) Beginning of the sliding. (c) End of sliding.

It is also observed that the displacement of lubricant from the contact point increases as sliding speed increases. At low speeds, the entire wear track is covered by lubricant because there is enough time for the displaced mobile lubricant to diffuse across the wear

track again. As speed increases, there is not enough time for the displaced lubricant to diffuse across the wear track between consecutive cycles [Albertson 1963]. This continuous displacement of lubricant from the wear track has led to lubricant starved solid-solid contact, which increases the COF, leading to subsequent wear. This proposed mechanism for lubricant displacement is also supported by optical micrographs of the counterface ball after the wear test and the worn surface, as shown in Table 7.1 (only for selected sliding velocities). The micrographs of the counterface ball in Zone 1 (0-0.12 m/s) show an obvious lubricant transfer film over them and the worn surface images show a progressive reduction in lubricant coverage of the wear track with the increase in speed. The wear debris of SU-8 transferred to the ball also increases with speed, which indicates increased asperity contact.

7.3.2.2 Lubrication Mechanism at Zones 2 and 3 (High Speeds)

Figure 7.5 (a) shows the high-speed sliding (at the start of Zone 2) where the majority of mobile lubricant is displaced from the surface, leaving a few layers of bonded and unbonded lubricant. There is less time for displaced mobile lubricant to flow back onto the wear track. Bonded monolayers with very little mobile lubricant may not withstand such severe operating conditions, and eventually fail, as demonstrated by Figure 7.5 (b). Once the wear process reaches the next layer of fresh lubricant droplets, lubrication occurs, as demonstrated by Figure 7.5 (c). Hence, a marginal drop in COF is observed at the beginning of Zone 2 (0.15-0.36 m/s). Then, the COF almost plateaus with little increase until Zone 3. This constant COF is attributed to the lubrication provided by the release of a new batch of lubricant.

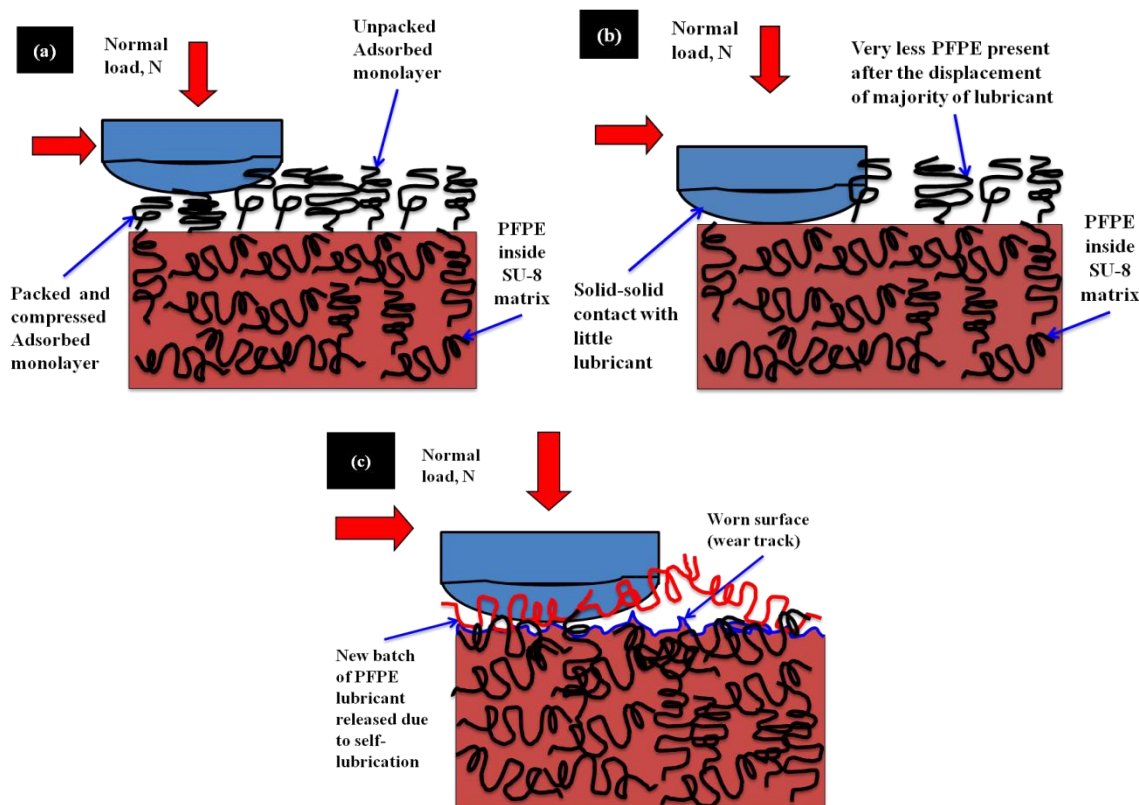


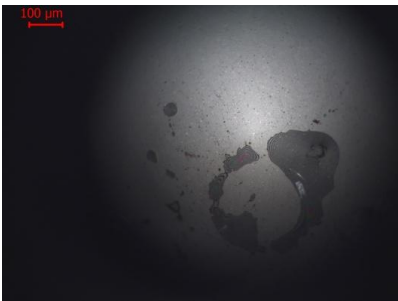
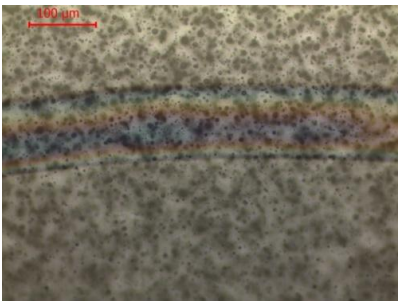
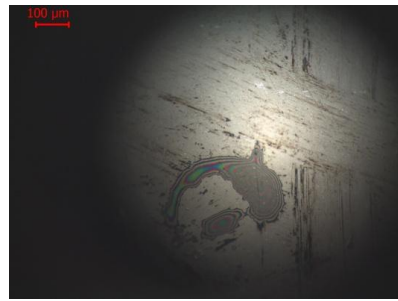
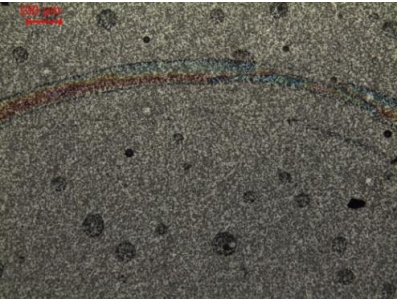
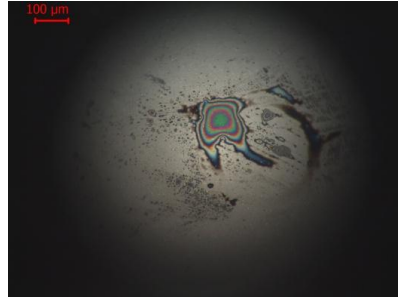
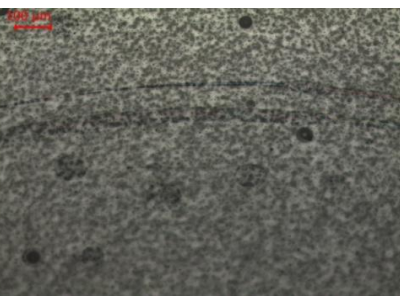
Figure 7.5: Possible sequence of lubrication mechanisms at the ball-surface interface during Zones 2 and 3, where high speed sliding takes place. (a) After a few sliding cycles. (b) Lubricant-starved contact. (c) Wear releases new batch of lubricant due to self-lubrication.

However, the lubrication was not as effective as compared to fresh surfaces because of the following possibilities. 1) Wear particles would destroy the boundary film, thus never maintaining an effective boundary film. 2) No boundary lubrication is attained because surface roughness would be much higher than film thickness. Hence, lubrication is provided by the slurry of the lubricant and wear particles rather than by the lubricant alone. Thus, the COF never drops to as low a value as the case of lubricant being solely present. Micrographs in Table 7.1 also show minimal lubricant on the surface and ball at the beginning of Zone 2, but suddenly much more lubricant on both was observed as speed increased.

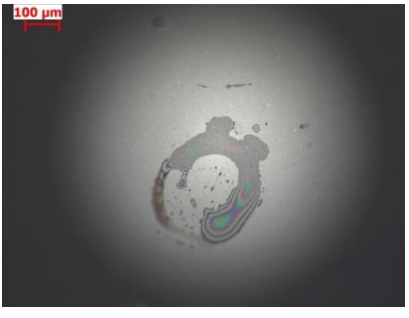


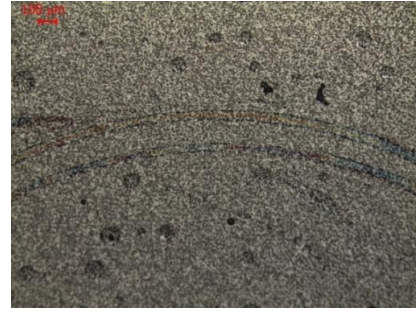
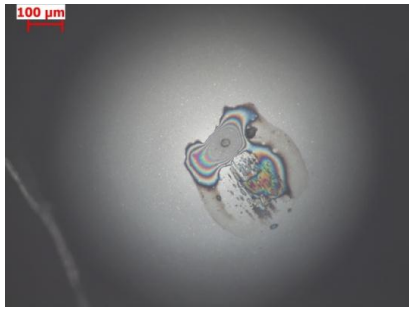
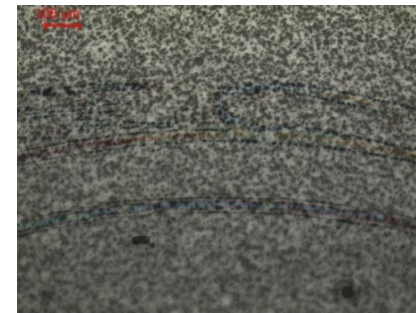
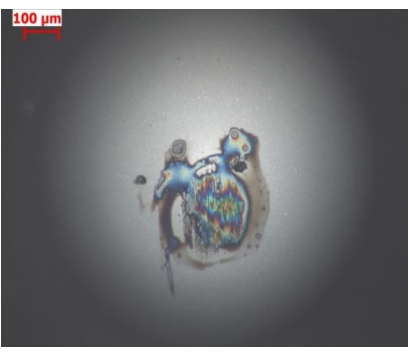
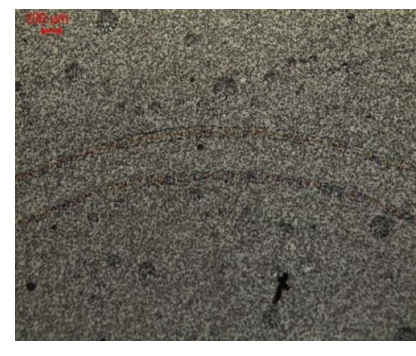

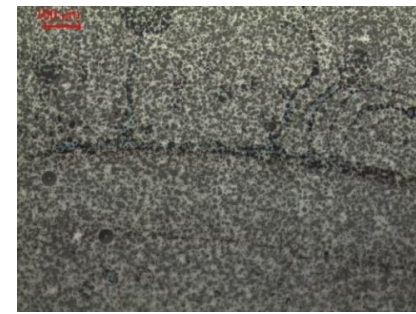
This also ascertains the new batch of lubricant released by the self-lubrication mechanism. Evidence for self-lubrication was presented in Chapters 5 and 6 [Prabakaran et al 2013 (b)]. When speed is further increased into Zone 3, COF started increasing linearly. This increase in COF is again attributed to lubricant displacement, and can be witnessed by optical micrographs in Table 7.1, which has no lubricant over either the ball or the surface. As soon as it reaches the dry contact at the sliding velocity of 0.73 m/s (3500 rpm), a new batch of lubricant is released and the COF drops to a lower value and stabilizes again. The same cycle may be repeated again and again. The sliding velocity of 0.73 m/s is the maximum velocity up to which we studied frictional behaviour in the present thesis.

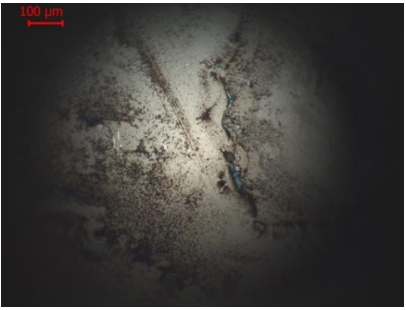
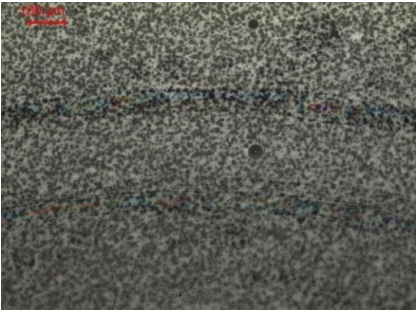
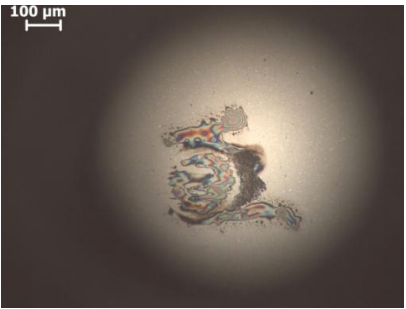
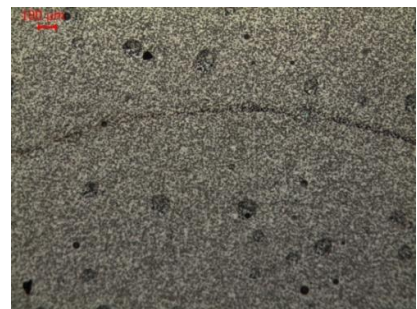
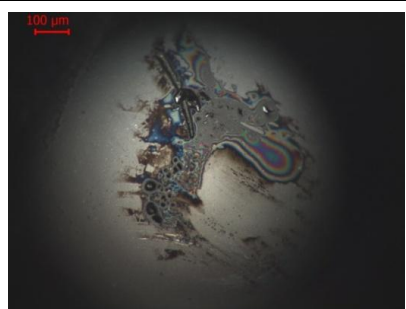

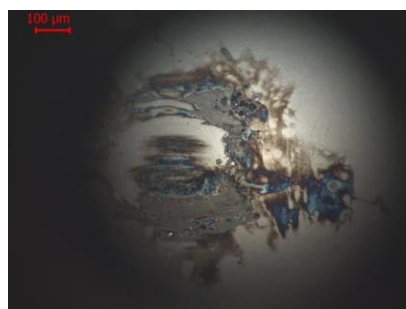

Table 7.1: Summary of coefficient of friction (μ_s) values for 5wt% SU-8+Z-dol composite obtained from sliding tests against 4 mm diameter Si_3N_4 ball at a fixed normal load of 300g and various sliding rotational speeds and their corresponding counterface ball and worn surface image after the sliding test, respectively.

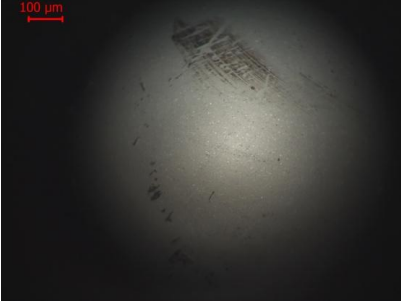
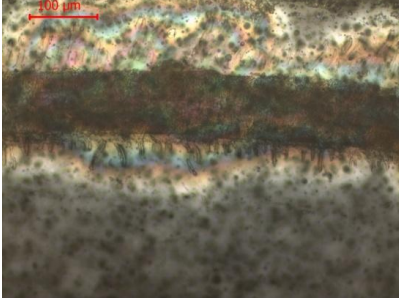
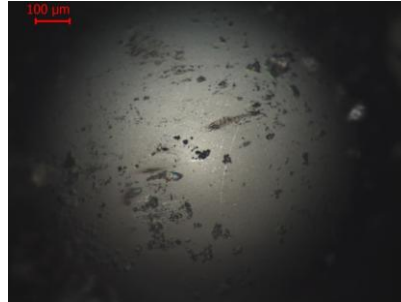

[Note: The data summarized here were obtained from the coefficient of friction Vs sliding speed shown in Figure 7.3. Z1, Z2 and Z3 are three regimes with differing frictional behaviour. Zone 1: COF increases steeply (0-0.12 m/s). Zone 2: COF increases marginally (0.15-0.36 m/s). Zone 3: COF increases linearly (0.41-0.73 m/s).]

| Sliding Velocity (m/s) | COF | Optical Images | Surface Images |
|---------------------------------------|-------|---|--|
| Zone 1 : COF increases steeply | | | |
| 0.0002 (1 RPM) | 0.025 |  |  |
| 0.001 (5 RPM) | 0.020 |  |  |
| 0.002 (10 RPM) | 0.020 |  |  |

Chapter 7: A Comprehensive Investigation of Physical Self-Lubrication Mechanisms of SU-8 Composites

| | | | |
|---------------------------|--------------|---|--|
| <p>0.005 (25 RPM)</p> | <p>0.021</p> |  |  |
| <p>0.01 (50 RPM)</p> | <p>0.023</p> |  |  |
| <p>0.02 (100 RPM)</p> | <p>0.026</p> |  |  |
| <p>0.05 (250 RPM)</p> | <p>0.074</p> |  |  |
| <p>0.12 (600 RPM)</p> | <p>0.11</p> |  |  |

| Zone 2 : COF increases marginally | | | |
|--|-------|---|--|
| 0.15 (750 RPM) | 0.098 |  |  |
| 0.20 (1000 RPM) | 0.105 |  |  |
| 0.31 (1500 RPM) | 0.118 |  |  |
| Zone 3: COF increases linearly | | | |
| 0.42 (2000 RPM) | 0.106 |  |  |

| | | | |
|--------------------------------|--------------|---|--|
| <p>0.52 (2500 RPM)</p> | <p>0.129</p> |  |  |
| <p>0.63 (3000 RPM)</p> | <p>0.173</p> |  |  |

7.3.3 Effects of Normal Load and Sliding Rotational Speed

Figures 7.6 (a) and (b) show the COF vs sliding speed and COF vs normal load plots of 5wt% SU-8+Z-dol composite respectively, tested for a fixed number of 10,000 cycles. The effect of sliding rotational speed on the frictional behaviour of 5wt% SU-8+Z-dol composite for various normal loads has been discussed using Figure 7.6(a). The coefficient of friction follows a rising trend for almost all normal loads such as 10, 50, 100, 200 and 300g for sliding speeds ranging between 1 – 3000 rpm. The normal load case of 10g proves an exception, where the COF drops after 1500 rpm due to effective self-lubrication. The COF for various normal loads at any given single speed has very marginal variation. For example, at 1500 rpm, the COF varies between 0.1-0.14 between the load range of 10-300g. However, the COF variation at specific loads for different speeds is substantial. It indicates that sliding speed plays an important role in the

frictional behaviour of these composites. The Zones discussed in Figure 7.3 may not occur at the same speed for different normal loads, but they all follow very similar trends and have very little effect from the normal load. Thus, the mechanism at the ball-surface interface is very much controlled by the lubricant's frictional properties, rather than the frictional properties of the SU-8-ball pair. The effect of normal load on the frictional behaviour of the 5wt% SU-8+Z-dol composite for various sliding rotational speeds has been discussed using Figure 7.6(b). The COF merely follows a constant trend with little variation between various normal loads at any given single sliding speed. A sliding speed of 100 rpm yields a COF of ~0.05 and 0.04, at 10g and 300g respectively. Hence, the variation of 0.01 is very much within the experimental error band. Conversely, the sliding speed of 3000 rpm gives a COF of ~0.11 and 0.18, at 10g and 300g respectively. The variation in COF is ~0.07, which is a noticeable experimental variation, signifying that the normal load has minimum effect on the frictional behaviour of SU-8+PFPE and is noticeable only at higher speeds than at lower speeds. However, the effect of sliding speed on friction is very significant as compared to the effect of normal load on friction.

The sudden small drop or increase in COF for certain speeds is not clearly understood, and it can be attributed to the self-lubrication mechanism. Overall, these results ascertain that sliding speed has great effect on the frictional behaviour of 5wt% SU-8+Z-dol than the normal load within the range studied. The sliding speed varies in three orders of magnitude (10^3), whereas the load varies only in two orders of magnitude (10^2) (because of experimental limitations of the machines). Therefore, the results obtained here may have some scale effects and further work is necessary to elucidate such effects.

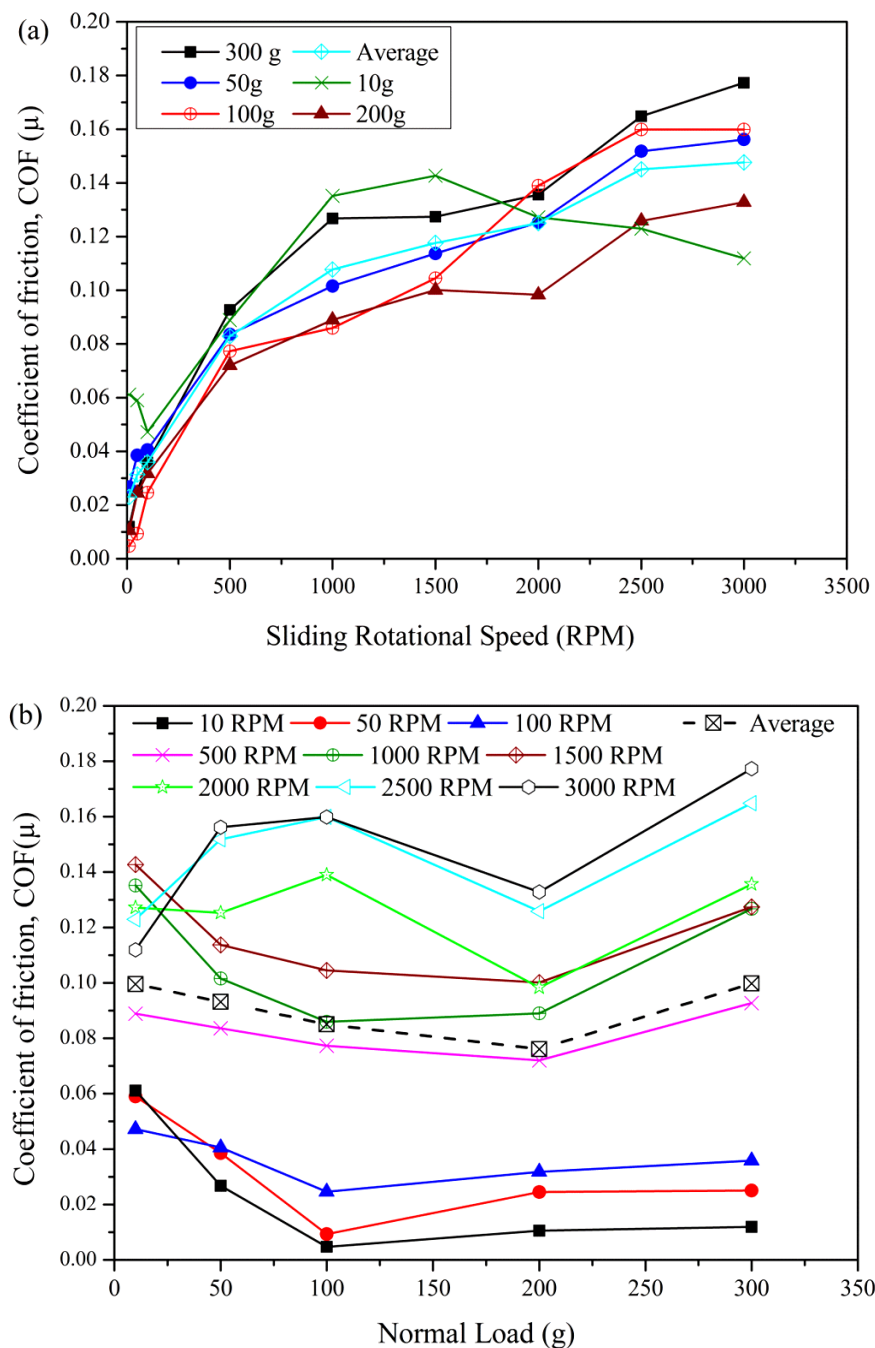


Figure 7.6: Effect of sliding rotational speed (V) and Normal load (N) on frictional behaviour of 5wt% SU-8+Z-dol composite tested against 4 mm diameter Si_3N_4 balls with the ball-on-disk sliding configuration at a different normal load and a sliding rotational speed. (a) COF Vs sliding rotational speed plot: 5wt% SU-8 +Z-dol composite tested at a range of sliding rotational speeds from 10 to 3000 RPM for normal loads from 10 to 300g. (b) COF Vs Normal load plot: 5wt% SU-8+Z-dol composite tested at a range of normal loads from 10-300g for sliding rotational speeds from 10 to 3000 RPM. [Standard Error: ± 0.02].

7.3.4 Tribological High-Low Speed Tests

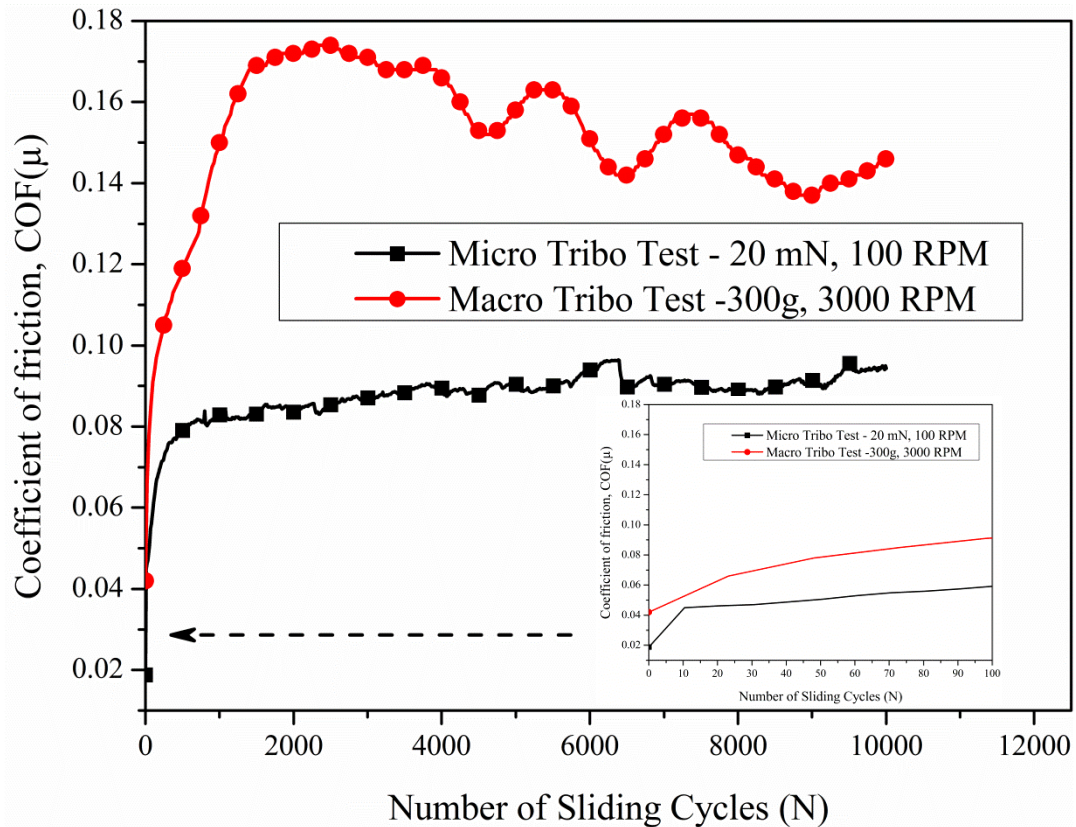


Figure 7.7: Typical coefficient of friction versus number of sliding cycles plot of 5wt% SU-8+Z-dol composite tested against 4 mm diameter Si_3N_4 ball with the ball-on-disk sliding configuration at different normal loads and sliding rotational speeds for a fixed test duration of 10,000 cycles. (—●—): Macro-tribological tests were conducted at a normal load of 300g and sliding speed of 3000 rpm on a fresh surface. (—■—): Micro-tribological tests were performed right after the macro-tribological test at the same wear track for a normal load and speed of 20 mN and 100 rpm.

Figure 7.7 shows the typical coefficient of friction versus number of sliding cycles plot of 5wt% SU-8+Z-dol composite tested at different loads and rotating sliding speeds for a fixed 10,000 cycles of operation over the same spot. The objective of these tests was to confirm the presence of PFPE over the worn surface after the operation of 10,000 cycles

at macro conditions such as normal load and speed of 300g and 3000 rpm respectively. A normal load and sliding speed of 300g and 3000 rpm respectively were applied over a fresh surface of 5wt% SU-8+Z-dol composite for 10,000 cycles. The fresh surface of 5wt% SU-8+Z-dol showed a steady-state coefficient friction (μ_s) of ~ 0.15 for 10,000 sliding cycles with a mild-wear track. It is also obvious that the majority of PFPE available at the surface was displaced from the wear track, which led to the wear.

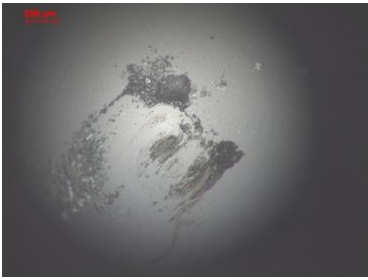

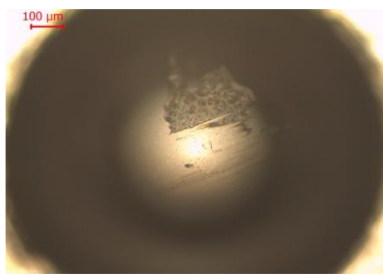
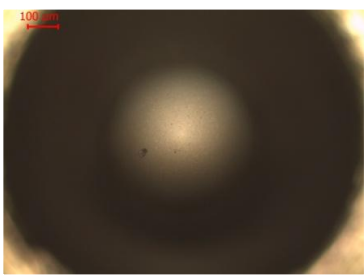
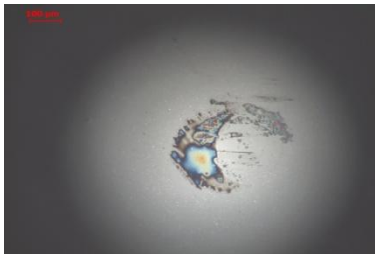
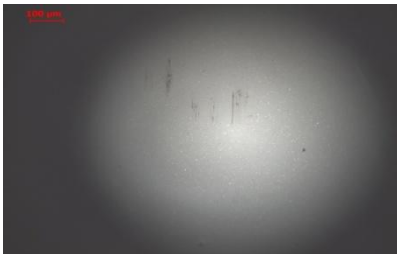
Since there was wear, it was necessary to confirm the presence of PFPE which might have migrated to the surface from the SU-8 matrix through the self-lubrication mechanism. Therefore, micro-tribological tests with normal load of 20 mN and sliding speed of 100 rpm were performed on the same wear track. Severe operating conditions such as high normal load of 300 g and speed of 3000 rpm respectively have not been chosen, due to the difficulty of PFPE displacement and damage to boundary film. Micro-tribological tests showed a steady-state coefficient of friction (μ_s) of ~ 0.08 with almost no additional wear. The results showed that the steady-state friction coefficient (μ_s) was reduced by ~ 2 times, which confirms the presence of PFPE, even after wear. The inset inside Figure 7.6 also shows the first few cycles of two wear tests. The micro-tribological test shows the COF, which is two times lesser than the COF of the macro-tribological test, proving self-lubrication was responsible for PFPE replenishment.

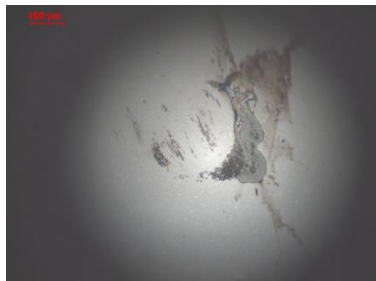
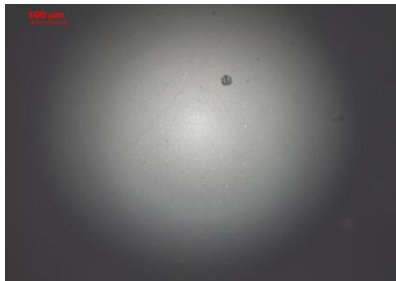


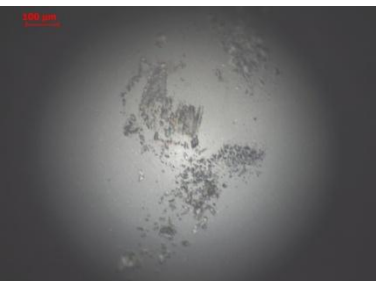

The presence of PFPE at the wear track is also confirmed by optical images captured after the wear tests. Table 7.2(a) shows the micrographs of the counterface ball after the macro-tribological test of 300 g and 3000 rpm respectively, and after cleaning the ball with acetone solvent, which was done to assess the damage to the ball. The counterface ball after the test shows the materials transferred onto it through abrasive

wear and also shows small scratches after cleaning. These images may indicate PFPE-starved contact between the ball and SU-8, or little PFPE present over the surface, which may not be effective at such severe operating conditions. Table 7.2 (b) shows the micrographs of the counterface ball after the micro-tribological test of 100 mN and 200 rpm respectively, and after cleaning the ball with solvent (acetone). The counterface ball after the test shows a film of PFPE transfer film with some wear debris. After cleaning, it shows a clean surface comparable to that of a new ball. These micrographs confirm the presence of PFPE at the wear track after severe operating conditions.

A few macro-tribological tests of a 300g normal load and different speeds such as 10 and 1000 rpm were performed on the same wear track, and corresponding micrographs are presented in Table 7.2 (c). The PFPE film, seen over the counterface ball at 10 rpm, has disappeared at 1000 rpm. These results confirm lubricant displacement at higher speeds. However, while the PFPE present over the wear track may not be effective in providing lubrication at such severe conditions, it can provide lubrication for less severe conditions such as micro-tribological conditions. EDS mapping and elemental analysis were also performed at random spots on the wear track and the results are presented in the next section.

Table 7.2: Summary of co-efficient of friction values of 5wt% SU-8 composites obtained from sliding tests using a 4 mm diameter Si₃N₄ ball, at fixed normal load of 300 g and various sliding rotational speeds. The corresponding optical micrographs of the counterface ball after sliding tests and micrographs of the counterface ball after cleaning with solvent are also shown. The sliding tests were conducted from a high speed of 3000 rpm to low speeds of 10, 100, 500 and 1000 rpm, respectively.

| Sliding Speed (RPM) | Coefficient of friction, COF(μ) | Counterface ball micrograph after sliding test | Counterface ball micrograph after cleaning with solvent |
|--|---------------------------------------|---|--|
| a) Macro tribo test : 5wt% SU-8+Z-dol composite, Normal load : 300g | | | |
| 3000 | 0.151 |  |  |
| b) Micro tribo test after macro test on the same spot, 20 mN | | | |
| 100 | 0.08 |  |  |
| c) Macro tribo tests performed on the same spot, Normal load : 300g | | | |
| 10 | 0.006 |  |  |

| | | | |
|------|------|--|---|
| 100 | 0.07 |  |  |
| 500 | 0.12 |  |  |
| 1000 | 0.13 |  |  |

7.3.5 EDS (Electron-Dispersive X-ray Spectroscopy) Elemental Mapping

Figure 7.8 shows EDS (Electron-Dispersive X-ray Spectroscopy) elemental mapping which was carried out on random spots of wear track of 5wt% SU-8+Z-dol composite tested at macro-tribological conditions of a normal load of 300g and sliding rotational speed of 3000 rpm, for 10,000 sliding cycles. It is necessary to analyze the presence of PFPE at the wear track after the macro-tribological test because of a high friction coefficient along with wear of material witnessed in the first image, Grey (upper left). SU-8 is an alkane, consisting mainly of carbon (C) and oxygen (O). The presence of PFPE

lubricant can be confirmed by fluorine (F). Hence, C, O and F were selected for elemental mapping.

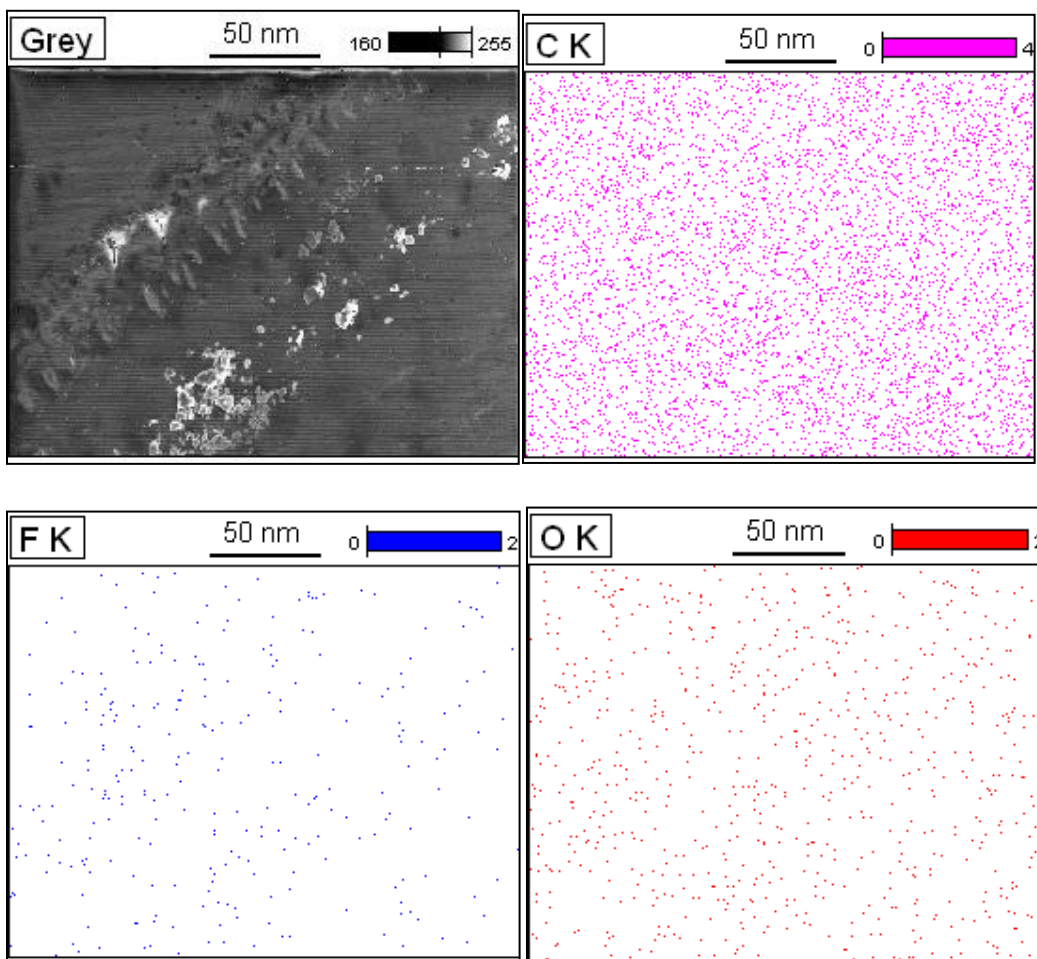


Figure 7.8: EDS elemental mapping carried out on the random spot of wear track (worn surface) of 5wt% SU-8+Z-dol composite tested at macro-tribological test conditions of normal load of 300 g and sliding rotational speed of 3000 rpm for a fixed test duration of 10,000 cycles. [Note: C-Carbon (UR); O-Oxygen (LL); F-Fluorine (LR)] [Legends: UR – Upper Right, LL – Lower Left and LR – Lower Right]

The concentration of elements scanned within the selected area of wear track is as follows: carbon (C) > oxygen (O) > fluorine (F), because SU-8 is about 95wt% of composite and PFPE is only 5wt%. The concentrations of C and O are well dispersed

throughout the scanned spot, whereas F is mostly concentrated in around the wear track than far away from the wear track. The above mapping demonstrated unusual fluorine (F) concentration in and around the wear track, confirming the presence of PFPE on the wear track. It also suggests that the PFPE present over the wear track may not be able to withstand such highly severe operating conditions for prolonged durations.

7.4 Conclusions

Coefficient of friction versus sliding velocity plot for 5wt% SU-8+Z-dol composite was constructed using results obtained from sliding tests conducted at a normal load of 300g and different sliding speeds until 10,000 sliding cycles. Three different Zones were identified based on their exhibited frictional behaviour with speed. Zone 1, Zone 2 and Zone 3 exhibit a steep increase, marginal increase and linear increase in COF respectively, with the increase in speed.

- At low speeds, the entire wear track is covered by lubricant because there is enough time for the displaced mobile lubricant to diffuse across the wear track again after each sliding. As the speed increases, there is not enough time for the displaced lubricant to diffuse across the wear track between consecutive cycles.
- Hence, the increase in sliding speed leads to increased asperity contact and initiates surface wear. Once the wear process reaches the next layer of fresh lubricant droplets, lubrication occurs. Then, the COF stabilizes.
- A further increase in speed increases the COF linearly. This increase in COF is again attributed to lubricant displacement. As soon as the contact became dry

- without any lubricant, a new batch of lubricant is released from the droplets and the COF drops to a lower value and stabilizes again.
- The effects of normal load and sliding speed were studied separately and it was found that the sliding speed has a greater effect on the frictional behaviour of 5wt% SU-8+Z-dol composites than the normal load. The macro- and micro-tribological, optical and EDS characterizations along with the existing literature, have supported the proposed tribological behaviour of 5wt% SU-8+Z-dol composite at various speeds.

Chapter 8

Effects of Curing Temperature and In-situ Heating on Thermal Stability of SU-8 Composites

This chapter presents the investigation of effects of in-situ heating and curing temperature on the thermal stability of SU-8 composites. Tribological and mechanical behaviours of SU-8 composites were evaluated at various in-situ temperatures and interpreted with regard to physical and chemical phenomena. The following presents the main objectives for this chapter: 1) To investigate the thermal stability of the SU-8 composite at higher temperatures above room temperature. 2) To investigate the effect of curing temperature on the performance of the SU-8 composites.

8.1 Introduction

Chapter 4 detailed the development of the self-lubricating SU-8+PFPE composite by blending liquid PFPE into SU-8. The SU-8+PFPE composite reduced the initial coefficient of friction (μ_i) by ~8 times, reduced the steady-state coefficient of friction (μ_s) by ~6 times and increased wear life by $>10^4$ times, as compared to pristine SU-8. Chapter 5 elaborated on the formation of an ether bond between the SU-8 and PFPE molecules, which provides high wear durability to the composite, as the lubricant molecules are not easily removed or worn. Chemical bonding, uniform dispersion of PFPE lubricant in bulk, and effective spreading of the lubricant over the surface are considered main factors controlling tribological performance of the SU8+PFPE composite [Prabakaran et al 2013

(a)]. It is therefore necessary to investigate the effect of curing conditions on the tribological behaviour of the SU-8 and SU-8 composites.

Ma et al [Ma et al 2001] have reported that higher temperatures accelerate the surface diffusion of Fomblin Z-dol and Z-type PFPE lubricants on amorphous carbon surfaces (widely used in hard disk drive (HDD) systems). They also reported that the reaction between the main chain and the carbon surface has no effect on the reactions between the end-groups and surface. In addition to that, they also postulated that no reaction was viable between the main chain and the carbon surface. Liu et al [Liu et al 2003] have studied the effect of temperature on molecularly thin films of Z-15 and Z-DOL type PFPE lubricants. They reported that an increase in temperature desorbs the moisture film over the surface and helps to reduce viscosity, which facilitates the orientation of molecules. However, no tribological data were reported in this work.

Unal et al [Unal et al 2012] have studied the friction and wear behaviour of pure polyimide-6 (PA-6), graphite-filled polyimide-6 and wax-filled polyimide-6, sliding against stainless steel under dry conditions. They concluded that the maximum wear resistance was exhibited by wax-filled PA6 composites. The wax-filled PA6 composites were 20 and 200 times more wear-resistant than graphite-filled PA6 composites and pure PA6 respectively, under dry sliding conditions. Bijwe et al [Bijwe et al 2013] have reported on the tribological behaviour of polyetherketone (PEK)-based composites containing carbon or glass fibers along with various solid lubricants. The short fibers of carbon and glass, along with solid graphite lubricant, have improved the friction and wear properties of PEK. From the results, it was concluded that graphite is more efficient than PTFE as a

solid lubricant, and that glass and carbon fibers lead to the lowest friction coefficient and highest wear resistance respectively.

In this chapter, *in-situ* heating effect on the tribological behaviour of the SU-8+PFPE composites was investigated. The *in-situ* heating experiments were conducted at temperatures ranging from room temperature (25°C) to 100°C, and yielded significant improvements in the tribological and mechanical properties of the SU-8+PFPE composite.

8.2 Materials and Experimental Procedures

8.2.1 Materials

The physical and chemical properties of SU-8 2050 and perfluoropolyether Z-dol 4000 lubricant have already been summarized in Chapter 3. The sample preparation procedure, from sizing the Si wafer substrates, to completely cured SU-8 and SU-8 film composites and other characterizations, was detailed in Chapter 3. 2wt% is the concentration of the lubricant used in this chapter.

8.2.2 Tribological Characterization

Friction and wear tests were carried out using the UMT-2 (Universal Micro Tribometer, CETR, USA), in a ball-on-disk setup where the coefficient of friction (μ) was measured with respect to the number of sliding cycles (N). Si₃N₄ balls of 4 mm diameter, with a surface roughness of 5 nm, were used as the counterface. The tests were conducted at a normal load of 300 g and sliding velocity of 7 mm/s. The complete experimental heating setup was operated in air at room temperature (25°C) and at a relative humidity of

approximately 60%, where the sliding tests were also performed. The schematic of the experimental heating set-up used is shown in Figure 8.1. From the sliding tests, an initial coefficient of friction (μ_i) was noted as an average of the first twenty sliding cycles.

The steady-state coefficient of friction (μ_s) was calculated as the average of all coefficient of friction values from the point where steady-state behaviour was observed, until the end of the test or until the failure point, whichever was earlier. The wear life for the tested conditions was taken as the number of sliding cycles after which the coefficient of friction exceeded 0.3, or when a visible wear track was observed on the substrate with abnormally fluctuating friction values, whichever occurred earlier.

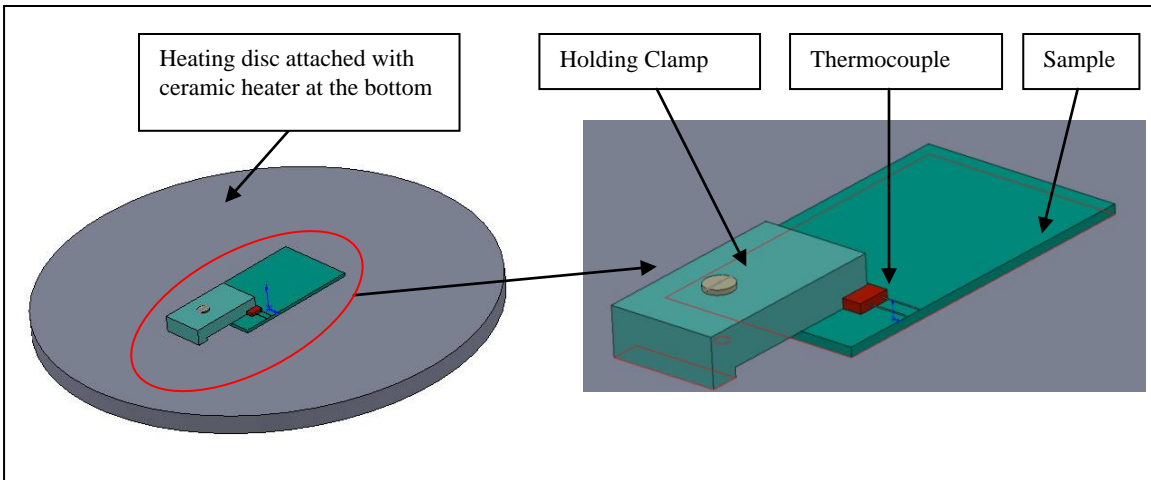


Figure 8.1: Schematic of the experimental heating set-up used for tribological characterization.

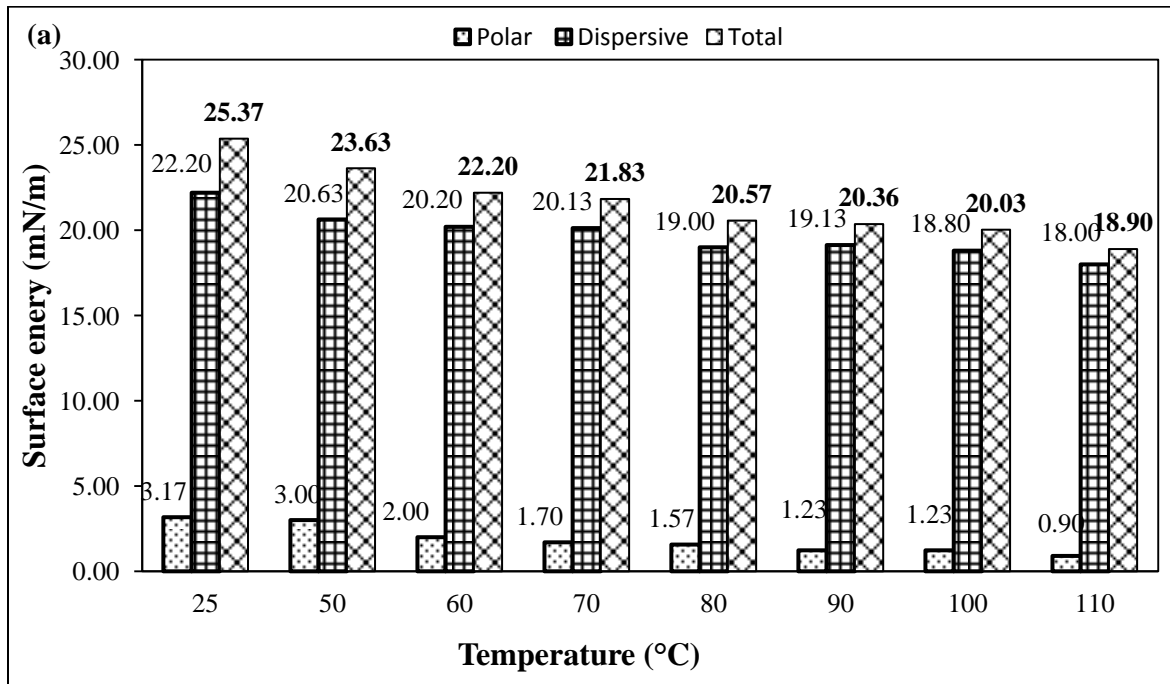
As will be shown in the results and discussion section, the lubricating property of the composites formed depends upon the ability of the composite to form a thin lubricating film *in situ*. A reduction in the thickness of the film (due to the lack of supply of lubricant) or displacement of lubricant molecules away from the interface leads to high friction and generates wear particles. Hence, for the present case, the wear-failure criteria

involving the coefficient of friction have been found to be sufficient. For each composite, at least 3 tests were repeated and the average data was reported. An optical microscope was used to image the worn surfaces after the sliding tests to assess the damage to the film surfaces and the ball respectively.

8.3 Results and Discussion

8.3.1 Surface Free Energy Calculations

Surface free energy calculations were carried out for pristine SU-8 and SU-8+PFPE composite, as shown in Figure 8.2. Pristine SU-8 (Figure 8.2(a)) shows the highest surface free energy of 25.3 mN/m at room temperature (25°C), and lowest surface free energy of 18.9 mN/m at 110°C.



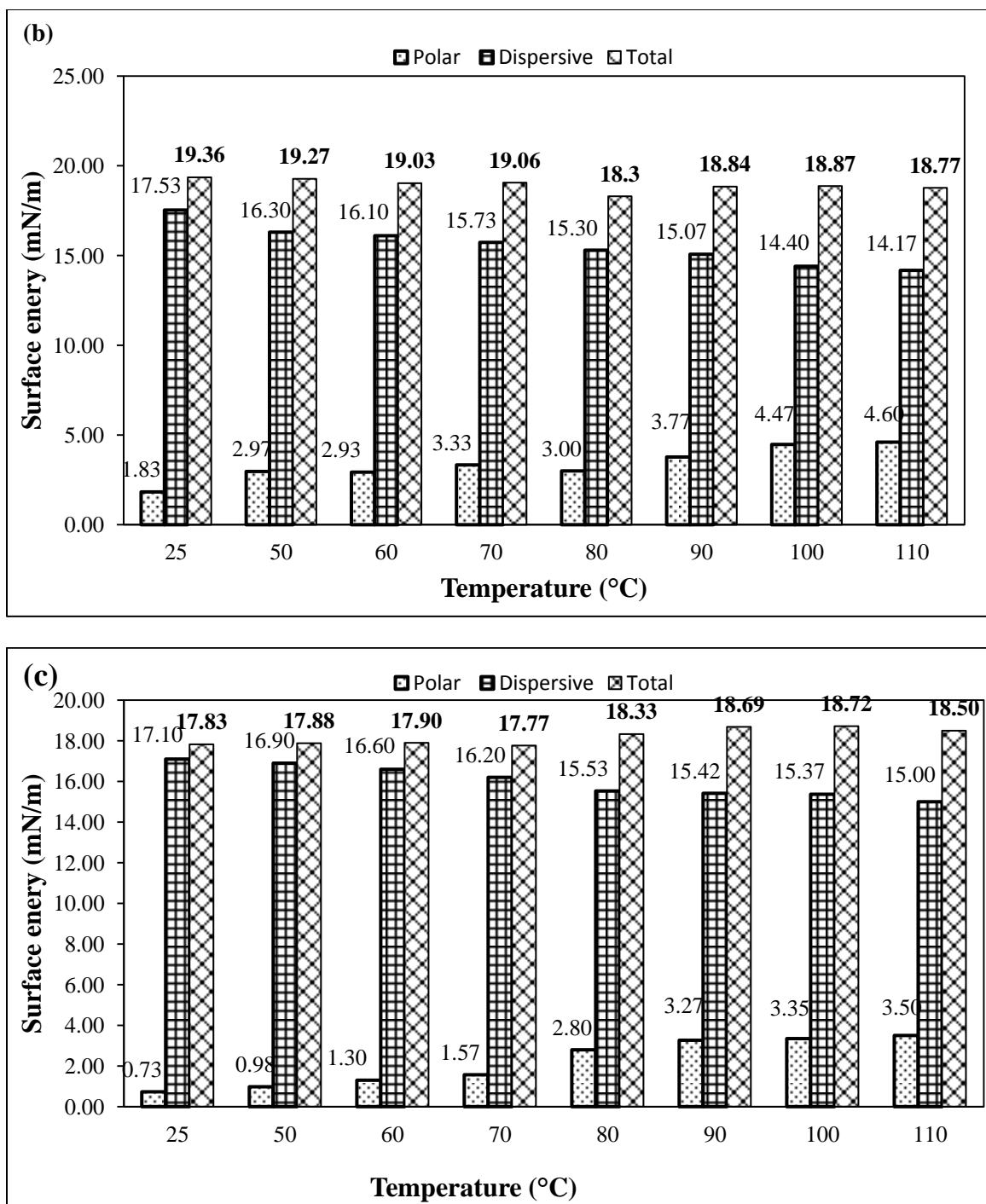


Figure 8.2: Polar, dispersive and total surface energies of pristine SU-8 and SU-8+PFPE composite at various temperatures from RT (25°C) to 110°C. (a) Pristine SU-8, (b) SU-8+PFPE composite fresh surface, and (c) SU-8+PFPE composite after washing. Standard error (S.E) is ± 0.2 for all cases.

There is a reduction in the polar and dispersive surface free energy of SU-8 as temperature increases. Overall, while the dispersive component continues to decrease as temperature increases, the polar component remains almost constant after a certain temperature. The fresh surface of SU-8+PFPE composite shows the highest and lowest surface free energy of 19.36 and 18.3 mN/m at room temperature (25°C) and 80°C respectively, as shown in Figure 8.2(b). The total surface free energy remains almost constant at all temperatures, with small deviations observed. More notably, with an increase in temperature, the dispersive component decreases, while the polar component increases significantly.

The increase in the polar component of surface free energy with respect to temperature could lead to a greater surface coverage by the PFPE lubricant due to increased availability of PFPE at the surface. This observation will have some influence on tribological properties, which will be discussed in the succeeding sections.

The fresh surface of SU-8+PFPE was washed with PFPE solvent (H-Galden SV 60) using ultrasonic cleaning, then subjected to surface free energy calculations as shown in Figure 8.2(c). The sample was washed for a duration of 1 hour, and this step was repeated thrice, for thorough washing. The objective was to remove the un-bonded PFPE over the surface, so as to only have the bonded monolayer of PFPE over the surface [Prabakaran et al 2013 (a)]. The total surface free energy remains almost constant at approximately 18 mN/m with little variation (~0.5 mN/m) for all temperatures. More notably, as the temperature increased, the dispersive component continued to decrease, while the polar component increased. This behaviour is identical to that of fresh surfaces, where increased availability of PFPE over the surface also leads to this observation. The

mobility of the bonded PFPE monolayer over the surface was restricted, since it was chemically attached to the surface [Hanging et al 2006]. Therefore, the gradual increase in polar component indicates that a higher amount of mobile PFPE was driven to the surface from another source. This source, that accounts for increased presence of PFPE, even after washing, will be discussed later.

8.3.2 Tribological Characterization

Tribological test results of pristine SU-8 and SU-8+PFPE composite (2wt%), which were tested at a normal load of 300 g and a linear sliding velocity of 7 mm/s until 200,000 sliding cycles, are summarized in Table 8.1. The data were taken from typical coefficient of friction (CoF) versus number of sliding cycles (n) plots, which are shown in Figure 8.3(a) and 8.3(b) respectively. The pristine SU-8 showed a high initial coefficient of friction of $\mu_i \sim 0.54$ and low wear life ($n \sim 0$) at room temperature (25°C). However, at all temperatures from 50°C to 100°C, pristine SU-8 showed an initial coefficient of friction (μ_i) and wear life (n) of approximately ~ 0.5 and ~ 0 respectively.

The SU-8+PFPE composite showed $\mu_i = 0.04$ and $\mu_s = 0.05$ until failure, where wear life was (n) $\sim 75,000$ at room temperature (25°C). At all temperatures from 50°C to 100°C, the initial coefficient of friction of the SU-8+PFPE sample remained almost constant at approximately $\sim 0.02-0.03$, while the steady-state coefficient of friction dropped from 0.07 to 0.007 and wear life (n) was more than 200,000 at 100°C. Overall, the *in-situ* heating of SU-8+PFPE reduced the initial (μ_i) and steady-state coefficient friction (μ_s) by ~ 2 and ~ 7 times respectively. The significant reduction in friction coefficients can be attributed to an increase in surface coverage by PFPE lubricant when

temperature rises. From the results, greater spreading of PFPE only occurs after 50°C, as before 50 °C frictional properties are similar to those at room temperature.

Table 8.1: Initial coefficient of friction (μ_i), steady-state coefficient of friction (μ_s) and wear life (number of sliding cycles) of pristine SU-8 and SU-8+PFPE composite obtained from sliding tests with 4 mm diameter Si_3N_4 ball for a normal load of 300 g and a sliding linear velocity of 7 mm/s at various temperatures.

| Temperature (°C) | Initial coefficient of friction, COF (μ_i) | Steady-state coefficient of friction, COF (μ_s) | Wear life (Number of cycles, n) |
|--|--|---|---------------------------------|
| Pristine SU-8 /Test Parameters: 300 g, 7 mm/s | | | |
| RT | 0.54 | - | 0 |
| 50 | 0.54 | - | 0 |
| 60 | 0.53 | - | 0 |
| 80 | 0.52 | - | 0 |
| 90 | 0.51 | - | 0 |
| 100 | 0.51 | - | 0 |
| SU-8+PFPE composite /Test Parameters: 300 g, 7 mm/s | | | |
| RT | 0.04 | 0.05 | 75,000±5,000 |
| 50 | 0.03 | 0.07 | >200,000 |
| 60 | 0.03 | 0.05 | >200,000 |
| 70 | 0.03 | 0.03 | >200,000 |
| 80 | 0.02 | 0.01 | >200,000 |
| 90 | 0.02 | 0.008 | >200,000 |
| 100 | 0.02 | 0.007 | >200,000 |

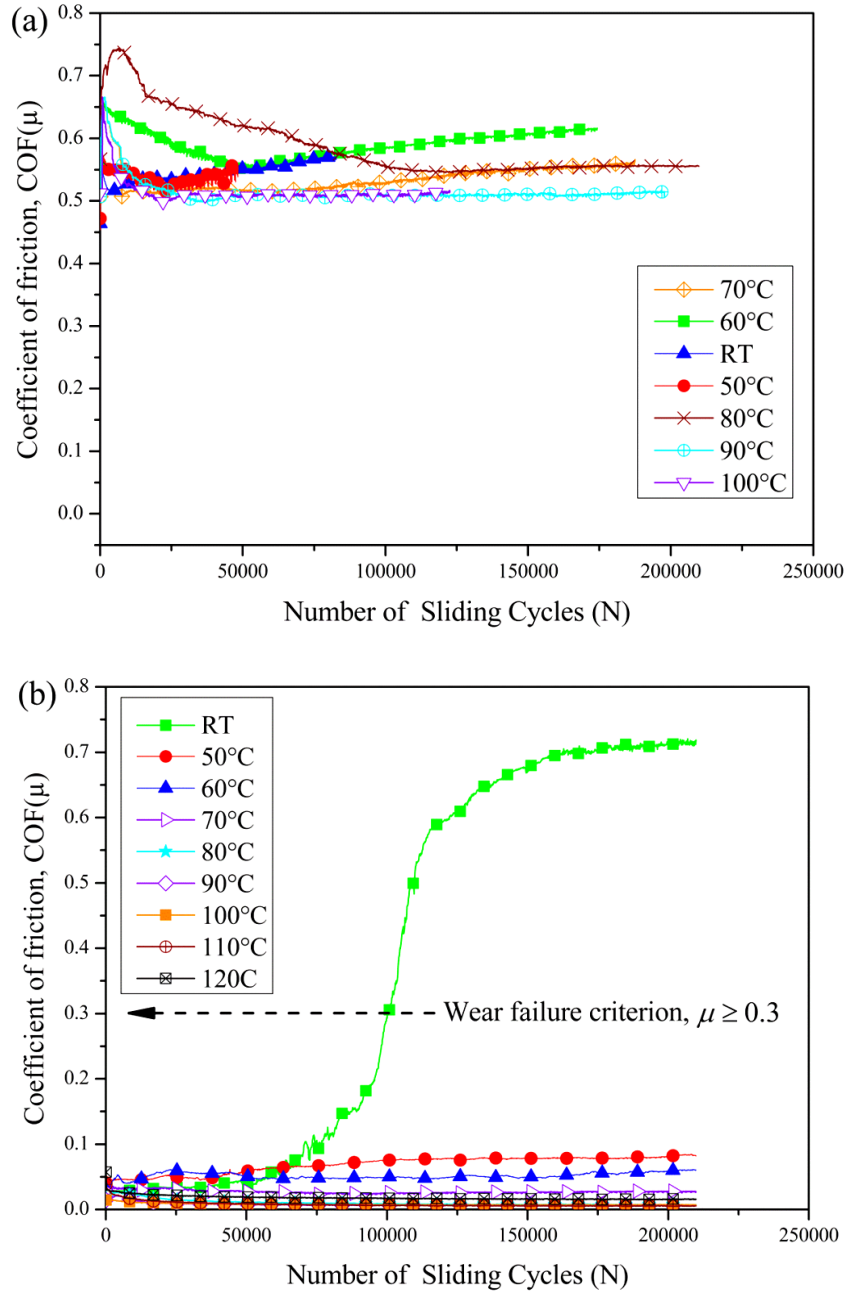


Figure 8.3: Typical coefficient of friction versus number of cycles plot for pristine SU-8 and SU-8+PFPE composite obtained from ball-on-disk sliding tests with 4 mm diameter Si_3N_4 ball at a normal load of 300g and a sliding velocity of 7 mm/s for different temperatures ranging from room temperature (25°C) to 100°C. (a) Pristine SU-8; (b) SU-8+PFPE composite. The tests stopped after 0.2 million cycles without any failure for the SU-8+PFPE composite at all temperatures (50-100°C).

From 60°C to 100°C, the tribological behaviour of SU-8+PFPE was much superior to those at room temperature. Both PFPE spreading and increased surface area coverage of PFPE provided superior surface protection, which will be shown qualitatively through optical micrographs in succeeding sections. The post-heating (not *in-situ*) experiments were also conducted after heating the samples for 2 hours at the corresponding temperature prior to tribological tests. The tribological results of post-heated samples were the same as those of in-situ heating, with marginal variation.

8.3.3 Migration of Lubricant

The nano-tribological test results of pristine SU-8 and SU-8+PFPE composites, which were tested at a normal load of 20 mN and a sliding rotational speed of 100 rpm at different surface conditions (i.e. after washing or after heating), are summarized in Table 8.1. The objective of these nano-tribological tests was to confirm whether the bulk to surface migration of PFPE occurs during the heating process. Migration is the phenomenon which facilitates the separation of low surface energy constituents, from the bulk to the air-surface interface in a blend/composite, with or without the application of heating to lower the overall free energy of the surface [Wei et al 2010, Yeo et al 2012, Nicolaas et al 2010, Zheng et al 2009, Goffri et al 2006, Harald et al 2006, Chirvase et al 2004]. It is possible that the PFPE trapped inside SU-8 could be diffused to the surface through pores in the SU-8 matrix as temperature rises [Prabakaran et al 2013 (a)].

The pore structure of SU-8 (with PFPE inside the pores) was ascertained in our earlier work [Prabakaran et al 2013(a)]. It is noted that the surface tension of PFPE is much lower than that of SU-8. The pristine SU-8 showed a high initial coefficient of

friction of $\mu_i \sim 0.67$ and low wear life ($n \sim 0$), as summarized in Table 8.1, obtained from the coefficient of friction versus number of cycles data shown in Figure 8.4. The inset inside the plot in Figure 8.4 also shows an enlarged view of μ_i in all cases, to distinguish the effects of heating and washing of the SU-8+PFPE composite. The fresh surface (case 1) of SU-8+PFPE composite showed a low initial and steady-state coefficients of friction of $\mu_i \sim 0.03$ and $\mu_s \sim 0.04$ respectively, and wear life of (n) $>10,000$.

Table 8.2: Initial coefficient of friction (μ_i), steady-state coefficient of friction (μ_s) and wear life (number of sliding cycles) of pristine SU-8 and SU-8+PFPE composite obtained from sliding tests using 2 mm diameter Si_3N_4 ball for a normal load of 20 mN and a sliding rotational speed of 100 rpm at various surface conditions.

| Composite Description | Initial coefficient of friction, COF (μ_i) | Steady- state coefficient of friction, COF (μ_s) | Wear Life (Number of Cycles, n) |
|---|--|--|---------------------------------|
| Pristine SU-8 /Test Parameters: 20 mN, 100 rpm | | | |
| Pristine SU-8 | 0.67 | - | 0 |
| SU-8+PFPE composite /Test Parameters: 20 mN, 100 rpm | | | |
| Fresh Surface (case 1) | 0.03 | 0.04 | $>10,000$ |
| Washing (case 2) | 0.22 | 0.19 | $>10,000$ |
| Heating at 100°C for 12hrs (case 3) | 0.19 | 0.14 | $>10,000$ |
| Washing (case 4) | 0.22 | 0.17 | $>10,000$ |

After thorough washing with PFPE solvent (H-Galden SV60), the washed surface (case 2) showed $\mu_i \sim 0.22$, $\mu_s \sim 0.19$ and wear life of (n) >10,000. This confirms the presence of PFPE over the surface (possibly one bonded monolayer) even after intensive washing, which protects the surface from friction and wear. The chemical bonding between PFPE and SU-8 molecules has already been postulated in our previous section [Prabakaran et al 2013 (b), Prabakaran et al 2014]. The same sample was subjected to heating at 100°C for 12 hours, and then subjected to nano-tribological tests.

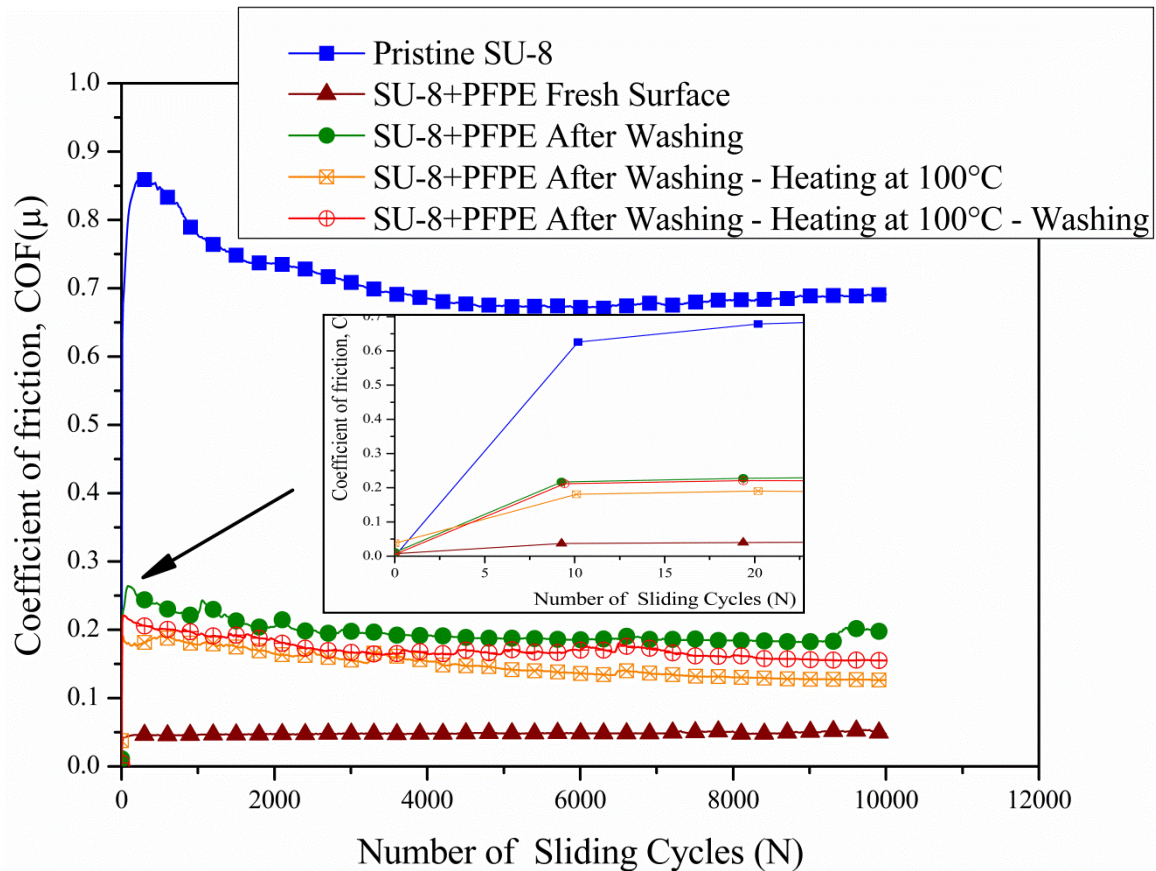


Figure 8.4: Coefficient of friction versus number of cycles plot for pristine SU-8 and SU-8+PFPE composite at various surface conditions, obtained from the ball-on-disk sliding tests using a 2 mm diameter Si_3N_4 ball at a normal load of 20 mN and a sliding speed of 100 rpm. The inset shows the initial co-efficient of friction (μ_i) of all series in the plot.

The surface after heating (case 3) shows $\mu_i \sim 0.19$, $\mu_s \sim 0.14$ and a wear life of (n) $> 10,000$. There is a reduction in the initial and steady-state friction coefficients before and after heating, which indicates a greater presence of PFPE on the surface. The bonded PFPE layer over the surface cannot spread further, since it is chemically attached to the surface. Therefore, it may be possible that heating diffuses PFPE from the bulk to the surface through migration, which helps to further reduce the friction coefficient [Prabakaran et al 2013 (a)].

The same sample was then washed again and subjected to tribological tests (case 4), which showed $\mu_i \sim 0.22$, $\mu_s \sim 0.17$ and wear life of (n) $> 10,000$. The excess mobile PFPE that migrated to the surface due to heat was removed by washing. Hence, the washed surface (case 4) exhibited similar tribological behaviour to when washed before heating (case 2), with very little deviation. This heating-induced PFPE diffusion from the bulk to the surface is very evident from the nano-tribology results. This concept can be understood from the schematic presented in Figure 8.5, which illustrates the phenomenon of migration in SU-8+PFPE composite due to heating. The PFPE molecules in the bulk start migrating to the surface when heating takes place.

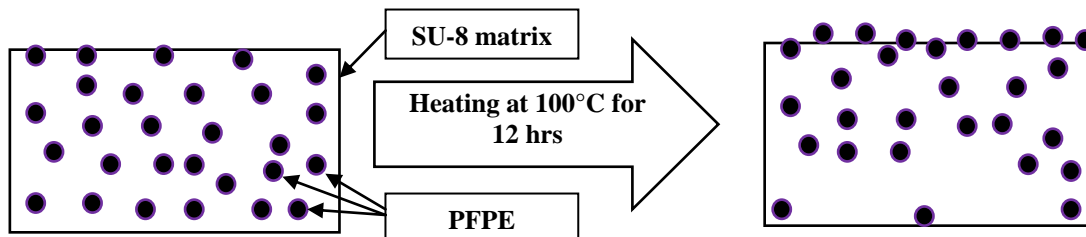


Figure 8.5: Schematic explaining possible migration of PFPE from bulk to surface after heating at 100°C for 12 hrs.

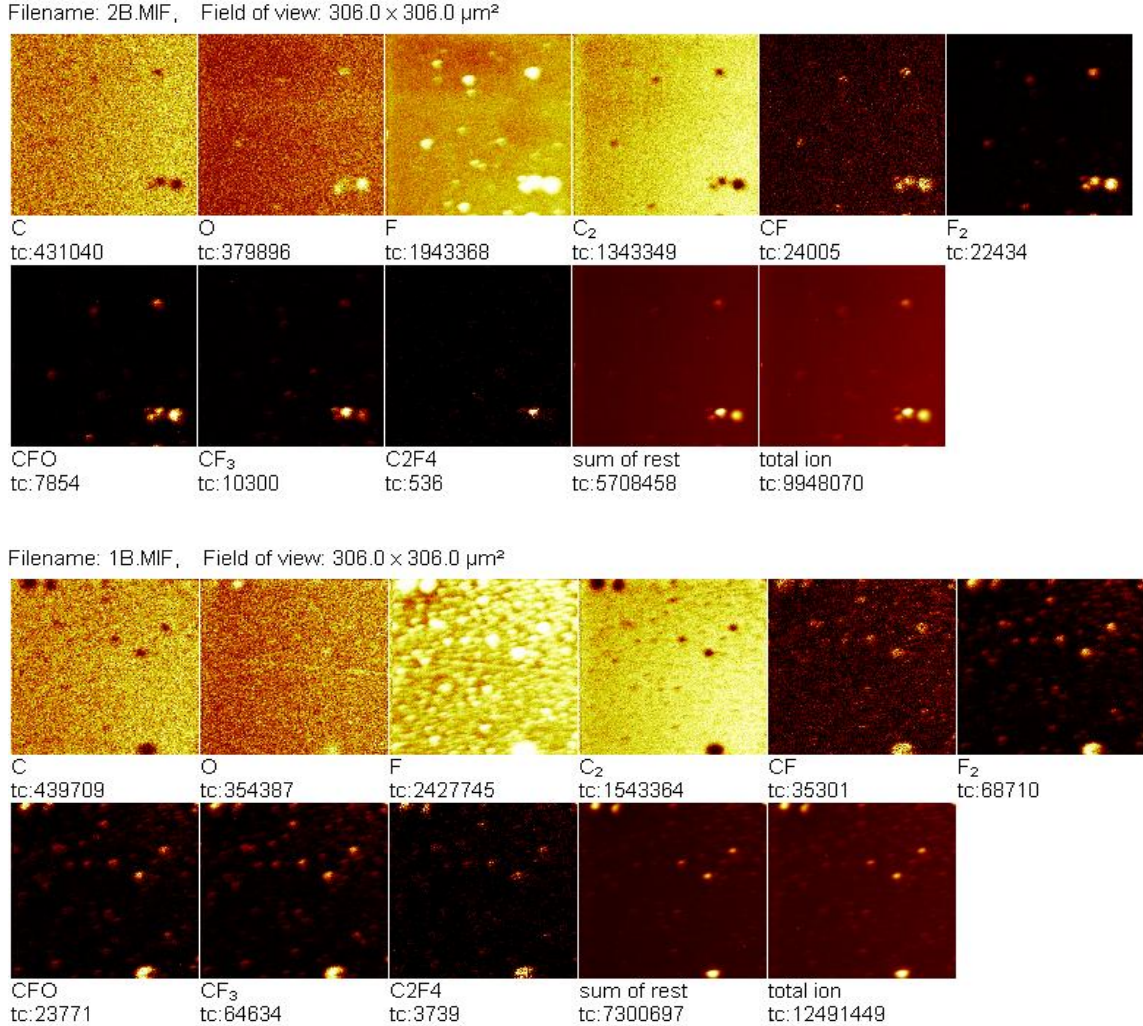


Figure 8.6: Typical 2D TOF-SIMS elemental mapping for SU-8+PFPE composite. (a) Elemental mapping for SU-8+PFPE after washing. (b) Elemental mapping for the same washed SU-8+PFPE after heating at 100°C for 12 hrs. The samples were preserved in a clean container before TOF-SIMS analysis to avoid any surface contamination. The total count numbers presented here are for one selected sample, with the same trend observed for other samples.

Usually, the low surface energy polymer in a polymer blend tends to move towards the air-surface interface rather than the substrate-composite interface, due to the surface tension of PFPE being much lower than SU-8. Hence, PFPE migrates to the surface [Wei et al 2010, Yeo et al 2012].

This migration of PFPE was again verified by TOF-SIMS results, which supports the concept explained earlier. Figures 8.6(a) and (b) show TOF-SIMS elemental mapping for the SU-8+PFPE composite after washing and heating respectively, and a summarized graphical illustration of the ratio of elemental counts from TOF-SIMS can be seen in Figure 8.7. From Figure 8.6(a), the total fluorine (F) count in SU-8+PFPE after washing was ~1,943,368, in which F represents the presence of PFPE. After heating the same washed sample at 100°C for 12 hours (Figure 8.6(b)), the fluorine (F) count increased to ~2,427,745, which is about a 5% (~484,377) increase. This increase in fluorine count at the surface after heating indicates greater PFPE presence on the surface.

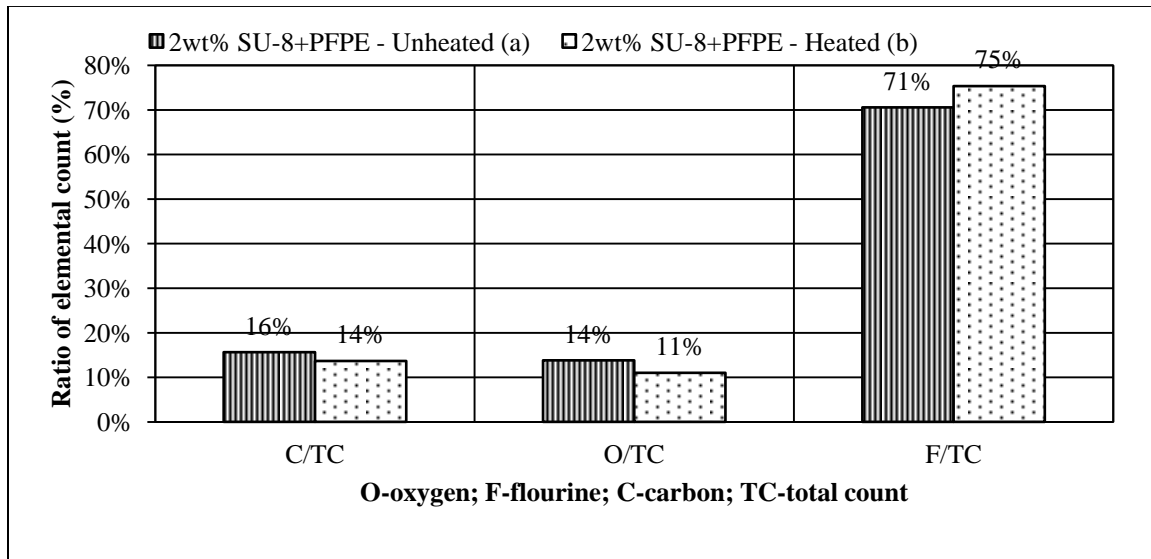


Figure 8.7: Graphical illustration of ratio between element counts for SU-8+PFPE composite. (a) Elemental count ratio for SU-8+PFPE after washing. (b) Elemental count ratio for the same washed SU-8+PFPE after heating at 100°C for 12 hrs.

This behaviour can be attributed to the migration of PFPE from the bulk to the surface as heating takes place. Only a certain fraction of this excess PFPE might have chemically bonded to the surface. But, it assists in bringing down friction and wear of the

composite due to an increase in the mobile fraction. Thus, the diffusion of PFPE from bulk to surface, by the migration mechanism, can be distinctly verified by TOF-SIMS results, coupled with nano-tribometer results.

8.3.4 Surface Area Coverage Calculation

The fractions of surface coverage by PFPEs were determined using Equation 8.1 [Hanging et al 2006] presented below:

$$\cos \theta = f_1 \cos \theta_1 + f_2 \cos \theta_2, \quad \text{where } f_1 + f_2 = 1 \quad (\text{Eq 8.1})$$

where θ is the measured apparent contact angle of the SU-8+PFPE surface, θ_1 is the measure apparent contact angle of the PFPE dip-coated SU-8 surface, and θ_2 is the measured apparent contact angle of the unlubricated SU-8 surface. The parameters f_1 and f_2 are the fractions of surface area covered by PFPE and the unlubricated SU-8 surface respectively.

Water and hexadecane were the two different solvents used to find the contact angle, in order to form two equations, which can be solved to give fractions of area. Both solvents have a higher dispersive surface energy than that of SU-8, SU-8+PFPE and PFPE dip-coated SU-8 surfaces. The area fractions at various temperatures ranging from room temperature (25 °C) to 120 °C were calculated using Equation 8.1 and presented in Figure 8.8.

At room temperature (25°C), the SU-8+PFPE composite has ~50% of its total area covered by PFPE (f_1) lubricant. These area fractions also have a strong influence on the tribological behaviour of the composite. When temperature increased to 70°C, the values of f_1 and f_2 changed from 49% and 51% to 63% and 37% respectively. The rise in

temperature enhances the spreading of PFPE for more surface coverage. At 100°C, the f_1 and f_2 values were 71% and 29% respectively, which changed to 93% and 7% at 120°C.

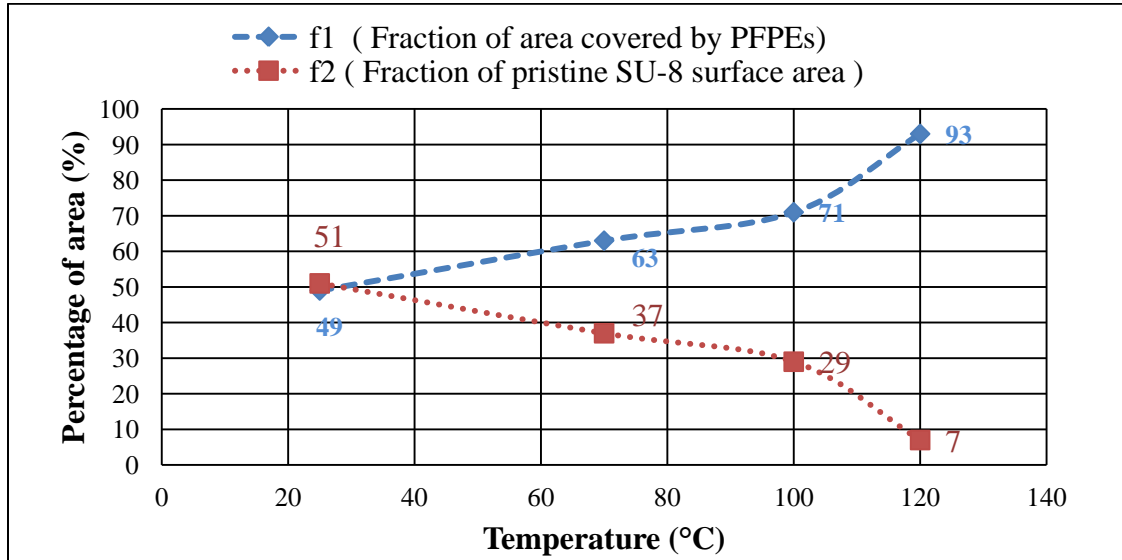


Figure 8.8: Surface area coverage calculations for the fresh surface of SU-8+PFPE composite at different temperatures.

The PFPE lubricant covers approximately 93 % of the total area at 120 °C. This shows that spreading, a diffusion-controlled phenomenon of PFPE, is more pervasive at high temperatures, and furthermore, additional PFPE molecules migrated to the surface from the bulk. The calculation for surface area coverage explains the improvement in tribological behaviour as temperature rises [Prabakaran et al 2013 (c)].

8.3.5 Nano-Mechanical Characterization

Heating enhances the mechanical properties of the pristine SU-8 and SU-8+PFPE composites, and the results of nano-indentation are shown in Figure 8.9. The pristine SU-8 showed hardness (H) and elastic modulus (E) values of 0.27 GPa and 3.8 GPa

respectively. After heating at 100 °C for about 12 hrs, it showed H and E values of 0.49 GPa and 4.2 GPa (~80% and 5% increases in H and E) respectively. On the other hand, the pristine SU-8+PFPE composite showed H and E values of 0.32 GPa and 4 GPa respectively.

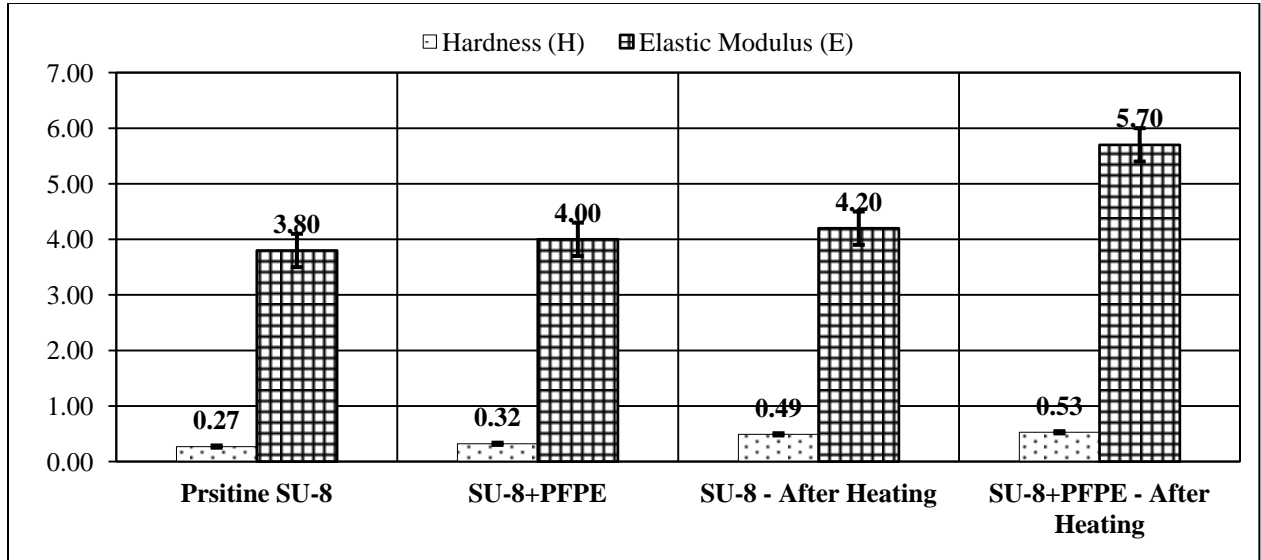


Figure 8.9: Hardness (*H*) and elastic modulus (*E*) values of pristine SU-8 and SU-8+PFPE composite before and after heating at 100°C for about 12 hrs, measured using nano-indentation characterization.

But after heating at 100 °C for about 12 hrs, it showed H and E values of 0.52 GPa and 5.7 GPa (~62% and ~42% increases in H and E) respectively, which are values greater than those of pristine SU-8. This significant increase in hardness and elastic modulus due to heating could be attributed to temperature-induced cross-linking. Most epoxy polymers are stable at high temperatures due to a cross-linked molecular structure, and harden further when temperature is moderately raised.

8.3.6 Surface Characterization of Worn Surfaces

Figure 8.10 shows optical micrographs of pristine SU-8 and SU-8+PFPE composite after sliding tests at a normal load of 300 g and a sliding linear velocity of 7 mm/s. Figures 8.10 (a), (g) and (m) correspond to optical micrographs of the wear track (worn surface) on SU-8, the counterface ball immediately after the test, and the counterface ball after cleaning with a solvent respectively, for pristine SU-8 at room temperature. The optical micrographs of pristine SU-8 at all temperatures, from room temperature to 100°C, are almost identical.

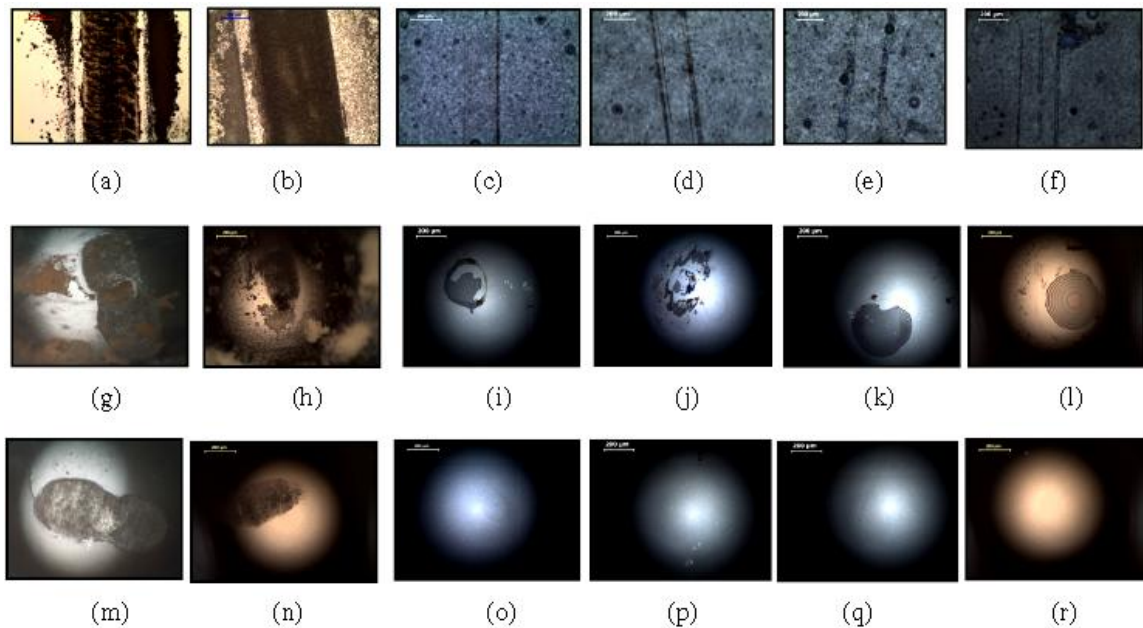


Figure 8.10: Optical micrographs of worn surfaces: (a) Pristine SU-8 (at 100,000 cycles). Images (b), (c), (d), (e) and (f): SU-8+PFPE composite at RT (25°C), 60°C, 80°C, 90°C and 100°C, respectively (at 200,000 cycles). Images (g), (h), (i), (j), (k), (l) are optical micrographs of the counterface ball surface after sliding tests. Images (m), (n), (o), (p), (q), (r) are micrographs of the tested counterface balls after cleaning with solvents corresponding to the worn surfaces shown in (a), (b), (c), (d), (e) and (f), respectively. The length of the scale bar is 200 µm in all images.

A physical observation of the counterface ball before and after cleaning reveals information about the amount of material transfer onto the counterface ball, mode of wear and damage caused to the counterface ball. Pristine SU-8 shows severe wear with a wide and deep wear track, and loss of material. The counterface ball also shows a thick layer of material with some damage, as distinct wear marks can be seen after cleaning with acetone. These images qualitatively support the tribological behaviour discussed in the preceding sections.

Figures 8.10 (b), (h) and (n) correspond to micrographs of the wear track on SU-8+PFPE composite at RT, counterface ball and counterface ball after cleaning with solvent. SU-8+PFPE showed a very deep wear track, with significant material removed, and damage to the counterface ball. Figure 8.10 (c), (d), (e) and (f) show optical micrographs of the wear track on SU-8+PFPE composite at 60, 80, 90 and 100 °C respectively. No distinct wear track can be seen other than a thin sliding trail (impression) on all surfaces and increased PFPE presence over the surface can be witnessed as temperature rises.

Likewise, Figures 8.10 (i), (j), (k), (l) and (o), (p), (q), (r) show micrographs of the counterface ball after sliding tests, and after cleaning with solvent at 60, 80, 90 and 100 °C respectively. A thin film of PFPE lubricant over the counterface ball can be seen in all cases and more notably, the PFPE film becomes very distinct and wide as temperature rises. This confirms the greater availability of lubricant over the surface as temperature rises, which is similar to one PFPE layer sliding against another (thin film lubrication), resulting in extremely superior tribological behaviour. After cleaning, no damage was observed to the counterface ball in all cases of 60-100 °C. Overall, the

presence and spreading of PFPE with respect to temperature were again confirmed by optical micrographs of the surfaces and the counterface balls.

8.4 Conclusions

Effects of *in-situ* heating on pristine SU-8 and SU-8+PFPE composite at temperatures from room temperature (25 °C) to 100 °C were investigated. The heating did not result in any improvement in tribological behaviour of pristine SU-8, whereas the heating of SU-8+PFPE reduced the initial and steady-state coefficients by ~2 and ~7 times respectively, and increased wear life (n) by more than three times. Increased surface area coverage by PFPE lubricant due to *in-situ* heating was confirmed by surface free energy and surface coverage calculations. A possible migration phenomenon also displaced an amount of PFPE from the bulk to the surface as temperature increased, which was deduced from nano-tribology and TOF-SIMS characterizations. Overall, these two aspects enriched the surface with more PFPE, which reduced friction and wear. The optical micrographs also showed a noticeable increase in PFPE coverage over the surface and transference of film over the counterface ball as temperature increased. This chapter shows that the SU-8+PFPE composite can find applications in conditions involving moderately high temperature, where tribology is a concern.

Chapter 9

Conclusions and Future Work

This chapter consolidates the conclusions derived from this PhD work towards achieving the objectives set for the entire thesis. The major conclusions are related to the development of self-lubricating SU-8 composites for MEMS applications and investigations of the physical and chemical mechanisms responsible for their superior tribological properties. The directions for future work and major limitations of this work are also elaborated.

9.1 Conclusions

9.1.1 Development of Self-lubricating SU-8 composites

The self-lubricating SU-8 hybrid composites were successfully developed by blending a liquid PFPE lubricant and nanoparticles such as SiO₂, CNTs and graphite. The liquid lubricant and nanoparticles were added for enhancement of the tribological and mechanical properties respectively.

- The developed SU-8 composite is hydrophobic (with a maximum water contact angle of 106° for SU-8+PFPE+SiO₂), highly lubricous with exceptional wear durability, and without any detriment to photo-sensitive curing.
- Compared with the pristine SU-8, the SU-8+PFPE and the SU-8+PFPE+nanoparticle composites reduced the initial coefficient of friction by ~6-9 times, increased wear life by more than 10⁴ times, and increased the elastic modulus and hardness by ~0.4 times.

- The presence of PFPE film at the counterface ball-SU-8 interface is maintained by a continuous supply of lubricant through a self-lubrication mechanism. The etherification between SU-8 and PFPE molecules was partially verified by XPS and water contact angle characterizations.
- These SU-8 composites can be used as self-lubricating structural materials for MEMS with no need for external lubrication. Apart from this, the SU-8 composite can also find applications as a lubricous and wear-resistant coating for several tribological components made from different materials, such as journal bearings, raceways for ball bearings, gears, medical equipments and tools, bio-devices, precision positioning stages, electronics components of cameras and printers, plastic bearings etc.

9.1.2 Wear Durability Study for Chemical Bonding Investigation

The superior tribological properties of self-lubricating SU-8 composites were further investigated using lubricants such as PFPE, base oil SN 150 and MAC oil as fillers. SU-8+PFPE, SU-8+SN 150 and SU-8+MAC enhanced the wear life of pristine SU-8 by 1000, 500 and 200 times respectively.

- In the case of SU-8+SN 150 and SU-8+MAC, physical self-lubrication mechanism is responsible for superior tribological properties. For SU-8+PFPE, the self-lubrication mechanism and the chemical reaction between SU-8 and PFPE molecules, are responsible for their superior tribological properties over those of other SU-8 composites.

- The presence of physical self-lubrication was confirmed by surface energy measurements, SEM images and XPS analysis on the wear track after sliding tests.
- The chemical reaction between SU-8 and PFPE was ascertained by the EDS analysis, AFM imaging after washing, high wear resistance of the rinsed specimen, nano-mechanical and optical characterizations.

The chemical bonding between SU-8 and PFPE molecules was further investigated. Two PFPE lubricants with identical backbone chains, but with different functional end groups, were chosen for this study. These functional end groups, -OH and -CF₃, are present in Z-dol and Z-03 respectively. Because of chemical bonding between SU-8 and Z-dol molecules, the SU-8+Z-dol composite showed superior wear life to SU-8+Z-03 and pristine SU-8, of ~8 times and over four orders of magnitude ($>10^4$) respectively. The following conclusions can be drawn:

- The dispersive surface free energy of SU-8+Z-dol was lower than that for SU-8+Z-03, which indicated that Z-dol had better dispersion and more affinity towards SU-8. This was verified by worn surface micrographs and wettability studies where Z-03 droplets showed hydrophobic behaviour towards SU-8 while Z-dol remained uniformly spread out across the SU-8 surface.
- From the XPS results, SU-8+Z-dol showed an increased amount of C-O groups compared to SU-8+Z-03, even though both have the same polymer backbone chain with no breakage.

- TGA characteristics of Z-dol dip-coated SU-8 samples proved that the Z-dol lubricant molecules were retained by chemical bonding with SU-8 molecules even after intensive solvent washing.

9.1.3 Physical Self-Lubrication Investigation

Coefficient of friction (COF) versus sliding velocity plot was constructed for the 5wt% SU-8+Z-dol composite which was tested at a normal load of 300g and different sliding speeds until 10,000 sliding cycles. Three different zones were identified based on their exhibited frictional behaviour with speed. Zones 1, 2 and 3 exhibit the steep increase, marginal increase and linear increase in COF respectively, as speed increases.

- At low speeds, the entire wear track is covered with lubricant because there is enough time for the displaced mobile lubricant to diffuse across the wear track. As speed increases, there is not enough time for the displaced lubricant to diffuse across the wear track between consecutive cycles.
- Hence, the increase in sliding speed leads to increasing asperity contact, initiating surface wear. Once the wear process reaches the next layer of fresh lubricant droplets, lubrication occurs. Then, the COF stabilizes.
- Further increases in speed increase the COF linearly. This increase in COF is again attributed to lubricant displacement. As soon as it reaches the dry contact, a new batch of lubricant is released, and the COF drops and stabilizes again.
- The effects of normal load and sliding speed were studied separately, and it was found that the sliding speed has a tremendous effect on the frictional behaviour of 5wt% SU-8+Z-dol composites, as compared to a normal load. The macro- and

micro-tribological, optical and EDS characterizations, along with the existing literature, have supported the proposed tribological behaviour of 5wt% SU-8+Z-dol composite at various speeds.

9.2 Limitations and Future Work

9.2.1 Adapting this Approach for Other Photo-resist Polymers

Other photo-resist polymers such as PMMA, PMGI, PA and other non photo-resistive polymers such as PDMS and PEDOT can be used for developing the new breed of self-lubricating composites using various polar lubricants. These new composites could help us to identify the unique properties of both polymers and lubricants to solve tribological problems. Meanwhile, these composites can be used as structural materials for MEMS applications. The chemical and physical interactions between various polar/non-polar polymers and polar/non-polar lubricants can be investigated using more sophisticated characterization techniques. However, this method of developing self-lubricating composites is limited only to photo-resist polymers. This limitation can be overcome by further work.

9.2.2. Utilizing SU-8 Composites in Real-time Applications

It has been already demonstrated that the addition of lubricants to SU-8 did not affect its photolithographic properties, through the construction of a gear with the SU-8 composite in one of our earlier works [Prabakaran et al 2013(a)]. However, it is still necessary to fabricate a MEMS device using the SU-8 composite and evaluate its performance in real-time applications, because that is where more issues of feasibility arise. Some examples

include a MEMS device that involves sliding, as well as rolling contacts, which may prove better configurations to study the tribological performance of SU-8 composites.

9.2.3 Addition of Additives and Surfactants

The dispersion of lubricant droplets inside the polymer matrix is not very uniform and many agglomerations can be found. Lubricant agglomeration is governed not only by the properties of the lubricant, but also by lubricant–polymer interactions. Interfacial polymer-lubricant interactions also affect the agglomeration. Thus, in addition to the proper selection of a polymer-lubricant combination, proper surfactants, additives and catalysts can also be used to obtain uniform dispersion of lubricant droplets. Polarity, chemical structure and electro-negativities of surfactants also have to be taken into consideration before selecting them. Thus, better tribological performance can be obtained.

9.2.4 Mechanical Properties of SU-8

Two main concerns have to be addressed in the design of a MEMS device. Firstly, the tribological properties of the material, which will affect the life span of the device. Secondly, the mechanical properties of the material, which will affect reliability and functionality of the device because of very stringent tolerance limits on a micro/nano scale. However, improvements in mechanical properties such as elastic modulus (E) and hardness (H) yielded by the addition of nanoparticles (SiO₂, CNT and Graphite) are insufficient. This is one crucial area to look at for improvement in the mechanical

properties of SU-8. The commercialization of SU-8 MEMS may not be realized in the near future unless the mechanical properties of SU-8 are improved to a level equivalent to that of Si.

9.2.5 Cross-linking Density Analysis of SU-8 and SU-8 Composites

The pristine SU-8 shows E and H values of 3.8 and 0.27 GPa respectively, whereas the SU-8+PFPE composite shows E ~4 GPa and H ~0.32 GPa. The improvement in mechanical property arising from the addition of PFPE was attributed to enhanced cross-linking as a result of chemical interactions between SU-8 and PFPE molecules. Mechanical properties are expected to deteriorate, due to the addition of lubricant fillers in normal cases. There is no sufficient evidence to prove this proposed hypothesis. Hence, further work is necessary to validate the proposed explanation by measuring the cross-linking densities. It is also essential to investigate whether the lubricant inside the droplets behaves in the same fashion as human cartilage, to withstand increased load.

9.2.6 Graphite-PFPE Lubrication

It was observed that the addition of graphite to the SU-8 composite did not improve its tribological properties. Graphite is known to be the best solid lubricant in humid environments, as it has a layered and planar structure, which allows it to shear off easily. It is therefore surprising that graphite showed inferior tribological properties to those of SU-8. It was suggested that the SU-8 matrix restricted the ability of graphite to shear off layer by layer. However, the SU-8+PFPE+graphite composite showed no advantage in lubrication as compared to graphite. It is believed that the graphite particles also do not

allow PFPE to maintain the boundary film as it does in the case of SU-8+PFPE alone. These suggested explanations require further study for validation, by conducting experiments on an atomic scale.

9.2.7 Dip-coating of SU-8 Composite for Commercial Applications

The performance of SU-8 composites as a coating on various substrates such as steel, aluminium, and glass can be evaluated to expand the commercial scope of SU-8 composites. The 100 micron thickness is able to withstand a normal load of 300g and sliding speed of 2000 rpm for more than one million cycles ($>10^5$). Thicker films of more than 1 mm can easily be fabricated using more viscous grades of SU-8. It is evident that these films could be used as a coating for protecting machine elements from friction and wear on a macro scale. Hence, further work is necessary in these aspects.

References

Abgrall, P., Gue, A. M., J. *Lab-on-chip technologies: making a microfluidic network and coupling it into a complete microsystem—a review.* J. Micromech. Microeng. 17(2007) R15–R49.

Albertson, C.E. *The Mechanism of Anti-Squawk Additive Behavior in Automatic Transmission Fluids.* ASLE Transactions, 6 (1963) 300-315.

Armani, D.K., Liu, C. *Microfabrication technology for polycaprolactone, a biodegradable polymer.* J. Micromech. Microeng. 10 (2000) 80-84.

Arocott, S., Garet, F., Mounaix, P., Duvillaret, L., Coutaz, J.-L., Lippens, D. *Terahertz time-domain spectroscopy of films fabricated from SU-8.* Electronics Letters 35 (3) (1999) 243.

Bailey, I.A., and Courtney-Pratt, J. S. *The area of real contact and the shear strength monomolecular layers of a boundary lubricant.* Proceedings of the Royal Society of London A, 227 (1955) 500-515.

Barthlott, W., and Neinhuis, C. *Purity of the sacred lotus, or escape from contamination in biological surfaces.* Planta, 202 (1997) 1–8.

Belanger, M.-C., Marois, Y. *Hemocompatibility, biocompatibility, inflammatory and in vivo studies of primary reference materials low-density polyethylene and polydimethylsiloxane: A review.* J. Biomed. Mater. Res., 58 (2001) 467- 477.

Bertsch, A., Lorenz, H., Renaud, P. *Combining micro stereolithography and thick resist UV lithography for 3D microfabrication.* in: IEEE MEMS '98 (1998) 18–23.

Bhushan, B. In: *Proc. Tribol. Issues and Opportunities in MEMS Workshop* , Kluwer Academic, Dordrecht (1998).

Bhushan, B. *Nanotribology and Materials Characterization of MEMS/NEMS and BioMEMS/BioNEMS Materials and Devices*. Springer Handbook of Nanotechnology. Springer Berlin Heidelberg (2007) 1575-1638.

Bhushan, B. *Nanotribology and nanomechanics of MEMS/NEMS and BioMEMS/BioNEMS materials and devices*. Microelectronic Engineering, 84 (2007) 387-412.

Bhushan, B. *Springer Handbook of Nanotechnology*. 2nd edition, Heidelberg: Springer (2007).

Bhushan, B. *Tribology and Mechanics of Magnetic Storage Devices*, 2nd edition, Springer-Verlag, New York (1996).

Bhushan, B., and Jung, Y.C. *Wetting study of patterned surfaces for superhydrophobicity*. Ultramicroscopy 107 (2007) 1033–41.

Bhushan, B., Hansford, D., Lee, K.K. *Surface Modification of Silicon and Polydimethylsiloxane surfaces with Vapor-Phase-Deposited Ultrathin Fluorosilane Biomedical Microdevices*. J. Vac. Sci. Technol. A, 24 (2006) 1197–1202.

Bhushan, B., Kasai, T., Kulik, G., Barbieri, L., Hoffman, P. *AFM study of perfluorosilane and alkylsilane self-assembled monolayers for anti-stiction in MEMS/NEMS*. Ultramicroscopy, 105 (2005) 176–188.

Bhushan, B., Kulkarni, A.V., Koinkar, V.N., Boehm, M., Odoni, L., Martelet, C., Belin, M. *Microtribological characterization of self-assembled and Langmuir-Blodgett monolayers by atomic and friction force microscopy*. Langmuir 11 (1995) 3189–3198.

Bielecki, R. M., Maura Crobu, Nicholas D. Spencer. *Polymer-Brush Lubrication in Oil: Sliding Beyond the Stribeck Curve*. Tribol Lett., 49 (2013) 263-272.

Bijwe Jayashree, Sanjeev Sharma, Mohit Sharma, Tushar Parida, Prakash Trivedi.

Exploration of potential of solid lubricants and short fibers in polyetherketone (PEK) composites. Wear 301(2013) 810-819.

Booser, R.E. *CRC Handbook of Lubrication (Theory and Practice of Tribology) 2, Theory and Design.* CRC Press, Inc., Boca Raton, Florida (1984) 275.

Borger, D.P., Frens, G. *Solvatochromism as an alternative for contact angle measurements in the characterization of modified polymer surfaces.* Colloids and Surfaces A., 161 (2000) 75-80.

Briscoe B. J., Yao, L. H. *In: K. C. Ludema (ed.), Wear of Material.* ASME, New York (1985) 725-741.

Briscoe, B.J., Evans, D.C.B. *The shear properties of Langmuir–Blodgett layers.* Proc. R. Soc.Lond. A 380 (1982) 389–407.

Bryzek, J., Petersen, K. and McCulley, W. *Micromachines on the march.* IEEE Spectrum, 31(1994) 20-31.

Burton, Z., Bhushan, B. *Surface characterization and adhesion and friction properties of hydrophobic leaf surfaces.* Ultramicroscopy 106 (2006) 709–16.

Cao, L., Mantell, S. and Polla, D. *Design and simulation of an implantable medical drug delivery system using microelectromechanical systems technology.* Sensors and Actuators A- Physical, 94 (2001) 117.

Carlen, E. T., Mastrangelo, C. H. J. *Surface micromachined Paraffin actuated valves.* J. Microelectromech. Syst. 11 (2002) 408-420.

Cassie, A., Baxter, S. *Wettability of Porous Surfaces.* Trans.Faraday Soc. 40 (1944) 546–51.

Chau, K. H. L., and Sulouff, R. E. *Technology for the high-volume manufacturing of integrated surface-micromachined accelerometer products.* Microelectronics Journal, 29 (1998) 579.

Chen, H., Lei Li., Merzlikine, A.G., Hsia, Y.T., and John, M.S. *Surface energy and adhesion of perfluoropolyether nanofilms on carbon overcoat: The end group and backbone chain effect.* Jour. Appl. Phy., 99 (2011) 08N103.

Chen, H., Myung S. John. *Relationship between surface coverage and end group functionality of molecularly thin perfluoropolyether films.* J. Appl. Phy., 103 (2006) 07F536.

Chiamori, H. C., Brown, J. W., Adhiprakasha, E. V., Hantsoo, E. T., Straalsund, J. B., Melosh, N. A., and Pruitt, B. L. *Suspension of nanoparticles in SU-8: Processing and characterization of nanocomposite polymers.* Microelectronics Journal 39 (2008) 228-236.

Chirvase, D., Parisi, J., Hummelenand, J.C., Dyakonov, V. *Influence of nanomorphology on the photovoltaic action of polymer–fullerene composites.* Nanotechnology 15 (2004)1317-1323.

Coulson, S.R., Woodward, I., and Badyal, J.P.S. *Super-repellent composite fluoropolymer surfaces.* J. Phys. Chem. B, 104 (2000) 8836–40.

Cui, T., Wang, J. *Polymer-based wide-bandwidth and high-sensitivity micromachined electron tunneling accelerometers using hot embossing.* J. Microelectromech. Syst., 14 (2005) 14, 895-902.

- Cutler, J.N., Sanders, J.H., Zabinski, J.S., John, P.J., McCutchen, J.R., Kasten, L.S., and Tan, K.H.** *Surface chemistry of new lubrication systems for high-speed spacecraft bearings.* Tribology Letters, 8 (2000) 17-23.
- Dalvi, V.H., and Rosky, P.J.** Molecular origins of fluorocarbon hydrophobicity. PNAS 107 (31) (2010) 13603-13607.
- Damean, N., Parviz, B. A., Lee, J. N., Odom, T., Whitesides, G. M.** Composite ferromagnetic photoresist for the fabrication of microelectromechanical systems. J. Micromech. Microeng. 15 (2005) 29–34.
- David, L.B., Boesl, B., Bourne, G.R., Sawyer, G.W.** *Polymeric nanocomposites for tribological applications.* Macromol. Mater. Eng., 292 (2007) 387–402.
- De Boer, M. P. and Mayer, T. M.** *Tribology of MEMS.* MRS Bulletin, 26 (2001) 302-304.
- De Boer, M. P., Knapp, J. A., Mayer, T. M., Michalske, T. A.** *The role of interfacial properties on MEMS performance and reliability.* Proc. SPIE, 3825 (1999) 2–15.
- Delille, R., Urdaneta, M. G., Moseley, S. J., Smela, E.** *Benchmark polymer MEMS.* IEEE/ASME J. Microelectromech. Syst. 15 (2006) 1108-1120.
- Dellmann, L., Roth, S., Beuret, C., Racine, G., Lorenz, H., Despont, M., Renaud, P., Vettiger, P., and de Rooij, N.** *Fabrication process of high aspect ratio elastic structures for piezoelectric motor applications.* In Proc. Transducers, Chicago (1997) 641-644.
- Douglass, M. R.** *DMD reliability: A MEMS success story, Reliability, Testing, and Characterization of MEMS/MOEMS II.* Proc. SPIE, 4980 (2003) 1–11.
- Dowson, D.** *History of Tribology*, 2nd edition. Professional Engineering Publishers, London, UK, 1998.

Dube, M.J., Bollea, D., Jones, jr, W.R., Marchetti, M., and Jansen, M.J. *A new synthetic hydrocarbon liquid lubricant for space applications.* Tribology Letters, 15 (2003) 3-8.

Duffy, D.C., McDonald, J.C., Schueller, O.J.A., Whitesides, G.M. *Rapid Prototyping of Microfluidic Systems in Poly(dimethylsiloxane).* Anal. Chem., 70 (1998) 4974 - 4984.

Eapen, K.C., Patton, S.T., and Zabinski, J.S. *Lubrication of microelectromechanical systems (MEMS) using bound and mobile phases of Fomblin Zdol[®].* Tribology Letters, 12 (2002) 35-41.

Engel, J., Chen, J., Fan, Z., Liu, C. *Polymer micromachined multimodal tactile sensors.* Sens. Actuators A, 117 (2005) 50-61.

Engel, J., Chen, J., Liu, C., Bullen, D. *Polyurethane rubber all-polymer artificial hair cell sensor.* J. Microelectromech. Syst., 15 (2006) 729-736.

Esa Puukilainen, Hanna Saarenpa"ä" and Tapani A. Pakkanen. *Compression -molded, lubricant-treated UHMWPE composites.* Journal of applied polymer science, 104 (2007) 1762-1768.

Ewan, H.C., and Moore, D. F. *SU-8 thick photoresist processing as a functional material for MEMS applications.* J. Micromech. Microeng. 12 (2002) 368–374.

Eyring, H. *Viscosity, plasticity, and diffusion as examples of absolute reaction rates.*

Fang, N., Sun, C., Zhang, X. *Diffusion-limited photopolymerization in scanning micro-stereolithography.* Appl. Phys. A, 79 (2004) 1839-1842.

Foulds, I. G., Parameswaran, M. *A planar self-sacrificial multilayer SU-8-based MEMS process utilizing a UV-blocking layer for the creation of freely moving parts.* J. Micromech. Microeng. 16 (2006) 2109–2115.

François Constantin, Françoise Fenouillot, Jean-Pierre Pascault and Roberto Juan Jose Williams. *Post-Crosslinkable Blends: Reactions between a Linear Poly (hydroxyl-amino ether) and a Diepoxy.* Macromolecular Materials and Engineering, 289 (2004) 1027-1032.

Frechette, J., Maboudian, R., Carraro, C. *Effect of temperature on in-use stiction of cantilever beams coated with perfluorinated alkylsiloxane monolayers.* J. Microelectromech.Syst., 15 (2006) 737-744.

Frechette, L.G., Jacobson, S.A., Breuer, K.S. *High-speed microfabricated silicon turbo-machinery and fluid film bearings.* J. MEMS, 14 (2005) 141–152.

Friedrich, K. *Sliding wear performance of different polyimide formulations.* Tribol. Intl., 22 (1989) 25-31.

Fusaro, R.L. *Self-lubricating polymer composites and polymer transfer film lubrication for space applications.* Tribol. Intl., 23 (1990) 105-122.

Gabriela Blagoi, Stephan Keller, Fredrik Persson, Anja Boisen, and Mogens Havsteen Jakobsen. *Photochemical Modification and Patterning of SU-8 Using Anthraquinone Photolinkers.* Langmuir 24 (2008) 9929-9932.

Garcia, E.J., Sniegowski, J.J. *Surface micromachined microengine.* Sensors Actuators A, 48 (1995) 203–214.

Gelorme, J.D., Cox, R.J., Gutierrez, S.A.R. *Photoresist composition and printed circuit boards and packages made herewith.* US Patent 4,882,245, 21 Nov 1989.

Gill, S., and Rowntree, A. *Liquid Lubricants for Spacecraft Applications*. Chapter 12 in *Chemistry and Technology of Lubricants*, 3rd Edition (Edited by Mortier, R. M., Fox, M. F. and Orszulik, S. T.) (2010) 375-387.

Giltrow, J. P. *Friction and wear of some polyimides*. *Tribology*, 6 (1973) 253-257.

Goffri, S., Müller, C., Stingelin-Stutzmann, N., Breiby, D. W., Radano, C. P., Andreasen, J. W., Thompson, R., Janssen, R. A. J., Nielsen, M. M., Smith, P., Sirringhaus, H. *Morphology evolution via self-organization and lateral and vertical diffusion in polymer:fullerene solar cell blends*. *Nature Mater.* 5 (2006)950-956.

Gong, D., Xue, Q., and Wang, H. *Study of the wear of filled polytetrafluoroethylene*. *Wear*, 134 (1989) 283-295

Guerin, L.J., Bossel, M., Demierre, M., Calmes, S., Renaud, P. *Simple and low cost fabrication of embedded micro-channels by using a new thick-film photoplastic*. in: *TRANSDUCERS '97*, Chicago, USA (1997)1419–1422.

Guo, Q.B., Lau, K.T., Zheng, B.F., Rong, M.Z., and Zhang, M.Q. *Imparting Ultra Low Friction and Wear Rate to Epoxy by the Incorporation of Microencapsulated Lubricant?*. *Macromolecular Materials and Engineering* 294 (2009) 20-24.

Hanging Chen and Myung S. John. *Relationship between surface coverage and end group functionality of molecularly thin perfluoropolyether films*. *J. Appl. Phys.*, 103 (2006) 07F536.

Hankins, M.G., Resnick, P.J., Clews, P.J., Mayer, T.M., Wheeler, D.R., Tanner, D.M., Plass, R.A. *Vapor deposition of amino-functionalized self-assembled monolayers on MEMS*. *Proc. SPIE*, 4980, SPIE, Bellingham, Washington (2003) 238–247.

Harald Hoppe and Niyazi Serdar Sariciftci. *Morphology of polymer/fullerene bulk heterojunction solar cells.* J. Matl. Chem.16 (2006) 45-61.

Harris, K. D., Bastiaansen, C. W. M., Broer, D. J. *Physical properties of anisotropically swelling hydrogen-bonded liquid crystal polymer actuators.* IEEE/ASME J. Microelectromech.Syst., 16 (2007) 480-488.

Henck, S.A. *Lubrication of digital micromirror devices.* Tribol. Lett. 3 (1997) 239–247.

Holmes, A.S., Saidam, S.M. *Sacrificial layer process with laser-driven release for batch assembly operations.* Journal of Microelectromechanical Systems 7 (4) (1998) 416.

Hornbeck, L.J. *A digital light processing TM update – status and future applications.* Proc. Soc. Photo-Opt. Eng. 3634, Projection Displays V, (1999) 158–170.

Hornbeck, L.J. *The DMDTM projection display chip: A MEMS –based technology.* MRS Bull., 26 (2001) 325–328.

Hornbeck, L.J., Nelson, W.E. *Bistable deformable mirror device.* OSA Technical Digest Series Vol. 8: Spatial Light Modulators and Applications (1988) 107–110.

Hozumi, A., and Takai, O. *Preparation of silicon oxide films having a water-repellent layer by multiple-step microwave plasma-enhanced chemical vapor deposition.* Thin Solid Films 334, (1998) 54–9.

<http://memscyclopedia.org/su8.html#reflow> - SU-8: Thick Photo-Resist for MEMS, 1999-2013

Hu, T., Zhang, Y., and Hu, L. *Tribological investigation of MoS₂ coatings deposited on the laser textured surface.* Wear 278-279 (2012) 77-82.

Ingram, M., J. Noles, R. Watts, S. Harris, H. A. Spikes. *Frictional Properties of Automatic Transmission Fluids: Part II—Origins of Friction—Sliding Speed Behavior.*

Tribology Transactions, 54 (2011) 154-167

Israelachvili, J. N., and Tabor, D. *The measurement of Van der waals dispersion forces in the range 1.5 to 130nm.* Proceedings of the Royal Society of London A, 331 (1972) 19-38.

J. Chem.Phys. 4 (1936) 283–291.

Jain, V. K., and Bahadur, S. *In K. C. Ludema (ed.), Wear of Materials.* ASME, New York, (1987) 389-395.

Jiguet, S., Bertsch, A., Hofmann, H., Renaud, P. *SU8-Silver photosensitive nanocomposite.* Adv. Eng.Mater. 6 (2004) 719–724.

Jiguet, S., Bertsch, A., Judelewicz, M., Hofmann, H., Renaud, P. *SU-8 nanocomposite photoresist with low stress properties for microfabrication applications.* Microelectron. Eng. 83 (2006) (b) 1966–1970

Jiguet, S., Judelewicz, M., Mischler, S., Bertch, A., Renaud, P. Effect of filler behavior on nanocomposite SU8 photoresist for moving micro- parts. Microelectron. Eng.83 (2006) (a) 1273–1276.

Jo, B. H., Lerberghe, L. M. V., Motsegood, K. M., Beebe. D. J. *Three-dimensional micro-channel fabrication in polydimethylsiloxane (PDMS) elastomer.* J. Microelectromech. Syst., 9 (2000) 76-81.

Jo, B.-H., Van Lerberghe, L.M., Motsegood, K.M., Beebe, D.J. *Three-dimensional micro-channel fabrication in polydimethylsiloxane (PDMS) elastomer.* Journal of Microelectromechanical Systems 9 (1) (2000) 76.

- Jung, Y.C., and Bhushan, B.** *Contact angle, adhesion and friction properties of micro- and nanopatterned polymers for superhydrophobicity.* Nanotechnology, 17 (2006) 4970–80.
- Jung, Y.C., and Bhushan, B.** *Wetting transition of water droplets on superhydrophobic patterned surfaces.* Scr. Mater., 57 (2007) 1057–60.
- Kasai, T., Bhushan, B., Kulik, G., Barbieri, L., Hoffman, P.** *Nanotribological study of perfluorosilane SAMs for anti-stiction and low wear.* J. Vac.Sci. Technol. B, 23 (2005) 995–1003.
- Khoo, M., Liu, C.** *Micro magnetic silicone elastomer membrane actuator.* Sens. Actuators A, 89 (2001) 259-266.
- Kim, B. H., Chung, T. D., Oh, C. H., Chun, K.** *A new organic modifier for anti-stiction.* J. Microelectromech.Syst., 10 (2001) 33-40.
- Kim, S.H., Asay, D.B., Dugger, M.T.** *Nanotribology and MEMS.* NanoToday, 2 (2007) 22–29.
- Komvopoulos, K.** *Surface engineering and microtribology for microelectromechanical systems.* Wear, 200 (1996) 305-327.
- Kuo, T.-C., Cannon, D.M., Chen, Y.N., Tulock, J.J., Shannon, M.A., Sweedler, J.V., Bohn, P.W.** *Gateable Nanofluidic Interconnects for Multilayered Microfluidic Separation Systems.* Anal. Chem., 75 (2003) 1861-1867.
- LaBianca, N., and Delorme, J.** *High aspect ratio resist for thick film applications.* Proc. SPIE, 2438 (1995) 846-852.

Labianca, N.C., Gelorme, J.D., Lee, K.Y., Sullivan, E.O., Shaw, J.M. *High aspect ratio optical resist chemistry for MEMS application.* in: Proceedings of 4th International Symposium on Magnetic Materials, Processes and Devices, Chicago (1993) 386–396.

Lancaster, J. K. *Lubrication of carbon fibre-reinforced polymers: Part II—Organic fluids.* *Wear*, 20 (1972) 335-351.

Lau, K. H., Archit Giridhar, Sekar Harikrishnan, Nalam Satyanarayana, Sujeet K. Sinha. *Releasing high aspect ratio SU-8 microstructures using AZ photoresist as a sacrificial layer on metallized Si substrates.* *Microsystem Technologies* 19 (2013) 1863-1871.

Lee, K.K., Bhushan, B., Hansford, D. *Nanotribological characterization of perfluoropolymer thin films for bioMEMS applications.* *J. Vac. Sci. Technol. A* 23 (2005) 804–810.

Lee, K.Y., LaBianca, N., Rishton, S.A., Zolgharnain, S. *Micromachining applications for a high resolution ultrathick photoresist,* *Journal of Vacuum Science and Technology B* 13 (6) (1995) 3012.

Leong, J. Y., Reddyhoff, Sinha, S. K., Holmes, A. S., Spikes, H. A. *Hydrodynamic Friction Reduction in a MAC-Hexadecane Lubricated MEMS Contact.* *Tribology Letters*, 49 (2013) 217-225.

Li, Lei., Yongjin Wang, Cassandra Gallaschun, Timothy Risch and Jianing Sun. *Why can a nanometer-thick polymer coated surface be more wettable to water than to oil?.* *J. Mater. Chem.*, 22 (2012) 16719-16722.

Liakopoulos, T.M., Ahn. Microfabricated toroidal planar inductors with different magnetic core schemes for MEMS and power electronic applications, *IEEE Transactions on Magnetic* 35 (52) (1999) 3679.

Lin, Li-Ju J., David D. Saperstein. *Process for Bonding Lubricants to Thin Film Recording Media*, US Patent 5,030,478, Date of Patent: Jul. 9, **1991**.

Liu, H., Bharat Bhushan. *Nanotribological characterization of molecularly thick lubricant films for applications to MEMS/NEMS by AFM.* *Ultramicroscopy* 97 (**2003**) 321-340.

Liu, H., Bhushan, B. *Nanotribological characterization of digital micromirror devices using an atomic force microscope.* *Ultramicroscopy*, 100 (**2004**) 391–412.

Liu, H., Bhushan, B. *Nanotribological characterization of molecularly thick lubricant films for applications to MEMS/NEMS by AFM.* *Ultramicroscopy*, 97 (**2003**) 321-340.

Liu, H., Bhushan, B. *Nanotribological properties and mechanisms of alkylthiol and biphenyl thiol self-assembled monolayers by atomic force microscopy.* *Phys. Rev. B*, 63 (**2001**) 245412:1–245412:11.

Loeb, G. I., and Schrader, M. E. *Modern Approaches to Wettability: Theory and Applications.* Plenum Press, NY, USA (**1992**) 1-27.

Lorenz, H., Despont, M., Fahrni, M., LaBianca, N., Vettiger, P., and Renaud, P. *SU-8: a low-cost negative resist for MEMS.* *J. Micromech. Microeng*, 7 (**1997**) 121-124.

Lorenz, H., Despont, M., Renaud, P. *High-aspect-ratio, ultrathick, negative-tone near-UV photoresist and its applications for MEMS,* *Sensors and Actuators A* 64 (1) (**1998**) 33.

Lorenz, H., Laudon, M., and Renaud, P. *Mechanical characterization of a new high-aspect-ratio near UV-photoresist.* Microelec. Engin. 41/42 (1998) 371-374.

Ma Xiaoding, Huan Tang, Jing Gui. *Temperature effect on spreading of perfluoropolyethers on amorphous carbon films.* Tribol. Lett., 10 (2001) 203-209.

Ma, J.Q., Mo, Y.F., and Bai, M.W. *Preparation and tribological behavior of multiply-alkylated cyclopentane-1H,1H,2H,2H-perfluorodecyltrichlorosilane dual-layer film on diamond-like carbon.* Journal of Engineering Tribology, 223 (2009) 705-714.

Ma, J.Q., Pang, C.J., Mo, Y.F., and Bai, M.W. *Preparation and tribological properties of multiply-alkylated cyclopentane (MAC)-octadecyltrichlorosilane (OTS) double-layer film on silicon.* Wear 263 (2007) 1000-1007.

Maboudian, R. and Howe, R. T. *Critical review: Adhesion in surface micromechanical structures.* Journal of Vacuum Science and Technology B, 15 (1997) 1-20.

Maboudian, R. *Surface processes in MEMS technology.* Surface Science Reports, 30 (1998) 207-269.

Madou, M. J. *Fundamentals of Microfabrication*, 2nd edition, CRC Press, New York (2002).

Mani, S.S., Fleming, J.G., Walraven, J.A., Sniegowski, J.J. *Effect of W coating on microengine performance.* Proc. 38th Annual Inter. Reliability Phys. Symp., IEEE, New York (2000) 146–151.

Mann, C.M. *Fabrication technologies for terahertz waveguide.* in: IEEE Sixth International Conference on Tera Hertz Electronics, Leeds, UK (1998) 46–49.

Maria Nordström, Alicia Johansson, Encarnacion Sánchez Nogueroń, Bjarne Clausen, Montserrat Calleja, Anja Boisen. *Investigation of the bond strength between*

the photo-sensitive polymer SU-8 and gold. Microelectronic Engineering 78–79 (2005) 152–157.

Mastrangelo, C. H. *Adhesion-related failure mechanisms in micromechanical devices, Tribology Letters*, 3 (1997) 223-238.

Mastrangelo, C. H., Hsu, C. H. *Mechanical stability and adhesion of microstructures under capillary forces – part I: Basic theory. J. MEMS*, 2 (1993) (a) 33–43.

Mastrangelo, C. H., Hsu, C. H. *Mechanical stability and adhesion of microstructures under capillary forces – part II: Experiments, J. MEMS*, 2 (1993) (b) 44–55.

Mate, C. M. *Tribology on the Small Scale - A Bottom Up Approach To Friction, Lubrication and Wear.* Oxford University Press, UK (2007).

Mate, C. M., McClelland, G. M., Erlandsson, R. and Chiang, S. *Atomic-scale friction of tungsten tip on a graphite surface. Physical Review Letters*, 59 (1987) 1942-1945.

Mathew, M.C., and Novotny, V.J. *Molecular conformation and disjoining pressure of polymeric liquid films. J. Chem. Phys.*, 94 (1991) 8420 -8427.

Menard, E., Nuzzo, R. G., Rogers. J. A. *Bendable single crystal silicon thin film transistors formed by printing on plastic substrates. Appl. Phys. Lett.*, 86 (2005) 093507.

Miller, W. M., Tanner, D. M., Miller, S. L., Peterson K. A. *MEMS Reliability: The Challenge and the Promise.* In: Proc. 4th Annual “The Reliability Challenge”, Dublin, Ireland (1998) 4.1-4.7.

Mionic, M., Jiguat, S., Judelewicz, M., Karimi, A., Forro, L. and Magrez, A. *Study of the mechanical response of carbon nanotubes-SU8 composites by nanoindentation. Phys. Status Solidi B* 247 (2010) 3072-3075.

- Miwa, M., Nakajima, A., Fujishima, A., Hashimoto, K., and Watanabe, T.** *Effects of the surface roughness on sliding angles of water droplets on superhydrophobic surfaces.* Langmuir, 16 (2000) 5754–60.
- Muller, R. S., Howe, R. T., Senturia, S. D., Smith, R. L. and White, R. M.** *Microsensors*, IEEE Press, New York (1990).
- Nahar, P., Naqvi, A., Basir, S.F.** *Sunlight-mediated activation of an inert polymer surface for covalent immobilization of a protein.* Anal Biochem, 327 (2004) 162-4.
- Neidhardt, J., Hultman, L., Broitman, E., Scharf, T. W., and Singer, I. L.** *Structural, mechanical and tribological behavior of fullerene-like and amorphous carbon nitride coatings.* Diamond & Related Materials 13 (2004) 1882-1888.
- Nicolaas-Alexander Gotzen, HeikoHuth, Christoph Schick, Guy Van Assche, CarineNeus, Bruno Van Mele.** *Phase separation in polymer blend thin films studied by differential AC chip calorimetry.* Polymer 51(2010) 647-654.
- Nosonovsky, M., and Bhushan, B.** *Roughness optimization for biomimetic superhydrophobic surfaces.* Microsyst. Technol., 11 (2005) 535–49.
- Ohno, N., Mia, S., Morita, S., and Obara, S.** *Friction and wear characteristics of advanced space lubricants.* Tribology Transactions, 53 (2010) 249-255.
- Okhlopkova, A.A., Petrova, P.N., Popov, S.N., and Fedorov, A.L.** *Tribological materials based on polytetrafluoroethylene modified by a liquid lubricant.* Journal of friction and wear, 29 (2008) 133-136.
- Oner, D., and McCarthy, T.J.** *Ultrahydrophobic surfaces: Effects of topography length scales on wettability.* Langmuir, 16 (2000) 7777–7782.

Owens, D. K. *The mechanism of corona and ultraviolet light-induced self-adhesion of poly (ethylene terephthalate) film.* Jour. of Appl. Poly. Sci., 19 (1975) 3315-3326.

Prabakaran, S., Satyanarayana, N., Sinha, S. K. *Self-lubricating SU-8 Nanocomposites for micromechanical systems applications.* Tribo. Lett. 49 (2013) (a) 169-178.

Prabakaran, S., Satyanarayana, N., Sinha, S.K. *Wear Durability Study on Self lubricating SU-8 composites with perfluoropolyther, multiply-alkylated cyclopentane and base oil as the fillers.* Tribol. Inter., 64 (2013) (b) 103-115.

Prabakaran, S., Satyanarayana, N., Sinha, S.K., and Duong Hai Minh. *An in-situ heating effect study on tribological behavior of SU-8+PFPE composite.* Wear 307 (2013) (c) 182–189.

Prabakaran, S., Sundaramurthy, J., Sinha, S.K., and Duong Hai Minh. *The Role of Functional End Groups of Perfluoropolyether (Z-dol and Z-03) Lubricants in Augmenting the Tribology of SU-8 Composites.* Tribo. Lett. 56 (2014) 423-434.

Prathima C. Nalam, Shivaprakash N. Ramakrishna, Rosa M. Espinosa-Marzal, and Nicholas D.Spencer. *Exploring Lubrication Regimes at the Nanoscale: Nanotribological Characterization of Silica and Polymer Brushes in Viscous Solvents.* Langmuir 29(32) (2013) 10149-10158.

Priest, C., Gruner, P. J., Szili, E. J., Al-Bataineh, S. A., Bradley, J. W., Ralston, J., Steele, D.A., Short, R.D. *Microplasma patterning of bonded microchannels using high-precision “injected” electrodes.* Lab Chip, 11 (2011) 541–544.

Raphael Heeb, Robert M. Bielecki, Seunghwan Lee, and Nicholas D. Spencer. *Room-Temperature, Aqueous-Phase Fabrication of Poly (methacrylic acid) Brushes by UV-*

LED-Induced, Controlled Radical Polymerization with High Selectivity for Surface-Bound Species. *Macromolecules* 42 (2009) 9124–9132.

Reichmanis, E., and Thompson, L. F. *Polymer materials for microlithography*. *Chem. Rev.*, 89 (1989) 1273-1289.

Renaud, P., van Lintel, H., Heuschkel, M., Guerin, L. *Photopolymer micromachannel technologies and applications in process*. in: *Process, TAS'98, Banff, Canada* (1998) 17–21.

Ruano-Lopez, J. M., Aguirregabiria, M., Tijero, M., Arroyo, M. T., Elizalde, J., Berganzo, J., Aranburu, I., Blanco, F.J., Mayor, K. *A new SU-8 process to integrate buried waveguidelines and sealed microchannels for a Lab-on-a-Chip*. *Sens. Actuators B Chem.* 114 (2006) 542–551.

Ruhe, J., Blackman, G., Novotny, V.J., Clarke, Street, G.B., and Kuan, S. *Terminal Attachment of Perfluorinated Polymers to Solid Surfaces*. *J. Appl. Poly. Science*, 53, (1994) 825 -836.

Ryu, K., Wang, X., Shaikh, K., Liu, C. *A method for precision patterning of silicone elastomer and its applications*. *J. Microelectromech.Syst.*, 13 (2004) 568-575.

Ryu, W., Fasching, R. J., Vyakarnam, M., Greco, R. S., Prinz, F. B. *Microfabrication technology of biodegradable polymers for interconnecting microstructures*. *IEEE/ASME J. Microelectromech. Syst.* 15 (2006) 1457-1465.

Samel, B., Griss, P., Stemme, G. *A Thermally Responsive PDMS Composite and Its Microfluidic Applications*. *J. Microelectromech.Syst.*, 16 (2007) 50-57.

- Satyanarayana, N., and Sinha, S. K.** *Tribology of PFPE overcoated self-assembled monolayers deposited on Si surface.* Journal of Physics D: Applied Physics 38 (2005) 3512-3522.
- Sharpe, W. N., Bagdahn, J.** *Fatigue testing of polysilicon - a review.* Mech. Mater., 36 (2004) 3-11.
- Sharpe, W. N., Jackson, K. M., Hemker, K. J., Xie, Z.** *Effect of specimen size on young's modulus and fracture strength of polysilicon.* J. Microelectromech. Syst.,10 (2001) 317 -326.
- Shen, X.-J., Pan, L.-W., Lin, L.** *Microplastic embossing process: experimental and theoretical characterizations.* Sens. Actuators A, 97-98 (2002) 428-433.
- Shi, w., Dong, H., and Bell, T.** *Tribological behaviour and microscopic wear mechanisms of UHMWPE sliding against thermal oxidation-treated Ti6Al4V.* Material Science and Engineering, A291 (2000) 27-36.
- Shibuichi, S., Onda, T., Satoh, N., and Tsujii, K.** *Super-water-repellent surfaces resulting from fractal structure.* J.Phys. Chem., 100 (1996) 19512-7.
- Singh, R. A., Satyanarayana, N., Kustandi, T. S., and Sinha, S. K.** *Tribo-functionalizing Si and SU8 materials by surface modification for application in MEMS/NEMS actuator-based devices.* Journal of Physics D: Applied Physics, 44 (2011) (a) 015301.
- Singh, R.A., Satyanarayana, N., and Sinha, S.K.** *Surface Chemical Modification for Exceptional Wear Life of MEMS Materials.* AIP Advances 1 (2011) (b) 042141.
- Situma, C., Wang, Y., Hupert, M., Barany, F., McCarley, R.L., and Soper, S.A.** *Fabrication of DNA microarrays onto poly (methyl methacrylate) with ultraviolet*

patterning and microfluidics for the detection of low-abundant point mutations. Anal Biochem, 340 (2004) 123-135.

Campen, S., Jonathan Green, Gordon Lamb, David Atkinson, Hugh Spikes. *On the Increase in Boundary Friction with Sliding Speed*. Tribology Letters 48 (2012) 237-248.

Spearing, S.M., Chen. K.S. *Micro-gas turbine engine materials and structures*. Ceramic Eng. Sci. Proc., 18 (2001) 11–18.

Spencer, N.D., and Tysoe, W.T. *Left of the Stribeck curve*. Tribology & Lubrication Technology 68(12) (2012) pp 96.

Spikes, H. A. *Mixed lubrication — an overview*. Lubrication Science, 9 (1997) 221–253.

Srinivasan, U., Houston, M. R., Howe, R. T., Maboudian, R. *Alkyltrichlorosilane-based self-assembled monolayer films for stiction reduction in silicon micromachines*. J. Microelectromech.Syst., 7 (1998) 252-260.

Stark, B. (ed): *MEMS Reliability Assurance Guidelines for Space Applications*. National Aeronautics Space Administration (NASA) and Jet Propulsion Laboratory (JPL), California Institute of Technology, Pasadena (1999).

Sugimoto, I., and Miyake, S. *Solid lubricating fluorine-containing polymer film synthesized by perfluoropolyether sputtering*. Thin Solid Films 158 (1988) 51-60.

Surface Coatings. *Raw Materials and Their Usage, Oil and Colour Chemist's Association*, 1993, vol 1, ISBN 0412552108.

Sze, S. M. *Semiconductor Sensors*, Wiley, New York (1994).

Tabor, D., and Winterton, R. H. S. *The direct measurement of normal and retarded van der Waals forces*. Proceedings of the Royal Society of London A, 312 (1969) 435-450.

Tai, Y.C., Fan, L.S., Muller, R.S. *IC –Processed micro-motors: Design, technology and testing*. In: Proc. IEEE Micro Electro Mechanical Systems, (1989) 1–6.

Tambe, N.S., Bhushan, B. *Nanotribological characterization of self assembled monolayers deposited on silicon and aluminum substrates*. Nanotechnology 16 (2005) 1549–1558.

Tanaka, Y., and Kakiuchi, H. *Study of Epoxy Compounds. Part VI. Curing Reactions of Epoxy Resin and Acid Anhydride with Amine, Acid, Alcohol, and Phenol as Catalysts*. Journal of Polymer Science Part A, 2 (1964) 3405-3430.

Tani, H., Tagawa, N. *Adhesion and Friction Properties of Molecularly Thin Perfluoropolyether Liquid Films on Solid Surface*. Langmuir 28 (2012) 3814-3820.

Tanner, D.M., Smith, N.F., Irwin, L.W. *MEMS Reliability: Infrastructure, Test Structures, Experiments, and Failure Modes*. SAND2000-0091, Sandia National Laboratories, Albuquerque, New Mexico (2000).

Tas, N., Sonnenberg, T., Jansen, H., Legtenberg, R., and Elwenspoek, M. *Stiction in surface micromachining*. Journal of Micromechanics and Microengineering, 6 (1996) 385-397.

Thomas Rohr, Frank Ogletree, D., Frantisek Svec and Frechet, J.M.J. *Surface Functionalization of Thermoplastic Polymers for the Fabrication of Microfluidic Devices by Photoinitiated Grafting*. Adv. Funct. Mater., 13, No.4 (2003) 264-270.

Thorsen, T., Maerkl, S. J., Quake, S. R. *Microfluidic Large-Scale Integration*. Science 298 (2002) 580-584.

Timpe, S. J., and Komvopoulos, K. *An experimental study of sidewall adhesion in microelectromechanical systems*. J. Microelectromech. Syst., 14 (2005) 1356-1363.

Tyndall, G. W., Karis, T. E., Jhon, M. S. *Spreading Profiles of Molecularly Thin Perfluoropolyether Films*. Tribology Transactions, 42:3 (1999) 463-470.

Ulman, A. *An Introduction to Ultrathin Organic Films: From Langmuir--Blodgett to Self-Assembly*, Academic press, San Diego (1991).

Unal, H., Mimaroglu, A. *Friction and wear performance of polyimide 6 and graphite and wax polyimide 6 composites under dry sliding conditions*. Wear 289(2012)132-137.

Unger, M. A., Chou, H.-P., Thorsen, T., Scherer, A., Quake, S. R. *Monolithic Microfabricated Valves and Pumps by Multilayer Soft Lithography*. Science 288 (2000) 113-116.

van Spengen, W. M. *MEMS reliability from a failure mechanisms perspective*, Microelectron. Reliab., 43 (2003) 1049–1060.

Venier, C.G., and Casserly, E.W. *Multiply-Alkylated Cyclopentanes (MACs): A New Class of Synthesized Hydrocarbon Fluids*. Lubrication Engineering, 47 (1991) 586-591.

Voigt, A., Heinrich, M., Martin, C., Liobera, A., Gruetzner, G., and Perez-Murano, F. *Improved properties of epoxy nanocomposites for specific applications in the field of MEMS/NEMS*. Microelectronic Engineering 84 (2007) 1075-1079.

Walther, F., Tanja Drobek, Alexander M. Gigler, Marc Hennemeyer, Michael Kaiser, Helmut Herberg, Tetsuji Shimitsu, Gregor E. Morfill and RobertW. Stark. *Surface hydrophilization of SU-8 by plasma and wet chemical processes*. Surface Interface Analysis, 42 (2010) 1735-1744.

Waltman, R.J., Yen, B.K., White, R.L. *The adhesion of monomolecular hydroxyl terminated perfluoropolyether liquid films on the sputtered silicon nitride surface as a function of end group acidity and mobility*. Tribo. Lett., 20 (2005) 69-81.

Wang, X., Engel, J., Liu, C. *Liquid crystal polymer (LCP) for MEMS: processes and applications.* J. Micromech. Microeng., 13(2003) 628-633.

Wang, Y., Mark Bachman, Christopher E. Sims, Li, G. P., and Nancy L. Allbritton. *Simple Photografting Method to Chemically Modify and Micropattern the Surface of SU-8 Photoresist.* Langmuir 22 (2006) 2719-2725.

Wang, Y., Mo, Y., Zhu, M., and Bai, M. *Wettability and nanotribological property of multiply alkylated cyclopentanes (MACs) on silicon substrates.* Tribology Transactions 53 (2010) 219-223.

Wei, H. X., Li, J., Q, Z., Xu, Y. Cai, J., Tang, X., Li, Y. Q. *Thermal annealing-induced vertical phase separation of copper phthalocyanine: Fullerene bulk hetero junction in organic photovoltaic cells.* Appl. Phys. Lett., 97 (2010) 083302.

Weisenberg, B. A., Mooradian, D. L. *Hemocompatibility of materials used in microelectromechanical systems: Platelet adhesion and morphology in vitro.* J. Biomed. Mater. Res.60 (2002) 283–291.

Welle, A., Horn, S., Schimmelpfeng, J., Kalka, D. *Photo-chemically patterned polymer surfaces for controlled PC-13 adhesion and neurite guidance.* J Neurosci Meth, 142 (2005) 243-50.

Wenmin Qu, Wenzel, C., Jahn, A., Zeidler, D. *UV-LIGA: a promising and low-cost variant for microsystem technology.* in: Proceedings of Optoelectronic and Microelectronic Materials Devices, Perth, Australia (1998) 380–383.

Wenzel, R.N. *Resistance of solid surfaces to wetting by water.* Ind. Eng. Chem., 28 (1936) 988–94.

West, G.H., and Seniort, J.M. *High temperature plastics bearing compositions.* Tribology, 6 (1973) 269-275.

www.microchem.com

www.somisys.ch/microfluidics.htm

www.solvayplastics.com

www.chevron.com/

www.nyelubricants.com/

Xia, Y., Whitesides. G. M. *Soft lithography.* Annu. Rev. Mater. Sci., 28 (1998) 153-184.

Xing, C.M., Deng, J.P., Yang, W.T. *Synthesis of antibacterial polypropylene film with surface immobilized polyvinylpyrrolidone-iodine complex.* J Appl Polym Sci, 97 (2005) 2026-31.

Yamaguchi, Y. *In: Tribology of Plastic Materials,* Tribology Series, 16, Elsevier, Amsterdam (1990) 192.

Yamaguchi, Y., and Sekiguchi, I. ASLE Proc., 3rd Znt. Solid Lubrication Conf, Denver, CO (1984) 187-195.

Yang, X., Grosjean, C., and Tai, Y.-C. *Design, fabrication, and testing of micromachined silicon rubber membrane valves.* J. Microelectromech. Syst., 8 (1999) 393-402.

Yeo, J.S., Yun, J.M., Kim, D.Y., Park, S., Kim, S.S., Yoon, M.H., Kim, T.W., Na. SI. *Significant Vertical Phase Separation in Solvent-Vapor-Annealed Poly(3,4-ethylenedioxythiophene):Poly(styrene sulfonate) Composite Films Leading to Better Conductivity and Work Function for High-Performance Indium Tin Oxide-Free Optoelectronics.* ACS Appl. Mat. Interfaces. 4 (2012) 2551-2560.

Yeow, T. W., Law, K. L. E. and Goldenberg, A. *MEMS optical switches.* IEEE Communications Magazine, 39 (2001) 158.

Yoon, Y.-K., Park, J.-H., Allen, M. G. *Multidirectional UV Lithography for Complex 3-D MEMS Structures.* J. Microelectromech.Syst., 15 (2006) 1121-1130.

Zhang, G., Chu, V., Conde, J. P. *Conductive blended polymer MEMS microresonators.* IEEE/ASME J. Microelectromech. Syst.16 (2007) 329-335.

Zhang, H., Mitsuya, Y., Imamura, M., Fukuoka, N., Fukuzawa, K. *Effect of ultraviolet irradiation on the interactions between perfluoropolyether lubricant and magnetic disk surfaces.* Tribo. Lett., 20 (2005) 191-199.

Zhang, H., Taiki Takimoto, Kenji Fukuzawa, and Shintaro Itoh. *Effect of Ultraviolet Irradiation on Adhesion of Nanometer-Thick Lubricant Films Coated on Magnetic Disk Surfaces.* IEEE Trans. On Magnetics, 47, No.1 (2011) 94-99.

Zheng Xu, Li-Min Chen, Guanwen Yang, Chun-Hao Huang, Jianhui Hou, Yue Wu, Gang Li, Chain-Shu Hsu, Yang Yang. *Vertical Phase Separation in Poly (3-hexylthiophene): Fullerene Derivative Blends and its Advantage for Inverted Structure Solar Cells.* Adv. Func. Matl. 19 (2009) 1227-1234.